University of Groningen

Inflation

Coone, Andries Alexander

IMPORTANT NOTE: You are advised to consult the publisher's version (publisher's PDF) if you wish to cite from it. Please check the document version below.

Document Version
Publisher's PDF, also known as Version of record

Publication date:
2018

Link to publication in University of Groningen/UMCG research database

Citation for published version (APA):
Coone, A. A. (2018). *Inflation: Generic predictions and nilpotent superfields*. [Thesis fully internal (DIV), University of Groningen]. Rijksuniversiteit Groningen.

Copyright
Other than for strictly personal use, it is not permitted to download or to forward/distribute the text or part of it without the consent of the author(s) and/or copyright holder(s), unless the work is under an open content license (like Creative Commons).

The publication may also be distributed here under the terms of Article 25fa of the Dutch Copyright Act, indicated by the "Taverne" license. More information can be found on the University of Groningen website: https://www.rug.nl/library/open-access/self-archiving-pure/taverne-amendment.

Take-down policy
If you believe that this document breaches copyright please contact us providing details, and we will remove access to the work immediately and investigate your claim.

Downloaded from the University of Groningen/UMCG research database (Pure): http://www.rug.nl/research/portal. For technical reasons the number of authors shown on this cover page is limited to 10 maximum.

Download date: 05-05-2023

Inflation: Generic Predictions and Nilpotent Superfields

Dries Coone

ISBN: 978-94-034-0697-8 (printed version)
ISBN: 978-94-034-0698-5 (electronic version)

© 2018 Dries Coone

Printed by Ipskamp Printing, The Netherlands.

university of groningen

VRIJE UNIVERSITEIT BRUSSEL

Inflation: Generic predictions and nilpotent superfields

Proefschrift

ter verkrijging van de graad van doctor
aan de Rijksuniversiteit Groningen
op gezag van de
rector magnificus prof. dr. E. Sterken
en volgens besluit van het College voor Promoties

en

ingediend met het oog op het behalen van de academische graad van
Doctor in de Wetenschappen aan de Vrije Universiteit Brussel.

Double PhD degree

De openbare verdediging zal plaatsvinden op

vrijdag 1 juni 2018 om 11:00 uur

door

Andries Alexander Coone

geboren op 17 juli 1988
te Groningen

Promotores
Prof. dr. B. Craps
Prof. dr. D. Roest

Copromotor
Prof. dr. A. Mariotti

Beoordelingscommissie
Prof. dr. A. Achúcarro
Prof. dr. W. Buchmüller
Prof. dr. E. Pallante
Prof. dr. A. Sevrin

Contents

Abstract

With the current observations of the Planck satellite, the measurements that probe cosmological scales are entering a new high precision era. This provides interesting information regarding the very early stages of the universe, including on the era of inflation which is studied in this thesis.

One of the observables is the cosmic microwave background (CMB) radiation, which was emitted when the universe was relatively young (380 000 years). This radiation encodes a wealth of information concerning the state of the universe when it was emitted and can therefore be regarded as a picture of the early universe. One of the interesting features of this 'picture' is that the observed deviations in the temperature of the CMB radiation are tiny, implying that the CMB radiation is isotropic.

A popular explanation for the isotropy of the universe is cosmological inflation, which is the main topic of this thesis. During the inflation era the universe rapidly expanded, generating a causal connection between points in the CMB radiation that were far apart at the moment this radiation was emitted. Therefore, inflation explains the isotropy of the universe. Quantum mechanics generates small differences for different patches of the universe during the inflationary phase, which are responsible for the small anisotropies – deviations from the perfect isotropy – in the CMB radiation. Indeed, dedicated experiments have observed these anisotropies, which are exactly as predicted by (single field) inflation. In addition to these small perturbations in the density of the universe, inflation also predicts a cosmological source of gravitational waves. Though the existence of these gravitational waves could be visible in the CMB radiation, they have not been observed.

The first line of research on which this thesis is based considers large ensembles of inflation models and compares them with the data from the CMB radiation observed by the Planck satellite. From these large ensembles generic predictions were deduced for given parametrizations. By comparing the predictions from a polynomial expanded inflation model to a model defined by the ratio of polynomials, we find that the latter (which represents plateau inflation) are in better

agreement with the data than the former. Therefore, we conclude that the current data favours plateau inflation. This observation is strengthened by our subsequent study of the strong coupling attractor inflation model, which also naturally have a plateau if a parameter (ξ) is chosen sufficiently large. Our study of generic predictions of this attractor showed that if $\xi = \mathcal{O}\left(10^4\right)$, these models are in perfect agreement with the data.

The second line of research studies inflation embedded in supergravity, which is an extension of both the standard model of particle physics and general relativity. In this study, we consider a particular embedding of inflation in supergravity, and study its theoretical consistency. In addition, we are able to address another problem in cosmology, which is that the total amount of matter in the universe is larger than the amount of observed matter. In part of the parameter space of our supergravity model the additional matter (dark matter) is naturally explained as originating from this new supersymmetric sector. Thus, we have a model that simultaneously describes supersymmetry breaking, inflation and dark matter.

Samenvatting

Binnen de natuurkunde wordt een grote verscheidenheid aan afstandsschalen bestudeerd. Zo worden bijvoorbeeld zeer precieze metingen verricht aan kosmologische datasets. Deze metingen genereren interessante informatie over het zeer vroege universum, inclusief de inflatieperiode die bestudeerd wordt in dit proefschrift.

Een van de kosmologische datasets is de kosmische achtergrondstraling (CMB). De CMB is straling die uitgezonden is toen het universum relatief jong (380 000 jaar) was. Deze straling werd uitgezonden in het vroege universum en bevat een grote hoeveelheid informatie over deze periode. Feitelijk kan het beschouwd worden als een meting van de temperatuur van het vroege universum. Vreemd genoeg bevat deze meting nagenoeg geen variaties in de temperatuur, hetgeen betekent dat de CMB isotroop is (merk op dat de CMB enkel waargenomen wordt in verschillende richtingen aan de hemel).

De populairste verklaring voor de isotropie van het universum is een vroege fase van kosmologische inflatie en het onderzoek hiernaar is het onderwerp van dit proefschrift. Tijdens inflatie expandeerde het universum versneld, hetgeen ervoor zorgde dat punten in de CMB causaal met elkaar verbonden raakten. Hiermee verklaart inflatie de isotropie van het universum. Echter, kwantummechanische fluctuaties genereerden tijdens inflatie zeer kleine veranderingen in de energiedichtheid van het universum die vervolgens anisotropieën in de CMB veroorzaakten. Deze anisotropieën zijn inderdaad gemeten en zijn precies zoals voorspeld door inflatie. Behalve deze anisotropieën voorspelt inflatie ook deformaties in het gravitationele veld die zich manifesteren als zwaartekrachtgolven. Hoewel de gevolgen van de zwaartekrachtgolven zichtbaar zouden moeten zijn in de CMB, is dit nog niet waargenomen.

De eerste tak van het onderzoek dat beschreven wordt in dit proefschrift is het vergelijken van grote ensembles van inflatiemodellen met de data van de CMB zoals gemeten door de Planck satelliet. Van deze grote ensembles kunnen generieke voorspellingen worden afgeleid voor de verschillende parametrisaties waarmee deze

ensembles zijn gemaakt. Door een parametrisatie van de potentiaal gebaseerd op een polynoom te vergelijken met modellen met een verhouding van polynomen, wordt geconcludeerd dat deze laatste modellen (die een realisatie zijn van plateau inflatiemodellen) beter overeenkomen met de CMB. We concluderen hieruit dat de huidige data suggereren dat inflatie geparametriseerd wordt door plateau inflatiemodellen. Deze observatie is versterkt door een studie van zogenaamde sterke koppeling attractormodellen die een natuurlijk plateau genereren als een parameter (ξ) groot genoeg wordt gekozen. Onze studie naar de generieke voorspellingen van deze modellen toonde aan dat als $\xi = \mathcal{O}\left(10^4\right)$ gekozen wordt, deze modellen in perfecte overeenstemming zijn met de data.

De tweede tak van het onderzoek bestudeert inflatiemodellen in supergravitatie, hetgeen een extensie is van zowel het standaardmodel van de deeltjesfysica als van de algemene relativiteitstheorie door middel van een nieuwe symmetrie genaamd supersymmetrie. In dit onderzoek bestuderen we een bepaalde inbedding van inflatie in supergravitatie en bestuderen we de theoretische consistentie. Daarnaast zijn we in staat om donkere materie, een ander probleem in de kosmologie, te bestuderen. In een deel van de parameterruimte van ons model wordt deze donkere materie verklaard door een deeltje in de supersymmetrische sector. Hierdoor zijn wij in staat om in ons model zowel supersymmetriebreking, inflatie als donkere materie te beschrijven.

CHAPTER 1

Introduction

1.1 Physics at extreme length scales

Contemporary physics experiments study events at a large variety of length scales. At the smallest length scales, the Large Hadron Collider (LHC) probes the elementary particles, while at the largest scales the initial state of the universe is probed by the Planck satellite [1] and the BICEP/KECK telescope [2] which observe the cosmic microwave background (CMB) radiation. Between these extremes, there are many orders of magnitude at which interesting physical phenomena occur. A few of these are shown in Fig. 1.1.

When considering this wide range of distance scales, it should be realised that for many observations it is sufficient to consider effective theories, instead of a theory that describes the full set of energy scales. For instance, when calculating the acceleration of a falling apple, at first order only the gravitational force needs to be included. In general, the physics of a falling apple is, as is most of the physics that we observe around us in daily life, well described by classical mechanics.

When considering small distance scales, quantum mechanics provides a better explanation for the observed effects. Within quantum mechanics, there is an intrinsic uncertainty for observable quantities given by the Heisenberg uncertainty principle. Due to this principle, the position and momentum operators do not commute in quantum mechanics, while such an effect is not encountered in classical physics. Therefore, there is an intrinsic length scale named de Broglie wavelength $\lambda_{\mathrm{dB}} = \hbar/p$ given by the momentum (p) of a particle at which quantum mechanical effects become relevant.

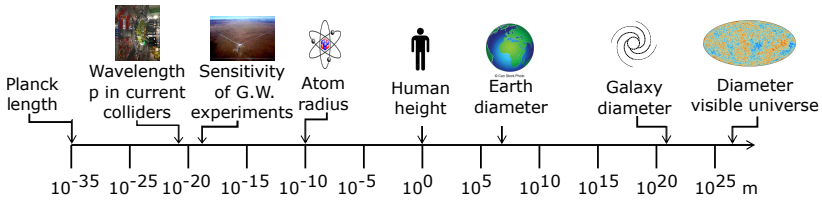

Figure 1.1: *The different observed distance scales, G.W. stands for gravitational waves. The wavelength of protons (denoted p) is the De Broglie wavelength and the diameter of the visible universe refers to the surface of the cosmic microwave background radiation that we observe. The total universe that can theoretically be observed, the current particle horizon, is larger.*

At large velocities close to the speed of light (hence also at large momenta) special relativistic effects become relevant, since the speed of light is the maximal possible velocity at which information can travel. In this extreme, the fact that the speed of light is the same for all inertial frames, *i.e.* non-accelerating frames, is relevant. Therefore, when boosting to a faster-moving inertial frame (thus without acquiring an acceleration), time in this new frame will run slower. This implies that the laws of physics are not invariant under independent transformations of space and time, as implied by Galilean relativity, but are invariant under the Lorentz transformations.

In the limit of small distance and large velocity, the de Broglie wavelength is smaller than the Compton wavelength $\lambda_C = \hbar/(mc)$. In this regime quantum field theory is the established theory, since it combines quantum mechanics and special relativity. The standard model of particle physics was developed within this paradigm and is a fundamental theory that is experimentally well verified. The standard model contains three types of particles: fermions, gauge bosons and the Brout-Englert-Higgs boson, which differ by their spin. Gauge bosons have spin 1, fermions spin 1/2 and the Brout-Englert-Higgs boson has spin 0. All observed matter, with the exception of dark matter, can be explained with this set of particles together with three of the four fundamental forces: the electromagnetic, the weak and the strong force. The gravitational force is not described in this framework, for it is extremely weak at the energy scales where the standard model of particle physics is tested. At the moment of writing this thesis, collider experiments did not observe any significant deviations from the standard model of particle physics.

When we study the physics at large distances, usually the involved masses become large. If, in addition, large velocities are considered, general relativistic effects must be taken into account. Within general relativity, space-time is curved

depending on the mass distribution inside it and a freely falling object follows the path with the shortest distance in this curved space. The difference of this path with respect to a straight line in flat space explains gravity. General relativity is typically relevant for describing the physics from the solar system scales, for instance the perihelion precession of Mercury, up to quantifying the shape of our universe.

At these large distance scales the standard model forces do not play an important role, since there are no charged structures. Moreover, the weak force has only a finite range and for distances beyond about 10^{-15} metre their effects are negligible. The strong force between two strongly charged objects grows with distance, therefore, if two quarks are separated, then the energy quickly increases and a new pair of quarks appear. This process is known as confinement, quarks are confined to be close together, thus at cosmological distance scales no strongly charged objects can exist. Though the dipole interaction resulting from the separation of the strong charges in nucleons does not confine, this force only has a finite length and is not of cosmological importance. This leaves us with only the gravitational force, which is – evidently – important when we are studying the universe.

Experimental studies showed that at large distances general relativity describes the astronomical data extremely well, if two new ingredients are taken into account. The first is that the total matter density is about a factor 4 larger than the luminous matter. The required additional matter, named dark matter, is not accounted for in the standard model of particle physics and is one of the motivations for studying extensions of this theory. Another new ingredient to explain the astronomical data is to add a source of acceleration for the late-time universe. The simplest approach to explain this acceleration is by adding a cosmological constant Λ to the Einstein equations. Thus parametrizing the two unknowns of current cosmology, the standard model of cosmology is named the ΛCDM (Λ Cold Dark Matter) model, where cold stands for the assumption that dark matter is non-relativistic. It is in good agreement with the data.

The ΛCDM model assumes that the evolution of the universe is described by general relativity, which postulates that the gravitational force attracts all matter equally due to the equivalence principle. Since gravity is for all objects in the universe an attractive force, structures are formed in the universe, like galaxies, galaxy clusters and superclusters. However, structures larger than superclusters (about 100 Mpc $\approx 3 \times 10^{25}$ m) have not been observed. This is in agreement with the cosmological principle, which postulates that for scales larger than approximately 100 Mpc the observations in the universe become independent on the position of the observer (homogeneity) and independent on the direction in which the universe is observed (isotropy). For a discussion on the cosmological principle and its emergence at large distances, see Ref. [3].

To further investigate the cosmological principle, one should realise that observing phenomena in cosmology at large spatial distance also implies a large temporal distance due to the finite speed of light. Therefore, by looking far away we observe

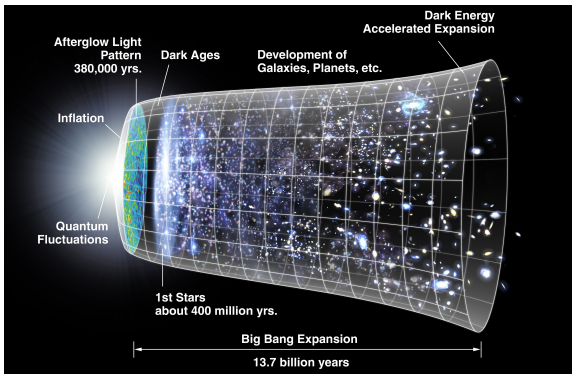

Figure 1.2: *History of the universe. Figure from Ref. [4], original from NASA.*

the early universe, of which the different eras are shown in Fig. 1.2. The current paradigm is that the universe started with a hot Big Bang, after which it was extremely hot. During this era, the universe was radiation dominated. However, the energy density contained in the radiation decreased faster than the energy density of the matter fluid, so after about 10^4 years the universe became matter dominated.

During this radiation dominated phase and the beginning of the matter dominated phase (the first 10^5 years), all matter in the universe was in the plasma phase and the mean free path of a photon in a plasma is small. Due to the expansion of the universe, the primordial plasma cooled down and at some moment the formation of neutral particles was energetically favourable, hence the universe entered the gas phase. Photons do not scatter as strongly in a gas as they do in a plasma, so the mean free path of the photons was greatly enhanced. The photons emitted at this phase transition are observable on the earth as the cosmic microwave background (CMB) radiation. Since before the CMB radiation was emitted the universe was not transparent, this is the earliest moment in the universe that is directly observed.

The CMB radiation was discovered by Penzias and Wilson in 1965 [5,6]. The signal that they observed was extremely isotropic. Moreover, the spectrum of the CMB radiation represents a perfect black body spectrum with a temperature of 2.7255 ± 0.0006 K [7]. The low temperature is caused by the expansion of the universe. When the CMB radiation was emitted, its spectrum was a black body with a temperature of the order of 3000 K [8]. After the first measurement of the CMB no deviations of the black body spectrum have been observed.

In 1992 the Cosmic Background Explorer (COBE) satellite measured small anisotropies in the sky [9], implying a breaking of the cosmological principle. These anisotropies were expected, since they are the seeds of the current density fluctua-

tions in the universe, like the galaxies, galaxy clusters and superclusters mentioned earlier. However, if there is no new era in the history of the universe, the CMB radiation should be completely uncorrelated at an angle in the sky larger than about 1.8 degrees [3]. Since the CMB radiation that we observe is correlated at larger angles, it is not clear how the universe became so isotropic and how this isotropy is slightly broken to generate the observed structures. This problem is known as the isotropy problem.

The isotropy problem can be translated into the homogeneity problem by using the Copernicus principle, which states that the earth is not situated at a centre of the universe. Since the only possibility that the universe is isotropic but not homogeneous is when the earth was located in the center of the universe, we conclude that the universe is also homogeneous. Recently, also direct observation of homogeneity became possible with large scale structure surveys. These observations confirm that at large scales the universe is homogeneous [10].

1.2 Inflation

In principle, it can be understood how a perfectly scale invariant universe came into existence, solving the question: 'why the universe is isotropic and homogeneous?' The argument is that if there was only one single possible initial condition of the universe, it should not come as a surprise that the final universe is highly scale invariant. But this does not explain the origin of the small anisotropies. Obviously, these can be solved by imposing that the initial conditions of the universe were such that it is nearly isotropic and homogeneous, with only small anisotropies and inhomogeneities. However, this approach is highly unsatisfactory since such initial conditions are rather artificial. A more elegant solution is to propose that the universe went through an extra era during which the observable part of the universe became homogeneous and isotropic, which was first investigated by Guth in [11]. This new epoch in the universe is called inflation and is the main subject of this thesis.

The era of inflation was a period during which the early universe underwent an accelerated expansion. Due to this expansion the universe was smoothed and flattened, not only explaining why the universe is nearly isotropic and homogeneous, but also why measurements show that it is extremely flat. This inflationary era can be described in quantum field theory by introducing a scalar field called the inflaton (multiple inflatons are possible, but not considered in this thesis) that slowly rolls down a potential. The slow roll condition implies that at leading order the kinetic energy of the inflaton can be neglected with respect to its potential energy. If the inflaton potential is positive, neglecting the kinetic energy generates effectively a de Sitter vacuum, which undergoes the above-mentioned accelerated expansion. When the inflaton has rolled sufficiently far down the potential, the kinetic energy overtakes the potential energy and inflation ends.

During inflation, the inflaton field undergoes quantum fluctuations. Due to these quantum fluctuations there are patches in the universe in which the inflaton was higher in the potential while in other patches the inflaton was lower. The accelerated expansion of the universe implies that some of these patches are not able to equilibrate. So, during inflation several patches in the universe became disconnected with a slightly different value for the inflaton field, meaning that they were unable to equalize their inflaton field value amongst them. Inflation ends at a certain value for the inflaton field, so these patches will stop inflating at different moments in cosmic time. This difference in the moment at which inflation ends implies a difference in the subsequent evolution of the universe, with small density perturbations appearing in the cosmic plasma.

At the moment the CMB radiation was emitted these density perturbations were transformed into temperature fluctuations, which are the anisotropies observed today. These anisotropies can be parametrized using two parameters, A_s and n_s. The parameter A_s measures the size of the perturbations, while the parameter n_s measures the deviation from a scale-independent spectrum. CMB observations show that $A_s = (2.14 \pm 0.05) \cdot 10^{-9}$ [12] and in addition the Planck satellite in Ref. [13] showed with 5σ confidence that the spectrum changes slightly with respect to the energy scale at which the fluctuations are measured. A more recent analysis from the same satellite resulted in the parameter $n_s = 0.965 \pm 0.004$ [14], where $n_s = 1$ corresponds to scale invariant fluctuations.

Another potentially observable feature of inflation is that it produces gravitational waves. That gravitational waves exist was observed by the Laser Interferometer Gravitational-wave Observatory (LIGO) in September 2015 [15], but the gravitational waves observed in this experiment were emitted relatively recently. Unfortunately, the gravitational waves emitted by inflation are today less energetic and therefore not directly observable. However, they leave imprints on the polarization of the CMB radiation, which can be measured by dedicated experiments. This results in the third important parameter for inflation, r, which is the ratio of the tensor (gravitational wave) power spectrum over the scalar power spectrum. Current experiments have set the upper bound $r < 0.07$ [16] with 95% confidence level [17], and it is expected that in the near future these bounds will strongly improve, or result in a detection.

The goal of inflationary physics is to explore the space of inflation models that satisfy the current measurements of n_s and A_s and the bound on r. These current constraints are strong enough to falsify a large set of the known inflation models, however also an extremely large number of models do satisfy the observations. Therefore, it is important to study classes of inflation models with a similar observable behaviour. Examples of these classes of inflation models are the attractor models, which introduce a special feature in the inflaton action so that n_s and r become nicely aligned with the observations.

Since the standard model of particle physics does not account for inflation, this study is also relevant for the study of extensions of the standard model of particle

physics. There is the possibility that the Brout-Engert-Higgs boson is the inflaton, but consistency with the observables requires for this scenario a non-minimal coupling of the Brout-Engert-Higgs boson with gravity. Therefore, inflation provides a view on physics beyond the standard model of particle physics.

Inflation is not the only hint that the standard model of particle physics is only an effective theory and that at sufficiently large energies, which in quantum field theory correspond to small distance scales, the theory should be altered. Another indication is the fact that the gravitational force is not incorporated in the standard model. Using dimensional analysis, it can be shown that effects from general relativity become important at energy scales of the order of 10^{18} GeV, which corresponds to 10^{-37} meters. Therefore, at least at these energies new physics should emerge.

A candidate for combining quantum field theory with general relativity is string theory, which can only be theoretically consistent if an additional symmetry is introduced. This symmetry, named supersymmetry, relates particles of different spin. The simplest version of supersymmetry relates every boson in the theory to a fermion and visa versa. Current experiments have not observed these superpartners of the standard model particles, but it is possible that their masses are beyond the energy scales that experiments can probe.

Extensions of both the standard model of particle physics and gravity, which include supersymmetry, have been studied. The minimal extension of the standard model with supersymmetry is named the MSSM (minimal supersymmetric standard model), which is currently being constrained by the experiments at the LHC. The gauging of supersymmetry (*i.e.* making the symmetry transformation dependent on position) results in an interesting quantum field theory that also describes the gravitational force. This is called supergravity. Since inflation takes place at large energies, and supersymmetric effects are supposed to become relevant at large energies as well, an important field of research is to study the embedding of inflation models in supersymmetry and supergravity.

1.3 Outline of the thesis

This thesis focusses on unravelling the characteristics of inflation models. This will be achieved through two approaches. The first will be to investigate the generic observational predictions from different parametrizations of inflation models. The second approach will be to study if a certain set of supergravity inflation models, known as nilpotent inflation models, can account for the inflationary observables and at the same time realise low energy supersymmetry breaking.

Before dealing with inflation, in chapter 2 the physics of the standard models of particle physics and cosmology will be reviewed and the problems leading to inflation will be highlighted. This chapter starts in section 2.1 with a review of the standard model of particle physics, followed by a review on the ΛCDM model

in the subsequent sections. In chapter 3, inflation will be reviewed.

Chapters 4, 5 and 6 deal with the problem of generating parametrizations for inflation models that have n_s and r generically in agreement with the observations. Chapter 4 reviews the inflationary flow code, which is a numerical method to compute predictions for large sets of inflation models and uses them for a polynomial Hubble function. In addition, another numerical method will be derived that can be used to obtain the general predictions from any parametrization of the inflation potential (or Hubble function). Using this code, it will be shown that n_s in polynomial inflation models is generically too small to explain the Planck data. In chapter 5 this numerical analysis is extended using a novel analytical method to solve the inflationary dynamics. In addition, another parametrization will be developed, which uses a ratio of polynomials known as the Padé approximant to parametrize the Hubble function. Since this parametrization generically agrees with the observed data much better than the polynomial parametrization, we conclude that it is not suitable to use the polynomial parametrization as a generic prescription for inflationary models (as was used in the literature). This analysis uses the same numerical tools that were developed for polynomial inflation in chapter 4. However, it raises the question of whether the Padé approximant is the correct parametrization, or that yet another alternative parametrization should be used.

The parametrization introduced in chapter 6 is inspired by the strong coupling attractor models, which has an interesting interpretation of being a theory non-minimally coupled to gravity. It will be shown analytically and using the above-mentioned numerical procedure that also for this parametrization the predictions generically agree with the observables, if the parameter ξ is sufficiently large.

Chapters 7 and 8 discuss the embedding of inflation in supergravity. For this purpose, chapter 7 shortly reviews supersymmetry and supergravity with the emphasis on supergravity inflation. Then, in chapter 8, a model will be introduced in which inflation is embedded in supergravity using the nilpotent inflation model. It will be shown that the consistency of this embedding is not always guaranteed, however an example of a new model that does have a valid inflationary phase will be provided.

After obtaining this valid supergravity embedding we compute the superparticle masses, which are in agreement with the current constraints from the LHC. In addition, we verify that the lowest supersymmetric particle, in our model the gravitino, does not overclose the universe. For part of the parameter space, the gravitino can account for dark matter. This thesis therefore provides one of the few known examples of an inflation model that includes supersymmetry breaking, the MSSM spectrum and dark matter.

The thesis is structured in three parts, as shown in the flow chart in Fig. 1.3. The introductory part consists of chapters 2 and 3. Then, the chapters 4 – 6 consider the general parametrization of inflation. The third part of the thesis contains the remaining chapters 7 and 8. The second and third part can be read separately,

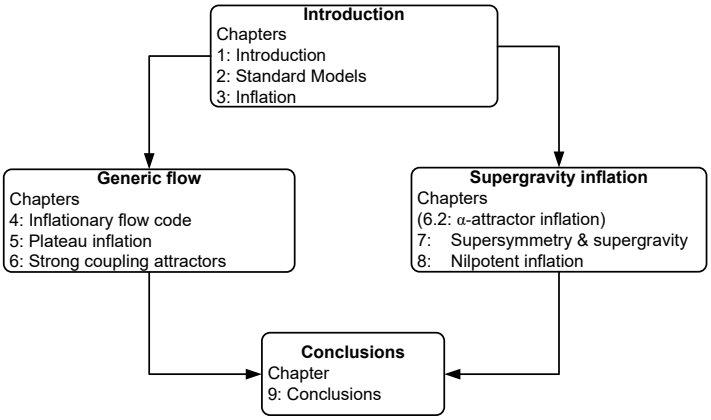

Figure 1.3: *Flow chart of the thesis.*

though section 6.2 reviews the α-attractor inflation model used in chapter 8. We conclude in chapter 9.

In the following natural units will be used, where $\hbar = c = 1$, and additionally we define the reduced Planck mass $M_{\rm p} = \frac{m_{\rm pl}}{\sqrt{4\pi}} = \sqrt{\frac{\hbar c}{G_N}}$. We assume that the reader is familiar with general relativity and quantum field theory.

CHAPTER 2

The standard models of cosmology and particle physics

Introduction

In this chapter the standard models of particle physics and cosmology will be briefly introduced. We will focus on the standard model of cosmology, since within this model inflation will be described in the next chapter. The standard model of particle physics, simply named the standard model in the following, will be extended with supersymmetry in chapter 7 to provide candidates for the inflaton.

This chapter will be structured as follows. First, in section 2.1 the standard model of particle physics will be discussed. Then, in section 2.2 and 2.3 the mathematical framework of our universe will be shortly reviewed, followed by an explanation of the Cosmic Microwave Background (CMB) radiation in section 2.4. Combining the standard model of particle physics and cosmology provides us with the history of the universe, as will be reviewed in section 2.5, while in section 2.6 will be shown that this generates the problems of dark energy and dark matter. Finally, we finish in section 2.7 with selected problems concerning the origin of our universe, of which some will be solved by the inflation paradigm in the next chapter.

More information concerning the ΛCDM cosmology can be found in the textbooks [3, 8, 18–20], while textbooks concerning the standard model of particle physics are Refs. [21–24].

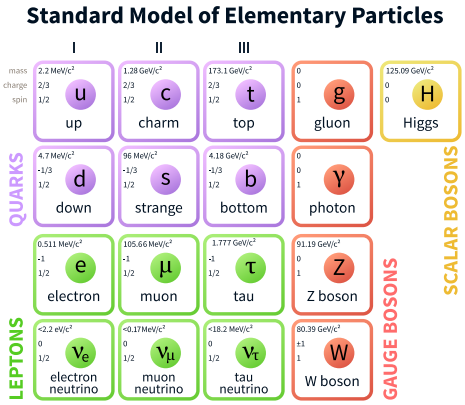

Figure 2.1: *The particle content of the standard model of particles. The figure is taken from [25], but the masses of the particles are extracted from [26]. The quoted neutrino masses are the masses in the flavour eigenbasis.*

2.1 The standard model of particle physics

The standard model of particle physics is defined as the most general renormalizable quantum field theory with the gauge symmetry $SU(3) \times SU(2)_L \times U(1)$ and the particle content seen in nature. This symmetry group represents the three fundamental forces that are described by the model, the electric force, the weak force and the strong force. The first two forces, the electric and the weak force, are unified within the standard model as the electroweak force (with the symmetry group $SU(2)_L \times U(1)$), while the strong force (the $SU(3)$ part) is for the energy scales probed so far fundamental. The $U(1)$ symmetry corresponds to a charge, the hypercharge. For the energy scales where the standard model is being tested, gravity is too weak to have observable effects and can be neglected.

The particle content of the standard model is shown in Fig. 2.1. The first three columns of Fig. 2.1 correspond to the three families of fermions, of which the first two rows are the quarks (in purple), and the bottom two are the leptons (in green). The particles in every generation are more massive than in the previous generation and are increasingly unstable, except for the neutrinos. Concerning the neutrinos it is known that they have a mass, however it is not known which neutrino is exactly the heaviest. Moreover, the neutrinos do not decay, but their mass matrix is not aligned with the flavour matrix (the basis with ν_e, ν_μ and ν_τ) so they oscillate into the different flavours. The last column contains the gauge bosons that carry the fundamental forces.

Quarks in the standard model are charged under all three forces [24]. Due to the strength of the strong force, all quarks with exception of the top quark form bound states called hadrons if the temperature of the medium is below 100 MeV and do not appear as distinguishable particles[1]. These bound states appear as $SU(3)$ singlets, hence they consist either of a quark and an antiquark, called mesons, or of three quarks which are called baryons. Due to the electroweak force, the mesons are unstable while the lightest baryon, the proton, is stable. The next-to-lightest baryon is the neutron, which has a half-life of about 14 minutes but is stable if it is in a bound state with protons.

The leptons, of which only the electron appears in everyday life, are only charged through the electroweak force and carry no strong charge. Muons can be observed due to interactions of cosmic radiation with the atmosphere, while to study tau particles collider experiments are necessary. Finally, the three neutrinos are electrically neutral and do not couple to the strong force, hence they couple solely through the weak charge (and gravity) with other particles. It requires large dedicated experiments to observe even a tiny part of the neutrino flux that permeates the earth, since to neutrinos the earth is nearly transparent [21].

In quantum field theory a force is characterized by a local symmetry of the Lagrangian. All known matter particles in the standard model are either in the singlet (trivial) or the fundamental representation of the gauge group. This means that the Lagrangian is invariant under the symmetry transformation[2] $\psi \to e^{i\alpha(x)}\psi$, if the particle ψ transforms under the fundamental representation of the gauge group and α is the parameter of the symmetry transformation. For a global symmetry α is space-independent, while for local symmetries α depends on the space-time coordinate x. This implies that the kinetic term of ψ in the Lagrangian, which includes $i\bar{\psi}\gamma_\mu\partial^\mu\psi$ (where γ_μ are the gamma matrices), is usually invariant under global symmetries, but if the symmetry is local the space-time dependence of α generates a term linear in $\partial_\mu\alpha(x)$. This term has to be eliminated by an additional vector field that transforms as $A_\mu \to A_\mu + \partial_\mu\alpha(x)$, which has to be introduced [22]. The resulting theory is known as a gauge theory, and the local symmetry group as the gauge group.

The number of introduced vector fields equals the dimension of the gauge group, hence the number of vector fields in the standard model is 12: 8 gluons (from $SU(3)$) + 3 W fields (from $SU(2)_L$) and the B field (from $U(1)$). Since the standard model preserves the $SU(3)$ symmetry of the strong force, the gluons are massless. However, the vacuum of the standard model is not invariant under the $U(1)_Y \times SU(2)_L$ (Y stands for hypercharge) part of the standard model gauge group which is broken to $U(1)_{EM}$ (electromagnetism). Due to this spontaneous symmetry breaking, the observable vector bosons are the massive $W^\pm$ and Z bosons and the massless photon (γ). Weak interactions are mediated by the $W^\pm$

[1] The top quark decays before it can hadronize.

[2] We use $U(1)$ as an example. Non-Abelian gauge theories transform similarly, but the equations are more cumbersome [22].

and Z bosons, while the electromagnetic force is mediated by the photon.

The weak force only couples to left-handed particles, which means for a Dirac particle that it couples only to the combination $\psi_L = \frac{1}{2}(1-\gamma_5)\psi$, where $\gamma_5 = i\gamma^0\gamma^1\gamma^2\gamma^3$. This implies that a left-handed muon decays into a left-handed electron, a left-handed muon neutrino and a right-handed electron antineutrino, but that no right-handed electron or neutrino is produced [21].

In the standard model Lagrangian, mass terms for the fermions and gauge bosons are forbidden because they are not invariant under the $U(1)_Y \times SU(2)_L$ symmetry. To give the fermions a mass, the $U(1)_Y \times SU(2)_L$ symmetry is broken spontaneously to $U(1)_{EM}$, meaning that the Lagrangian is invariant under the $U(1)_Y \times SU(2)_L$ symmetry but the ground state is not. To describe this spontaneous symmetry breaking the Brout-Englert-Higgs doublet (named Higgs doublet in the following) was introduced in Refs. [27, 28]. This doublet consists of two complex scalar fields that are charged under the $U(1)_Y \times SU(2)_L$ group. The renormalizable potential for the Higgs field that breaks the $U(1)_Y \times SU(2)_L$ symmetry spontaneously is [21]

$$\mathcal{L}_H = D_\nu H^\dagger D^\nu H + \mu H^\dagger H - \lambda (H^\dagger H)^2, \tag{2.1}$$

where μ and λ are constant parameters, and D_ν is the gauge covariant derivative. It is easy to see that, if μ and λ are positive, in the vacuum the Higgs doublet can be written as

$$H = \frac{1}{\sqrt{2}} \begin{pmatrix} 0 \\ v \end{pmatrix}, \tag{2.2}$$

where the Higgs vacuum expectation value is $v = \frac{\mu}{\sqrt{\lambda}}$.

Since the Higgs field consists of two complex scalar fields, four scalar particles should appear in nature. This is not the case, as can be seen from a counting of degrees of freedom in the gauge sector. If a local symmetry is exact, the corresponding gauge bosons are massless. However, if the symmetry is broken, the gauge bosons corresponding to the broken symmetry acquire a mass and therefore also an additional degree of freedom. Hence the breaking of gauge symmetry introduced by the Higgs field increases the total number of degrees of freedom in the standard model with 3 (2 for the $W^\pm$ bosons and 1 for the Z boson). Since the number of degrees of freedom in the vacuum of the model is the same as the number of degrees of freedom in the Lagrangian, 3 of the 4 degrees of freedom of the original Higgs field are absorbed by the gauge fields. In the end the Higgs field only contains a single propagating scalar boson, with the three longitudinal components being part of the (now massive) $W^\pm$ and Z bosons.

The remaining symmetry group of the standard model, $U(1)_{EM} \times SU(3)$ is unbroken, hence the gauge mediators of these forces (photon and gluons) are massless. This is indeed observed in nature, so the full expression for the standard model Lagrangian can be obtained. This expression is rather long, but can be represented

as

$$\mathcal{L} = \mathcal{L}_F + \mathcal{L}_V + \mathcal{L}_H + \mathcal{L}_Y \,, \tag{2.3}$$

where $\mathcal{L}_F$ contains the fermionic kinetic terms, $\mathcal{L}_V$ contains the gauge interaction terms, $\mathcal{L}_H$ (defined in Eq. (2.1)) contains the Higgs kinetic term and self-interaction terms and $\mathcal{L}_Y$ contains the Higgs-fermion couplings. In this thesis only the Higgs Lagrangian $\mathcal{L}_H$ will be explicitly used, the expressions of the other Lagrangians are defined in Ref. [21].

2.1.1 Some problems in the standard model

There are several issues with the standard model of particle physics that ask for an explanation. In this section some of these will be shortly discussed, while a longer discussion on dark matter will be given in section 2.6.

The first problem is the Higgs naturalness problem. Naturalness is the theoretical assumption that no small parameters should exist in a low energy description of a model if setting the parameter to zero does not introduce a symmetry [29]. Since the theory does not acquire additional symmetry if the Higgs mass is zero, it is expected that the Higgs mass is of the same order as the cut-off scale of the standard model. If the cut-off scale would be much larger than the Higgs mass, small deviations in the bare parameters of the high-energy (UV) theory will considerably change the (low-energy) Higgs mass. Therefore, any UV-theory of the standard model must be fine-tuned such that the standard model Higgs mass is 125 GeV. Such a strong dependence of the parameters in the low-energy theory on the high-energy completion is undesirable.

The Higgs naturalness problem can be solved by imposing a large amount of tuning in the bare parameters of the UV theory, but this is rather unnatural. Other solutions to this problem exist. In chapter 7 we will consider supersymmetry to solve the hierarchy problem, though the Large Hadron Collider is constraining the favourable parameter range considerably. Other solutions impose for instance that the Higgs is a composite particle [30] or use extra dimensions [31]. Cosmologically, the relaxion mechanism is interesting, in which the Higgs VEV was reached in the very early universe due to a dynamical relaxation process [32]. Explaining all solutions to the Higgs hierarchy problem deviates too much from the thesis, see Refs. [33, 34] for reviews.

Another issue that will be relevant in this thesis is the stability of the Higgs vacuum. As is shown in Fig. 2.2, the Higgs quartic coupling (λ) runs to negative values at an energy below the Planck scale, so the vacuum of the standard model given in Eq. (2.2) is metastable [35]. Fortunately, the lifetime of the current vacuum is orders of magnitude larger than the age of universe, so the probability that the universe has already decayed to the true vacuum is negligible, but at some moment in the future it might decay. Whether this is a true problem is, at this stage, philosophical, since there is no reason that in the distant future the universe might not completely change. As was explained in chapter 1 the early universe

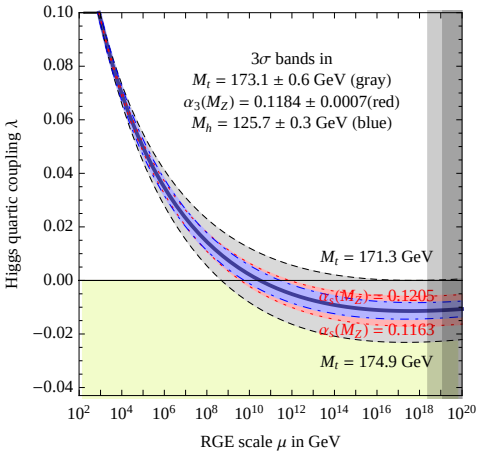

Figure 2.2: *Running of the Higgs quartic coupling. The error bars correspond to the* 1 *and* 2σ *errors on the top quark mass measurement. The quartic coupling, and therefore the potential, becomes negative unless the top quark mass is more than* 2 *standard deviations lighter than its measured value. Figure from Ref. [35].*

had an extremely large energy density, thus a problem is why the standard model is in a metastable state in the first place. Fortunately, finite temperature effects converge the Higgs VEV to zero, so that at low energies the universe is confined to the present metastable state [36, 37]. But if inflation is driven by the Brout-Englert-Higgs field this problem will be important, as will be explained in section 3.4.3.

Another issue in the standard model is the strong CP problem. According to the current paradigm, it is compulsory to construct a field theory from all renormalizable terms invariant under the given symmetry group and matter content. The gauge sector consists of two terms [24]

$$-\frac{1}{4}F^a_{\mu\nu}F^{\mu\mu a} + \frac{g_3^2\Theta}{64\pi^2}\epsilon_{\mu\nu\rho\sigma}F^{\mu\nu a}F^{\rho\sigma a}, \tag{2.4}$$

where a runs over the gluons, $\epsilon_{\mu\nu\rho\sigma}$ is a fully anti-symmetric tensor, g_3 is the QCD coupling and Θ is the QCD theta parameter. The second term in Eq. (2.4) is only possibly for QCD, since in Abelian gauge theories a term similar to Eq. (2.4) has no physical effects [39] and for the $SU(2)_L$ group it can be rotated away [38][3]. The theta parameter can be measured since it invokes a breaking of CP symmetry in strong decays, which has not been observed. The current constraint is that $\theta < 10^{-9}$ [39].

[3]In the electroweak theory all fermions charged under $SU(2)_L$ are massless.

The strong CP problem would not have been a problem if the standard model as a whole was CP invariant, however the electroweak force breaks CP. Therefore, imposing that the strong force is CP invariant while the electroweak force is unnatural. A solution is to impose that the whole standard model at some high energy scale is CP invariant, which is then broken by a new particle named the axion (χ) [39]. This axion will enter the action with the dimension-5 operator [24]

$$\frac{\chi}{\Lambda}\epsilon_{\mu\nu\rho\sigma}F^{\mu\nu a}F^{\rho\sigma a}. \tag{2.5}$$

If the vacuum expectation value of the axion is sufficiently small, this coupling will be naturally suppressed.

A fourth issue are the neutrino masses. It is shown experimentally that the neutrinos oscillate between the different flavour states of Fig. 2.1 [40, 41]. Such an oscillation can only exist if the neutrinos are massive and the mass eigenstates of the neutrinos are not aligned with the flavour eigenstates. Using cosmological data, the bound $\sum_{i=1}^{3} m_{\nu_i} < 0.234$ eV [12] for the neutrino mass in the mass eigenbase can be obtained. Though the resulting mixing matrix can be defined, as is shown in Refs. [21,23], there is no renormalizable interaction in the standard model that gives mass to the neutrinos. Different proposals are in Refs. [21, 42], but the origin of the neutrino masses will not be studied in this thesis.

Finally, the standard model is not well defined at large energies. At energy scales of the order of the Planck scale $M_{\mathrm{p}} \approx 2.44 \cdot 10^{18}$ GeV gravitational effects become relevant with respect to the forces introduced in the standard model. To make predictions of what happens at these energies a quantum theory of gravity is required. To go beyond this energy scale we need a description that unifies the standard model with gravity, like string theory, but also other solutions were posed, for instance by imposing that the standard model is scale invariant [43].

It would be somewhat surprising if there is no new physics up to the Planck scale, especially since there are interesting theories that postulate new physics at energy scales far below the Planck scale. An example are the grand unification theories [44]. These theories postulate that at a certain energy scale physics is represented by a simple group, instead of a product group as is the standard model. At the grand unification scale the three standard model groups, $SU(3) \times SU(2)_L \times U(1)$, appear due to a spontaneous symmetry breaking. Several interesting features of the standard model can be explained in grand unification theories, for instance why electric charge is quantized.

However, at the grand unification scale all the standard model couplings must be equal. Extrapolating the (running) couplings to higher energies shows that they do not [44], implying that grand unification is not possible if the standard model is not extended at lower energy scales. Possible extensions have been proposed, for instance if the standard model is supersymmetric the couplings can combine and grand unification is possible.

2.2 The expanding universe

2.2.1 The FLRW universe

After reviewing the standard model of particle physics, we continue in the remainder of this chapter with reviewing the standard model of cosmology: the ΛCDM model. The most relevant assumption in this model is that our universe can be considered homogeneous and isotropic at large distance scales, implying that it is the same at all locations [3, 10]. Within general relativity the unique metric that describes such a universe is the Friedmann-Lemaître-Robinson-Walker (FLRW) metric [8, 45]

$$ds^2 = -dt^2 + a(t)^2 \left[\frac{dr^2}{1 - kr^2} + r^2(d\theta^2 + \sin^2\theta d\phi^2) \right], \tag{2.6}$$

where $a(t)$ is the scale factor, t is the cosmic time, r is the comoving radial coordinate and θ and ϕ are the comoving angular coordinates. The parameter k labels the curvature of the universe, if $k > 0$ the universe is positively curved (spherical), if $k < 0$ the universe is negatively curved (hyperbolic) and if $k = 0$ the universe is flat. To simplify the analyses, the metric (2.6) can be rewritten as

$$ds^2 = -dt^2 + \tilde{a}(t)^2 \left[d\chi^2 + f(\chi^2)(d\theta^2 + \sin^2\theta d\phi^2) \right], \tag{2.7}$$

where

$$r^2 = f(\chi^2) = \begin{cases} \sinh^2\chi & \kappa = -1 \\ \chi^2 & \kappa = 0 \\ \sin^2\chi & \kappa = +1 \end{cases} \tag{2.8}$$

In Eq. (2.7) the scale factor $\tilde{a}(t)$ is normalized such that $\kappa = \operatorname{sign} k$, where the sign function represents the sign of the argument, *i.e.* $\operatorname{sign} k = \frac{k}{|k|}$. Since the sign of the curvature of space is time invariant this choice is constant in time.

The FLRW metric only contains one unspecified function of time, the scale factor $a(t)$, that defines the time-dependent size of the universe. In a static universe $a(t)$ is constant in time, however Edwin Hubble observed in 1929 that the wavelength of the emitted light from distant galaxies scales linearly with the distance to these galaxies [46]. Within the FLRW metric (2.6), this observation can be interpreted by considering an object at which no external forces act. Such an object has a constant comoving distance r to the observer, that we consider to be located at $r = 0$. The physical distance between the observer and the object (d) is obtained from the comoving distance (χ) as $d = a(t)\chi$, where the angular coordinates in Eq. (2.7) are ignored due to the isotropy of the universe. Using this definition for physical distance, the physical velocity of this object is

$$\dot{d} = \dot{a}\chi = \frac{\dot{a}}{a} d = Hd, \tag{2.9}$$

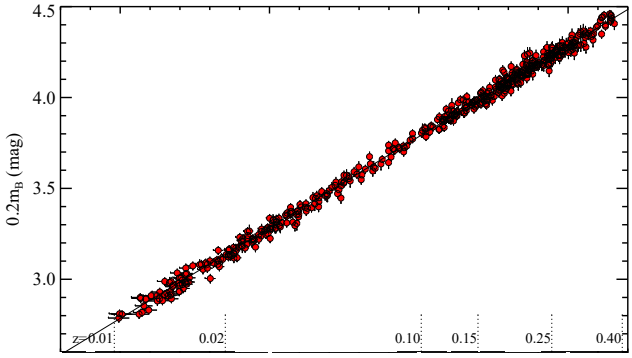

Figure 2.3: *Hubble diagram showing the redshift of supernovae Ia with respect to their luminosity, which is a probe for the distance. The figure is obtained from [47].*

where a dot denotes a derivative with respect to time, *i.e.* $\dot{f} \equiv \frac{\mathrm{d}f}{\mathrm{d}t}$ and the Hubble parameter $H \equiv \frac{\dot{a}}{a}$. The parameter that Hubble calculated in his seminal paper [46][4] is $H_0 = H(t_0)$, where 0 denotes the current value, since during the evolution of the universe the Hubble parameter changed.

In the coordinate system used to define the FLRW metric in Eq. (2.6), light does not move with a constant velocity but its velocity depends on the scale factor. Obviously, this is a result of the coordinate choice, and it is more convenient to use conformal time τ, defined as

$$dt = a(\tau)d\tau\,, \tag{2.10}$$

for which the speed of light is constant during the evolution of the universe. Using conformal time, the FLRW metric becomes

$$ds^2 = a(\tau)^2\left[-d\tau^2 + d\chi^2 + f(\chi^2)(d\theta^2 + \sin^2\theta d\sigma^2)\right]\,. \tag{2.11}$$

Another way to compute the expansion is to use the amount of redshift of light as a time parameter. Due to the expansion of the universe, electromagnetic waves get stretched out, so their wavelength increases. Therefore, there is a difference between a certain measured wavelength λ_{obs} and the actually emitted wavelength λ_{em}. The redshift z is defined as the fraction between the two

$$z = \frac{\lambda_{\mathrm{obs}} - \lambda_{\mathrm{em}}}{\lambda_{\mathrm{em}}} = H_0 d, \tag{2.12}$$

[4]Though he was off by a large factor due to an error in the measurement of the distances to the galaxies.

where H_0 denotes the current Hubble constant. Observationally, the redshift is used to probe the distance to an object, since for most sources the parallax, which can be used to measure distances directly, is not observable.

However, to measure distances using redshift the Hubble constant has to be known, which is observed in multiple experiments. For example, if the emitted brightness of a certain object is known, the object is named a standard candle and the distance can be obtained from its apparent brightness. Several standard candles were used in the analysis in Ref. [47] to produce Fig. 2.3. In this survey the Hubble parameter was found to be $H_0 = 73 \pm 1$ km s^{-1} Mpc^{-1}. Another measurement of the Hubble constant uses the cosmic microwave background radiation that will be described in section 2.4, however this measurement resulted in a significantly lower Hubble parameter $H_0 = 67.3 \pm 0.7$ km s^{-1} Mpc^{-1} [12]. Though the discrepancy between the data sets is large, it might originate from errors in either of the two experiments, since the extraction of the Hubble parameter is subtle. Moreover, there are indications that the measurement of the local measurement of H_0 is a statistical outlier [48].

Since this is an important tension between the CMB experiments and local experiments, much ongoing investigations attempt to remove it. An interesting development is the observation of a gravitational wave signal together with a gamma ray burst. Combining the two observations, $H = 70 \pm 12$ km s^{-1} Mpc^{-1} was obtained [49], which is not yet competitive. However, if more neutron star mergers are observed in the future, this provides a useful third measurement of the local Hubble constant [49].

2.2.2 Horizons

Another property of the FLRW universe is the appearance of horizons [50, 51]. In this thesis the most important horizon will be the particle horizon, which is the maximal distance such that two objects in the universe could have been in causal contact. Using that the maximal velocity is the speed of light, the particle horizon distance at time t can be obtained from the FLRW metric (2.6) as [8]

$$d_{\text{part}} = \int_0^t \frac{\mathrm{d}t}{a(t)}. \tag{2.13}$$

It will be shown in the next section that normal cosmologies are either dominated by non-relativistic matter or by radiation. Using the results of that section it is easily verified that the integral in Eq. (2.13) converges. Therefore, at a certain time t there is a finite distance d_{part} beyond which two objects have never been in causal contact. In section 2.7 we will see that this generates problems in the early universe.

Another useful quantity is the comoving Hubble sphere, which is the distance at which the velocity[5] due to the expansion of the universe exceeds the speed of

[5]Formally this is not a velocity, since both objects are at rest in their own rest frames.

light

$$D_H = \frac{1}{aH}. \tag{2.14}$$

Since the expansion of the universe is a general relativistic effect this quantity does not correspond to a physical horizon, *i.e.* objects outside our Hubble sphere might be inside the particle horizon. However, for a universe where $a \propto t^q$ all the way to $t = 0$, which corresponds to the single-component universes studied in the next section, the comoving Hubble sphere equals the particle horizon.

2.3 Components of the universe

Our universe is not entirely empty, but it is filled with matter and radiation. To describe the universe we observe, we write the most general energy-momentum tensor for an isotropic and homogeneous universe as $T_{00} = -\rho$, $T_{ii} = p$ where $i = \{1, 2, 3\}$ are not summed over and the off-diagonal components of T are zero. This energy-momentum tensor corresponds to a perfect fluid with an energy density ρ and pressure p. For such a fluid the Einstein equation

$$R_{\mu\nu} - (\tfrac{1}{2}R - \Lambda)g_{\mu\nu} = \frac{1}{M_{\mathrm{p}}^2} T_{\mu\nu}\,, \tag{2.15}$$

where $R_{\mu\nu}$ is the Ricci tensor, R the Ricci scalar and Λ the cosmological constant, can be rewritten as the Friedmann equations [8, 19, 20][6]

$$H^2 = \frac{1}{3M_{\mathrm{p}}^2}\rho - \frac{k}{a^2} + \frac{\Lambda}{3}, \tag{2.16a}$$

$$\dot{H} + H^2 = -\frac{1}{6M_{\mathrm{p}}^2}\left(\rho + 3p\right), \tag{2.16b}$$

$$0 = \frac{\mathrm{d}\rho}{\mathrm{d}t} + 3H\left(\rho + p\right), \tag{2.16c}$$

where the third equation describes energy conservation and can be derived from the first two.

When studying the universe, it is convenient to consider the equation of state parameter $w \equiv \frac{p}{\rho}$. The equation of state can be computed in the different limits at which matter manifests itself. In non-relativistic matter, also named dust, the energy density is dominated by the relativistic mass while the pressure is parametrically smaller. This implies that $w \approx 0$. In contrast, in an isotropic universe the equation of state parameter for relativistic matter is $w = 1/3$. In both limits the equation of state is independent of time and integrating the energy conservation equation (2.16c) gives [8]

$$\rho \propto a^{-3(1+w)}\,. \tag{2.17}$$

However, the rest frames themselves move apart [51].

[6] A derivation without using general relativity is provided in [18].

	w	$a(t)$	$H(t)$	$\rho(t)$
Matter	0	$\propto t^{2/3}$	$\frac{2}{3t}$	$\propto \frac{1}{t^2}$
Radiation	1/3	$\propto t^{1/2}$	$\frac{1}{2t}$	$\propto \frac{1}{t^2}$
Λ	-1	$\propto e^{t/t_0}$	$\frac{1}{t_0}$	const.

Table 2.1: *Time dependence of several cosmological quantities in a universe dominated by matter, radiation or the cosmological constant (Λ). The Hubble constant is exact, for the others the proportionality constant is not shown.*

Thus, for a radiation-dominated universe the energy density scales as $\rho_{\text{rad}} \propto a^{-4}$, while for a matter dominated universe it scales as $\rho_{\text{mat}} \propto a^{-3}$. This is not surprising: If the universe consists of only a single heavy particle with mass M, the energy density for matter is $\rho_{\text{mat}} = MN/V$, where N is the number of particles in volume V. In an expanding universe, the number of particles and their masses are constant, while the volume scales as a^3, hence the total energy density scales as a^{-3}. For the radiation dominated universe the statement is similar, except that the mass of the particle is replaced by its energy. Since in an expanding universe the energy of radiation decreases as a^{-1} due to redshift, the energy density of radiation scales as a^{-4} [18].

Combining the energy density of Eq. (2.17) with the Friedmann equation (2.16a) (and setting $\Lambda = 0$), the scale factor dependence of the Hubble constant can be obtained. Finally, solving the subsequent differential equation (using $H \equiv \frac{\dot{a}}{a}$), the time dependence of the scale factor is

$$a \propto t^{\frac{2}{3(1+w)}} , \tag{2.18}$$

from which the time dependence of the energy density and Hubble function are easily obtained. An overview of the different components of the universe is given in Table 2.1.

Note that the energy densities of matter and radiation scale differently when the universe expands, as is shown in Fig. 2.4. If the universe is small, hence if a is small, the energy density of radiation is larger than the energy density of matter, while if a is large the matter energy density dominates. This indicates that the very early universe was radiation dominated, while afterwards the universe became matter dominated. The moment at which the universe became matter dominated is known as the matter-radiation equilibrium point.

Current measurements show that the universe is expanding in an accelerating manner, hence that $\ddot{a} > 0$ [52, 53]. The particles known to us satisfy the strong energy condition, which implies that $\rho + 3p > 0$. From Eq. (2.16) follows that matter satisfying this condition always generates a decelerating universe [18, 45]. To explain these measurements a nonzero cosmological constant Λ was added to the Einstein equations. This constant term can be interpreted as an energy of the vacuum, hence an energy density that is independent of the volume. Since also

in an expanding universe the energy density generated by a cosmological constant is constant, it will be the leading contribution to the total energy density if a is sufficiently large. Also this is shown in Fig. 2.4. However, in order to explain the present acceleration of the universe Λ must be very small, $\Lambda \approx 10^{-122} M_{\rm p}^2$ [12]. This tuning problem is known as the cosmological constant problem, and will be shortly addressed in section 2.6.

Using the above arguments, the history of the energy densities in the universe is shown in Fig. 2.4. Shortly after the Big Bang, the universe was small and therefore dominated by radiation. In this era the energy density of the universe was coupled to the temperature of the plasma since, using the black body spectrum, [8]

$$\rho_{\rm rad} = \frac{g\pi^2}{30} T^4, \tag{2.19}$$

where g is the number of relativistic degree of freedom. For fermionic degrees of freedom $g = 7/8$, while for bosons $g = 1$. Due to the expansion of the universe, the energy density of the plasma decreased, hence it cooled down and after some time the energy density of matter became larger than the energy density of radiation. When the universe cooled down even further, the energy density of matter got below the energy density generated by the cosmological constant. Currently the cosmological constant is the main contribution of the total energy of the universe.

There is a peculiar phenomenon in Fig. 2.4, which is that the cosmological constant started to dominate the universe relatively recently[7]. This is known as the coincidence problem: why do we live so close to the moment that the cosmological constant became the dominant contribution of the total energy density [54]. Another way to phrase the coincidence problem is to ask why currently the energy density generated by the cosmological constant is roughly equal to the matter energy density, as is also visible in Fig. 2.4. This indicates that we are living in a rather peculiar moment in the universe.

The coincidence problem and the cosmological constant problem are linked, since if the cosmological constant had been larger, the matter-Λ equilibrium time would have been different. A solution to these problems is the anthropic principle, which states that we cannot live in a universe in which life is impossible. For instance, if the matter-Λ equilibrium would have occurred much earlier, the current universe would have diluted so much that life is impossible. Using this philosophy, Weinberg and Vilenkin predicted a value in Refs. [55, 56] for Λ which agrees with what is measured by current observations.

The density of the universe depends on the Hubble parameter H and the curvature k. From these, a critical density can be defined as the energy density for which the universe is exactly flat. This density is, neglecting the cosmological constant, obtained from Eq. (2.16) as [8]

$$\rho_c = 3M_{\rm p}^2 H^2. \tag{2.20}$$

[7]Note that due to the logarithmic axis and in the definition of redshift of Eq. (2.12) the number of years is large, 10^{10} years, see Table 2.2, but corresponds to a redshift of $z = 0.4$.

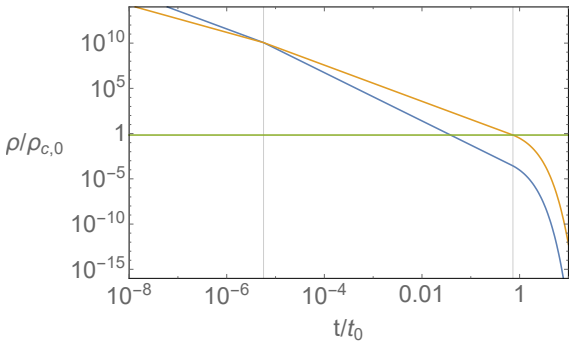

Figure 2.4: *Evolution of the energy density of matter (blue), radiation (orange) and cosmological constant (green) in the universe as a function of time. The densities are normalized to the current critical density in Eq. (2.20), such that the present time is at $t = t_0$. The dotted lines correspond to the matter-radiation equilibrium and matter-Λ equilibrium. Since the single fluid approximation is not sufficient around these equilibria, this analysis is not sufficient to study their precise position.*

Note that due to the appearance of the Hubble parameter, which is time dependent, the critical density of the universe changes in time. Since our universe is extremely flat, as will be discussed in more detail in section 2.7, the total density of the universe is very close to the critical density. It is therefore customary to express the densities of the different components that make up the energy density in the universe as fractions of the critical density

$$\Omega_i = \frac{\rho_i}{\rho_c}, \tag{2.21}$$

where i denotes the component of the energy density. The energy density parameters Ω are a function of time since the density of most components in the universe are time-dependent and since the critical density depends on time. The density parameter of the substance that contributes mostly to the total energy of the universe is constant, as can easily been seen from Table 2.1.

2.4 CMB

When the temperature of the universe was of the order of 3×10^3 K, it was dominated by a plasma of protons, electrons and traces of heavier elements like Deuterium, Helium and Lithium [20]. Protons require for nuclear fusion an energy of 10^5 eV, which is much more than available at the energy of the universe at that

time, so no fusion events happened. Also neutrinos existed in the universe, but their interaction with the matter is so tiny that they can be considered decoupled from the plasma to first approximation. When the temperature of the plasma decreased, the plasma formed a hydrogen gas, in a phase transition named recombination. Since photons do not couple as strongly to hydrogen as to a plasma, the mean free path of photons got enhanced and after recombination they were able to permeate the universe. The surface at which the photons last scattered[8] from the electrons that we currently observe with the CMB is named the surface of last scattering. The photons that were emitted from this surface make up the CMB radiation.

When the CMB was emitted, it had a black body profile with a temperature of the order of 3×10^3 K [8]. Due to the expansion of the universe, the photons lost their energy and the temperature of the radiation decreased to the value observed today, which is 2.7255 ± 0.0006 K [7]. Since the redshift leaves the profile of the CMB invariant, the CMB can be interpreted as a picture of the universe at the time it was emitted. A tiny fluctuation of the temperature of the universe at the moment the CMB was emitted is represented in a small change in the current temperature spectrum. This section will give a short overview of the CMB physics, leaving a more technical description to section 3.3.

When observing the CMB carefully, very small temperature fluctuations of the order of $\frac{\delta T}{T} \approx 10^{-5}$ are found. A map of these fluctuations in the sky as measured by the Planck satellite is shown in Fig. 2.5. These temperature fluctuations can be interpreted as originating from very tiny density fluctuations in the universe at the time of last scattering. They can be quantified using the correlation between two temperatures separated with an angle θ. Then expanding in spherical harmonics leads to the parameter l, which can be understood as $l \approx \frac{180^\circ}{\theta}$ [3].

The mechanism that creates these density fluctuations depend on the value of l. At small l, the anisotropies purely originate from gravitational effects known as the Sachs-Wolfe effect. Light that leaves a minimum in the gravitational potential, named a gravitational well, which is caused by an overdensity in the primordial plasma experiences a gravitational redshift, while the light gets blue-shifted if it is emitted towards an overdensity. Thus the CMB temperature observed from points that were matter overdensities on the surface of last scattering is lower compared to the CMB emitted at underdensities [3].

The Sachs-Wolfe effect is mainly important for large angular distances, since there was no causal connection between the different patches that sent out the CMB. When, on the contrary, we consider small θ, causal mechanisms are relevant. In this regime the deviations in the gravitational potential of the universe during CMB emission are mainly caused by deviations in the density of the so-called dark matter. Dark matter, which will be explained in more detail in section 2.6, is only gravitationally coupled to baryons and to radiation. Since the baryons and photons are coupled through the standard model forces, the universe before re-

[8]The duration of last scattering, hence the thickness of this surface, is negligibly small.

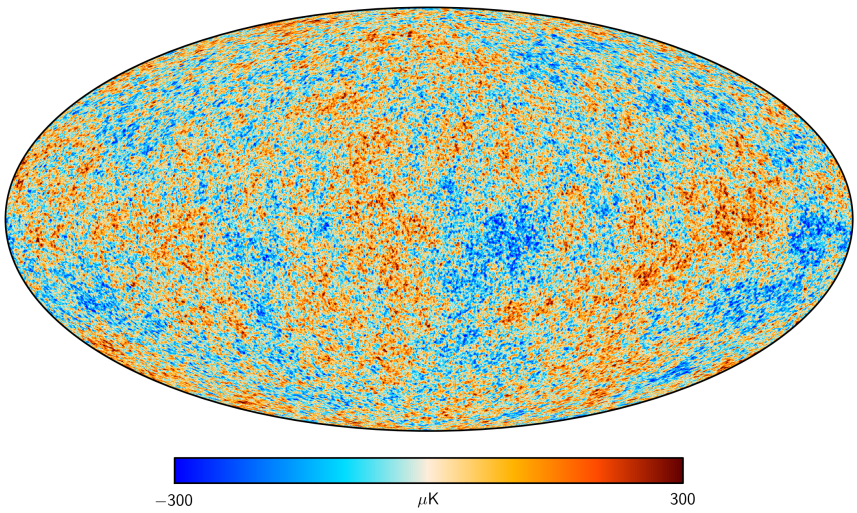

Figure 2.5: *Map of the anisotropies observed by the Planck satellite [12].*

combination can be interpreted as a baryon-photon fluid moving in a gravitational potential caused by the dark matter. This baryon-photon fluid flows towards the gravitational wells. However, in a gravitational well the fluid gets compressed, the pressure rises (w is not exactly 0 due to the photons) and the fluid will move out of the gravitational well. At the maximum of these acoustic oscillations (this process resembles sound), the matter is denser and therefore also hotter, generating hot spots in the CMB. The matter that flows away or towards the overdensities will also cause a Doppler effect in the light. These two effects, the rarefaction of the matter and the Doppler effect, together produce the large-l anisotropy spectrum. The large-l temperature fluctuations in the CMB are therefore a probe to measure the density profile of the very early universe [3].

The density fluctuations at the CMB surface are observed to be randomly spread across the sky, thus their defining features are encoded in statistical averages. For this reason the averages over the sky of 2-point correlation functions are studied. If the primordial density fluctuations are Gaussian, the higher order correlation functions are all determined by this two-point function. Also 3-point functions are studied, but no deviations from the Gaussian hypothesis were found [57].

The CMB power spectrum, which will be explained in more detail in section 3.3 and is shown in Fig. 3.3, has several interesting features. For instance, the power spectrum consists of several peaks, that appear due to the density fluctuations in the plasma. The location of the first peak is caused by modes that are of the size of the Hubble sphere at the moment of last scattering [3]. The size of the Hubble

sphere that we observe in the sky depends on the curvature of the universe. If the universe is positively curved, the light from different parts of the Hubble sphere during last scattering will arrive at the earth from a slightly larger angle compared to when the universe is hyperbolic. The location of the first peak in the power spectrum at $l = 200$ implies that our current universe is flat.

Another relevant piece of information from the CMB is the height of the different peaks, which are generated by gravitational collapse of overdensities in the cosmic plasma. This collapse also generated the additional peaks in the spectrum and the relative height of the secondary peaks in the CMB give a measure on the amount of matter in the universe and the amount of standard model matter [3]. The peak structure requires the introduction an additional non-observed particle, the dark matter particle. For a longer discussion on how the CMB can be used to measure the energy densities of the universe, see Ref. [58]. Solutions to the problem of dark matter will be discussed in more detail in section 2.6.

2.5 The radiation dominated universe

The different eras in the history of the universe are shown in Table 2.2. As is shown in this table, before the CMB was emitted the universe went through an era of radiation domination that (according to the ΛCDM model) lasted from the Planck scale until the moment of matter-radiation equality. What happened when the energy density was above the Planck scale is unknown, since in this regime quantum gravity effects become relevant. After the Planck dominated era the universe slowly cooled down during which phase transitions occurred.

Most of these phase transitions follow the same pattern. While the temperature of the universe decreases, at some point the thermal bath does not contain enough energy to create a heavy particle in a sufficiently large amount to sustain its abundance in the thermal bath. Such a particle typically scatters and decays into lighter particles[9], hence the particle disappears from the thermal bath. Since the particles in a thermal bath have a range of energies, the typical temperature at which this (so called freeze-out) process happens is roughly at $T = \mathcal{O}(M/10)$, with M the mass of the heavy particle.

This happened with most of the particles of the standard model of particle physics. For instance, the high energy universe contained free quarks, which hadronized when the temperature was $T \approx 100$ MeV. After the hadronization, the protons and neutrons were formed at a temperature $T \approx 8$ MeV. This was a rather critical moment in the history of the universe, since neutrons are unstable, they decay with a half-life of roughly 10 minutes unless they are bound to the protons as helium nuclei. It was energetically possible to generate Helium and other light elements in a process known as Big Bang nucleosynthesis (BBN) 3

[9] If the particle does not decay, a fraction of its abundance stays in the universe, as explained in section 2.6.2.

minutes after neutrons were formed [8]. During this process light elements up to ^{7}Be were formed, after which the universe was not hot enough to support nuclear fusion. The abundances of these elements – at least the stable ones, ^{7}Be decays to ^{7}Li – are measured in very old stars. There are some discrepancies in the ^{7}Li abundance [58], but in general the consistency between the theory of BBN and the observations is remarkably good. Indeed, the measurement of the cosmic abundances of light elements is a strong indication that the ΛCDM model is the correct description of the early universe, at least up to these energies.

Before the BBN, when the temperature of the universe was 1 MeV, the neutrinos decoupled from matter and generated the cosmic neutrino background radiation [8, 59]. These neutrinos, just as the photons in the CMB, move through the universe nearly without interactions and form a small part of the radiation density in the universe[10]. But since the neutrinos hardly interact with matter, this radiation has not been observed.

All the eras described above contain standard model physics that is well tested, hence they could have occurred in the early universe. However, there are some features observed in the universe that the standard model cannot explain. The first feature is dark matter, which will be discussed in the next section. Neither is it understood how the number of particles versus the number of antiparticles $\eta = \frac{n_B - n_{\bar{B}}}{n_\gamma} \approx (6.1 \pm 0.2) \times 10^{-10}$ [60] (where n_γ is the photon number density) became so large, since from the usual evolution of the universe it is expected that η is significantly smaller. Within the standard model, it is not possible that such a large difference between the abundances of particles and antiparticles is generated, but by introducing new physics this asymmetry can be created, which is called baryogenesis [8, 60]. In most models baryogenesis happens at very high temperature, of the order of $T \approx 10^{10}$ GeV.

2.6 Problems of the late time universe

When combining the standard model of particle physics with cosmological data of the current universe, two striking discrepancies appear. In section 2.3 it was mentioned that relatively recently the expansion of the universe started to accelerate, while in a matter dominated universe the expansion decelerates. In addition, when computing the total matter density of the universe there seems to be more matter in the universe than the standard model can account for. The additional energy that generates the acceleration is called dark energy and the additional matter is known as dark matter. In this section both will be explained in more detail.

[10] If the neutrinos are massive, they might currently be non-relativistic [59].

	Time	Energy
Planck era (?)	$< 10^{-43}$ s	$> 10^{18}$ GeV
Inflation (?)	$> 10^{-34}$ s	$< 10^{15}$ GeV
Electroweak transition	10^{-10} s	1 TeV
Quark-hadron transition	10^{-4} s	100 MeV
Nucleon freeze-out	0.01 s	10 MeV
Neutrino freeze-out	1 s	1 MeV
BBN	3 min	0.1 MeV
Matter-radiation equality	10^4 yr	1 eV
Recombination	10^5 yr	0.1 eV
Dark ages	10^5 – 10^8 yr	0.1 eV – 1 meV
Reionization	10^8 yr	1 meV
Galaxy formation	6×10^8 yr	1 meV
Matter-Λ equality	10^9 yr	0.3 meV
Present time	10^{10} yr	0.2 meV

Table 2.2: *Major eras during the evolution of the universe. It is not certain if any of the eras before BBN actually occurred. The energies correspond to the temperature of the radiation medium (except during inflation). Table from [45].*

2.6.1 Dark energy

A minimal explanation for dark energy is that the cosmological constant in the Einstein equation (2.15) is nonzero and positive, as explained in section 2.3. In Table 2.1 it is shown that a cosmological constant dominated universe is indeed expanding exponentially fast. However, to explain the current observations the cosmological constant has to be of the order of $\Lambda \approx 10^{-122} M_{\rm p}^2$ [12], which is extremely small. Using the interpretation that the cosmological constant is a vacuum energy, dimensional analysis shows that the vacuum energy is $\rho_\Lambda = \Lambda^2 M_p^2 \approx M^4$, where M is the cut-off scale of the theory. The maximal cut-off scale for a field theory without gravity is the Planck scale, so the expected vacuum energy is of the order of $M_{\rm p}^4$, which leads to $\Lambda \approx M_{\rm p}^2$. This value for the cosmological constant is a factor of 10^{122} too large [58]. Another way to phrase this is that the current measurement of Λ implies that the energy scale of the physics that describes the cosmological constant, M, is $10^{-30} M_{\rm p} \approx 10^{-12}$ GeV, which is far below the mass scales in the standard model of particle physics [58].

The cosmological constant problem can be solved in two different ways. The first is to accept that the cosmological constant is as it is and to explain why it is so small. One attempt in this direction is to use an anthropic statement. It was shown by Weinberg and Vilenkin in Refs. [55, 56] that it is not possible for life to be formed if the cosmological constant is much different than what is observed. If the original universe was a multiverse, containing many different patches with different values for the cosmological constant, then there would be a set of patches where we could live and patches where we cannot. Even if a large majority of these patches has a cosmological constant that is much larger than ours, since we cannot live in these patches we do not need to consider them as natural universes.

However, a problem with the multiverse argument is that the measure over the set of universes is not known, a problem known as the measure problem. This measure should be provided by a theory that explains the origin of our universe, like string theory. But though string theory indeed predicts a multiverse, the precise measure is not known. Therefore also other solutions are probed. These solution for the cosmological constant problem either change general relativity, as for instance in Refs. [61,62], or introduce a scalar field that mimics the cosmological constant [63–65]. This last idea is very similar to inflation, which will be introduced in the next chapter. Indeed, some of the models introduce a scalar field that generates both the late time accelerated expansion of the universe and drives inflation at early times, which are known as quintessential inflation models [64,65].

Alternative solutions of the cosmological constant problem often predict that the equation of state of dark energy $w_{\rm de}$ is different from the prediction of a cosmological constant $w_\Lambda = -1$. The equation of state is directly related to the acceleration of the universe and the Hubble parameter and observations show that $w_{\rm de} = -1.023 \pm 0.1$ (95% confidence) [12], which is compatible with the hypothesis that dark energy is due to a cosmological constant.

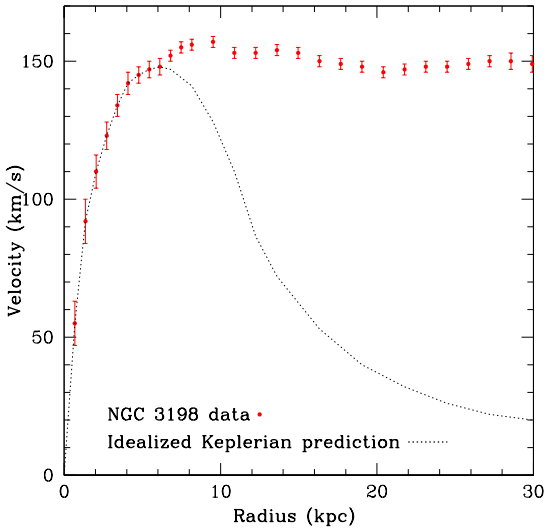

Figure 2.6: *Galaxy rotation curves as measured in the galaxy NGC 3198 versus the Keplerian curve from Eq. (2.22). Figure taken from Ref. [66].*

2.6.2 Dark matter

Several observations show the existence of dark matter. The first is the velocity distribution of matter in galaxies and clusters [3]. In both objects, at large distances the velocity of the observable matter seems to be flattening, while Newtonian physics[11] expects that the velocity scales as [3]

$$v = \sqrt{\frac{GM(R)}{R}}\,, \tag{2.22}$$

where $M(R)$ is the mass inside a sphere of size R. Since at large distances only a negligible amount of mass is prevalent, we expect that $v \propto 1/\sqrt{R}$, hence decreases. The measured velocities shown in Fig. 2.6 instead flatten for large distance, contrary to what is predicted [66].

Another probe for the amount of dark matter comes from the acoustic CMB peaks as explained in section 2.4. These peaks can be interpreted as appearing due to a resonance effect in the primordial plasma at the time the CMB was emitted. This resonance effect depends on the amount of gravitationally interacting matter, and it exceeds the size of the peaks predicted by the matter density observed today.

[11] In this regime relativistic effects are negligible.

Finally, dark matter can be indirectly observed using the movement of stars and due to lensing of light [3]. During a collision of two clusters the (non-interacting) dark matter continues without interacting, while the (interacting) visible matter feels a friction force and slows down, separating the two types of matter. In these clusters, of which the bullet cluster is the most famous example [67], the dark matter is therefore displaced from the normal matter (mainly hot gas). This separation is made visible by comparing data from gravitational lensing of background light with the X-ray data collected from the hot interstellar gas.

The nature of dark matter is not known, though there are some hints. The first hint is that the bullet cluster measurement is best explained using a very weakly interacting particle and also the early universe arguments imply that this particle should not interact with the cosmic plasma at the time of BBN. In addition, the dark matter particle has to be heavy enough since light dark matter will, due to a larger free streaming length, wash away structures in the universe [8]. By measuring Lyman-α lines from structures in the early universe the structure formation rate can be estimated. These experiments give a bound on the dark matter mass of $m_{DM} > 5.3$ keV [68].

The only weakly interacting massive particle in the standard model is the neutrino, but the Lymann-α bound on the dark matter mass is above the sum of the standard model neutrino masses, $\sum m_\nu < 0.236$ eV [12]. This scenario can be made consistent if an additional heavy neutrino (known as the sterile neutrino) us added to the standard model spectrum that will play the role of dark matter, see for instance [69] and references therein.

The standard paradigm for dark matter is that there is a stable non-standard model particle in the thermal plasma that freezes out before BBN to obtain the current day abundance [19]. In the freeze-out process the dark matter particle is in thermal equilibrium in the very early universe, meaning that the annihilation process is as fast as the creation process. When the temperature drops below the mass of the dark matter particle, the creation process becomes thermally suppressed, and the dark matter particle density decreases nearly exponentially. If the dark matter particle is stable, its only interaction is through annihilations and due to the sharp drop in the number density two dark matter particles cannot 'find each other', hence they freeze out.

The components in the cosmic plasma are described by a set of Boltzmann equations. The Boltzmann equation that characterizes the abundance of dark matter is [19]

$$a^{-3}\frac{\mathrm{d}(n_{DM}a^3)}{\mathrm{d}t} = \langle\sigma v\rangle\left((n_{DM}^{eq})^2 - n_{DM}^2\right), \tag{2.23}$$

where $\langle\sigma v\rangle$ is the thermal average of the cross section times velocity of the dark matter particle and n_{DM} the dark matter number density. At high temperatures, the equilibrium dark matter density (n_{DM}^{eq}) is large, and the dark matter abundance follows it. After the dark matter decouples from the thermal bath, the number density (n_{DM}) is much larger then the equilibrium density and the latter

can be ignored.

Before solving Eq. (2.23), it is convenient to define some terminology. Instead of using the scale factor and time, it is useful to define $x \equiv m/T$, where the temperature is rewritten as $T \propto a^{-1}$. In addition, instead of number densities it is convenient to work with the yield $Y \equiv n/s$, where s is the entropy density[12]. In terms of these parameters the Boltzmann equation (2.23) becomes a Riccati equation [19]

$$\frac{\mathrm{d}Y}{\mathrm{d}x} \approx -\frac{\lambda Y^2}{x^2}\,, \tag{2.24}$$

where

$$\lambda = \frac{2\pi^2 g_*}{45}\frac{m^3\langle\sigma v\rangle}{H(m)}\,, \tag{2.25}$$

and g_*, the number of relativistic degrees of freedom at decoupling, is assumed constant. When also assuming that λ is constant in time, it is possible to integrate (2.24) between the moment of freeze-out x_f and current time $x_0 = m/T_0$

$$Y = \frac{\lambda^{-1}}{x_f^{-1} - x_0^{-1}} \approx \frac{x_f}{\lambda} \tag{2.26}$$

where the last expression assumes that the yield after freeze-out is large compared to the yield at late time. Typically, the parameter λ can be rather large and $x_f = \mathcal{O}(10)$. Thus, at late times there exists a small non-zero dark matter density, given by (2.26).

If the universe had continued expanding without any extra energy injections, the dark matter density would have been unchanged after decoupling. However, annihilations of other particles after dark matter freeze-out will increase the temperature of the medium with respect to the dark matter density[13]. Assuming that these energy injections are adiabatic, the current day dark matter density can be obtained using Eq. (2.21) [19]

$$\Omega_{DM} = \frac{mY_\infty T_0^3}{\rho_c}\left(\frac{a_0 T_0}{a_1 T_1}\right)^2 = \frac{\pi}{9}\frac{x_f}{\langle\sigma v\rangle}\sqrt{\frac{g_*(a_{DM})^2}{10 g_*(a_0)}}\frac{T_0^3}{M_\mathrm{p}^3 H_0^2}\,, \tag{2.27}$$

where for the second equality was used that in an adiabatic process the entropy density $s = g_*(aT)^3$ is conserved. Demanding $\Omega_{DM}h^2 \approx 0.1198 \pm 0.0015$ [12] and that the mass of the dark matter particle is roughly at the weak scale, we find that $\langle\sigma v\rangle \approx 0.1\sqrt{G_F}$, where G_F is the Fermi coupling. This observation, known as the WIMP miracle [70], means that a massive dark matter particle is expected to be interacting with the weak force or a force similar in strength.

[12] Note that the yield can also be defined as $Y \equiv n/T^3$.

[13] The photon density will decrease less compared to the dark matter density, but it never increases [19].

Unfortunately, experimental observations currently constrain most of the parameter space for WIMP dark matter candidates. There are three different search methods for dark matter. The first is to search for dark matter in collider experiments, where the dark matter particles are visible as missing transverse momentum [71]. The second method is to search for recoils of dark matter particles with the nucleus or the electrons of some material, for instance silicon [72]. Finally, if dark matter annihilates there could be an electromagnetic or neutrino signal from regions where the dark matter clusters, *i.e.* at the center of a galaxy or the sun. From these experiments, there is a hint of a detection from an electromagnetic signal with an energy of 3.5 keV from the center of several galaxy clusters [73,74]. However, this signal is debated [74]. In other experiments no signal of dark matter was found [71,72,74].

Another production mechanism for dark matter, which is less constraint by observations, is freeze-in [75]. In freeze-in the original dark matter density was negligibly small and some particle in the thermal plasma decayed or annihilated into the dark matter particle. Therefore, the dark matter particle can be extremely weakly coupled to the known standard model particles, while the intermediate particle might have a mass beyond the reach of current colliders.

Freeze-in can occur both by decay processes $B_1 \to B_2 + X$, where the B_i are bath particles and X is the dark matter particle, or freeze-in can occur using a scattering $B_1 + B_2 \to X + X$ (or annihilation, if $B_1 = B_2$). If in the former scenario, the Boltzmann equation for the dark matter particle is [75]

$$\dot{n}_X + 3n_x H \approx \frac{g_{B_1} m_{B_1}^2 \Gamma}{2\pi^2} T K_1 \left(\frac{m_{B_1}}{T}\right), \tag{2.28}$$

where g is the number of internal spin degrees of freedom, Γ is the partial decay width of B_1 into B_2 and X, and K_1 is the modified Bessel function of the second kind. In Eq. (2.28) the effects of Pauli blocking and stimulated emission are neglected. The yield $Y = n/S$ can be obtained, adding the possibility of multiple particles decaying into the dark matter particle, as [75]

$$Y_{\text{freeze-in}} = \sum_i \frac{45\sqrt{90} g_i}{4\pi^5 g_*^{3/2}} \frac{\Gamma_i M_{\text{p}}}{m_i^2} \int_{x_{i,\min}}^{x_{i,\max}} K_1(x) x^3 \mathrm{d}x \,, \tag{2.29}$$

where i runs over all particle states that decay to the dark matter particle, Γ_i is the partial decay width of particle i to the dark matter particle and g_i its internal number of degrees of freedom.

The current temperature of the universe is much smaller than the mass of the dark matter particle, hence sending $x_{\max} \to \infty$ is a good approximation. If it can also be assumed that the original temperature of the universe is much larger than m_1, hence if $x_{\min} \approx 0$, the integral of (2.29) can be solved analytically and is $3\pi/2$. In section 3.5 it will be shown that when assuming inflation, the maximal temperature of the radiation era of the universe is the reheating temperature. If

the masses of the fields decaying into X are close to the reheating temperature, then $x_{\rm min} = 0$ is not a proper choice. It is possible to analytically perform the integral, but it is simpler to use an interpolating function, that we numerically found to be

$$I = \frac{2}{3\pi}\int_x^\infty K_1(y) y^3 \mathrm{d}y \approx \begin{cases} 1 & \text{if } x < 1, \\ \frac{1}{3}e^{-x}\left(0.07x^3 + 2.2x^2 + 2x + 4\right) & \text{if } x > 1, \end{cases} \tag{2.30}$$

where $x = x_{\rm min}$. Note that if $x_{\rm min} < 1$ this interpolation function coincides with the value given in [75]. Finally, the dark matter abundance can be obtained from the yield using

$$\Omega_{DM} = \frac{s_0 m_{DM} Y}{(\rho_c/h^2) M_{\rm p}^2}\,, \tag{2.31}$$

where $s_0 = 2\pi^2 g_{*0} T_0^3/45$ is the current entropy density ($T_0 = 2.735K$ is the CMB temperature and $g_{*0} = 43/11$ the current number of relativistic degrees of freedom), $\rho_c = 3H_0^2 M_{\rm p}^2$ is the critical density and $H_0/h = 100$ km s^{-1}Mpc^{-1}.

Note that for freeze-in the main contribution to the dark matter density comes from the particle with the lowest mass and highest partial decay width into X. This is a general freeze-in effect, that the strongest interacting particle has the strongest contribution to the process. The result of this is that freeze-in is dominated by the contribution at the moment this bath particle freezes out of the thermal bath. This can be presented in a nice form using phase diagrams, as in Ref. [76].

In addition to particle dark matter, the observations leading to dark matter can be caused by a modification of gravity. Typically, modified gravity theories are able to explain the galaxy rotation curves better than particle dark matter. But to explain the early universe probes of dark matter with modified gravity is challenging. Nevertheless, some models are studied, see for instance Refs. [62, 77]

2.7 Initial condition problems

The universe described above agrees extremely well with the universe we observe, with only a few small discrepancies. Three of these, the existence of dark energy and dark matter and the question why there is a large difference between the amounts of matter and antimatter were discussed in the previous sections. These problems are problems in the current universe, while in this section we will discuss some problems related to the extrapolation of our universe to very early times. Some of these problems of the standard Big Bang model will be solved with the introduction of a new phase in the history of the universe, the inflation phase, in the next chapter.

The clearest problem of the Big Bang model is the initial singularity. At the moment that the coordinate time $t = 0$, the scale factor vanishes, meaning that the matter density given in Eq. (2.17) diverges. In this thesis, the initial singularity

problem will not be considered, since due to the era of inflation introduced in the next chapter no physical observations can be related to it. Instead, we will assume that at some moment the universe had an energy density $\rho_i \approx M_{\mathrm{p}}^4$ and will not deal with the reason how this emerged. Note that the era of inflation, that will be introduced in the next section, will make the initial condition of the universe unobservable.

Another initial condition problem of the ΛCDM model is the horizon or isotropy problem. The reason is that two different universes can be realised. The first is a universe that is highly inhomogeneous and anisotropic. The initial condition of such a universe are completely random. The second kind of universe is instead completely homogeneous and isotropic, in such a universe there existed only a single initial condition, and the universe evolved from that point onwards.

However, it turns out that we live in neither of these two universes. In section 2.4 was explained that the temperature of the CMB is extremely similar in different directions. This is strange, since there has not been a moment of causal contact between points in the CMB surface which are separated by more than about 0.4 Mpc, which corresponds today to points separated by an angle of 1.8° in the sky [3]. In the ΛCDM model there is no causal mechanism that can generate such an isotropic CMB surface [70].

This statement can be made mathematically explicit by using the particle horizon. The particle horizon was defined in section 2.2.2 as the maximal distance that information could have travelled during the evolution of the universe and it can be computed using Eq. (2.13) [70]

$$\begin{aligned} d_{\mathrm{part}}(t) =& \int_0^{a(t)} \frac{\mathrm{d}\log\ a}{aH} = \tau(t) - \tau_{\mathrm{i}} \\ =& \frac{2}{H_0(1+3w)} \left[a^{\frac{1}{2}(1+3w)} - a_{\mathrm{i}}^{\frac{1}{2}(1+3w)} \right], \end{aligned} \tag{2.32}$$

where τ is the conformal time defined in Eq. (2.10) and the subscript i defines the initial time $a(t_{\mathrm{i}} = 0)$. The second line assumes that the equation of state w is constant. The problem is that both during radiation domination as well as during matter domination the particle horizon converged. Therefore, the particle horizon at last scattering was much smaller than the particle horizon now, since the amount of conformal time from the start of the Big Bang until the moment of recombination was smaller than the conformal time up to now. This is shown schematically in Fig. 2.7. The conformal time is shown on the vertical axis, while the size of the particle horizon is shown on the horizontal axis. At the start of the universe, where $\tau = 0$, the two points at the CMB surface could not have been in causal contact, since their particle horizons (the orange cones) do not overlap [45].

The angular scales in the sky that correspond to the particle horizon at the moment of last scattering can be computed using the distance to the CMB, and result in the above-mentioned angle of about 1.8°, corresponding to $l \approx 100$ in the CMB power spectrum [3]. This means that, according to the standard Big Bang

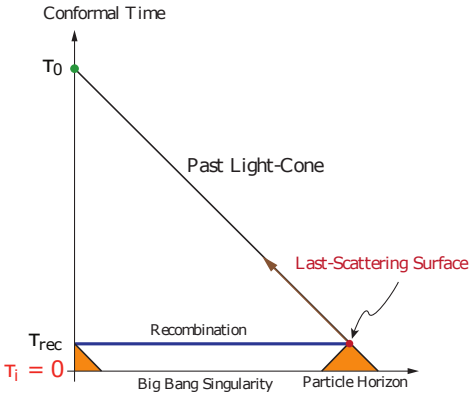

Figure 2.7: *Schematic representation of the horizon problem from Ref. [45]. The orange cones represent the particles horizons of two points on the surface that emitted the CMB. The cones do not overlap, hence the points are causally disconnected. Since the causally connected patches at the moment of recombination are much smaller than the observed CMB sphere, the CMB anisotropies should have been highly anisotropic.*

model, points in the CMB separated in the sky by more than 1.8° cannot have a causal reason to be isotropic.

A related problem is the homogeneity problem. It is easily seen that the universe is not completely homogeneous: in a perfectly homogeneous universe there would be no earth. The universe around us does become homogeneous when considering very large distances, as can be observed using large scale structure studies. These studies show an amount of homogeneity that is consistent with the ΛCDM model and the cosmological principle [10].

The cosmological principle is an additional reason for the homogeneity problem. From the definition of isotropy follows that it is possible for a universe to be isotropic but not homogeneous if it is rotationally symmetric with the observer in the center [3]. Hence, the isotropy of the universe can be explained by postulating that we are located in the center, however this is in conflict with the Copernicus principle which states that we are not.

The last problem we consider here is related to the curvature of our universe. Using the definition of the critical density of Eq. (2.20) and writing the cosmological constant as an energy density, $\Omega_\Lambda = \frac{\Lambda M_\mathrm{p}^2}{\rho_c}$, the Friedmann equation (2.16a) can be written as [70]

$$1 - \Omega_{\mathrm{tot}}(t) = -\frac{k}{a^2 H^2}\,, \tag{2.33}$$

where $\Omega_{\mathrm{tot}} = \sum_i \rho_i$ and i runs over all the constituents of the universe including Λ.

From the Friedmann equation follows that the curvature k is independent of time, so the energy density generated by the term given in Eq. (2.33) increases with time. The current energy density due to curvature is measured to be $|1 - \Omega_{\text{tot}}| < 0.005$ [12], hence the curvature at last scattering was $1 - \Omega_{\text{tot}} \leq \mathcal{O}\left(10^{-14}\right)$, while the curvature at Planck time was $1 - \Omega_{\text{tot}} \leq \mathcal{O}\left(10^{-60}\right)$. The flatness problem is therefore how it is possible that such a small curvature originated from the Big Bang process.

Mathematically, the change of the flatness of the universe in time can be expressed as [70]

$$\frac{\mathrm{d}|\Omega_{\text{tot}} - 1|}{\mathrm{d}\ln a} = (1 + 3w)\Omega_{\text{tot}}(\Omega_{\text{tot}} - 1)\,, \tag{2.34}$$

where w is the equation of state of the universe defined in section 2.3. During the evolution of the universe, Table 2.1 shows that the scale factor always increased and during radiation and matter domination $w < -\frac{1}{3}$. Hence $\Omega - 1 = 0$ is an unstable fixed point, so it is expected that the universe has a very large curvature. This is in contrast to observations.

Note that these problems in the early universe can be solved by choosing the proper initial condition [45]. If initially the universe was not curved, the bounds in the previous paragraph would be trivially satisfied. However, a very small deviation from complete flatness will generate an enormous curvature at large scales. The horizon problem is more difficult to solve, since Fig. 2.5 shows that in the early universe there were small but nonzero anisotropies. Therefore, the universe started from a state that was not completely isotropic, but had small ripples. Though in principle the problems are initial condition problems and the initial conditions of the universe are not known [70], in the next chapter inflation will be introduced. Inflation will provide a solution for these problems without the need to set very specific initial conditions of the universe.

CHAPTER 3

Inflation

Introduction

In section 2.7 the horizon and flatness problems of the ΛCDM model were posed. The horizon problem originates from the observation that the CMB is isotropic at angular scales beyond the size of the causal patches at the time of recombination, meaning that it is more isotropic than causal physics can account for. This problem is related to the homogeneity problem, which asks how the nearby universe became inhomogeneous, and why the distant universe is homogeneous. In addition to being homogeneous and isotropic, the current universe is also spatially flat, which is not explained in the ΛCDM model.

A solution to these problems is to impose a very specific initial condition for the universe. However, it requires a large amount of fine-tuning to explain the isotropy in the temperature of the CMB. A more appealing solution is to impose that there is a new phase in the history of the universe that generated this homogeneity, isotropy and flattened the universe.

In this thesis we will assume that the universe had such an additional phase called inflation in which it experienced an accelerated expansion. Though inflation is the main paradigm for solving these early universe problems, other ideas are proposed as well. For instance, in an ekpyrotic universe [78], the horizon and flatness problems are solved during an era of rapid contraction of the universe, followed by a bounce.

The structure of this chapter is as follows. In section 3.1 inflation will be defined and it will be shown that it solves the initial condition problems of the

ΛCDM model. However, the model proposed in this section will not include an end of inflation, so in section 3.2 inflation with a dynamical scalar field is introduced, which results in the theory of slow roll inflation. In section 3.3 the anisotropies in the CMB will be explained using the theory of single field slow roll inflation and in section 3.4 some selected inflation models will be reviewed. This chapter finishes with section 3.5 concerning reheating, during which the inflaton decayed to produce the radiation dominated era.

This chapter is based on the Refs. [8, 20, 45, 79].

3.1 Solving the horizon and flatness problems

The main idea of inflation is to impose that the early universe went through an era of accelerated expansion, hence when $\ddot{a} > 0$. This can be related to the conditions [70]

$$\frac{\mathrm{d}}{\mathrm{d}t}\left(\frac{1}{aH}\right) < 0, \qquad (1+3w) < 0. \tag{3.1}$$

Then, if the inflationary phase continues until the start of the universe where $a = 0$, the second line of Eq. (2.32) diverges so that the conformal time $\tau_i \to -\infty$ [70]. Therefore, inflation can be interpreted as a phase that stretches the amount of conformal time to large negative values, which solves the horizon problem. This is shown pictorially in Fig. 3.1.

The conditions for inflation in Eqs. (3.1) are satisfied in a universe dominated by a cosmological constant, which is described in section 2.3. Using the results from a cosmological constant dominated universe summarized in table 2.1, we find that the scale factor can be parametrized as [3]

$$a(t) = e^{-N(t)} a_{\mathrm{end}}, \tag{3.2}$$

where a_{end} is the scale factor at the end of inflation and $N(t)$ the number of e-folds. Since the final state of inflation is known, rather than the initial state, the number of e-folds is defined counting backwards with respect to time[1].

An example is a universe dominated by a cosmological constant. For such a universe

$$\frac{1}{aH} \propto e^{-t/t_0} \tag{3.3}$$

hence the universe undergoes an accelerated expansion. In the flow equation (2.34) this implies that while the universe is Λ dominated, a flat universe is an attractor solution. Hence, the flatness problem is solved if the universe accelerated for enough e-folds. For reasonable values of the parameters, it can be found that the required number of e-folds is between 60 and 70, as is shown in Ref. [79]. However,

[1] Note that different definitions are used for the number of e-folds, including the definition starting from t_i, as well as the above definition without the minus sign (rendering $N(t)$ negative during inflation). If these definitions are used N increases during inflation.

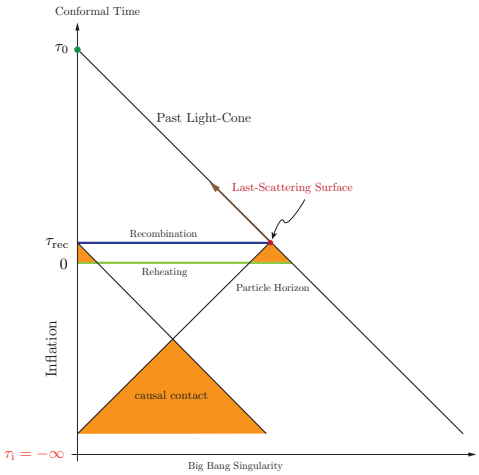

Figure 3.1: *Schematic picture of the solution of the horizon problem, compare with Fig. 2.7. Inflation extends the amount of conformal time before recombination, so that the particle horizon at recombination is increased. If inflation lasted long enough, the horizon problem is solved. Figure from Baumann's Tasi lectures [45].*

this depends on the post-inflationary evolution of the universe, as will be discussed in section 3.5. In addition, during inflation the particle horizon increases as

$$d_{\rm part}(t_{\rm end}) = a(t_{\rm end}) \int_{t_{\rm i}}^{t_{\rm end}} \frac{{\rm d}t}{a(t)} \propto \frac{e^N}{H} e^{H(t_{\rm end}-t_{\rm i})} \,. \tag{3.4}$$

Therefore, if N is sufficiently large, the horizon distance at last scattering will be beyond the size of current observations. If inflation lasted for 60 e-folds, also the horizon problem is solved, as is shown in Ref. [79].

Other issues with the early universe are also solved by an inflation era. One of the problems of many UV-completions of the standard model is that they postulate very massive stable particles, for example cosmic strings and magnetic monopoles [3]. These particles could easily be measured even if their abundance is small. Since they are not observed, either the UV-completion is incorrect or there is a mechanism that efficiently dilutes these particles. During inflation the total volume of the universe greatly increased and since the density of a set of particles scales as $\rho_{\rm M} \propto a^{-3} \propto e^{-3N_{\rm tot}}$ during inflation, any pre-inflationary abundance of particles is efficiently washed out. If after inflation these particles are not created, their current density will be unobservably small.

Unfortunately, the above inflation model is not complete. The model lacks a mechanism to end inflation and start a radiation dominated phase, which is

necessary for Big Bang nucleosynthesis. Therefore, in the next section, inflation models will be considered that use a scalar field, the inflaton. Then the dynamics of the inflaton provides the end of inflation.

3.2 Inflation with a scalar field

Three main proposals were raised to explain inflation; old, new and chaotic inflation. In the following these proposals will be discussed, and it will be explained why old inflation does not explain the observations. Then, the equations of motion for the remaining dynamical inflation scenarios will be reviewed, which leads to the Hamilton-Jacobi description of inflation and potential slow roll inflation. This section finishes with a comment on the stability of the inflation trajectory calculated with these methods.

3.2.1 Old, new and chaotic inflation

The first model of inflation is now known as 'old inflation', and was first posed by Guth in [11]. In old inflation, the early universe is trapped in a false vacuum state, depicted with a dot in the left frame of Fig. 3.2. At very early times, the value for the inflaton field ϕ is large, and it rolls down the right potential hill towards the local minimum denoted with the black dot. While being trapped in the false vacuum state, the universe is expanding exponentially fast and the scale factor can be parametrized with the number of e-folds, as in Eq. (3.2). After a sufficiently long expansion in the inflating local minimum, the inflaton tunnels through the potential barrier and inflation ends.

At the time that Guth posed old inflation, the anisotropies in the CMB were not yet observed. However, a rough bound on the amount of breaking of homogeneity was known, parametrized by the amount of density fluctuations in the energy density in the universe over the total energy density $\frac{\delta\rho}{\rho}$. These density fluctuations could be explained by posing that the bubbles generated by the first order phase transition that ended inflation were sufficiently small [11].

However, the end of inflation is paradoxical. To have enough inflation, the inflaton had to stay sufficiently long in the local minimum before tunnelling to the global minimum, while a quick phase transition is required to generate many small bubbles. Therefore, the Guth model of inflation was abandoned in favour of new and chaotic inflation.

Shortly after Guth introduced the theory of old inflation, Albrecht and Steinhardt [80] and Linde [81] proposed new inflation in which the inflaton rolls slowly to the bottom of the potential after the tunnelling towards the true vacuum. An example of such a potential is schematically shown in the middle frame of Fig. 3.2. Note that the potential on the left of the local minimum in this frame is much flatter compared to the potential in old inflation to provide a phase in which the inflaton slowly rolls down the potential. During this slow roll phase, the speed of

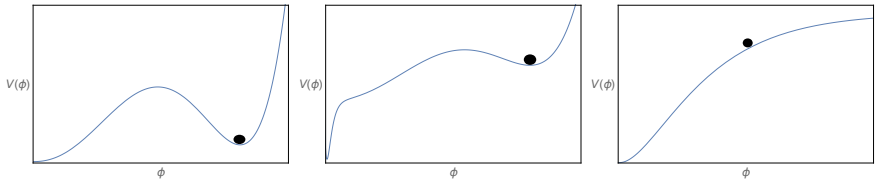

Figure 3.2: *From left to right, examples of potentials for old, new and chaotic inflation. During old and new inflation, the inflaton (which acts as the parameter of the phase transition) is situated on the right (local) minimum, but tunnels to the global minimum after some time. After tunnelling, the new inflation potential is sufficiently flat to maintain inflation, while old inflation stops with the tunnelling. Chaotic inflation has no initial metastable minimum, but slowly rolls down a sufficiently flat potential.*

rolling is small compared to the potential energy and the field is approximately a cosmological constant. This effective cosmological constant generates a nearly exponential expansion, similar to old inflation, which ends when the inflaton stopped to roll slowly. Because during the slow roll era the universe still expands nearly exponentially fast, the whole observable universe will be dominated by a single bubble. New inflation solves the early universe problems similarly as the Guth inflation model, with the difference that the number of e-folds is a more complicated function of time.

A similar model, that did not require a phase transition to start inflation, was proposed by Linde in Ref. [82]. It is schematically depicted in the right frame of Fig. 3.2. In this model the inflaton field value obtains a random initial condition in the early universe, such that it starts with its field value displaced from the origin. Due to this random initial condition the name chaotic inflation was given to this inflation model[2].

To make qualitative predictions for new and chaotic inflation models, the equations of motion for a scalar field in an FLRW background have to be obtained. These are most easily found by observing that for a scalar field with a canonical kinetic term and a minimal coupling to gravity which has a potential V, the energy-momentum tensor behaves as a perfect fluid with [79]

$$\rho = \frac{1}{2}\dot{\phi}^2 + V(\phi), \qquad p = \frac{1}{2}\dot{\phi}^2 - V(\phi)\,. \tag{3.5}$$

Using Eq. (2.6) the Friedmann and Klein Gordon equations are obtained

$$H^2 = \frac{1}{3M_\mathrm{p}^2}\left(\frac{1}{2}\dot{\phi}^2 + V(\phi)\right), \tag{3.6a}$$

$$0 = \ddot{\phi} + 3H\dot{\phi} + V'(\phi)\,, \tag{3.6b}$$

[2]The name chaotic inflation was also given to the ϕ^n and quadratic inflation models.

where the prime corresponds to differentiation with respect to ϕ. The Klein-Gordon equation describes a harmonic oscillator with a damping due to the cosmic expansion generated by the inflaton field.

To model inflation, it is useful to rewrite the third equation of (2.6) as [79]

$$\frac{\ddot{a}}{a} = H^2(1-\epsilon_{\rm H}), \qquad \epsilon_{\rm H} \equiv -\frac{\dot{H}}{H^2} = \frac{3}{2}(1+w)\,, \tag{3.7}$$

where $\epsilon_{\rm H}$ is the first Hubble slow roll parameter. The inflationary phase is defined to be the era in which the universe underwent an accelerated expansion, which can be cast into the condition

$$\epsilon_{\rm H} < 1. \tag{3.8}$$

Computationally, condition (3.8) is simpler to use than the conditions $\ddot{a} > 0$ or (3.1). It implies, using (3.7), that inflation occurs if the change in time of H is smaller than H^2. Hence for inflation to occur the Hubble parameter of the universe has to decrease slowly.

The number of e-folds (N) is defined by Eq. (3.2), as in the Guth model of inflation. The number of e-folds and the Hubble parameter H are the most natural quantities obtained from the scale factor a considering that multiplying a with a constant does not have physical implications.

3.2.2 Hamilton Jacobi

For most purposes, it is convenient to consider the inflaton field value instead of a time parameter (t or τ) or the number of e-folds to parametrize inflation. Obviously, this is only consistent if $\dot{\phi}$ never vanishes during inflation, hence if the inflaton field does not initially roll up the potential and returns its path. In the following it will be assumed that the inflaton field is moving down its potential during the full part of the inflationary trajectory under consideration. Then the Hubble parameter is expressed as $H(\phi)$ and by differentiating the Friedmann equation in (3.6) and plugging that into the Klein-Gordon equation (3.6b), we obtain [83]

$$\dot{\phi} = -2M_{\rm p}^2 H'(\phi), \qquad V = 3M_{\rm p}^2 H(\phi)^2 - 2M_{\rm p}^4 H'(\phi)^2. \tag{3.9}$$

The second equation is the Hamilton Jacobi equation, which relates the Hubble function to the inflaton potential. Using this equation any $H(\phi)$ can be mapped to a unique potential. In addition, from the first relation of (3.9) another relation for $\epsilon_{\rm H}$ is obtained [84]

$$\epsilon_{\rm H} = 2M_{\rm p}^2 \left(\frac{H'(\phi)}{H(\phi)}\right)^2. \tag{3.10}$$

Finally, differentiating Eq. (3.2) with respect to time an expression relating the number of e-folds with the field value is

$$N = \int_{\phi_{end}}^{\phi} \frac{{\rm d}\phi}{M_{\rm p}\sqrt{2\epsilon_{\rm H}(\phi)}}\,. \tag{3.11}$$

Inflation is completely specified if $H(\phi)$ is known [83]. From the Hubble function the first slow roll parameter ($\epsilon_{\rm H}$) can be obtained using Eq. (3.10) and when this parameter is smaller than one inflation takes place. In section 3.1 was shown that inflation needs to last for at least 60-70 efolds. During these e-folds $\epsilon_{\rm H}$ must be smaller than one, so the derivative of $\epsilon_{\rm H}$ with respect to the number of e-folds must be small. For this purpose the second slow roll parameter is defined as [84]

$$\eta_{\rm H} = 2M_{\rm p}^2 \frac{H''(\phi)}{H(\phi)} \,. \tag{3.12}$$

With this definition, η corresponds to the acceleration of the inflaton velocity within the Hubble function. For inflation to persist it is typically required that $|\eta_{\rm H}| < 1$ [70].

In addition, in this framework a very large and positive $\eta_{\rm H}$ is never allowed, since from Eq. (3.9)

$$V'(\phi) = 2M_{\rm p}^2 H'(\phi) H(\phi) \left(3 - \eta_{\rm H}\right), \tag{3.13}$$

and if $\eta_{\rm H} > 3$ either the potential or the Hubble function increases with time. From the second equation of Eq. (3.8) it is easily verified that the Hubble function decreases during inflation, hence $\eta_{\rm H} > 3$ corresponds to a model in which the inflaton rolls up the potential. This situation can be obtained for certain initial conditions of the inflaton, but at some point the inflaton field will loose its momentum and will start to move down the potential. This is not consistent with the ansatz that ϕ is a monotonic function, so we require that $\eta_{\rm H} < 3$. In fact, some inflation models, named ultra-slow roll inflation, exist in which $\eta_{\rm H} = 3$ [85]. For this type of models the full field equations in Eqs. (3.6) have to be used instead of the Hamilton-Jacobi equation.

3.2.3 Potential frame

In the Hamilton-Jacobi frame of inflation the Hubble function is specified and the potential is derived from Eq. (3.9). To embed inflation in particle physics it is more convenient to specify the potential and derive the Hubble function instead. Numerically this is possible, as the Hubble function can be found using Eq. (3.9), but since this is a first order quadratic differential equation it is usually not possible analytically. Therefore, in this section the slow roll conditions $(\epsilon_{\rm H}, |\eta_{\rm H}|) \ll 1$ will be used to solve Eq. (3.9) order by order. Only the first order analysis is shown here, but more information regarding higher orders in slow roll can be found in Ref. [83].

The potential slow roll parameters are defined analogously to Eqs. (3.10) and (3.12) [86],

$$\epsilon_{\rm V}(\phi) \equiv \frac{M_{\rm p}^2}{2} \left(\frac{V'(\phi)}{V(\phi)}\right)^2, \qquad \eta_{\rm V}(\phi) \equiv M_{\rm p}^2 \frac{V''(\phi)}{V(\phi)} \tag{3.14}$$

and can be related to the Hubble slow roll parameters using Eq. (3.9)

$$\epsilon_{\mathrm{V}} = \epsilon_{\mathrm{H}} + \mathcal{O}\left(\epsilon_H^2\right), \qquad \eta_{\mathrm{V}} = \epsilon_{\mathrm{H}} + \eta_{\mathrm{H}} + \mathcal{O}\left(\epsilon_H^2\right), \tag{3.15}$$

where $\mathcal{O}\left(\epsilon_H^2\right)$ implies corrections of second order in the slow roll parameters (hence also terms of order η_H^2 and $\epsilon_{\mathrm{H}}\eta_{\mathrm{H}}$). Since $\epsilon_{\mathrm{V}} \approx \epsilon_{\mathrm{H}}$, the relation for N in Eq. (3.11) is the same interchanging ϵ_{H} for ϵ_{V}.

Expanding Eq. (3.15) to higher order in slow roll is not difficult, but the results are not very illuminating [83]. However, the resulting expression cannot be given in terms of ϵ_{V} and η_{V} only, but will depend on derivatives of these quantities. These derivatives can be nicely captured in a generic set of higher order slow roll parameters [83]

$$\epsilon_{\mathrm{V}} = \frac{M_{\mathrm{p}}^2}{2}\left(\frac{V'(\phi)}{V(\phi)}\right)^2, \tag{3.16a}$$

$${}^n\lambda_{\mathrm{V}}(\phi) = M_{\mathrm{p}}^{2n}\frac{V'(\phi)^{n-1}V^{(n+1)}(\phi)}{V(\phi)^n}, \tag{3.16b}$$

where ${}^1\lambda_{\mathrm{V}} = \eta_{\mathrm{V}}$. In addition, for slow roll inflation to occur it is necessary that for all n, $|{}^n\lambda_{\mathrm{V}}| < |{}^{n-1}\lambda_{\mathrm{V}}|$, but due to the structure of the parameters this is usually satisfied if $\epsilon_{\mathrm{V}} < 1$ and $|\eta_{\mathrm{V}}| < 1$.

The slow roll phase of inflation is defined as the period in which the potential slow roll parameters ϵ_{V} and $|\eta_{\mathrm{V}}|$ are below one. Theoretically the end of this phase does not have to be the end of inflation, but the end of inflation typically follows soon after the end of the slow roll era. The location at which inflation ends is mainly important for computing the number of e-folds, but since if $\epsilon_{\mathrm{V}} > 1$, also $\epsilon_{\mathrm{H}} \approx 1$ and the integrand of (3.11) is small, hence the error that is made when using the end of slow roll is typically small. An example with models with $\epsilon_{\mathrm{V}} < 0$ but $\epsilon_{\mathrm{H}} > 0$ was explored in [87], though in this regime always $|\eta_{\mathrm{V}}| > 1$, so formally there was no slow roll inflation.

3.2.4 Slow roll attractor

The slow roll inflation model as described above chooses a specific trajectory through the two dimensional phase space of the inflaton spanned by the inflaton field value and its time derivative. Therefore, in this section we study if the slow roll trajectory given by Eqs. (3.9) is stable with respect to small perturbations. This analysis is based on Ref. [83].

Consider a Hubble function $H_0(\phi)$ that satisfies the Hamilton-Jacobi equation (3.9) for a specific potential V and add a small perturbation $\delta H(\phi)$. For this Hubble function, the Hamilton-Jacobi equation becomes

$$M_{\mathrm{p}}^2 H_0'(\phi)\delta H'(\phi) = H_0(\phi)\delta H(\phi), \tag{3.17}$$

where the prime refers to differentiation to ϕ. The perturbation equation (3.17) can be solved as

$$\delta H(\phi) = \delta H\left(\phi_{\mathrm{i}}\right) \exp\left(-3\int_{t_{\mathrm{i}}}^{t} H_0(\phi(t))\mathrm{d}t\right) = \delta H\left(\phi_{\mathrm{i}}\right) e^{-3|N_{\mathrm{i}}-N(\phi)|}\,, \tag{3.18}$$

where the first equation of (3.9) was used to change integration from ϕ to t and the index i corresponds to the initial condition of the perturbation. The last equality in Eq. (3.18) denotes that the size of the perturbation is exponentially suppressed when inflation proceeds. Therefore the slow roll trajectory is stable with respect to small perturbations.

However, inflation might have started at a point in phase space far from the inflationary attractor. It can be shown [83], that in this scenario for a large part of phase space the final inflation model converges to the attractor. Hence, the basin of attraction of the inflationary attractor is large [83, 88–90]. There are points in phase space, usually where the initial velocity is very large, that do not reach the attractor and for which the slow roll description of inflation is not sufficient. We will not discuss the initial conditions for inflation in this thesis, but assume that the inflationary attractor is reached before any observable features, explained in the next section, appear.

In addition, note that the above analyses are all assuming that the inflaton trajectory is classical. If the inflaton is moving so slowly that the classical motion is subleading with respect to the quantum oscillations, the quantum corrections will push up the inflaton more than that it is rolling down. This theory is called eternal inflation [91], but for the observable part of the inflation trajectory eternal inflation seldom occurs and is not studied in this thesis. For the non-observable part of the trajectory eternal inflation is often encountered and is one of the criticisms for inflation, see for instance Ref. [92], while Ref. [93] claims that eternal inflation can also be interpreted as a good feature of inflation.

In the following we will assume that inflation is in the slow roll attractor, and that the dynamics is sufficiently fast that the classical path is the correct one (up to the small quantum corrections that appear in the CMB, which will be discussed in the next section).

3.3 The CMB anisotropies

Having defined the dynamics of inflation, it is time to study the observable predictions of inflation. The observables for inflation originate from quantum fluctuations during inflation, as will be shown in section 3.3.3. These perturbations source fluctuations in the matter density of the universe $\delta\rho$. Constraints on the breaking of homogeneity due to $\frac{\delta\rho}{\rho}$ using large scale structure observations were used to constrain the first inflation models [94–99].

However, since the evolution of gravity is non-linear at late times, it is difficult to infer the primordial density perturbations from the current distribution of matter. Therefore, currently the strongest constraints for inflation originate from the anisotropies in the CMB. In the following of this section, first the description of the density fluctuations in the CMB of section 2.4 is extended. Since inflation also predicts observable features in the polarisation of the CMB photons, these will be discussed in section 3.3.2. Then the derivation of the power spectrum will be sketched for a single field slow roll inflation model. The purpose of this derivation is to provide the inflationary observables A_{s}, n_{s} and r, so that inflation models can be tested with the data. We finish with some comments on inflation with multiple fields and a reformulation of the horizon problem into a stronger statement.

3.3.1 The CMB power spectrum

The CMB was qualitatively considered in section 2.4, where it was explained that it is actually measured on the surface of a sphere around us. Therefore, it is convenient to expand temperature deviations of the CMB in spherical harmonics $Y_{lm}(\hat{n})$ [70]

$$\Delta T = T(\hat{n}) - T_0 = \sum_{l,m} a_{lm} Y_{lm}(\hat{n})\,, \tag{3.19}$$

where T_0 is the average CMB temperature. Of interest will be correlation functions averaged over the sky, defined as $\langle \Delta T(\hat{n}_1)\Delta T(\hat{n}_2)...\rangle$. The first non-zero correlation function is the two-point function, which will generate the observables for inflation that will be used in this thesis. Since the two-point function is averaged over the sky, it can be expanded as [8]

$$\langle \Delta T(0)\Delta T(\theta)\rangle = \sum_{l} \frac{2l+1}{4\pi} C_l P_l(\cos\theta)\,, \tag{3.20}$$

where the P_l are the Legendre polynomials. In this expansion, the values $l = 1$ and $l = 2$ correspond to the monopole and dipole respectively, and do not contain measurable information about cosmological anisotropies. The monopole corresponds to the average CMB temperature, while the unknown motion of the local group with respect to the CMB generates a dipole that cannot be subtracted from the data.

By combining Eqs. (3.19) and (3.20) the two-point function can be written as [70]

$$C_l^{TT} = \frac{1}{2l+1} \sum_{m=-l}^{l} \langle a_{lm}^* a_{lm}\rangle\,, \tag{3.21}$$

where T stands for the temperature spectrum, opposed to the polarisation data that will be considered in section 3.3.2. In Fig. 3.3 the power spectrum is shown as the combination

$$D_l^{TT} = \frac{l(l+1)}{4\pi} C_l^{TT}, \tag{3.22}$$

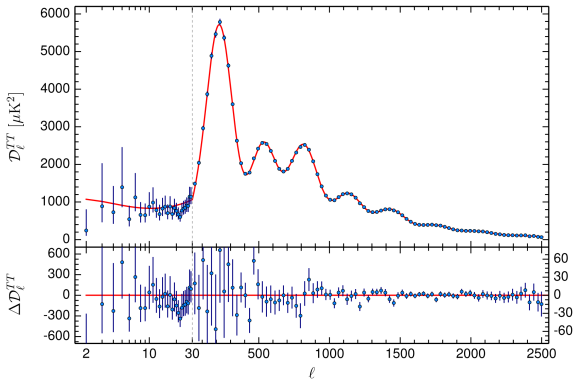

Figure 3.3: *The TT power spectrum* $\langle \Delta T(\hat{n}) \Delta T(\hat{n}') \rangle$ *(more precisely defined in Eq. (3.22)) as measured by the Planck satellite [12]. For* $l < 30$ *a different instrument was used and there the x-axis is in log-space, while for* $l > 30$ *it is linear.*

which is flat for a conformally invariant universe. Indeed, in Fig. 3.3 the spectrum at low-l is rather flat, but the small tilt indicates that there is a small deviation from conformal invariance.

3.3.2 Polarization

Additional information can be extracted from the CMB by studying the polarization of the CMB photons. If there are quadrupole anisotropies in the cosmic plasma during CMB emission, the emitted photons will be polarized due to Thomson scattering [100]. If a medium emits uniform radiation and this radiation is scattered by an electron, the light becomes polarized in the direction orthogonal to the scattering plane. Hence, if two photons originating from a hot and a cold spot are scattered, the scattered light gets a linear polarization, as is pictured in Fig. 3.4. When the light scatters often it will get depolarized, hence the observed polarization originates only from the very last scatterings at the very end of last scattering. Though the polarization of the CMB is therefore small, current experiments are sensitive enough to test it.

Polarization can be represented using the Stokes parameters I, Q, U and V [8]. The parameters I and V, which are related to the total intensity of the polarization and to the circular polarisation respectively, can be ignored. The remaining parameters are combined as $Q \pm iU$ which transform under rotations with an overall factor $Q' \pm iU' = e^{\pm i\psi}[Q \pm iU]$, where ψ is the phase of the rotation. As for the temperature power spectrum above, these parameters are

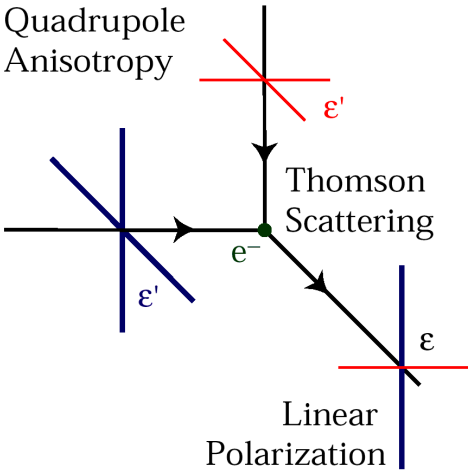

Figure 3.4: *Origin of the linear polarization in the CMB. Two photons originating from a quadrupole anisotropy scatter off an electron and get a net linear polarization. Figure from [101].*

expanded in spherical harmonics

$$(Q+iU)(\vec{n}) = \sum_{l\leq 2,|m|<l} a_{\pm 2l,m\pm 2}\tilde{Y}_l^m(n)\,, \tag{3.23}$$

where $\tilde{Y}$ transform under rotations as $Q+iU$ does.

The two different polarization patterns of the CMB can also be distinguished by their parity. This defines the E and B mode polarizations. The E-mode polarization is even under a parity transformation and the B-mode polarization is odd. From Eq. (3.23), the E and B modes are defined as [8]

$$E(\vec{n}) = \sum_{l\leq 2,|m|<l} a^E_{l,m}Y_l^m(\vec{n}), \qquad a^E_{lm} = -\frac{a_{2lm}+a^*_{-2lm}}{2}\,, \tag{3.24a}$$

$$B(\vec{n}) = \sum_{l\leq 2,|m|<l} a^B_{l,m}Y_l^m(\vec{n}), \qquad a^B_{lm} = -\frac{a_{2lm}-a^*_{-2lm}}{2i}\,. \tag{3.24b}$$

This definition has the additional feature that a^E_{lm} and a^B_{lm} are real. Analogously to the unpolarized part of the CMB spectrum in Eq. (3.22), the (cross-) correlation functions are defined as

$$C_l^{EE} = \langle a^E_{lm}a^E_{lm}\rangle, \qquad C_l^{BB} = \langle a^B_{lm}a^B_{lm}\rangle, \qquad C_l^{TE} = \langle a^T_{lm}a^E_{lm}\rangle, \tag{3.25}$$

while the correlation functions C_l^{BT} and C_l^{BE} are zero for symmetry reasons.

The primordial EE spectrum was first detected by the DASI experiment in 2002 [102], while a cosmological B spectrum has not been observed so far and much effort is made to measure this. The Planck satellite measured both the EE spectrum, as well as the TE cross-correlation spectrum with high accuracy [12].

3.3.3 The inflationary origin

According to the inflationary paradigm, the anisotropies in the CMB originate from quantum fluctuations of the inflaton field value during inflation [103, 104]. These fluctuations from the homogeneous solution, which appear in both the metric and the inflaton field, can be expanded as

$$\phi(\vec{x},t) = \bar{\phi}(t) + \delta\phi(\vec{x},t), \qquad g_{\mu\nu}(\vec{x},t) = \bar{g}_{\mu\nu}(t) + \delta g_{\mu\nu}(\vec{x},t)\,, \tag{3.26}$$

where the bar corresponds to the background value, which is space independent due to homogeneity and isotropy, and δ denotes the fluctuation. The fluctuations of the metric field can be expanded in a scalar, a vector and a tensor part [8]

$$\delta g_{\mu\nu}dx^\mu dx^\nu = -2\Phi dt^2 + 2aB_i dx^i dt + a^2\left(-2\Psi\delta_{ij} + E_{ij}\right)dx^i dx^j\,, \tag{3.27}$$

where $E_{ij} = 2\partial^2 E + 2\partial_{(i}F_{j)} + h_{ij}$. Because the scalar fluctuations are not space-time invariant, it is beneficial to define a gauge invariant perturbation $\mathcal{R} \equiv \Psi - \frac{H}{\dot{\phi}}\delta\phi$ and gauge $\Phi = \Psi$ and $E = 0$. Vector perturbations are usually not created at linear order in perturbation theory during inflation and decay during the evolution of the universe, hence also B_i and F_i are set to zero. The tensor perturbations of $h_{\mu\nu}$ are gauge-invariant and correspond to the tensor modes that are emitted during inflation.

From the gauge invariant scalar perturbation $\mathcal{R}$, the two-point function [70]

$$\langle \mathcal{R}_k\, \mathcal{R}_{k'}\rangle = (2\pi)^3\delta(k+k')\,\mathrm{P}_{\mathcal{R}}(k), \qquad \Delta_s^2 = \frac{k^3}{(2\pi)^3}\,\mathrm{P}_{\mathcal{R}}(k)\,, \tag{3.28}$$

can be defined, where Δ_s^2 is the scalar power spectrum. The powers of k in the definition of Δ_s^2 are chosen such that Δ_s^2 is constant if the perturbations are scale-independent. Observations show that indeed the scalar perturbations are close to scale invariant, hence expanding Δ_s^2 around a scale invariant ansatz

$$\Delta_s^2(k) = A_{\mathrm{s}}(k_*)\left(\frac{k}{k_*}\right)^{(n_{\mathrm{s}}(k_*)-1)+\frac{1}{2}\alpha_s(k_*)\ln(k/k_*)+\ldots} \tag{3.29}$$

is a good starting point. Here and in the following a star will be assigned to quantities at the moment of horizon crossing. The reference scale $k_* = a_* H_*$ is known as the pivot scale and depends on the typical size of the perturbation under consideration. Typical choices are $k_* = 0.002\ \mathrm{Mpc}^{-1}$ for the Planck satellite [14]

and $k_* = 0.05$ Mpc^{-1} for the BICEP/Keck array [105]. The deviations from scale invariance are parametrized by the scalar spectral index $n_{\rm s}$, which is 1 for a scale-independent spectrum, while the scale dependence of $n_{\rm s}$ is encoded by the running α_s. Higher order quantities can be defined as the running of the running and so on, but these are difficult to observe.

Similarly, the power spectrum of the tensor modes h_{ij} can be obtained. The tensor modes are gauge-invariant, hence no redefinitions are required and the power spectrum of the tensor modes is

$$\langle h_k h_{k'} \rangle = (2\pi)^3 \delta(k+k')\, \mathrm{P}_h(k), \qquad \Delta_t^2 = 2\delta_h^2 = \frac{k^3}{2\pi^2} P_h(k)\,, \tag{3.30}$$

where the factor 2 originates from the two polarizations of tensor modes (which are gravitational waves). The tensor power spectrum is expanded around a scale invariant ansatz

$$\Delta_t^2(k) = A_t(k_*) \left(\frac{k}{k_*}\right)^{n_t(k_*)+\frac{1}{2}\alpha_t \ln(k/k_*)+\ldots} . \tag{3.31}$$

Note that, for historical reasons, the tensor spectral index n_t for a scale-invariant spectrum is 0. In addition, instead of computing the tensor power spectrum (A_t), the tensor to scalar ratio is defined as

$$r \equiv \frac{\Delta_t^2}{\Delta_s^2}\,. \tag{3.32}$$

To compute the power spectra of Eqs. (3.29) and (3.31), a second quantisation description for $\mathcal{R}$ and h is used, as described in Ref. [45]. This leads, for the scalar power spectrum, to the Mukhanov equation

$$v_k'' + \left(k^2 - \frac{z''}{z}\right) v_k = 0\,, \tag{3.33}$$

where $v_k \equiv z\,\mathcal{R}$, $z^2 = 2a^2\epsilon_{\rm H}$ and primes are derivatives with respect to conformal time τ.

When performing the second quantization the vacuum is defined as the state that is annihilated by the annihilation operator. However, within a curved space-time the vacuum is not well-defined, as is nicely explained in Ref. [70]. The standard choice for the vacuum is to assume that the very early universe was completely de Sitter, hence $z''/z = 2/\tau^2$ and from solving Eq. (3.33) in this vacuum we obtain

$$v_k = e^{-ik\tau}\sqrt{2k}\left(1 - \frac{i}{k\tau}\right), \tag{3.34}$$

which is known as the Bunch-Davies mode function.

The dependence of the perturbation spectrum on the vacuum is unexpected, since inflation should remove the initial conditions of the universe. There are

examples in which the Bunch-Davies mode function is replaced by another solution [106–108]. For instance in Ref. [107, 108] was shown that if the universe went through a bounce, a small shift in the low-l data can be expected. Though there is observationally a hint that such a shift exists, as can be seen from Fig. 3.3, this is not statistically significant [14].

In this thesis we will use the Bunch-Davies vacuum for the scalar and the tensor modes. Assuming this vacuum, the power spectra at leading order in slow roll are [70]

$$\Delta_s^2 = \frac{H_*^2}{8\pi^2\epsilon_{\rm H}(k_*)M_{\rm p}^2}, \qquad \Delta_t^2 = \frac{2H_*^2}{\pi^2 M_{\rm p}^2}\,. \tag{3.35}$$

From the definitions of the slow roll parameters, the scalar indices and the tensor to scalar ratio defined in Eqs. (3.29) and (3.31) are

$$n_{\rm s} = 1 + 2\eta_{\rm V} - 6\epsilon_{\rm V} \tag{3.36a}$$

$$r = 16\epsilon_{\rm V} \tag{3.36b}$$

$$\alpha = 16\epsilon_{\rm V}\eta_{\rm V} - 24\epsilon_{\rm V}^2 - 2({}^2\lambda_{\rm V}) \tag{3.36c}$$

$$n_t = -2\epsilon_{\rm V}\,, \tag{3.36d}$$

where we neglected terms next-to-leading order in slow roll. The parameter ${}^2\lambda_{\rm V}$ is defined in Eq. (3.16) and is second order in slow roll. Note that higher orders terms of the power spectrum are also higher order in slow roll, e.g. $n_{\rm s} - 1$ is first order in slow roll, while α is second order. Therefore slow roll inflation predicts that α is much smaller than $n_{\rm s}$ and that the scale dependence of α (named δ), is much smaller than α, etcetera.

As qualitatively explained in section 2.4, the density fluctuations generated during inflation seed the temperature fluctuations in the CMB. This is particularly true for the low-l data, which probe distance scales outside of the causal horizon at last scattering. However, for the large-l data there are some effects that change the power spectrum, as explained in section 2.4. These effects are accounted for by a transfer function Δ_{Tl}, which relates the temperature anisotropies measured in the CMB with the perturbations generated during inflation. This leads to [70]

$$C_l^{TT} = \frac{2}{\pi}\int k^2 {\rm d}k\; P_{\mathcal{R}}(k)\Delta_{Tl}(k)\Delta_{Tl}(k)\,, \tag{3.37}$$

where C_l^{TT} was defined in Eq. (3.21). Finding these transfer functions goes beyond the scope of this thesis, the relevant information is that the anisotropies in the temperature spectrum of the CMB are directly related to the scalar perturbations generated in the CMB.

Scalar modes generate in the CMB only temperature perturbations and E-mode perturbations, but do not produce any B-mode polarisation. Tensor modes – which are gravitational waves – do produce B-mode polarisation[3] [70]. Therefore,

[3] Also E-mode polarization and temperature anisotropies are produced, but from the current non-measurement of any B-mode spectrum follows that these contribution are negligible.

if B-mode polarisation is found in the CMB this will correspond to a measurement of A_t, and hence of r. This is the most promising signal of the tensor power spectrum, since the gravitational waves emitted by inflation are far to weak to be detected by gravitational wave experiments. Unfortunately, experiments have not seen any primordial B-modes in the CMB [17].

From these parameters, only A_s and n_s are observed. Observations show that [14]

$$A_\mathrm{s} = (2.14 \pm 0.05) \cdot 10^{-9} \tag{3.38a}$$

$$n_\mathrm{s} = 0.9645 \pm 0.0049 \tag{3.38b}$$

$$r < 0.11 \tag{3.38c}$$

$$\alpha = -0.0057 \pm 0.0071 \tag{3.38d}$$

where the errors are 1σ, but the bound on r is the 95% confidence limit. This analysis assumed that the running of the running $\delta = \mathrm{d}\alpha/\mathrm{d}\log(k)$ is zero. The Planck satellite also considered the possibility of a nonzero running of the running, which was found to be nonzero at roughly 1σ. Thus with the current data the measurement of the running of the running is consistent with 0.

3.3.4 Signatures from multi-field inflation

Inflation scenarios where inflation is driven by multiple fields can generate specific features in the CMB. For instance perturbations orthogonal to the inflaton trajectory might generate so-called isocurvature modes. The propagation of these modes to the CMB depends on the background dynamics and a full analysis goes beyond this thesis, see for instance Ref. [45]. If isocurvature perturbations survive to the CMB they can be observed by a distortion of the peaks in the TT and EE power spectra, which have not been observed [14].

In addition, multi-field inflation models predict a larger contribution to non-Gaussian features in the CMB power spectrum [45]. These non-Gaussianities appear in the three-point function or bispectrum[4]. In the single field inflation paradigm the produced density fluctuations are very Gaussian, hence the bispectrum is mostly dominated by the contribution from the two-point function. If multiple fields drive the physics of inflation, larger non-Gaussianities can be produced. The measurements of the Planck satellite did not show any hints of non-Gaussianities in the CMB radiation [14], putting strong constraints on models with multiple fields.

In addition to multi-field inflation models, non-Gaussianities can also appear in single field models with higher derivative operators. These models can be distinguished from the multi-field inflation models by considering the shape in which the three-point function is maximal [45]. But, since in this thesis we will not consider

[4] Also higher point functions could be compared, but these are observationally much less constraint [14].

multi-field models or models with higher derivative operators, the full analysis is beyond the thesis.

3.3.5 Predictions of (single field) slow roll inflation

The historical reasons for assuming an inflation phase were explained above, being the horizon, the flatness and the monopole problems. In this section a few additional reasons for inflation will be phrased that use the current CMB observations.

In the derivation of the spectra, it was found that Δ_s^2 is related to the temperature power spectrum, while r is related to the B-mode power spectrum. However, no quantities were introduced to parametrize the E-mode power spectrum, nor to explain the spectrum of the ET cross-correlations. The reason is that if inflation took place, these spectra are fixed by the shape of the TT and BB spectra. The Planck satellite observed both the EE and TE spectra with high significance and the result shown in Figs. 3.5 shows the remarkable agreement between theory (the red line) and experiment (data points). The red line in the right frame of Figs. 3.5 is the prediction of ΛCDM with inflation, and is not a fit. That the line overlaps the data points so well is therefore a strong indication that the theory of inflation is correct.

Another prediction is a phase-coherence of the oscillations in the primordial plasma. The observed overdensities in the CMB are the correlated spectra of different sound waves. Due to inflation, all modes leave the horizon with the same phase. If the initial phases of the different sound waves was not coherent, the sum of the different modes would have averaged out so no anisotropies would be observed in the CMB. However, the anisotropies are observed, so the initial phases for the sound waves in the CMB have to be coherent [109].

For most modes observed in the CMB the acoustic peaks occur inside the horizon and there could be a causal mechanism that generates them. This is not the case for modes that are outside of the horizon. At the moment that the CMB is emitted, the electrons in the cosmic plasma behave as a fluid. Using energy conservation, the fluid equation for density perturbations is [109]

$$\dot{\rho} = -\vec{\nabla} \cdot (\rho \vec{v}) \,, \tag{3.39}$$

where $\vec{v}$ is the velocity of the electrons. This implies that the derivative of the monopole (left-hand site of Eq. (3.39)) equals the dipole. Since the temperature anisotropies produce monopole radiation, while E-mode polarization is a dipole, the TT power spectrum is a squared monopole, while the TE power spectrum will represent the signatures of the dipole spectrum. The temperature perturbations have a maximum at $l \approx 100$ in Fig. 3.3 and at this point the TE power spectrum is expected to be negative due to the minus sign in Eq. (3.39). This is indeed observed in Fig. 3.5b. Since for these small values of l the modes were not inside the horizon, some mechanism that sets the initial conditions of the anisotropies is necessary. Inflation is such a mechanism [109].

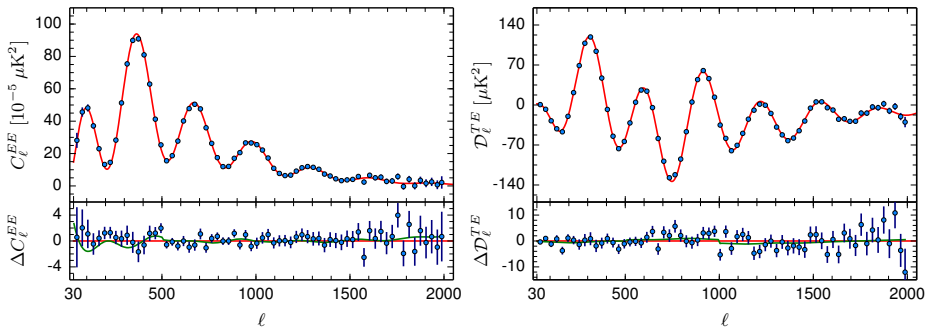

(a) (b)

Figure 3.5: *On the left the EE power spectrum and on the right the TE power spectrum, as measured by the Planck satellite [12]. The red line is the ΛCDM prediction.*

3.4 Selected inflation models

In the previous sections the requirements and the observables of inflation were studied. In the this sections a few selected inflation models will be discussed. For a more complete set of inflation models, see [110].

3.4.1 Quadratic inflation

The simplest inflation model is the model of a free massive scalar field. This model has a quadratic potential $V = \frac{1}{2}m^2\phi^2$ [111] and is a benchmark model which is studied in most reviews on inflation [45,112]. Quadratic inflation is closely related to the quartic potential first studied by Linde in [81], but quartic inflation is strongly excluded by the observations of n_s and r while quadratic inflation only mildly.

The potential slow roll parameters for quadratic inflation are obtained from Eq. (3.14)

$$\epsilon_\mathrm{V} = \eta_\mathrm{V} = \frac{2M_\mathrm{p}^2}{\phi^2}\,. \tag{3.40}$$

After the condition for the end of inflation inflation, $\epsilon_\mathrm{V}(\phi_\mathrm{end}) = 1$ and obtaining the number of e-folds N from Eq. (3.11), the observables A_s, n_s and r can be expressed in N using Eqs. (3.36)

$$n_\mathrm{s} = 1 - \frac{4}{2N+1}, \qquad r = \frac{16}{2N+1}, \qquad A_\mathrm{s} = \frac{(2N+1)^2}{12\pi^2}\left(\frac{m}{M_\mathrm{p}}\right)^2. \tag{3.41}$$

Note that n_s and r are independent of the overall scale m^2. This is a generic feature, since n_s and r depend, due to the structure of Eqs. (3.16) and (3.36), on ratios of the potential and its derivatives. The overall scale of the potential only enters through the size of the CMB anisotropies, A_s. Using that $A_s = 2.2 \cdot 10^{-9}$, the mass of the inflaton field is fixed to [45]

$$\left(\frac{m}{M_p}\right)^2 = \frac{12\pi^2}{(2N+1)^2} A_s \approx \left(7 \times 10^{-6} \left(\frac{50}{N_*}\right)\right)^2 . \tag{3.42}$$

Typically the number of e-folds is between 50 and 60, yielding a mass of the order of 10^{13} GeV, far from the range of current particle colliders. Unfortunately, for $N_* = 50 - 60$ the tensor to scalar ratio $r \approx 0.13 - 0.16$, which is in tension with current observations [17]. This is shown in Fig. 3.6, where the predictions from quadratic inflation are shown in black dots representing 50 (small dot) and 60 e-folds. Though the simplicity of quadratic inflation makes it a very pedagogical example, it is not realised in nature.

Quadratic inflation is an example of a model with a large field excursion [45]. For this set of models the field excursion during inflation $\Delta\phi = \phi_* - \phi_e > M_p$, where ϕ_e is the value of the field at which inflation ends. A super-Planckian field excursion poses problems related to the corrections of the effective theory, since the cutoff scale of any effective theory that does not take into account gravity is maximally the Planck scale. Generically operators of the form $\frac{\phi^{n+4}}{M_p^n}$ are expected, which will dominate over $\frac{1}{2}m^2\phi^2$ ruining the predictability of the theory. We will return to this issue in section 7.5.

3.4.2 Starobinsky inflation

Another relatively simple inflation model is a modification of gravity that was originally posed by Starobinky in [113] to study small deviations from general relativity. The action of this model is most elegantly written in the Jordan frame as

$$S_J = \frac{M_p^2}{2} \int \mathrm{d}^4x \, \sqrt{-g_J} \left(R + \frac{1}{6M^2} R^2\right) . \tag{3.43}$$

Due to the R^2 term, this action contains a metric and a scalar. The scalar degree of freedom can be made explicit by defining an auxiliary field ϕ with the classical equation of motion $\phi = R$ [114]

$$S_J = M_p^2 \int \mathrm{d}^4x \, \sqrt{-g_J} \left[\tfrac{1}{2}\left(1 + 2\beta\phi\right) R - \beta\phi^2\right] , \tag{3.44}$$

where $\beta \equiv 1/(6M^2)$. This auxiliary field is non-minimally coupled to gravity, but by performing a conformal transformation on the metric,

$$g^E_{\mu\nu} = \left(1 + 2\beta\phi\right) g^J_{\mu\nu} , \tag{3.45}$$

it becomes minimally coupled. In this frame, named the Einstein frame, the action is [115]

$$S_E = M_{\rm p}^2 \int {\rm d}^4x \, \sqrt{-g_E} \left[\tfrac{1}{2} R - \tfrac{1}{2} \left(\frac{6\beta^2}{(1+2\beta\phi)^2} \right) \partial_\mu \phi \partial^\mu \phi - \frac{\beta \phi^2}{(1+2\beta\phi)^2} \right], \quad (3.46)$$

which represents a scalar field coupled to a minimal theory of gravity. The slow roll parameters introduced in Eq. (3.14) were assuming a canonical kinetic term for the inflaton. With the field transformation $\chi = \sqrt{\frac{3}{2}} \log(1+2\beta\phi)$ the action is transformed to

$$S_E = M_{\rm p}^2 \int {\rm d}^4x \, \sqrt{-g_J} \left[\tfrac{1}{2} R - \tfrac{1}{2} \partial_\mu \chi \partial^\mu \chi + \frac{1}{4\beta} \left(1 - e^{-\sqrt{\frac{3}{2}}\chi} \right)^2 \right], \quad (3.47)$$

which has a canonical kinetic term.

Using Eq. (3.14) the CMB observables can be obtained. These are

$$n_{\rm s} = 1 - \frac{2}{N}, \qquad r = \frac{12}{N^2} \qquad A_{\rm s} = \frac{N^2}{72\pi^2 M_{\rm p}^2 \beta}, \quad (3.48)$$

where the parameters were expanded at leading order in $1/N$ and at leading order in slow roll. In Starobinsky inflation r is suppressed by an additional factor of $1/N$ compared to the quadratic model in Eq. (3.41). Due to this extra factor, the Starobinsky model is in perfect agreement with observations, as is shown in Fig. 3.6 where the Starobinsky model is represented with orange dots. Finally, the scalaron mass M is can be found from measurement of $A_{\rm s}$

$$M = 2.4 \cdot 10^{13} \text{ GeV} \frac{50}{N}, \quad (3.49)$$

which is, as was the case for quadratic inflation, far beyond reach for current collider experiments.

It is interesting to consider general $F(R)$ models, where $F(R)$ is an arbitrary function of R including the linear term [116,117]. When changing the power of the Starobinsky term, so that $F(R) = R + R^p$, then for $p < 2$ the potential typically becomes steeper, while increasing the power $p > 2$ generates a hilltop-like shape. A steep potential is disfavoured by the non-observation of r, and hilltop potentials have a too small $n_{\rm s}$, hence only the values $2 > p > 1.92$ are allowed [116, 117].

Another reason to investigate $f(R)$ theories is that these models are a candidate for dark energy. For solving the dark energy problem, the late-time (small R) force of gravity is modified by adding a term with $p < 0$. However, negative p implies early time singularities, which can be solved by adding a term $R^{p'}$ to $f(R)$, with $p' \approx 2$ [116].

3.4.3 Higgs inflation

Inflation is driven by a scalar particle, hence either a new particle has to be introduced as in quadratic inflation or modified gravity has to be considered as in Starobinsky inflation. But it is also possible to use the scalar from the standard model. As discussed in section 2.1, the standard model contains only one scalar field, the Higgs field, which is a natural candidate for inflation. Even before considering Higgs inflation, there is an important issue. When computing the running of the Higgs parameters, using the current measurements for the top quark mass, our current vacuum is metastable [118]. Hence, inflation will be running from a hill-top and the spectral index will be too small. Moreover, if inflation runs into the true minimum the potential becomes negative and the universe deflates. In this section we assume that the Higgs vacuum is stable.

The Higgs potential in unitary gauge is

$$V = m^2 h^2 + \lambda h^4, \tag{3.50}$$

where m is the Higgs mass and λ the self-coupling. At a large value of the Higgs field, the potential becomes λh^4 which corresponds to quartic inflation, which is completely ruled out by the data. In addition, the COBE measurement of A_s fixes $\lambda \approx 10^{-14}$, which is much smaller than the value deduced from the standard model masses, $\lambda_{SM} = 0.1$. The running of λ from energy scales of a GeV to the energy scale at which inflation is taking place might reduce λ, but to reach 10^{-14} will require considerable fine-tuning. Therefore, this implementation of Higgs inflation does not agree with the observed universe.

To solve these issues with Higgs inflation, Bezrukov and Shaposhnikov proposed in Ref. [119] to couple the Higgs field non-minimally to gravity. In unitary gauge the Jordan frame Lagrangian of the Higgs inflation model is

$$\mathcal{L}_J = \sqrt{-g_J}\left[\left(\tfrac{1}{2}M_{\mathrm{p}}^2 + \xi h^2\right) R_J + \partial_\mu h \partial^\mu h - V_J\right], \tag{3.51}$$

where the Jordan frame Higgs potential $V_J(h)$ is the potential defined in (3.50) and ξ is the coupling constant of the non-minimal coupling to gravity. As in the Starobinsky inflation scenario described above, the conformal transformation

$$g^E_{\mu\nu} = \left(1 + \frac{\xi h^2}{M_{\mathrm{p}}^2}\right)^2 g^J_{\mu\nu} \tag{3.52}$$

rotates the Lagrangian (3.51) to the Einstein frame, in which the Higgs field is non-minimally coupled to gravity. The Einstein frame Lagrangian of Higgs inflation is [119]

$$\mathcal{L}_E = \sqrt{-g_E}\left[\tfrac{1}{2}M_{\mathrm{p}}^2 R_E - \frac{1}{2\Omega^2}\left(1 + \frac{6\xi^2}{M_{\mathrm{p}}^2\Omega^2}h^2\right)\partial_\mu h \partial^\mu h - \frac{V_J(h)}{\Omega^2}\right], \tag{3.53}$$

where the Higgs field has a non-canonical kinetic term but is coupled minimally to gravity and we defined the frame function $\Omega \equiv (1 + \xi h^2/M_{\mathrm{p}}^2)$. The non-canonical

kinetic term can be removed with a field redefinition, which gives the canonical Einstein frame Lagrangian

$$\mathcal{L}_E = \sqrt{-g_J}\left[\tfrac{1}{2}M_{\rm p}^2 R_E + \partial_\mu\phi\partial^\mu\phi - \frac{\lambda M_{\rm p}^4}{4\xi^2}\left(1+e^{-\frac{2\phi}{\sqrt{6}M_{\rm p}}}\right)^{-2}\right], \tag{3.54}$$

where the Higgs mass term was neglected.

The value for ξ can be related to λ using the COBE normalisation $\xi \approx 49000\sqrt{\lambda}$. As explained in the introduction, the precise value of λ at the energy scale of inflation is not known, since the running of λ depends on physics between the LHC scale and the inflationary scale, but if $\lambda = \mathcal{O}(1)$ then $\xi \approx 5\cdot 10^4$ which is rather large. At leading order in $1/N$ and $1/\xi$, the observables $n_{\rm s}$ and r are [119]

$$n_{\rm s} = 1 - \frac{2}{N}\,, \qquad r = \frac{12}{N^2}\,, \tag{3.55}$$

which are the same as in Starobinsky inflation (3.48).

Higgs inflation has the nice feature that it fits extremely well with the data, while due to its embedding in the standard model it is also very well motivated. However, the large non-minimal coupling term that enters in the Higgs potential raised questions related to unitarity [120, 121]. Though some studies showed that there was a problem with perturbative unitarity during Higgs inflation, mainly caused by a mixing of the kinetic terms of the different components of the Higgs multiplet [122, 123], this has been under debate [124, 125]. Recently, the unitarity problem was studied in Refs. [126, 127] and these authors showed that Higgs inflation is unitary. The reason of that unitarity is maintained in Higgs inflation is that in the limit $h \to \infty$ the theory is conformal. This approximate conformal symmetry is not only the basis of the success of Higgs inflation, but will also appear in the attractor theories that we will study in section 6.2.

As will be shown in section 6.2, Higgs inflation is a realisation of a set of models called the strong coupling attractors. The interesting feature of strong coupling attractor models is that the results for $n_{\rm s}$ and r are independent of the specific model. Due to this attractor behaviour the Higgs inflation model will be insensitive to small corrections, for instance in Ref. [128] it was shown that Higgs inflation is insensitive to logarithmic corrections to the potential, which often appear in perturbation theory.

To conclude, there is another proposal for Higgs inflation. In this scenario the Higgs field is coupled non-minimally to the Einstein tensor $G_{\mu\nu}$ [129, 130]

$$\mathcal{L} = \frac{M_{\rm p}^2}{2}R - \left(g_{\mu\nu} - \omega^2 G_{\mu\nu}\right)\partial^\mu h\partial^\nu h - \lambda h^4\,, \tag{3.56}$$

where for inflation to be valid, $\frac{M_{\rm p}^2}{\omega} \approx 8\cdot 10^{-8}$. This inflation scenario has good observational features, but the asymptotic scale invariance that characterizes Higgs

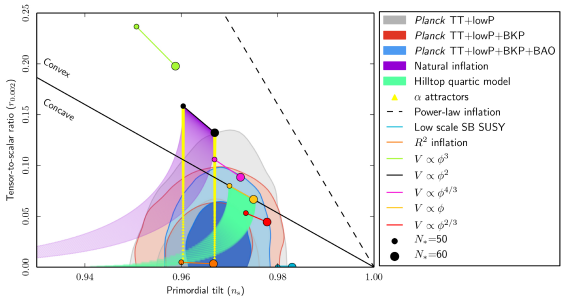

Figure 3.6: *Experimental constraints from the Planck 2015 paper [14], together with some inflation models. The black dots correspond to quadratic inflation, the orange dots to Starobinsky (R^2) inflation, Higgs inflation and the strong coupling attractor. The yellow lines interpolating between the black and orange dots is the α-attractor model for different values for α. The strong coupling attractor and the α-attractor will be discussed in section 6.2.*

inflation has not been identified. It is therefore questionable if small quantum corrections do not pose a problem to this scenario [125].

The problem that the Higgs vacuum is likely metastable is haunting both models. Typical solutions to this issue involve adding additional particles to the spectrum, however this solutions break the minimality of Higgs inflation [131–135].

3.4.4 Multi-field inflation

Finally there is active ongoing research on inflation with multiple scalar fields. In general, this research can be divided in four categories, with increasing importance of the additional fields. The orthogonal fields only play a minor role in the theory of hybrid inflation [80], in which there are one or multiple additional fields which end inflation immediately after they become dynamical. The second category are the curvaton models [136, 137], where the curvature perturbations are generated by another field than the field that generates the expansion of the universe. The third category are models with a modest number of extra fields, which can still be computed analytically or with numerical tools similar to the ones that will be described in section 4.3 [138–140]. Finally, interesting developments were made in the theory of inflation with a sufficient number of fields that the Hessian matrix could be generated with random matrix theory [141–143].

Evidently, the idea of adding additional fields to the inflationary sector is well motivated, as most high-energy extensions of the standard model require additional scalar fields. However, adding more fields also complicates the model, generating new observable features as discussed in section 3.3.4. The most important addi-

tional observables are the bispectrum and isocurvature modes. The bispectrum is defined by the CMB three-point function, which obtains a contribution from the Gaussian two-point function plus a term originating from non-Gaussianities parametrized by $f_{\rm NL}$. For single field slow roll inflation $f_{\rm NL}$ is proportional to the slow roll parameters [144–146] and very small, but for multi-field inflation non-Gaussianities can be considerably larger. Observationally, the Planck satellite did not observe any non-Gaussianities [57], putting the limit $|f_{\rm NL}| < 5$, [5] concluding that there is no evidence for additional fields.

3.5 Reheating

After inflation ended was the universe extremely cold and very empty except for the inflaton field that permeated it. Since our current universe is neither (that) cold nor empty, some process after inflation generated a hot and dense thermal bath. This mechanism is named reheating, and will be discussed in this section. This analysis will be relevant in chapter 8, while for considering the generic inflationary behaviour analysed in chapters 5 until 6 the reheating era will be ignored.

Since reheating is a vast domain of research, only some properties will be highlighted that are relevant for this thesis. In the following, first the main physics during reheating will be reviewed, resulting in the reheating temperature. Than will be explained how reheating determines the number of e-folds during inflation, and we finish with some comments concerning dark matter production related to the reheating era. For more information on reheating, see Refs. [147–149].

A quick summary of the reheating phase of the universe is as follows. After inflation ended the universe was still quickly expanding and while the universe is expanding faster than the inflaton decays, the universe is inflaton dominated. When the expansion of the universe cannot keep up with the decay time of the inflaton, the inflaton condensate that permeates the universe quickly decays, generating a large number of particles. These particles thermalize and generate a thermal plasma which continues with the evolution of the universe explained in section 2.5.

By definition, reheating started at the end of inflation. After inflation ended, the inflaton moved to the minimum of its potential. The equation of motion of the inflaton Eq. (3.6b) represents a damped oscillator with the damping term given by H. It follows that if H is smaller than the effective mass of the inflaton $m_{\rm eff}^2 = V''(\phi)$, the inflaton oscillates around its minimum. During these oscillations the decay of the inflaton generates an additional damping term, and Eq. (3.6b) is modified to [149]

$$\ddot{\phi} + (\Gamma + 3H)\dot{\phi} + V'(\phi) = 0\,, \tag{3.57}$$

where Γ is the total decay width of the inflaton.

[5] Though the bound can be considerably weaker depending on the shape of the triangle in which the three-point function is evaluated.

As was shown in section 2.3, the quantity that determines the dynamics of the universe is the equation of state. During reheating, the equation of state is not constant, but changes from $w_{\rm end} = 1$ when inflation ended to $w_{\rm reh} = 1/3$ at the onset of the radiation era. Fortunately, for the computations of interest in this section only the equation of state averaged over the reheating era [150]

$$\bar{w} = \frac{1}{\Delta N_{\rm reh}} \int_{N_{\rm end}}^{N_{\rm reh}} \frac{P(n)}{\rho(n)} \mathrm{d}n \tag{3.58}$$

is relevant, where $\Delta N_{\rm reh} = N_{\rm reh} - N_{\rm end}$ is the number of e-folds the universe expanded during reheating, with $N_{\rm end}$ the number of e-folds at the end of inflation. As in most of this thesis, we will set $N_{\rm end} = 0$. In Ref. [151] it was found that $\bar{w}$ is dominated by the potential of the inflaton at the end of reheating. When Taylor expanding the potential around the minimum to lowest order $V = V_0 + \lambda\phi^p + \mathcal{O}\left(\phi^{p+1}\right)$, the average equation of state is [151]

$$\bar{w} = \frac{p-2}{p+2} \,. \tag{3.59}$$

In many models of inflation, the inflaton has a mass term and $p = 2$, hence $\bar{w} = 0$. This result is expected since if the inflaton is much heavier than the Hubble function the inflaton acts as non-relativistic matter which has a vanishing equation of state parameter.

The maximal temperature of the plasma during the radiation dominated era ($T_{\rm reh}$) is related to the moment reheating ended, which is defined as the moment at which [149, 152]

$$H_{\rm reh} = \Gamma \,, \tag{3.60}$$

where the subscript reh is used for quantities at the moment reheating ends. From the Friedmann equation (2.16) and the Planck equation (2.19) the reheating temperature can be obtained for a universe with vanishingly small cosmological constant and curvature. Assuming that the universe thermalized instantaneously follows that

$$T_{\rm reh}^2 = \sqrt{\frac{90}{\pi^2 g_*}} \Gamma M_{\rm p} \,, \tag{3.61}$$

where g_* represents the number of relativistic degrees of freedom at the moment of reheating. If at the moment of reheating only the standard model particles are in the thermal plasma, $g_* = 106.75$ [70], but if more particles are added (i.e. supersymmetry), the number of relativistic degrees of freedom is larger.

The value of the reheating temperature of the universe depends on the interactions of the inflaton with matter. Since the reheating temperature is the maximal temperature the universe reaches during the radiation dominated era, it should be above the temperature of the known processes of section 2.5. This means that the reheating temperature has to be at least above the temperature of nucleosynthesis

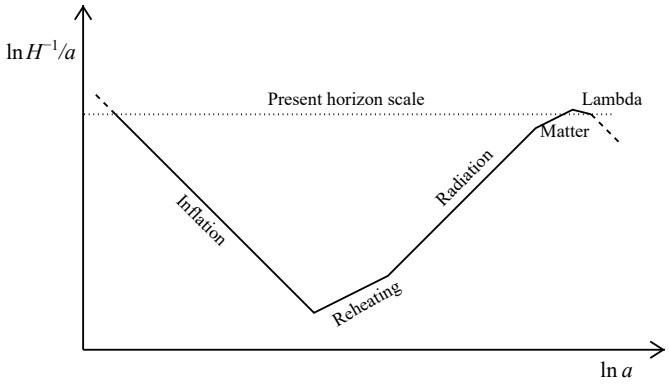

Figure 3.7: *Evolution of the Hubble sphere including reheating. The horizontal axis shows the number of e-folds $N \propto \ln a$, hence if the inflation and reheating phases are understood, the number of e-folds between the end of inflation and the current horizon size can be obtained. Figure from [147].*

at $T \approx 10$ MeV [153,154]. This is the weakest bound on the reheating temperature, while a stronger bound can be defined by demanding that the reheating temperature is above the typical temperature of baryogenesis, when the current unbalance between matter and anti-matter was generated, which is at 10^{10} GeV. However, since the mechanism of baryogenesis is unknown, it could have occurred at a much lower temperature. Therefore, in this thesis the weak bound $T_{\rm reh} > 10$ MeV will be used.

The importance of studying the era of reheating is that it is the only remaining unknown phase of the universe. Therefore, if reheating is understood the size of the CMB anisotropies can be mapped to a moment during inflation [147]. This is shown in Fig. 3.7, where the solid line represents the horizon size at a certain moment, while the dotted line represents a perturbation with the size of the current universe. The number of e-folds during inflation (N_k) is related to the distance that a mode with wavelength k has moved outside of the Hubble sphere before inflation ended. Afterwards the Hubble sphere expands and the mode will start to enter the horizon again. The amount of expansion of the universe after inflation ended is therefore related to the number of e-folds during inflation.

The average speed of the expansion during reheating, which is the slope of the line in Fig. 3.7, is given by $\bar{w}$. For a given inflation model and given reheating model, parametrized by $T_{\rm reh}$ and $\bar{w}$, the number of e-folds during inflation can be found. Using that the amount the universe expanded during reheating can be parametrized by the number of e-folds

$$e^{N_{\rm reh}} = \frac{a_{\rm reh}}{a_{\rm end}} \tag{3.62}$$

and with some mathematics, explained for instance in Refs. [147,155], the number of e-folds during inflation N_* is

$$N_* = \frac{1}{4}N_{\rm reh} - \log\left(\frac{k}{a_0 T_0}\right) - \frac{1}{4}\log\left(\frac{30}{g_*\pi^2}\right) - \frac{1}{3}\log\left(\frac{11g_*}{43}\right) - \frac{1}{4}\log\left((1+\lambda)\frac{V_{\rm end}}{M_{\rm p}^4}\right) + \frac{1}{2}\log\left(\frac{\pi^2 r A_{\rm s}}{2}\right), \tag{3.63}$$

where λ is the ratio of kinetic to potential energy at the end of inflation. If inflation ends with $\epsilon_{\rm H} = 1$, then $\lambda = 1/2$. Furthermore, the number of e-folds during reheating can be obtained from combining the reheating temperature [155]

$$T_{\rm reh} = \left(\frac{3(1+\lambda)}{10\pi^2}\right)^{1/4} V_{\rm end}^{1/4} e^{-\frac{3}{4}(1+\bar{w})N_{\rm reh}}\,. \tag{3.64}$$

with Eq. (3.61).

With the sensitivity of the current CMB experiments, computing the reheating temperature is only marginally relevant since the experimental errors on $n_{\rm s}$ and r are usually larger than the spread of roughly 10 e-folds induced by reheating, as can be seen in Fig. 3.6. However, if in the future the experimental data becomes better, calculating the number of e-folds using reheating might become a necessary analysis for comparing inflation models with the data [150, 156]. This will be demonstrated in the model obtained in chapter 8, for which the predictions are similar to the predictions of Starobinsky inflation in Eq. (3.48) but since $N_* \approx 48$–49 they are in the 2σ region of the Planck measurements.

The theory of reheating is in full generality more complex than described above. An important aspect that was not mentioned above is that for some theories it is possible that during the first oscillations of the inflaton field a large number of particles is produced due to non-perturbative effects when the field crosses the origin of the potential [148, 149, 157–159]. This effect is named parametric reheating, or preheating, and it can be sufficiently strong that reheating ends with this process. Though potentially relevant, the preheating era will not be considered in this thesis.

The reheating era is also of potential interest for solving the dark matter problem. If the inflaton decayed into the dark matter particle, a substantial part, even all, of the dark matter density could have been produce during reheating [160,161]. As described in section 2.6, the dark matter density is defined with the yield $Y \equiv n_X/s$, which is the dark matter number density over the entropy density. The dark matter yield from inflaton decay is [160, 161]

$$Y = \frac{3T_{\rm reh}}{4m_\phi}\frac{2\Gamma_{\phi\to XX}}{\Gamma_\phi}\,, \tag{3.65}$$

where $\Gamma_{\phi\to XX}$ is the partial decay width of the inflaton into dark matter particle X and Γ_ϕ the total inflaton decay width. The ratio $\Gamma_{\phi\to XX}/\Gamma_\phi$ is also known

as the branching ratio of ϕ to XX. The total number density of dark matter can be obtained from Eq. (2.31). This is irrelevant if the dark matter is strongly interacting with the thermal bath, since in that scenario the current dark matter abundance is obtained by the freeze-out process. However, if the dark matter does not interact with the thermal bath, the density of dark matter obtained from inflaton decay must be the current dark matter density unless a freeze-in process occurred after reheating that increased it.

If all dark matter originates from inflaton decay it can be boosted with respect to the thermal plasma. This is an important difference with dark matter produced from freeze-out, because then the dark matter particles are produced in the rest frame of the universe. Boosted dark matter is distinguishable from non-boosted dark matter since it has a higher temperature, which will wash out structures in the universe. This scenario was investigated in Ref. [161] using the parametrization

$$X_{\text{FS}} = \frac{2m_X}{\epsilon m_\phi}\sqrt{\frac{\sqrt{3}\Gamma}{z_{\text{eq}}H_0}}\,, \tag{3.66}$$

where z_{eq} is the red-shift at matter-radiation equilibrium and ϵ a factor depending on the energy fraction given to the dark matter particles if the decay of the inflaton is towards a dark matter and a bath particle. In the standard scenario where the inflaton decays into two dark matter particles, $\epsilon = 1$. The free streaming length of dark matter can be written in terms of X as [161]

$$\lambda_{\text{FS}} = \frac{1}{H_0\sqrt{1+z_{\text{eq}}}}X^{-1}\sinh^{-1}X\,. \tag{3.67}$$

Observations of the Lyman-α lines in the universe show that $\lambda_{\text{FS}} < 1$ Mpc, which implies that $X > 450$.

In addition, the decay of the inflaton field is a stochastic process, hence part of the inflaton field decayed before the end of reheating, generating a thermal plasma if thermalization is faster than the inflaton decay. This does not affect the evolution of the universe, since the energy density of the inflaton field exceeded the energy density of the plasma. However, freeze-out and freeze-in can occur in this radiation bath during reheating [162]. The density of dark matter in such a scenario is reduced with respect to the scenario that the universe is radiation dominated. This has two reasons, first the amount of radiation during the reheating era was smaller than during the radiation dominated era. Secondly, during a matter dominated reheating era the dark matter behaved as a radiation component, therefore its energy density decreases faster than the energy density of the inflaton, which later becomes the energy density of visible matter. Therefore, this phase will be neglected in the analysis of gravitino dark matter in chapter 8. That this might be a relevant effect is shown in Refs. [162–165], while in the scenario in Ref. [166] the effect was negligible.

Finally, when the freeze-in dark matter was introduced in section 2.6, it was assumed that the initial abundance of dark matter in the universe was negligibly

small. This was actually a statement about reheating, since it implies that the dark matter particle is very weakly coupled to the inflaton, so that reheating does not produce a large dark matter abundance. This might not be the generic situation. For instance, in chapter 8 we will consider a model with a dark matter particle for which the dark matter abundance is obtained both through inflaton decay and through freeze-in. Another example is shown in Ref. [167].

CHAPTER 4

Flows

Introduction

The theory of inflation developed in the previous chapter proposes candidate theories for the UV-completion of the standard model. A few examples of inflation models are given in section 3.4. However this section does not include all inflation models, see for instance Ref. [110] for more than a hundred additional inflation models. To investigate which type of inflation models are compatible with the data, and can therefore be part of a high energy completion of the standard model, all inflation models can be compared on a case-to-case study, as was done in Refs. [110, 150, 168, 169]. However, the vastness of inflation models makes this approach difficult.

In this thesis another strategy will be followed, which is to study generic results for a given parametrization of inflation models. There are two directions for this study. The first is to consider a large set of arbitrarily generated inflation models, as was first investigated by Hoffman, Turner and Kinney in Refs. [89,170]. The second direction is to study inflationary attractors, which have their generic predictions built-in.

In this chapter the first approach to generic inflation models, utilizing random inflation models, will be reviewed. For this purpose, sections 4.1 and 4.2 will be dedicated to generic slow roll parameters. In this section the Hubble slow roll parameters in Eqs. (3.10) and (3.12) will be extended similarly to the potential slow roll parameters of Eqs. (3.16). Using these slow roll parameters, in section 4.3 the inflationary flow code of Kinney [170] will be introduced and compared with

the data. Afterwards, in section 4.4, this code will be improved following an idea of Ramirez and Liddle in Refs. [171,172]. This last code is simpler when evaluating inflation models with generic Hubble functions, and will be used in chapters 5 and 6.

The analysis of the Hubble flow code will be continued in chapter 5, where another parametrization of inflation models will be considered and an analytical tool will be developed to solve the flow equations analytically. Afterwards, in chapter 6, a similar code as developed in section 4.4 will be used to study the strong coupling attractor model.

The final section of the present chapter, section 4.5, will be dedicated to parametrizing inflation with only geometric quantities, hence without the inflaton field. This section combines literature and unpublished research performed with Diederik Roest and Marco Scalisi.

4.1 Relations between the slow roll parameters

In section 3.2, two sets of slow roll parameters were defined, the Hubble slow roll parameters in Eqs. (3.10) and (3.12) and the potential slow roll parameters in Eqs. (3.16). Note that the definition of the latter included a set of infinite parameters, while for the former only the first two slow roll parameters were defined. This was not problematic in the analysis of chapter 3, since only the potential slow roll parameters were used.

In this section two extensions of ϵ_{H} will be provided, which will be used in the remainder of this chapter and in chapter 5 to make general predictions of inflation. In addition, this section will close with an observation on the parametrization of inflation, that might be of use for the interpretation of these sections.

4.1.1 Slow roll parameters

The first complete set of Hubble slow roll parameters are obtained similar to the potential slow roll parameters in Eq. (3.16), by acting with higher order derivatives on the Hubble parameter [83,170]

$$\epsilon_{\mathrm{H}} = -\frac{\dot{H}}{H^2} = 2M_{\mathrm{p}}^2\left(\frac{H'(\phi)}{H(\phi)}\right)^2, \tag{4.1a}$$

$${}^{n}\lambda_{\mathrm{H}}(\phi) \equiv \prod_{i=1}^{n}\left[-\frac{\mathrm{d}\log H^{(i)}(\phi)}{\mathrm{d}\ln a}\right] = \left(2M_{\mathrm{p}}^2\right)^n \frac{H'(\phi)^{n-1}H^{(n+1)}(\phi)}{H(\phi)^n}, \tag{4.1b}$$

where primes in this chapter refer to taking the derivative with respect to the inflaton field ϕ, $H^{(n+1)}(\phi)$ represents $\frac{\mathrm{d}^{n+1}H(\phi)}{\mathrm{d}\phi^{n+1}}$ and ${}^{1}\lambda_{\mathrm{H}} = \eta_{\mathrm{H}}$.

For the slow roll approximation to be valid, it is required that $|{}^{n}\lambda_{\mathrm{H}}| < |{}^{n-1}\lambda_{\mathrm{H}}|$. However, note that the slow roll approximation is not required for the computation

of the end of inflation or the number of e-folds. Only in the derivation of the power spectrum of the CMB, the Mukhanov equation (3.33) is solved order by order in slow roll. This analysis was done for the power spectrum of the CMB at second order in slow roll in Refs. [173,174], leading to

$$\begin{aligned} n_{\mathrm{s}} &= 1 + 2\eta_{\mathrm{H}} - 4\epsilon_{\mathrm{H}} - 8\epsilon_{\mathrm{H}}^2(1+C) + 2\epsilon_{\mathrm{H}}\eta_{\mathrm{H}}(3+5C) - 2C\left({}^2\lambda_{\mathrm{H}}\right), \\ r &= 16\epsilon_{\mathrm{H}}\left(1 + 2C(\epsilon_{\mathrm{H}} - \eta_{\mathrm{H}})\right), \end{aligned} \tag{4.2}$$

where $C \equiv \gamma_{\mathrm{E}} + \ln 2 - 2 \simeq -0.7296$ and γ_{E} is the Euler constant. Also higher order expressions are known, see for instance Refs. [174,175], but these expressions will not be used in this thesis.

During inflation, the Hubble slow roll parameters are obviously not constant. Their dynamics is determined by the flow equations [170]

$$\frac{\mathrm{d}\epsilon_{\mathrm{H}}}{dN} = 2\epsilon_{\mathrm{H}}(\eta_{\mathrm{H}} - \epsilon_{\mathrm{H}}), \tag{4.3a}$$

$$\frac{\mathrm{d}\eta_{\mathrm{H}}}{dN} = -\epsilon_{\mathrm{H}}\eta_{\mathrm{H}} + {}^2\lambda_{\mathrm{H}}, \tag{4.3b}$$

$$\frac{\mathrm{d}({}^n\lambda_{\mathrm{H}})}{dN} = \left[(n-1)\eta_{\mathrm{H}} - n\epsilon_{\mathrm{H}}\right]{}^n\lambda_{\mathrm{H}} + {}^{n+1}\lambda_{\mathrm{H}}, \tag{4.3c}$$

which are found using the definitions of the slow roll parameters and the Eqs. (3.9). In Eqs. (4.3) the number of e-folds $N \equiv -\log(a/a_{\mathrm{end}})$ replaces the notion of time, and decreases when time proceeds. Solving the flow equations will be one of the main topics of this chapter and the next.

It is possible to define another set of slow roll parameters for which the flow equations are simpler. These parameters are known as the horizon flow functions and are defined in Refs. [176,177] as satisfying the flow equations

$$\epsilon_0 \equiv \frac{H}{H_0}, \quad \frac{\mathrm{d}\epsilon_n}{\mathrm{d}N} = \epsilon_n\epsilon_{n+1}\,, \tag{4.4}$$

where H_0 is a (constant) reference value. It is straightforward that $\epsilon_1 = \epsilon_{\mathrm{H}}$, but the higher order terms will be different from the λ_{H} hierarchy. These functions can be written in terms of the Hubble function $H(\phi)$ and its derivatives. For the lowest order ϵ_n parameters, one has

$$\epsilon_1 = 2M_{\mathrm{p}}^2\left(\frac{H'}{H}\right)^2, \tag{4.5a}$$

$$\epsilon_2 = 4M_{\mathrm{p}}^2\left[\left(\frac{H'}{H}\right)^2 - \frac{H''}{H}\right], \tag{4.5b}$$

$$\epsilon_3 = 2M_{\mathrm{p}}^2\left[2\left(\frac{H'}{H}\right)^2 + \frac{H'''}{H'} - 3\frac{H''}{H}\right]\left(1 - \frac{HH''}{H'^2}\right)^{-1}. \tag{4.5c}$$

For the horizon flow functions to converge, all ϵ_n have to be smaller then 1, but there is no intrinsic hierarchy between the different orders. The parameter ϵ_n will only appear with terms of order $n-1$ in slow roll. Therefore, $n_{\rm s}$ and r can be expanded to second order in this frame as [174]

$$\begin{aligned} n_{\rm s} &= 1 - 2\epsilon_{1*} - \epsilon_{2*} - 2\epsilon_{1*}^2 - (2C+3)\epsilon_{1*}\epsilon_{2*} - C\epsilon_{2*}\epsilon_{3*}\,, \\ r &= 16\epsilon_{1*}\left(1 + C\epsilon_{2*}\right)\,. \end{aligned} \tag{4.6}$$

4.1.2 Frames of inflation models

The different parametrizations introduced above are related to different frames in which inflation can be described. The Hamilton-Jacobi frame defined in section 3.2.2 corresponds to the $\lambda_{\rm H}$ and ϵ_i parametrizations of Eqs. (4.1) and (4.4). This frame is natural from a geometric point of view, since the Hubble function is directly related to the scale factor. The other popular frame is the potential frame where the most natural slow roll parameters are the potential slow roll parameters of Eq. (3.16).

Both frames describe the same physical system, hence if the slow roll approximation is not applied the predictions are the same. However, at finite order in slow roll the two sets of slow roll parameters will yield different predictions. The simplest example is the end of the phase of slow roll inflation. In Ref. [83] is shown that the relation $\epsilon_{\rm H} \approx \epsilon_{\rm V}$ has corrections of order ϵ_V^2. Therefore, at the end of slow roll, where $\epsilon_{\rm V} = \mathcal{O}(1)$, the condition $\epsilon_{\rm V} = 1$ for the end of inflation is ambiguous. The standard lore is to impose in addition the constraint $|\eta_{\rm V}| = 1$, which indeed often signals the end of inflation.

Other approaches to relate the two slow roll parameters were to use a Padé approximant in Ref. [83] or a central manifold extension in Ref. [178]. Despite the interesting results of these groups, in this thesis we will be using $\epsilon_{\rm V} = 1$ as the end of inflation. The reason is that the number of e-folds defined in Eq. (3.11)

$$N = \int_{\phi_{end}}^{\phi} \frac{{\rm d}\phi}{M_{\rm p}\sqrt{2\epsilon_{\rm H}(\phi)}}\,, \tag{4.7}$$

gets its main contribution from regions where $\epsilon_{\rm H} \ll 1$, hence where slow roll is expected to be valid. The error made due to mistaking the end of inflation is therefore typically less than one e-fold, which is subleading to the error in the number of e-folds originating from reheating, which is roughly 10 e-folds [147]. Moreover, posing the condition $\epsilon_{\rm V} = 1$ is much simpler, and faster, than considering a Padé approximant or a center manifold extension.

Inflation can also be parametrized solely by $\epsilon_{\rm H}$ [179], which we will call the $\epsilon_{\rm H}$ frame. This frame is most obvious for analysing inflation, since $\epsilon_{\rm H}$ defines when inflation is taking place, but the physical origin is less obvious. A well-known example of the $\epsilon_{\rm H}$ frame is when inflation is described as an imperfect fluid. The

equation of state w of the imperfect fluid is related to $\epsilon_{\rm H}$ from Eq. (3.7)

$$w = \frac{2}{3}\epsilon_{\rm H} - 1\,, \tag{4.8}$$

and is used to define the inflation phase for these models. Another example of the $\epsilon_{\rm H}$ parametrization is when inflation is modelled as the renormalization group flow of a dual conformal field theory using dS/CFT. In this case the β function of the CFT is dual to $-2M_{\rm p}H'(\phi)/H(\phi) = \pm\sqrt{2\epsilon_{\rm H}}$ [180]. The arbitrary sign in the last equality follows from the square in the definition of $\epsilon_{\rm H}$.

In principle all three frames can be used to generically model inflation. However, the most natural choice is the Hubble frame, since this corresponds most clearly to physics while the slow roll assumption does not have to hold during inflation. Therefore, in this chapter the Hubble slow roll parameters will be used to compute arbitrary inflation models.

4.2 Flow equations

To study generic models of inflation, as will be done explicitly in the next section, the flow functions of Eqs. (4.3) or (4.4) can be studied. In this section the Hubble slow roll equations of Eq. (4.3) will be chosen, though a similar analysis can be performed with the flow functions.

The Eqs. (4.3) make up a set of first order differential equations and before trying to solve this dynamical system, it is customary to perform a fixed point analysis. The system (4.3) has two fixed points [170, 181],

1. The $r = 0$ fixed point, with $\epsilon_{\rm H} = {}^{n}\lambda_{\rm H} = 0$ and $\eta_{\rm H}$ is constant.
2. The power law fixed point, where $\epsilon_{\rm H} > 0$, $\eta_{\rm H} = \epsilon_{\rm H}$, ${}^{2}\lambda_{\rm H} = \epsilon_{\rm H}\eta_{\rm H}$ and ${}^{n+1}\lambda_{\rm H} = \epsilon_{\rm H}({}^{n}\lambda_{\rm H})$. This fixed point represents power law inflation where $H \propto e^{\kappa\phi}$.

Physically, the $r = 0$ fixed point corresponds to an extremum of the Hubble function where inflation lasts forever. The power law attractor corresponds to the situation where the potential is strongly increasing, like a quadratic Hubble function at large ϕ.

The signs of the eigenvalues of the Hessian matrix of Eqs. (4.3) correspond to the linear stability of the system. If all eigenvalues are positive the fixed point is an attractor, while if the eigenvalues are negative the fixed point is repulsive. The sign convention is because an attractor fixed point is defined here as an attractor at late time, hence for small N. At the $r = 0$ fixed point the eigenvalues are proportional[1] to η. Therefore, this fixed point is a late-time attractor if $\eta > 0$ [170, 181]. For the power law fixed point the eigenvalues are all negative, hence this is an early time

[1] There is also a zero eigenvalue, but since the eigenvector corresponding to this eigenvalue is orthogonal to the flow of ϵ this is not considered.

fixed point. Therefore inflation will generically flow from a power law fixed point or from the $r = 0$ fixed point with $\eta < 0$ in the past to the $r = 0$ fixed point in the future. Hence we can postulate that generically inflation will move from a power law fixed point to an $r = 0$ fixed point.

Below we will continue with solving the flow equations numerically. In chapter 5 the system of flow equations will be reconsidered, where we will obtain an analytic solution for the dynamical system.

4.3 Monte Carlo inflation: The Hubble flow code

Having solved the asymptotic dynamics of the flow equations, numerical techniques can be used to completely solve them for given initial conditions. In this section, this analysis will be used to obtain generic predictions based on the Hubble slow roll parameters defined in Eq. (4.1). The motivation of this analysis is that the physics that drives inflation is completely unknown. Instead of proposing some theory that includes inflation, we will assume that the Hubble function induced by the new physics is some complicated unknown function of the inflaton field, but at some point during the evolution of inflation the slow roll conditions are satisfied. Then, using the flow equations in Eqs. (4.3), the predictions of this unknown theory are obtained. With the Hubble flow code a large set of these theories can be considered, and generic predictions studied.

In section 4.1 we defined a natural hierarchy of slow roll parameters in Eqs. (4.1) and (4.3). Using the hierarchy of Eqs. (4.1), Kinney in Ref. [170] introduced the Hubble flow code to study the general inflationary predictions from a large number of randomly generated inflation models. In this algorithm, named the inflationary flow code, a value for $\epsilon_{\rm H}$, $\eta_{\rm H}$ and ${}^n\lambda_{\rm H}$ is chosen randomly from a prior distribution function, typically chosen as [170, 182, 183]

$$\epsilon_{\rm H} \in [0, 0.8], \tag{4.9a}$$

$$2\eta_{\rm H} - 4\epsilon_{\rm H} \in [-0.5, 0.5], \tag{4.9b}$$

$${}^n\lambda_{\rm H} \in [-5/10^n, 5/10^n], \tag{4.9c}$$

where [.] corresponds to a flat interval and the combination of $\epsilon_{\rm H}$ and $\eta_{\rm H}$ in the second line represents $n_{\rm s}$ at first order in slow roll. Other intervals have been studied in [172, 184, 185], with only minor changes in the observations. Due to the falloff of the priors for the higher slow roll parameters, the system is saturated at sixth order. This implies that the observables do not significantly change when considering sixth or seventh order in the slow roll hierarchy of Eqs. (4.9). In this chapter we will consider ${}^n\lambda_{\rm H} = 0$ for $n \geq 10$. Note that the derivative of ${}^n\lambda_{\rm H}$ in (4.3c) is proportional to ${}^n\lambda_{\rm H}$ and ${}^{n+1}\lambda_{\rm H}$, so during inflation the truncation ${}^n\lambda_{\rm H} = 0$ for $n > N$ is conserved.

By drawing the slow roll parameters the inflation model is prepared at a special location $\phi_{\rm ex}$ in a potential $V(\phi)$. Numerically, the end of inflation is then found

using the flow equations for the slow roll parameters of Eqs. (4.3). Then the flow equations can be solved without explicitly determining neither $\phi_{\rm ex}$ nor $V(\phi)$.

For the end of inflation there are three possibilities: either inflation moves to $\epsilon_{\rm H} = 1$ where inflation ends, the parameter $\epsilon_{\rm H}$ approaches 0 and inflation does not end, or it stays between 0 and 1 during the evolution of the numerical code. The second late-time behaviour corresponds to the $r = 0$ attractor, while the last ending will usually be a numerical artefact. After finding the end of inflation, the flow equations (4.3) can be used to trace back the inflation model for N_* e-folds and if $\epsilon_{\rm H} < 1$ along this flow, observables like the scalar spectral index and the tensor to scalar ratio can be calculated. This gives the following possible outcomes for the inflationary flow code [170]

1. Inflation ends at the bottom of the scalar field potential in the late-time fixed point with $\epsilon_{\rm H} = 0$, hence inflation does not have a graceful exit. In the fixed point inflation can end by activation of an additional field, as in hybrid inflation [186]. Since at the end of inflation $\epsilon_{\rm H}$ is still small, we assume that N_* is reached at the minimum of the potential and $n_{\rm s}$ and r are calculated at this point. At the fixed point $\eta > 0$, hence $n_{\rm s} > 1$. Since this is strongly excluded by the Planck data this scenario will not be considered[2].

2. During the numerical evolution $\epsilon_{\rm H}$ reaches neither 0 nor 1 within some fixed number of e-folds. Since we do not want to continue these trajectories too long, the configuration is stopped.

3. Inflation ends, but $\epsilon_{\rm H}$ becomes 1 before N_*. These trajectories do not have enough e-folds to explain the anisotropies in the CMB and are disregarded.

4. Inflation ends, and $\epsilon_{\rm H} < 1$ for at least N_* before this. Using Eq. (4.1) the observables $n_{\rm s}$ and r are computed at N_*. In this chapter we will use $N_* = 50$.

As can be understood from the fixed point analysis, the most generic outcome of polynomial inflation is scenario 1 in which inflation does not terminate. Using the method described above, a large ensemble of points was generated and Table 4.1 provides the probability for the different outcomes. Indeed, by far the most likely outcome is that inflation does not terminate. The probability of a viable single field inflation scenario is about 6%.

In addition, using the numerical data the density profile in the $n_{\rm s}$, r was obtained. The distribution of points in the $n_{\rm s}$, r plane is shown in Fig. 4.1a and the 1σ density contour in Fig. 4.1b. The 2σ contour spreads roughly the full plane and could not be resolved due to lack of statistics. Fig. 4.1b also displays the Planck 1 and 2 σ contours [14], which show that the observed data is more than a standard deviation away from the predictions of the inflationary flow code. This will be

[2]Another option for this scenarios is that the onset of the additional field is somewhere during inflation. We do not consider this situation, since it renders the model unpredictable.

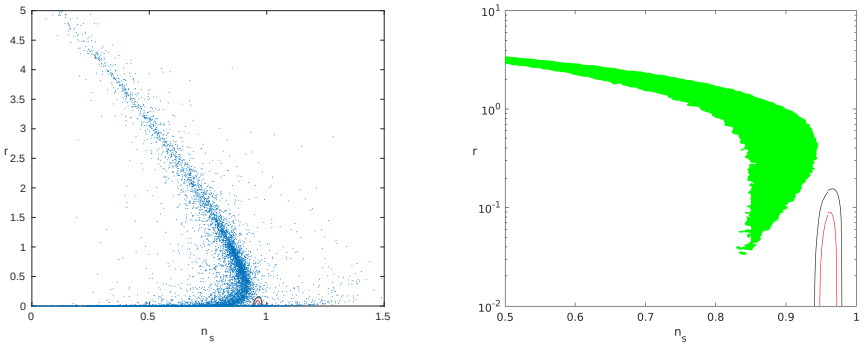

(a) (b)

Figure 4.1: *The CMB predictions for the horizon flow code [170] described in section 4.3. The left figure shows a scatter plot of n_s and r using 10^4 points. The right plot shows in green the 1σ contour using the full data set of 10^6 points. Both plots show the 1σ and 2σ contours of the Planck data from Ref. [14] in red and black, respectively. Note that the left plot has r on a linear scale, while the plot on the right has r logarithmic.*

more thoroughly investigated in the chapters 5 and 6, where different methods will be presented which fit the data much better.

Ensembles of inflation models, obtained with the method shown above, are used to study generic features of inflation and to fit the correct inflation model to the observed spectrum. Studying the general features of inflation using the Hubble flow code resulted in the relation [170, 172, 187]

$$1 - n_s = 3r \text{ or } r = 0 \tag{4.10}$$

and a relation between the field excursion and r [182] similar to the Lyth bound [188,189]. Another use of the Monte Carlo simulations is to reconstruct the inflaton potential using Eq. (3.9) as was done in Refs. [14, 184, 187, 190].

However, since Fig. 4.1 shows that the predictions of the inflationary flow code are not compatible with the observations, nature seems not to be represented by the type of inflation models that are used by the inflationary flow code. Therefore, the above analysis should be performed with a choice for the shape of the Hubble function that agrees more with the current data. This will be the main topic of chapters 5 and 6.

	Outcome	Percentage of outcomes
1	Fixed point $\epsilon_{\rm H} = 0$	92.9%
2	No end of inflation	0.01%
3	Insufficient $N_{\rm tot}$	0.2%
4	Good inflation models	6.8%

Table 4.1: *Percentage of model outcomes of the code of Kinney using a total of* 10^6 *tries. The data uses the priors for the slow roll parameters of Eqs. (4.9) and insists on 60 e-folds of inflation.*

4.4 The generic flow code

As described above, the Hubble flow code uses the $\lambda_{\rm H}$ parameters to define a set of inflation theories. This was motivated by claiming that the Hubble function, which can in principle be any arbitrary function, is Taylor expanded[3]. However, the Hubble flow code can also be viewed in the $\epsilon_{\rm H}$ frame [171, 172], where $\epsilon_{\rm H}$ is obtained from the Hubble function and used to characterize inflation. Using this philosophy, a faster code can be built since it does not require the numerical integration of the flow equations. In addition, the code can be easily modified to use arbitrary Hubble function shapes, instead of polynomials. This allows us to investigate a crucial aspect of flow parametrizations, namely the dependence (or lack thereof) of the results on the prior choice for the parameters of the expansion.

In this section we will explain this code with a Hubble function expanded as a polynomial

$$H(\phi) = \sum_{k=1}^{M} a_k \phi^k, \tag{4.11}$$

but generalizing this to another Hubble function should be obvious. Note that in this section ϕ is considered dimensionless, or equivalently we consider $M_{\rm p} = 1$. The random scan assumes that the Hubble function is expanded around a certain point, which we denote as $\phi_{\rm ex}$. In the Hubble flow code of section 4.3, $\phi_{\rm ex}$ corresponded to the value of ϕ at which the slow roll parameters were the values drawn by the random procedure. The algorithm of Refs. [171, 172] proceeds as follows

(i) Draw the parameters a_k appearing in Eq. (4.11) according to some prior distribution (see below).

(ii) For this specific Hubble function, calculate $\epsilon_{\rm H}(\phi)$ through Eq. (4.1).

(iii) If $\epsilon_{\rm H}(\phi_{\rm ex}) > 1$, restart from (i). Otherwise go to (iv).

[3] Although the prior distribution of the coefficients of the Taylor expansion are not chosen in a simple window, but in the distribution of Eq. (4.12).

(iv) Calculate the set of values $\{\phi_0\}$ where $\epsilon_{\rm H} = 0$ and $\{\phi_1\}$ where $\epsilon_{\rm H} = 1$.

(v) If $H'(\phi_{\rm ex}) > 0$, inflation proceeds at decreasing values of ϕ. Amongst the elements of $\{\phi_0\}$ and $\{\phi_1\}$, find which value is the closest to $\phi_{\rm ex}$ while being smaller than $\phi_{\rm ex}$. If this value belongs to $\{\phi_0\}$, the $r = 0$ fixed point is reached and we chose not to consider such (hybrid) trajectories. If, on the other hand, it belongs to $\{\phi_1\}$, identify $\phi_{\rm end}$ with this value. Apply a similar procedure if $H'(\phi_{\rm ex}) < 0$.

(vi) Calculate the value ϕ_* of ϕ, $N_* = 50$ e-folds prior to $\epsilon_{\rm H} = 1$, by integrating Eq. (4.7) and inverting the result. If a sufficient number of e-folds cannot be obtained, go back to (i).

(vii) Calculate the slow-roll parameters $\epsilon_{\rm H}$, $\eta_{\rm H}$ and ${}^2\lambda_{\rm H}$ using Eqs. (4.1), and the values for $n_{\rm s}$ and r from Eqs. (4.2).

In practice, we iterate this procedure until we obtain 10^6 successful realizations.

In step (i), the coefficients of the expansion are drawn according to some priors that we now specify. We studied three classes of priors. The first one consists in drawing all coefficients a_k from a flat distribution between $[-p/q^k, p/q^k]$, where p and q are two fixed numbers. In the following, it is referred to as the "power-law" priors. In the second class of priors, the a_k are drawn from flat distributions in the interval $[-\frac{p}{k!}, \frac{p}{k!}]$, where p is a constant. This prior is chosen such that at the boundary of the prior domain, all M derivatives of the Hubble function at $\phi = 0$ are 1. This prescription is referred to as the "binomial priors". Finally, the third prior class was chosen to resemble the original procedure proposed by Kinney in Eq. (4.9). This prior choice relies on drawing

$$a_k \in (\sqrt{2}/((2q)^k(k+1)!))[-p,p]/[0,1]^{(k-1)/2}, \tag{4.12}$$

where $[-p,p]/[0,1]^{(k-1)/2}$ stands for the ratio of two numbers, one drawn in the flat interval $[-p,p]$ and the other one drawn in $[0,1]$ and taken to the $(k-1)/2$ power. This corresponds to taking power-law priors on the values of the λ flow parameters, defined in Eq. (4.9), at $\phi_{\rm ex} = 0$.

The 1σ contour obtained with the third prescription is shown in the right panel of Fig. 4.1, and it was checked that the results represent the Hubble flow code. Unfortunately, other natural prior choices for the Taylor expansion coefficients, such as the power-law or the binomial priors introduced above, fail to converge as M increases. In other words, the obtained results have a large dependence on the order of truncation, an undesirable property. More precisely, in the power-law case, since the radius of convergence of the Taylor series is $\phi = q$, the model converges only when q is sufficiently large. This is shown in the left panel of Fig. 4.2, where the power law models disappear in the $M = 10$ data. For such priors, the higher order terms are strongly suppressed and, in practice, the simple results of the second order truncation with $M = 2$ are obtained. This case will be

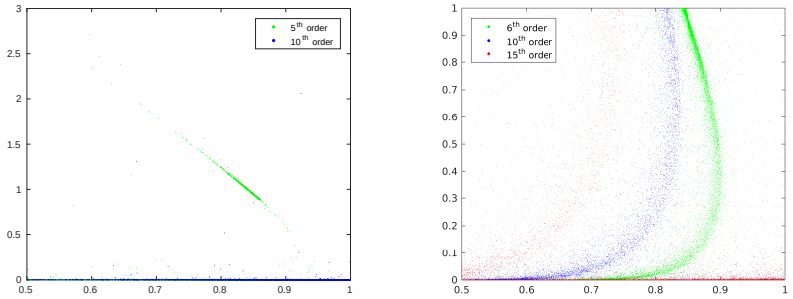

Figure 4.2: *Predictions of a Taylor expanded Hubble function, truncated at different orders M, when the coefficients are drawn from the power-law prior on the left and a binomial prior on the right.*

studied extensively in chapter 5. In the binomial case, the radius of convergence is even smaller, $\phi = 1$. Indeed, when the different orders of truncation are displayed in the right panel of Fig. 4.2, it is obvious that the model does not converge. Therefore, it seems difficult to design alternative parametrizations relying on a Taylor expansion.

Another approach would be to parametrize the potential, or parametrize directly $\epsilon_{\rm H}$. This approach was followed by Ramirez and Liddle in Ref. [172], where they found little difference between a Taylor expanded potential, a Taylor expanded Hubble function and $\epsilon_{\rm H}$ expanded as a ratio of polynomials. Expanding $\epsilon_{\rm H}$ as a polynomial strongly changes the result, but since $\epsilon_{\rm H}$ is positively defined, this expansion is not well motivated.

4.5 Geometric parametrizations of inflation

In the above sections the Hubble function was parametrized as a function of the inflaton field. Another choice for parametrizing the Hubble function is the number of e-folds. This has the interesting feature that both H and N are geometric quantities. This model will be studied in this section. This analysis is based on unpublished work in collaboration with Marco Scalisi and Diederik Roest. Afterwards a short overview will be given of other ideas that parametrize inflation in a geometric setting, being $\epsilon(N)$ and $w(\rho)$.

Expanding the Hubble function as a function of the number of e-folds was considered in Ref. [191], but these authors expanded H linearly in N. This is not consistent for our approach since $N \gg 1$, so generalizing Ref. [191] to a full Taylor

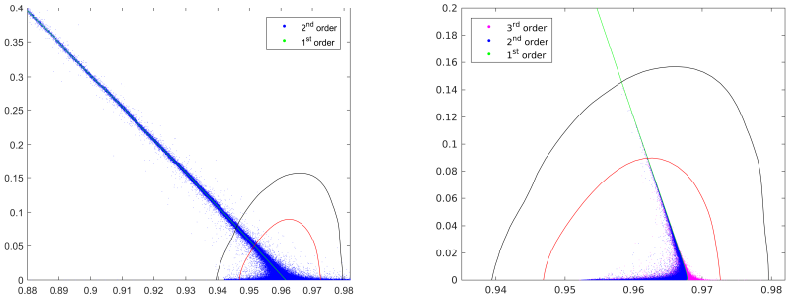

Figure 4.3: *Scatter plot with the different truncation orders for theories with the Hubble parameter expanded as in Eq. (4.13). On the left the effective description is used, while on the right inflation is forced to end at $N = 1$. The highest order shown in the figure is the order at which the series is saturated.*

series[4] is not possible. Instead, in this section we assume that the Hubble function can be expanded in $1/N$, thus that

$$H(\tilde{N}) = H_0 \left(a_0 + \sum_k^M \frac{a_k}{\tilde{N}^k} \right), \tag{4.13}$$

where a_k are parametrized with the binomial prior[5].

The meaning of $\tilde{N}$ depends on the interpretation of Eq. (4.13). If this relation is considered to hold only at large N, then $\tilde{N} = N_*$ and the condition $\epsilon_{\rm H}(N = 0) = 1$ is not imposed. This implies that the Hubble function is only parametrized for large N_*, while the specific end of inflation is not incorporated. The predictions of this model are shown on the left frame of Fig. 4.3. Though part of the possible values for $n_{\rm s}$ and r lies outside the Planck contours, most of the points are inside.

The other interpretation is to consider the expansion of Eq. (4.13) as a more fundamental expansion of the Hubble function that also holds for small N. In this case, we force that $\epsilon_{\rm H}(\tilde{N}_1) = 1$ and define the number of e-folds as $N = \tilde{N} - \tilde{N}_1$. A preliminary scan with the generic predictions for $n_{\rm s}$ and r is shown in the right panel of Fig. 4.3. This analysis did not include a sufficiently large number of configurations to construct the contour levels, but from the plot it can be expected that these contours are completely inside the Planck contours, with an extremely small value for r. Points using $M > 3$ are not shown, for they completely overlap the $M = 3$ data. The particular scenario where the series of Eq. (4.13) is truncated at first order contains only a single free parameter and can be solved analytically.

[4]Which the authors of Ref. [191] did not intend to do.
[5]The 'power-law' prior was not considered.

A nice feature of the geometric parametrization of Eq. (4.13) is that the Lagrangian can be written as a function of the number of e-folds in the simple form [64]

$$\mathcal{L} = -\epsilon_{\rm H}(N)\partial_\mu N \partial^\mu N - V(N). \tag{4.14}$$

In addition, for this model the Hamilton-Jacobi equation 3.9 becomes linear in the derivative (instead of quadratic) hence integrable. Using Eq. (4.14) to solve for H is not possible because of the appearance of $\epsilon_{\rm H}$, which is usually not known. However, when considering generic theories with a non-canonical kinetic term this limit might be of interest.

In addition to the Taylor expansion of the Hubble function in Eq. (4.13), H can also be expanded as a Padé approximant

$$H(\tilde{N}) = H_0 \frac{1 + \sum_{k=1}^{K} \frac{a_k}{\tilde{N}^k}}{1 + \sum_{l=1}^{L} \frac{b_l}{\tilde{N}^l}}, \tag{4.15}$$

where a_k and b_l are arbitrary coefficients and K and L the truncation orders of the two sums. The Padé approximant has the feature that it is a double expansion around $\tilde{N} = 0$ and $\tilde{N} \to \infty$, therefore both the end of inflation and the moment in which the CMB modes left the horizon can be parametrized simultaneously. A thorough study of this parametrization is left for future work.

Other geometric parametrizations were considered in the literature. An example is to parametrize $\epsilon_{\rm H}$ in $1/N$, which was studied in Ref. [192–196]. Using the observation that $n_{\rm s} \approx \alpha/N$ requires the parameter $\alpha = \mathcal{O}(1)$, $\epsilon_{\rm H}(N)$ can be found by solving a first order differential equation obtained from filling in the definition of ϵ_2 of Eq. (4.4) in Eq. (4.6) at first order in slow roll. This leads to [192–195]

$$\epsilon_{\rm H} = \frac{1}{2(\alpha-1)^{-1}N + AN^\alpha}, \tag{4.16}$$

where A is a constant parameter. Two regimes can be defined: If the first term in the denominator is leading, $r \propto 1/N$, as in the polynomial inflation model explained in section 3.4.1. However, if the second term in the denominator dominates and $\alpha > 1$, r is stronger suppressed. For instance, if $\alpha = 2$, Eq. (4.16) corresponds to the leading order expansion of the Starobinsky model explained in section 3.4.2, while if $\alpha > 2$, the model corresponds to hilltop inflation models. See for a complete classification of this model Ref. [194].

Finally, inflation can be parametrized with an equation of state $w(\rho)$ that deviates from the perfect fluid assumption ($w =$ constant) [191, 197–200]. During a de Sitter expansion of the universe, the equation of state represents a perfect fluid where $w = -1$. However, since inflation ends the medium during inflation has to be characterized by a deviation from the perfect fluid [191], or for instance using a van der Waals equation of state [200]. The fluid description of inflation can be considered a geometric parametrization since through Eqs. (3.7) and 2.16 the

equation of state can be rewritten as $\epsilon_{\mathrm{H}}(H)$, which are both geometrical quantities. In Ref. [192, 201] w was parametrized in $1/N$, which therefore closely resembles the parametrization of Eq. (4.16).

CHAPTER 5

The Hubble flow of plateau inflation

Introduction

In the preceding two chapters, two approaches were followed to study inflation models. In section 3.4, inflation was considered model-by-model, while in chapter 4 the Hubble function was expanded to study numerically a large class of inflation models. In this chapter and the following the second approach to inflation will be followed. The reason for this study is that the Hubble flow code with the parametrization introduced in chapter 4 is generically ruled out. In this chapter another parametrization of inflation will be introduced, in which the Hubble function is parametrized with a ratio of polynomials and it will be shown that this parametrization does generically agree with the data.

The outline of this chapter is as follows. In section 5.1 the flow equations introduced in section 4.3 will be shortly reviewed and a new method is defined to integrate the dynamical system. In section 5.2, we apply this method at low order Taylor and Padé expansions of the Hubble function and compare the results. (In appendix A, we also give the results for an inverse Taylor expansion, in order to further illustrate how our method works in practice.) In section 5.3 we perform a numerical scan over the Padé approximant of the Hubble function which enables us to expand to higher orders and to compare this 'generic' model with the Planck data. In this section we consider the dependence on the truncation order and the prior dependence of the numerical analysis. Finally, in section 5.4, we recap

our main results and draw a few conclusions, including comments on potential reconstruction with this method. The analysis of this chapter will be continued in chapter 6 with a similar setup, but then by considering a theory that is non-minimally coupled to gravity. In this chapter we set the reduced Planck mass $M_{\rm p} = 1$ and primes refer to taking the derivative with respect to the inflaton field ϕ.

This chapter is based on publication [202].

5.1 Hubble flow dynamics

The horizon flow formalism relies on the introduction of a set of flow parameters characterizing the way the Hubble scale evolves in time. Several possible sets of such parameters were introduced in section 4.1 and 3.2.3. In this chapter, we will use the Hubble flow parameters ϵ_i defined in Eq. (4.4) [176,177].

The horizon flow strategy that will be followed in this chapter rests on solving a truncated hierarchy of flow equations for a given set of flow parameters, as was explained in section 4.4. Since these flow parameters can always be written in terms of the Hubble function and its derivatives, as in Eqs. (4.5), this procedure thus relies on the assumption that some combination of H and its derivatives, corresponding to the first vanishing flow parameter, is zero. Interpreted as a differential equation for the Hubble function, this means that $H(\phi)$ is parametrized in a certain manner, involving a finite number of constant free parameters.

For example, if the Hubble flow hierarchy is truncated at some order M, *i.e.* if one assumes $\epsilon_l = 0$ for $l > M$, then ϵ_M is constant, and $H \propto \exp(a_1 \exp(a_2 \cdots \exp(a_M N) \cdots))$ where the exponential function is composed M times. As another example, one can make use of the ${}^l\lambda$ of Eq. (4.1). Truncating this hierarchy at order M means that $\mathrm{d}^{M+1}H/\mathrm{d}\phi^{M+1} = 0$, hence $H(\phi)$ has a polynomial form of degree M. In general, one can see that truncating a specific flow hierarchy always boils down to parametrizing the Hubble function in a specific manner.

Conversely, to any parametrization of the Hubble function, one can associate a specific dynamical system. Let $H(\phi, a_1, a_2, \ldots, a_n)$ be a given parametrization, where the coefficients a_i stem from some (e.g. Taylor or Padé) expansion truncated at some order n. The $n+1$ first derivatives of this function with respect to the inflaton field ϕ can be calculated, and one can invert the system to extract the $n+2$ variables $\left\{\phi, a_1, a_2, \ldots, a_n, H^{(n+1)}\right\}$ in terms of $\left\{H, H', H'', \ldots, H^{(n)}\right\}$. Of particular interest is the last entry of this solution, which relates the $(n+1)^{\rm th}$ derivative of the Hubble function $H^{(n+1)}$ to the lower order ones. In terms of the Hubble flow hierarchy, this means that ϵ_{n+1} can be expressed in terms of the n first Hubble flow parameters only. The flow equations (4.4), for $1 \leq i \leq n$, thus form a closed dynamical system. It is important to stress that all physical input resides in this truncation: how ϵ_{n+1} is expressed in terms of all preceding flow parameters

fully determines the dynamical system and hence the inflationary predictions.

Moreover, the flow dynamics (4.4) is insensitive to the actual value of the inflaton field ϕ and hence the transformation $\phi \to \phi + \delta\phi$ leaves this system invariant. For the expansions that we consider, indeed, the functional form of $H(\phi)$ does not change under this shift, implying that there is a degeneracy in the parameters. Amongst the n parameters, one combination can therefore be absorbed by the shift transformation, while the remaining $n-1$ combinations are invariant. The latter are therefore constants of motion, and the space of inflationary solutions has dimension $n-1$.

This formal description will become more clear in the following section, where we will show how these constants of motion can be derived in practice and apply this method to second order Taylor and Padé expansions of the Hubble function. In these cases, a single constant of motion will be obtained. Therefore, at fixed number of e-folds ΔN_* between the Hubble exit time of the CMB pivot scale and the end of inflation, a one-to-one relation between $n_{\rm s}$ and r will be obtained.

A last remark is in order. Though the systems will be solved exactly and independently of the slow-roll approximation, in practice, the scalar spectral index and the tensor-to-scalar ratio will be calculated from the flow parameters at Hubble exit time shown in Eq. (4.6), which are valid at second order in slow roll. In the regions preferred by the observations of the Planck satellite, the above expressions are valid and can therefore be used to compare predictions with observations.

5.2 Analytical integration of the Hubble flow

In this section, we apply the method sketched in section 5.1 to two toy cases: a Taylor expansion of the Hubble function at quadratic order and a Padé expansion at linear order. We obtain analytical expressions for the inflationary trajectories in the parameter space (ϵ_1, ϵ_2), as well as for the number of e-folds realized along these trajectories. Finally, we display in each case the corresponding values of $n_{\rm s}$ and r.

5.2.1 Taylor expansion

We first illustrate our method by considering the well-known case of a quadratic Hubble function:

$$H = H_0 \left(1 + a\phi + b\phi^2\right) , \tag{5.1}$$

which was already solved in Ref. [87] but here we employ a different approach. Using Eqs. (4.5), the two first flow parameters are given by

$$\epsilon_1 = 2\left(\frac{a+2b\phi}{1+a\phi+b\phi^2}\right)^2 , \quad \epsilon_2 = 4\left[\left(\frac{a+2b\phi}{1+a\phi+b\phi^2}\right)^2 - \frac{2b}{1+a\phi+b\phi^2}\right] . \tag{5.2}$$

Let us derive the constant of motion. Under the inflaton shift transformation $\phi \to \phi + \delta\phi$, the functional form of Eq. (5.1) remains unchanged if the coefficients of the expansion change according to

$$a \to \frac{a + 2b\delta\phi}{1 + a\delta\phi + b\delta\phi^2}\,, \quad b \to \frac{b}{1 + a\delta\phi + b\delta\phi^2}\,, \tag{5.3}$$

where H_0 has also to be rescaled according to $H_0 \to H_0\left(1 + a\delta\phi + b\delta\phi^2\right)$. If one moves to the specific gauge where a vanishes, *i.e.* if one takes $\delta\phi = -a/(2b)$, then the shifted b coefficient, $4b^2/(4b - a^2)$, is gauge invariant. This implies that the following combination is invariant under the inflaton shift[1]:

$$\gamma = \frac{32b^2}{a^2 - 4b} = \frac{(2\epsilon_1 - \epsilon_2)^2}{\epsilon_2 - \epsilon_1}\,, \tag{5.4}$$

where the second equality has been obtained from Eq. (5.2).

As pointed out in section 5.1, a given parametrization of the Hubble function can be translated into a specific dynamical system. For the case at hand, since Eq. (5.1) implies that $H''' = 0$, Eqs. (4.5) give rise to

$$\epsilon_3 = 3\epsilon_1 - 2\frac{\epsilon_1^2}{\epsilon_2}\,. \tag{5.5}$$

This truncates the infinite set of flow equations (4.4) for all the ϵ_i into a set of two differential equations for the first two flow parameters:

$$\frac{\mathrm{d}\epsilon_1}{\mathrm{d}N} = \epsilon_1\epsilon_2\,, \qquad \frac{\mathrm{d}\epsilon_2}{\mathrm{d}N} = -2\epsilon_1^2 + 3\epsilon_1\epsilon_2\,. \tag{5.6}$$

This dynamical system generates a flow through the two dimensional space (ϵ_1, ϵ_2), which is displayed in the left panel of Fig. 5.1. Different trajectories can be labelled by different values of the invariant parameter γ. It can easily be checked that Eqs. (5.6) indeed leave this particular combination invariant.

Moreover, by inverting Eq. (5.4), one can relate one of the remaining two slow-roll parameters to the other:

$$\epsilon_2 = 2\epsilon_1 + \frac{\gamma}{2} + \frac{\xi}{2}\sqrt{\gamma^2 + 4\gamma\epsilon_1}\,, \tag{5.7}$$

where $\xi = \pm 1 = \mathrm{sign}\left[(2\epsilon_1 - \epsilon_2)\epsilon_2(\epsilon_1 - \epsilon_2)\right]$ and the argument of the square root is always positive. Inserting Eq. (5.7) into the first of Eqs. (5.6) then leads to a first order differential equation for $\epsilon_1(N)$ that can be solved, and one obtains

$$\Delta N = N\left(\epsilon_1\right) - N\left(\epsilon_{1,\mathrm{end}}\right)\,, \tag{5.8a}$$

$$N\left(\epsilon_1\right) = \frac{2}{\gamma + \xi\sqrt{\gamma^2 + 4\gamma\epsilon_1}} + \frac{\xi}{\gamma}\log\left|\frac{\sqrt{\gamma^2 + 4\gamma\epsilon_1} - \gamma}{\sqrt{\gamma^2 + 4\gamma\epsilon_1} + \gamma}\right|\,, \tag{5.8b}$$

[1] The case with $a^2 = 4b$ or, equivalently, $\epsilon_1 = \epsilon_2$, is singular and needs to be treated separately. It is straightforward to show that, in this case, one simply has $\epsilon_1 = \epsilon_2 = 1/(1 + \Delta N)$.

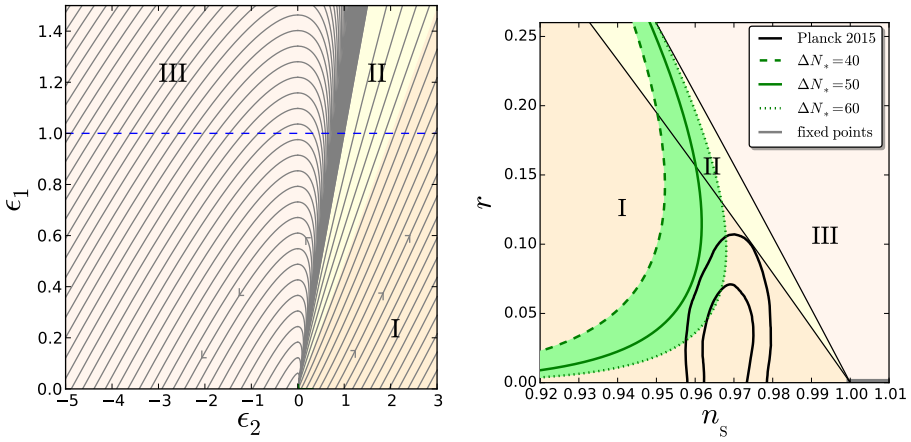

Figure 5.1: *Second order Taylor expansion for the Hubble function. Left panel: flow lines of the system (5.6) in the plane* (ϵ_1, ϵ_2)*. The arrows indicate in which direction inflation proceeds. The blue dashed line corresponds to* $\epsilon_1 = 1$ *where inflation stops. The three regions* I, II *and* III *refer to the discussion in the main text. Right panel: Observational predictions in the* (n_s, r) *plane, compared with the Planck 2015* 1σ *and* 2σ *contours. The green lines stand for the values of* n_s *and* r *computed 40 e-folds before the end of inflation (dashed line), 50 e-folds (solid line) and 60 e-folds (dotted line). The grey segment at the bottom right stand for the fixed points* $(\epsilon_1 = 0, \epsilon_2 < 0)$*.*

where $\epsilon_{1,\mathrm{end}} = 1$ (we only consider cases where inflation has a graceful exit). This expression can be inverted to yield ϵ_1 as a function of N,

$$\epsilon_1 = \frac{-\gamma W_\chi\left(-e^{\gamma\Delta N-1}\right)}{\left[1+W_\chi\left(-e^{\gamma\Delta N-1}\right)\right]^2}\,, \quad \chi = \begin{cases} -1 & \text{if } \gamma(2\epsilon_1-\epsilon_2)<0 \\ 0 & \text{if } \gamma(2\epsilon_1-\epsilon_2)>0 \end{cases}\,, \tag{5.9}$$

where χ determines which branch of the Lambert function W_χ is to be used. Note that the sign of the combination $2\epsilon_1 - \epsilon_2$ appearing in the definition of χ does not change during inflation, as the Hubble flow equations imply that $\mathrm{d}(2\epsilon_1-\epsilon_2)/\mathrm{d}N = \epsilon_1(2\epsilon_1-\epsilon_2)$. Therefore, the branch of the Lambert function does not change during inflation. One can check that the above formula matches Eqs. (66-70) of Ref. [87] where it was first derived.

Let us now discuss the structure of the phase space diagram plotted in the left panel of Fig. 5.1. According to the type of Hubble function one is dealing with, three possibilities must be distinguished:

- In regime I, $\epsilon_2 > 2\epsilon_1$. In this regime ϵ_1 vanishes in the far past while ϵ_2 takes a positive value. During inflation, both monotonically increase. This corresponds to a Hubble function that has an inverted parabolic profile whose maximum is positive. In this case, $\gamma > 0$ and $\xi = +1$.

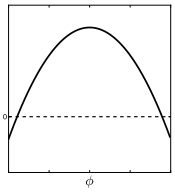

- In regime II, $\epsilon_1 < \epsilon_2 < 2\epsilon_1$, hence both slow-roll parameters are vanishing in the far past and monotonically increasing during inflation. The corresponding Hubble function has a parabolic profile with a negative minimum. In this case, $\gamma > 0$ and $\xi = -1$.

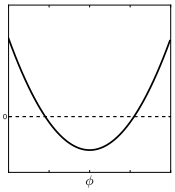

- Finally, in regime III, if $\epsilon_2 < \epsilon_1$, both slow-roll parameters are again vanishing in the far past. However, during inflation, ϵ_1 reaches a maximum, and then decreases back to zero, while ϵ_2 asymptotes to a negative value in the future. This stems from a Hubble function with a positive minimum. In this case, $\gamma < 0$, while $\xi = +1$ before ϵ_1 crosses its maximum and $\xi = -1$ afterwards.

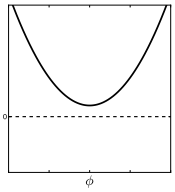

These three regions are shaded with different colors in the left panel of Fig. 5.1. One should note that thanks to the conservation of the sign of γ defined in Eq. (5.4), a given inflationary trajectory never changes region. Amongst the third category, one can distinguish two cases. If the maximum value of ϵ_1 is smaller than one, inflation never ends and reaches the $r = 0$ fixed point ($\epsilon_1 = 0, \epsilon_2 < 0$). If, on the other hand, the maximum value of ϵ_1 is larger than one, and if one starts inflating with $\epsilon_2 > 0$, then inflation ends naturally when $\epsilon_1 = 1$. This happens when $\gamma < -4$.

Combining Eqs. (5.9) and (5.7) with the expressions of n_{s} and r in Eq. (4.6), the inflationary predictions of this class of models can be obtained and are displayed in the right panel of Fig. 5.1 for $40 < \Delta N_* < 60$. One should note that Eqs. (4.6) also make use of ϵ_3, but ϵ_3 is related to ϵ_1 and ϵ_2 thanks to Eq. (5.5). For "large-field" scenarios (region II), r is too large, and the model asymptotes the line $r = 16(1 - n_{\mathrm{s}})/3$ mentioned at the end of section 4.3 and commented on in Ref. [87], which separates regions II and III. For "hilltop" or "small-field" scenarios (region I), r is small, but n_{s} is generically too red. When interpolating between these two cases, there is a small range of models for which $r \sim 0.1$ and the spectral index n_{s} has marginally the right value for low values of N_*. However, one can check that this corresponds to very fine-tuned initial values of the flow parameters (or, equivalently, values of γ). Moreover, we will find in section 5.3 that higher-order terms change this result significantly.

5.2.2 Padé expansion

Let us further illustrate our method by considering the case of a lowest order Padé expansion,

$$\frac{H}{H_0} = \frac{1+a\phi}{1+b\phi}\,. \tag{5.10}$$

This case has not been considered in the literature before and provides a simple implementation of the idea of "plateau inflation". The first two slow-roll parameters can be obtained from Eqs. (4.5), and one has

$$\epsilon_1 = \frac{2\,(a-b)^2}{(1+a\phi)^2\,(1+b\phi)^2}\,, \quad \epsilon_2 = \frac{4\,(a-b)\,(a+b+2ab\phi)}{(1+a\phi)^2\,(1+b\phi)^2}\,. \tag{5.11}$$

Here, we follow exactly the same approach as the one used for the Taylor expansion in section 5.2.1. For instance, under shift transformations $\phi \to \phi + \delta\phi$, the functional form (5.10) is unchanged provided

$$a \to \frac{a}{1+a\delta\phi}\,, \quad b \to \frac{b}{1+b\delta\phi}\,, \qquad H_0 \to H_0\,\frac{1+a\delta\phi}{1+b\delta\phi}\,. \tag{5.12}$$

By moving to the gauge where the constant term in the numerator of Eq. (5.10) vanishes, *i.e.* $\delta\phi = -1/a$, the b coefficient becomes $b/(1-b/a)$, which is gauge invariant. This implies that

$$\gamma = \frac{16\sqrt{2}ab}{|a-b|} = \frac{\epsilon_2^2 - 4\epsilon_1^2}{\epsilon_1^{3/2}} \tag{5.13}$$

is a constant of motion and can be used to label the different trajectories.

Let us recall that a given parametrization for the Hubble function can always be cast in a single dynamical system in the flow parameters space. For the present case, making use of the same procedure as before, Eq. (5.10) implies that $H''' = 3(H'')^2/(2H')$, and Eqs. (4.5) give rise to

$$\epsilon_3 = \frac{\epsilon_1^2}{\epsilon_2} + \frac{3}{4}\epsilon_2\,. \tag{5.14}$$

Again, this truncates the dynamical system to a closed set of differential equations for (ϵ_1, ϵ_2), given by

$$\frac{\mathrm{d}\epsilon_1}{\mathrm{d}N} = -\epsilon_1\epsilon_2\,, \qquad \frac{\mathrm{d}\epsilon_2}{\mathrm{d}N} = -\left(\epsilon_1^2 + \frac{3}{4}\epsilon_2^2\right)\,. \tag{5.15}$$

In particular, one can check that the combination γ defined in Eq. (5.13) is left invariant. The equation for ϵ_1 is the same as in Eq. (5.6), since it just defines ϵ_2. However, the equation for ϵ_2 is different. In general indeed, only the flow

equation for the last flow parameter encodes the physical information about the model, and propagates back to yield a specific dynamics for all flow parameters. The integrated flow lines of the above system are displayed in the left panel of Fig. 5.2.

Let us now see how this system can be integrated analytically. By inverting Eq. (5.13), one can express ϵ_2 as a function of ϵ_1,

$$\epsilon_2 = \xi\sqrt{4\epsilon_1^2 + \gamma\epsilon_1^{3/2}}\,, \tag{5.16}$$

where $\xi = \pm 1 = \mathrm{sign}(\epsilon_2)$ changes when ϵ_1 crosses its minimum value. As before, inserting Eq. (5.16) into Eqs. (5.15) yields a first order differential equation for $\epsilon_1(N)$ that can be solved, and one obtains

$$\Delta N_* = N(\epsilon_{1*}) - N(\epsilon_{1,\mathrm{end}})\,, \qquad N(\epsilon_1) = \xi\frac{4\left(8\sqrt{\epsilon_1} - \gamma\right)\sqrt{4\epsilon_1 + \gamma}}{3\epsilon_1^{3/4}\gamma^2}\,, \tag{5.17}$$

where again $\epsilon_{1,\mathrm{end}} = 1$. Contrary to the result obtained in section 5.2.1, this expression cannot be inverted analytically.

Let us now discuss the structure of the phase space diagram plotted in the left panel of Fig. 5.2. According to the type of Hubble function, three possibilities must again be distinguished:

- In regime I, $\epsilon_2 > 2\epsilon_1$, hence both ϵ_1 and ϵ_2 increase as inflation proceeds, from the fixed point $\epsilon_1 = \epsilon_2 = 0$ reached in the infinite past. Inflation ends naturally when $\epsilon_1 = 1$. This implements the idea of "plateau inflation" where the Hubble function is concave with a non vanishing plateau where inflation proceeds. In this case, $\gamma > 0$ and $\xi = +1$.

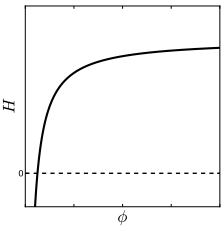

- In regime II, $-2\epsilon_1 < \epsilon_2 < 2\epsilon_1$ and $\epsilon_1 = 1$ is reached both in the past and in the future. In between, a finite period of inflation takes place where ϵ_2 increases and ϵ_1 goes through a minimum. The corresponding Hubble function is convex and vanishes before the plateau is reached (region II). In this case, $\gamma < 0$ while $\xi = -1$ before ϵ_1 reaches its minimum, and $\xi = -1$ afterwards.

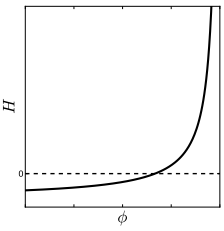

- Finally, in regime III, $\epsilon_2 < -2\epsilon_1$, ϵ_1 decreases as inflation proceeds, while ϵ_2 increases. The (attractive) fixed point $\epsilon_1 = \epsilon_2 = 0$ is reached in the asymptotic future. This corresponds to a convex Hubble function for which the plateau is positive (region III). In this case, $\gamma > 0$ and $\xi = -1$.

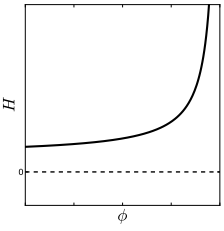

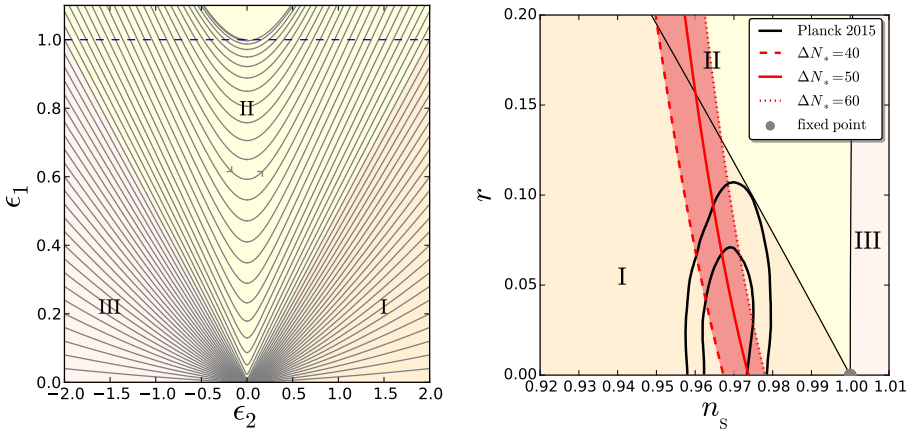

Figure 5.2: *First order Padé expansion for the Hubble function. Left panel: flow lines of the system (5.15) in the plane* (ϵ_1, ϵ_2)*. The arrows indicate in which direction inflation proceeds. The blue dashed line corresponds to* $\epsilon_1 = 1$ *where inflation stops. The three regions* I*,* II *and* III *refer to the discussion in the main text. Right panel: Observational predictions in the* $(n_{\rm s}, r)$ *plane, compared with the Planck 2015* 1σ *and* 2σ *contours. The red lines stand for the values of* $n_{\rm s}$ *and* r *computed 40 e-folds before the end of inflation (dashed line), 50 e-folds (solid line) and 60 e-folds (dotted line). The grey dot at the bottom right stands for the fixed point* $(\epsilon_1 = 0, \epsilon_2 = 0)$*.*

In particular, making use of Eq. (5.17), one can check that an infinite number of e-folds can be realized in cases I and III. However, in case II, only a finite number of e-folds can be obtained. Parametrizing a given trajectory within region II by $\epsilon_{2,\rm end} = \sqrt{\gamma + 4}$, the value of the second flow parameter at the end of inflation, the total number of e-folds is given by

$$N_{\rm max} = \frac{8}{3}\epsilon_{2,\rm end}\frac{12 - \epsilon_{2,\rm end}^2}{\left(\epsilon_{2,\rm end}^2 - 4\right)^2}\,. \tag{5.18}$$

As expected, this number vanishes when $\epsilon_{2,\rm end}$ approaches 0 and diverges when $\epsilon_{2,\rm end}$ approaches 2.

As before, combining Eqs. (5.17) and (5.16) with the expressions of $n_{\rm s}$ and r in Eqs. (4.6), the inflationary predictions of this class of models can be obtained and are displayed in the right panel of Fig. 5.2 for $40 < \Delta N_* < 60$. In Eqs. (4.6), ϵ_3 is related to ϵ_1 and ϵ_2 thanks to Eq. (5.14). When inflation proceeds in region I, in the limit $\epsilon_{2\rm end} \gg 1$, one recovers the "typical" predictions of plateau inflation where r is small and $n_{\rm s}$ is in good agreement with the observational constraints.

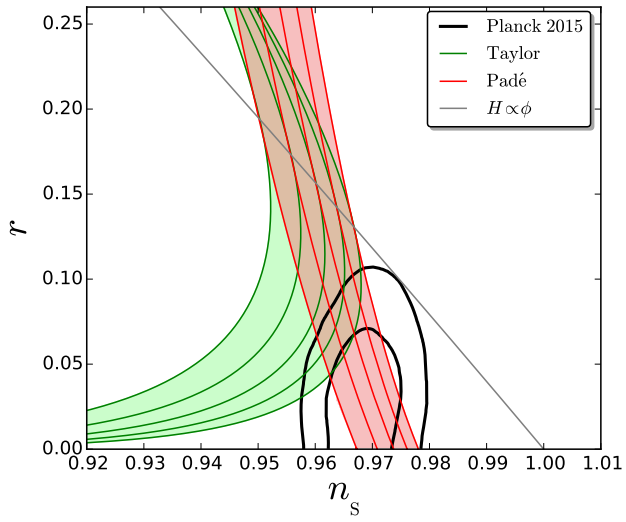

Figure 5.3: *Compared predictions of the Taylor model (5.1) (green) and the Padé model (5.10) (red), for* $40 < \Delta N_* < 60$*, in the* (n_{s}, r) *plane. The black lines are the* 1σ *and* 2σ *contours of Planck 2015. The grey solid line stands for the model* $H/H_0 = \phi$*, which is a special case of both parametrizations and for which* $\epsilon_3 = \epsilon_2 = 2\epsilon_1$*.*

In this limit, Eq. (5.16) gives rise to $\epsilon_2 \simeq \sqrt{\gamma}\epsilon_1^{3/4}$, and one has

$$\epsilon_{1*} \simeq \left(\frac{4}{3\sqrt{\gamma}\Delta N_*}\right)^{4/3}, \qquad \epsilon_{2*} \simeq \frac{4}{3\Delta N_*}. \tag{5.19}$$

This translates into $n_{\mathrm{s}} \simeq 1 - 4/(3\Delta N_*)$ and $r \sim \Delta N_*^{-4/3} \ll 1$, which is what one would expect from a plateau inflation model with a $1/\phi$ fall-off [192, 193].

Finally, let us note that this regime is interesting because $\epsilon_{2\mathrm{end}} \gg 1$ means that the last stage of the inflationary phase is realized far away from slow roll (let us recall that, here, the inflationary dynamics is solved *without* resorting to the slow-roll approximation). However, the number of e-folds realized between the time when $\epsilon_2 = 1$ and the end if inflation when $\epsilon_1 = 1$ can be calculated thanks to Eq. (5.17), and in the limit where $\epsilon_{2\mathrm{end}} \gg 1$, one obtains $4/3$ e-folds. This is why, ΔN_* e-folds before the end of inflation, slow roll is well valid and the system gives rise to predictions that are in good agreement with observations.

5.2.3 Comparison

In order to summarize the analysis of the two toy models discussed in the present section, in Fig. 5.3, we have superimposed their predictions in the $(n_{\rm s}, r)$ plane, for a few fixed values of $\Delta N_* \in [40, 60]$. One can see that Taylor and Padé lines are tangential, along the $\epsilon_3 = \epsilon_2 = 2\epsilon_1$ line, which is associated to the model $H/H_0 = \phi$. This should not come as a surprise for the following reason. After a suitable gauge transformation, Eq. (5.1) can be cast in the form

$$\frac{H}{H_0} = \phi + \sqrt{\frac{\gamma}{2}}\frac{\phi^2}{4}\,, \tag{5.20}$$

where γ has been defined in Eq. (5.4). Similarly, Eq. (5.10) can be cast in the form

$$\frac{H}{H_0} = \frac{\phi}{1 + \frac{\gamma}{16\sqrt{2}}\phi}\,, \tag{5.21}$$

where γ has been defined in Eq. (5.13). As a consequence, a linear Hubble is a special case of both parametrizations, corresponding to $\gamma = 0$. However, obviously, the way γ modifies this linear $H(\phi)$ function is different for both parametrizations.

5.3 Numerical integration of the Hubble flow

The above results indicate that inflationary dynamics is better parametrized by Padé expansions of the Hubble function rather than Taylor expansions. However, one might worry that this statement relies on the low truncation order we have worked with. This is why in this section, we generalize our approach by numerically including higher order terms. Notice that the analytical method developed in section 5.2 can in principle be used to deal with arbitrarily large order expansions, however, one would not gain much by displaying the corresponding cumbersome formulas. This is why, here, we directly compute the predictions of the models we study, which consist in Hubble functions of the form

$$H\left(\phi\right) = H\left[m, n\right]\left(\phi\right) \equiv \frac{\sum_{k=0}^{m} c_k \phi^k}{\sum_{l=0}^{n} d_l \phi^l}\,. \tag{5.22}$$

In practice, we consider orders $[M, 0]$, which correspond to Taylor expansions of the Hubble function, and orders $[M, M]$, which correspond to Hubble functions that asymptotes to a non-vanishing plateau at large-field values. We study different values of M in order to test the robustness of the predictions under increasing the order of truncation and we report the results below.

The numerical procedure is explained in section 4.4. This procedure requires, except of the parametrization of the Hubble function, the field value for the start of the exploration, $\phi_{\rm ex}$ and prior distribution for the coefficients. As explained in

section 4.4, expanding the Hubble function as a Taylor series requires $\phi_{\rm ex} = 0$ and the prior choice of Eq. (4.9), which corresponds to the prior choice first chosen by Kinney in Ref. [170]. A Padé approximant is a simultaneous expansion around $\phi = 0$ and $\phi = \infty$, which allows us to either start the exploration of the Padé Hubble function at $\phi_{\rm ex} = 0$ or $\phi_{\rm ex} = \infty$. This last case corresponds to plateau inflation and we expect it to be in best agreement with the data.

The coefficients of the Pade expansion are drawn according to some priors that were also used in section 4.4. There we studied, except of the specific prior choice to reproduce the results from Kinney, two classes of priors. The first one are the power-law priors, which consists in drawing all coefficients c_k and d_k from a flat distribution between $[-p/q^k, p/q^k]$, where p and q are two fixed numbers. In the second class of priors, the binomial priors, the coefficients c_k and d_k are drawn from flat distributions in the interval $[-pf_k, pf_k]$, where p is a constant and the set $\{f_k\}$ is defined such that if $c_k = (-1)^k d_k = f_k$ for all k, all M derivatives of the Hubble function at $\phi = 0$ are 1. This gives rise to

$$\text{Pade}: \;\; f_k = \frac{\binom{M}{k}}{\binom{2M}{k} k!}\,, \qquad \text{Taylor}: \;\; f_k = \frac{1}{k!}. \tag{5.23}$$

As was explained in section 4.4, the Taylor parametrization only converged if the priors were chosen following Eq. (4.12), which represents the analysis by Kinney. The 1σ contour is shown in Fig. 4.1b, and has no overlap with the Planck data. Therefore, only a small fraction of the points, 0.2%, was in the Planck 2σ region. We should stress that these results correspond to the standard "horizon flow" procedure as commonly used in the literature. They again motivate our search for alternative parametrizations.

Let us now consider Padé approximants. First of all, we have checked that with the two classes of priors proposed above, the results always converge (indeed, it is well known that Padé approximants have better convergence properties than Taylor expansions). In practice, we find that $M = 6$ is enough to reproduce all higher order results with a very good accuracy. The next question is how much the results depend on the class of priors. In Fig. 5.4, we have displayed the 1 and 2σ contours obtained with the power-law and binomial priors, in the case where $\phi_{\rm ex} = 0$ (left panel) and $\phi_{\rm ex} = \infty$ (right panel).

When $\phi_{\rm ex} = 0$, the binomial prior gives rise to wide spread contours (the 2σ contour entirely lies outside the plot frame). They are consistent with the power-law results, but scan larger sets of inflationary trajectories. For this reason, the percentage of points inside the Planck 2σ contour is smaller, 5% for the binomial distribution and 38% with the power-law prior.

When $\phi_{\rm ex} = \infty$, we find that both priors give rise to rather narrow contours, in agreement with each other at the 1σ level. In this case, large fractions of points lie inside the Planck 2σ contour: 18% for the binomial prior choice and 90% when the power-law prior is used. These models correspond indeed to one's intuitive representation of "plateau inflation". Interestingly also, a lower bound on r is

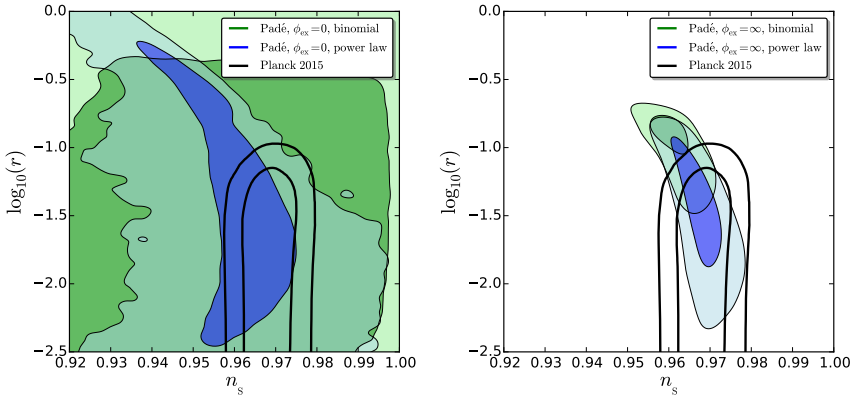

Figure 5.4: *1 and 2σ contours for the two prior choices (power law and binomial), for a Padé expansion of the Hubble function. The left panel corresponds to $\phi_{\rm ex} = 0$ and the right panel to $\phi_{\rm ex} = \infty$.*

found, which means that this class of inflationary dynamics could in principal be ruled out by future experiments.

This analysis thus reveals that up to a moderate prior dependence, Padé expansions of the Hubble function give rise to predictions in agreement with observations, and possess good convergence properties. Given what we observationally know, they seem better suited to parametrize inflationary dynamics than Taylor expansions, on which the standard horizon flow procedure rests.

5.4 Conclusion

Let us summarize our main findings. Whenever inflation is parametrized by a truncated dynamical system for the flow parameters, it can equivalently be described by an expansion scheme for the Hubble function $H(\phi)$, at some finite order. Conversely, any functional shape for the Hubble function (such as a Taylor expansion, a Padé expansion, or any other expansion involving a finite set of free coefficients) can be related to a single dynamical system in the flow parameters space.

Making use of the shift symmetry $\phi \to \phi+\delta\phi$ of the problem, we have explained how constants of motion can be derived for such systems, and how their dynamics can be integrated. For illustrative purpose, we have applied this new method to the case of a second order Taylor expansion (section 5.2.1), a first order Padé expansion (section 5.2.2), and a second order inverse Taylor expansion (appendix A). For the second order Taylor case, we have found that generically, either r is too large and the famous horizon flow relation $r \approx 16(1-n_{\rm s})/3$ is recovered, or r is small enough

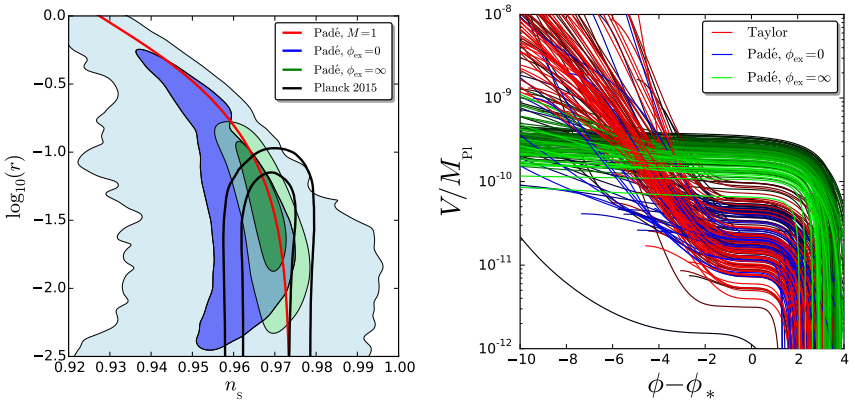

Figure 5.5: *Left frame:* 1σ *and* 2σ *contours for the two Padé parametrization around* $\phi = 0$ *and* $\phi = \infty$*, both with power-law priors. The predictions of the first order Padé expansion, as obtained in section 5.2.2, are displayed too. Right frame: potential reconstruction for the the most likely* 100 *trajectories (using the Planck likelihood [14]), for the standard horizon flow procedure based on a Taylor expansion of the Hubble function, a Padé expansion around* $\phi = 0$*, and a Padé expansion around* $\phi = \infty$*. Darker colors stand for smaller likelihood of the predicted values for* n_s *and* r*. The potentials are normalized so that the amplitude of the curvature power spectrum,* $\mathcal{P}_\zeta = V_*/(24\pi^2\epsilon_{1*}M_p^4) \simeq 2.203 \times 10^{-9}$*, is correctly obtained.*

but n_s is too red. For the first order Padé expansion on the other hand, the typical predictions $n_s \simeq 1 - 4/(3\Delta N_*)$ and $r \sim \Delta N_*^{-4/3} \ll 1$ have been obtained, in good agreement with observations.

We have then extended these results to higher order expansions with numerical tools in section 5.3, and studied the dependence of the predictions on the priors chosen for the coefficients of the expansions. We have confirmed that Padé expansions of the Hubble function are more suited to parametrize inflation than Taylor expansions, since they show good convergence properties, mild prior dependence, and, most notably, much better agreement with observations.

When using Padé approximants, we have distinguished the case where inflation proceeds close to $\phi = 0$ and close to $\phi = \infty$. These two prescriptions give rise to results that are compared in the left panel of Fig. 5.5, where we also display the first order Padé result of section 5.2.2. It is clear that, given observational constraints, they provide a better parametrization of inflationary dynamics than the usual horizon flow procedure.

These results illustrate why "model-independent" parametrizations of inflation, such as expansion schemes for the Hubble function or truncated flow dynamical

systems, always make non trivial assumptions about its dynamics. This is why, a priori, parametrizations yielding predictions that are in contradiction with the data cannot be used to infer physical information from them.

As an example, in the right panel of Fig. 5.5, we show the best 100 potentials, obtained from the Hamilton-Jacobi equation (3.9), for the three cases: Taylor expansion with the priors corresponding to the usual "horizon flow" procedure, Padé expansion around $\phi = 0$, and Padé expansion around $\phi = \infty$. From here, it is clear that different parametrizations sample inflation along different classes of potentials, even when restricted to the best possible realizations. Taylor and Padé expansions around $\phi = 0$ seem to prefer inflationary potentials with a flat inflection point. Because this is a rather fine-tuned configuration from a generic Taylor expansion, we understand why the standard horizon flow procedure, which is based on a generic Taylor expansion, produces trajectories that are most of the time excluded by observations. On the contrary, Padé expansions around $\phi = \infty$ mostly samples plateau inflation, as expected.

As a consequence, it is clear that "reconstructing" the potential with either of these parametrizations biases the result towards the class of potentials that it relies on. This is in essence a "prior effect". However, phenomenological descriptions are still very useful to address a number of other issues in the Early Universe, where the background is effectively "sourcing" some physical effects. Therefore, the question becomes: "How can we best obtain and parametrize a class of inflationary trajectories that are in agreement with current observational constraints?" From a Bayesian perspective, the priors for analysing the n^{th} generation of data come from the information provided by the $n - 1^{\text{th}}$ survey. In this respect, we have shown that after Planck, Padé expansions (or other types of expansion schemes implementing the plateau structure) should be preferred over the standard Taylor parametrizations of the Hubble flow dynamics.

CHAPTER 6

Plateau inflation from random non-minimal coupling

6.1 Introduction

In the previous chapter we found that if the Hubble function is chosen to be flat at large field values, i.e. has a Padé shape, the cosmological observations generically agree better with the CMB data than if the Hubble function is Taylor expanded. In this section, this analysis will be extended by considering the strong coupling attractor, which is a generalization of Higgs inflation studied in section 3.4.

The strong coupling attractor models studied in the literature use a specific relation between the potential and the frame function, which governs the coupling between the inflaton and the Ricci scalar. In this chapter, we aim to investigate arbitrary corrections with a more generic ansatz and thus introduce a method to generically alleviate the η-problem of arbitrary potentials.

This chapter is structured as follows. We start in section 6.2 with a short review of different attractor models in inflation, being the strong-coupling attractor and the α-attractor. In section 6.3 we continue to generalize the strong-coupling attractor to arbitrary non-minimal coupling functions and potentials and demonstrate how the coupling strength ξ may ensure a sufficient amount of observationally viable inflation. After outlining the analytic approximate expressions for the inflationary observables, we employ numerical methods to scan the landscape of possible inflationary scenarios with arbitrary coefficients in section 6.4. We conclude in section 6.5 with a discussion and outline further numerical evidence in

the appendix. In this chapter we set the reduced Planck mass $M_{\rm p} = 1$.

This chapter is based on publication [203].

6.2 Attractors of inflation models

In this section we review attractor inflation models, which predict for a certain part of their parameter space the same values for $n_{\rm s}$ and r independently of the potential[1]. Two classes will be discussed, the strong coupling attractor which consists of a coupling between the inflaton field and the Ricci scalar and the α-attractor which uses a particular kinetic term. In the end of this section the pole-attractor will be shortly reviewed, which combines the two kinds of attractors. In the remainder of this chapter a more generic version of the strong coupling attractor will be studied, while the α-attractor will be used in the next chapters.

6.2.1 Strong coupling attractor

Higgs inflation, explained in section 3.4.3, shows how an extremely bad inflation model, in terms of observations, characterized by the potential $V \propto h^4$ became a perfectly viable theory (Starobinsky-like) by introducing a large coupling between the inflaton field and the Ricci scalar. This attractor towards Starobinsky-like predictions is a generic feature of a group of related inflation theories, known as strong coupling attractors [103, 204] .

Analogously to Higgs inflation, the strong coupling attractor involves an inflaton coupled non-minimally to the Ricci scalar in the Jordan frame, but it allows for an arbitrary Jordan frame potential $V_J(\phi)$ and frame function (or non-minimal coupling term) $\Omega(\phi)$

$$\mathcal{L}_J = \sqrt{-g_J}\left[\tfrac{1}{2}\Omega(\phi)R_J - \tfrac{1}{2}\partial_\mu\phi\partial^\mu\phi - V_J(\phi)\right]. \tag{6.1}$$

In the original models [103, 204], the frame function and potential were related via

$$\Omega(\phi) = 1 + \xi f(\phi), \qquad V_J(\phi) = \lambda^2 f^2(\phi)\,, \tag{6.2}$$

where $f(\phi)$ is an arbitrary function of ϕ and λ is a positive parameter. As in the Higgs inflation model, Eq. (6.1) can be rotated to the Einstein frame using the conformal rotation $g^E_{\mu\nu} = \Omega(\phi)g^J_{\mu\nu}$,

$$\mathcal{L}_E = \sqrt{-g_E}\left(\tfrac{1}{2}R_E - \tfrac{1}{2}\left[\frac{1}{\Omega(\phi)} + \frac{3}{2}\left(\frac{\mathrm{d}\log\Omega(\phi)}{\mathrm{d}\phi}\right)^2\right]\partial_\mu\phi\partial^\mu\phi - \frac{V_J(\phi)}{\Omega(\phi)^2}\right). \tag{6.3}$$

When using a polynomial approximation for $f(\phi)$, the main features of this inflationary model are, as a function of the coupling strength ξ, [204]:

[1] This type of attractor is unrelated to the slow roll attractor discussed in section 3.2.4.

- $\xi = 0$: The minimally coupled case with a random scalar potential yields inflationary predictions $n_{\mathrm{s}}^{(0)}$ and $r^{(0)}$ that interpolate between small-field plateau and large-field chaotic inflation described in section 4.3. Almost all of these are ruled out by the Planck results.

- Very small ξ: At weak coupling, there is a universal behaviour for the inflationary predictions. Retaining only linear terms in the coupling strength ξ one finds [204]

$$n_{\mathrm{s}} = n_{\mathrm{s}}^{(0)} + \tfrac{1}{16}\xi f r^{(0)}, \quad r = r^{(0)} - \xi f r^{(0)}\,. \tag{6.4}$$

  Note that the inflationary predictions therefore have the same behaviour in the (n_{s}, r) plane, corresponding to a downward line with a slope of -16.

- Finite $\xi < \mathcal{O}(1)$: The original behaviour will be flattened at large field values that are beyond the region probed by the cosmic microwave background; horizon exit of CMB scales takes place closer to the minimum and hence allows for a wide range of inflationary predictions depending on the specifics of the polynomial potential. In particular, in this regime one looses the simplicity of the linear approximation, resulting in a wide range of different behaviours.

  For Higgs inflation, this regime is a particularly simple straight line, again with a slope of -16, that interpolates between quartic and Starobinsky inflation; for other starting points, the results of this regime are very different and generically complicated.

- Finite $\xi \gtrsim \mathcal{O}(1)$: Increasing the non-minimal coupling to and beyond order-one values pushes the plateau sufficiently close to the minimum of the scalar potential, yielding predictions that are indistinguishable from Starobinsky inflation, which are at next-to-leading order in $1/N$:

$$n_{\mathrm{s}} = 1 - \frac{2}{N_*} + \frac{3}{2}\frac{\log(N_*)}{N_*^2} + \dots\,, \tag{6.5a}$$

$$r = \frac{12}{N_*^2} - 18\frac{\log(N_*)}{N_*^3} + \dots \tag{6.5b}$$

  where the subleading corrections from [193] are included to the well known leading order result. The exact value of ξ where this happens depends on the specific choice of scalar potential.

An example of a strong coupling attractor model for different ξ is shown in Fig. 6.1. The model does not completely follow Eq. (6.2), and the intermediate and large-ξ behaviours are visible even for the large values for ξ considered. This will be the main motivation of the study in section 6.3. Note that for this particular model, the potential in the $\xi = 0$ limit is too steep to have 55 e-folds of inflation.

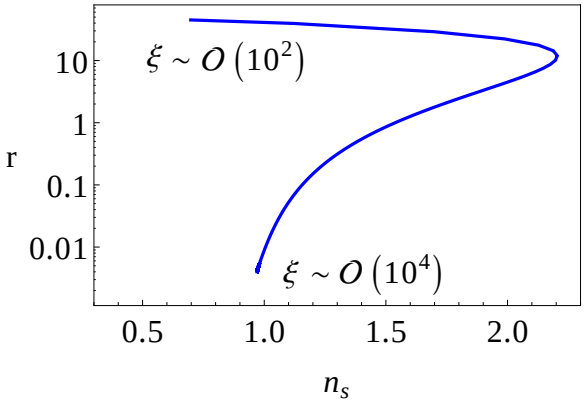

Figure 6.1: *The n_s, r predictions for gradually increased non-minimal coupling ξ at $N_* = 55$ of an example with $\Omega = 1 + \xi\phi$ and $V_J = e^{\phi} - (1 + \phi)$.*

The simplification of the latter limit arise as the first term in the kinetic function is sufficiently suppressed:

$$\Omega \ll \frac{3}{2}\Omega'^2 \,. \tag{6.6}$$

In terms of a canonically normalized scalar field χ,

$$\Omega(\chi) = e^{\sqrt{2/3}\chi}, \tag{6.7}$$

the scalar potential becomes

$$V_E = \frac{\lambda}{\xi^2}\left(1 - e^{-\sqrt{2/3}\,\chi}\right)^2 . \tag{6.8}$$

This is conformally dual to R^2-inflation (3.47), and results in the relation

$$N_* \sim \frac{3}{4}(\Omega - 1)\,, \tag{6.9}$$

for the number of e-folds.

Already in the original paper [204] it was argued that taking an independent scalar potential

$$\Omega = 1 + \xi f(\phi)\,, \quad V_J = \lambda\, g(\phi)\,. \tag{6.10}$$

does not change the leading inflationary predictions as long as the function $g(\phi)$ and the square of $f(\phi)$ share the order of their first zero while the non-minimal coupling is taken sufficiently strong.

A first quantitative investigation for a toy model of higher order corrections demonstrated that the leading order behaviour of the universal attractor can indeed be made robust once a certain value of the non-minimal coupling ξ is chosen [205]. Specifically, the Jordan frame potential was taken to be a function of the non-minimal coupling $f(\phi)$,

$$V_J(\phi) \to V_J(f(\phi)). \tag{6.11}$$

This allowed the function $f(\phi)$ to be left completely unspecified. The deviation of $V_J(f)$ from a quadratic function was then used to model corrections to the universal attractor behaviour. Different types of expansions with $\mathcal{O}(1)$ coefficients were employed, from simple monomials to different series. Remarkably, it was found that a coupling strength of $\xi \sim \mathcal{O}(10^4)$ was sufficient to maintain the leading order inflationary predictions.

The observation that a sufficiently large ξ can, regardless of an infinite tower of higher order corrections with order one coefficients, induce a Starobinsky-like inflationary plateau over a finite field range derives from ξ being able to drive $\Delta\phi < 1$ when increased. Hence all higher order terms in the Jordan frame potential are sub-leading. In other words, the effect of higher order terms can simply be pushed far away in canonical field space by sufficiently enlarging the non-minimal coupling strength ξ.

In the next sections, this observation will be further strengthened using arbitrary functions for $g(\phi)$ and $f(\phi)$. However, to have a more complete picture on the space of attractor inflation models, below we will shortly introduce the α-attractor and the pole attractor. A reader not interested in these attractors can skip the remainder of this section.

6.2.2 α-attractor

Another attractor, that was first investigated in Ref. [206], is the T-model α-attractor [207–214]. This attractor is defined as

$$\mathcal{L} = \sqrt{-g}\left(\tfrac{1}{2}R - \frac{\alpha}{1-\frac{1}{6}\phi^2}\partial_\mu\phi\partial^\mu\phi - f^2\left(\frac{\phi}{\sqrt{6}}\right)\right), \tag{6.12}$$

where $f(\phi)$ is an arbitrary function and α is a positive parameter. The value 6 is included for aesthetic reasons. As before, a canonical kinetic term can be obtained by utilizing the field redefinition [206]

$$\frac{\phi}{\sqrt{6\alpha}} = \tanh\frac{\varphi}{\sqrt{6\alpha}}, \qquad \mathcal{L} = \sqrt{-g}\left(\tfrac{1}{2}R - \partial_\mu\varphi\partial^\mu\varphi - f^2\left(\tanh\frac{\varphi}{\sqrt{6\alpha}}\right)\right). \tag{6.13}$$

Since the hyperbolic tangent is approximately shift symmetric if the argument is large, the potential will flatten for large field values if $f(\phi)$ is not diverging for $x < 1$. The flat potential in the canonical frame implies that the value of r is

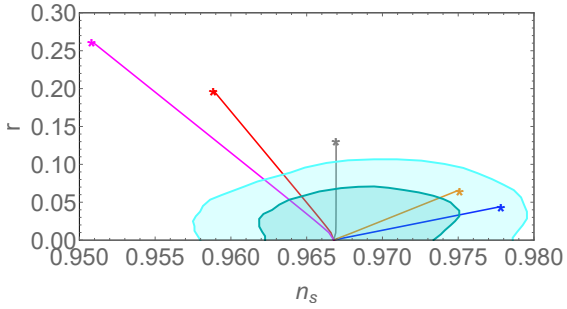

Figure 6.2: *Predictions of n_s and r for different α-attractor scenarios and $N_* = 50$ with $n = \{\frac{2}{3}, 1, 2, 3, 4\}$ for the colours blue, orange, gray, red and magenta. The stars correspond to the prediction of $V \propto \phi^n$ inflation. The cyan contour regions are the 1 and 2σ contour regions of Planck [14]. The figure is inspired on Ref. [209].*

very small, indeed for small α the large N expansion of the α-attractor for the observables, to second order in slow roll using Eqs. (4.2) is

$$n_s = 1 - \frac{2}{N} + \frac{1}{N^2}\left(\frac{4}{3} - 2C + \alpha\left(\frac{1}{n}\rho - \frac{3}{2}\right)\right), \tag{6.14a}$$

$$r = \frac{12\alpha}{N^2}\left(1 - \frac{1}{N}\left(\frac{2}{3} - 2C + \alpha\frac{1}{n}\rho)\right)\right), \tag{6.14b}$$

$$\rho = \sqrt{9 + \frac{3n^2}{\alpha}}\,, \tag{6.14c}$$

where we expanded the expression to second order in slow roll and the potential is assumed to be $f^2(\phi) = \lambda\phi^n$. The value $\alpha = 1$ corresponds to first order in $1/N$ to the Starobinsky and strong coupling attractor models in Eq. (6.5), but deviates at second order [215]. The predictions for the different inflation models are shown in Figs. 6.2 and 3.6.

From Fig. 6.2 can be inferred that in the opposite limit, where $\alpha \to \infty$, the original predictions of chaotic inflation in Eq. (3.41) are retrieved [209]. Thus is the α-attractor a method to interpolate polynomial inflation models at large α to models where $r = 0$ at low α.

An interpretation of the meaning of the parameter α is by considering the geometry of the moduli space, given by the kinetic term of the inflaton [216]. The metric of this moduli space represents the metric of a hyperbolic surface, which has a negative curvature $R = -\frac{2}{3\alpha}$. In addition, when considering a complex inflaton field, which will be the standard in supergravity realisations of inflation in section 7.5, the moduli space will represent a two-dimensional hyperbolic space with the same curvature. Therefore can the α-attractor mechanism be interpreted

as originating from a theory with a hyperbolic geometry in the moduli space, while the above analysis showed that the curvature of this space has to be large.

The peculiar structure of the non-canonical term in (6.12) can be explained using a broken conformal symmetry. Consider the following two-field conformal Lagrangian [206, 209]

$$\mathcal{L}_c = \sqrt{-g}\left[\tfrac{1}{2}\partial_\mu\chi\partial^\mu\chi - \tfrac{1}{2}\partial_\mu\phi\partial^\mu\phi + \frac{1}{12}\left(\chi^2-\phi^2\right)R - V(\phi,\chi)\right]. \tag{6.15}$$

This model contains an $SO(1,1)$ symmetry in the $\phi^2-\chi^2$ direction if $V(\phi,\chi) = V_c(\phi^2-\chi^2)$. The Lagrangian of Eq. (6.15) is in Jordan frame, but the gauge choice $\phi^2-\chi^2=6$ rotates it to the Einstein frame. In this gauge the conformal potential V_c is explicitly conformally invariant (*i.e.* flat).

The Starobinsky and the α-attractor models can be obtained from (6.15) by adding an explicit conformal symmetry breaking term. For the Starobinsky model, the required Lagrangian is [206]

$$\frac{\mathcal{L}}{\sqrt{-g}} = \frac{\mathcal{L}_c(\phi^2-\chi^2)}{\sqrt{-g}} - \frac{\lambda}{4}\phi^2\left(\phi-\chi\right)^2. \tag{6.16}$$

The gauge choice, $\phi^2-\chi^2=6$, which is solved for the fields as

$$\phi = \sqrt{6}\sinh\frac{\varphi}{\sqrt{6}} \qquad \chi = \sqrt{6}\cosh\frac{\varphi}{\sqrt{6}}, \tag{6.17}$$

leads to the Einstein frame Lagrangian of the Starobinsky model of Eq. (3.46). Similarly the T-mode α-attractor can be obtained from (6.15) by breaking the conformal symmetry with

$$\frac{\mathcal{L}}{\sqrt{-g}} = \frac{\mathcal{L}_c(\phi^2-\chi^2)}{\sqrt{-g}} - V\left(\frac{\phi}{\chi}\right)\left(\phi^2-\chi^2\right)^2. \tag{6.18}$$

With the same gauge choice $\phi^2-\chi^2=6$, this Lagrangian corresponds to the α-attractor model of Eq. (6.13).

There exists another type of α-attractor, named the E-model α-attractor, which is defined with the Lagrangian [206]

$$\mathcal{L} = \sqrt{-g}\left[\tfrac{1}{2}R - \tfrac{1}{2}\partial_\mu\phi\partial^\mu\phi - \Lambda^4\left(1-e^{-\sqrt{\frac{2}{3\alpha}}\frac{\phi}{M_\mathrm{P}}}\right)^n\right], \tag{6.19}$$

where n and α are (positive) parameters. This type of α-attractor is the large field limit of Eq. (6.13), and has observationally the same behaviour at leading order in $1/N$. However, in this thesis this attractor will not be further considered.

6.2.3 Pole attractor

The Starobinsky model, the strong coupling attractor and the α-attractor have all in common that the theories can be written with a singularity in the kinetic term and a non-singular potential. This led to the introduction of the pole attractor (or generic attractor) defined in Ref. [217], where it was shown that any Lagrangian with a pole in the kinetic function and a regular potential will have its large-N inflationary dynamics dictated by the order of this pole. Close to the pole, inflaton will evolve slowly, since its kinetic function is large which requires much energy to roll. With a field redefinition the pole in the kinetic term can be removed, and the resulting canonical inflation model will have a nearly flat potential. Since a flat potential corresponds to a small value for r, this corresponds to a small tensor-to-scalar ratio, which is currently preferred by the data. As can be read of from Eqs. (6.3) and (6.12), all attractor models shown above have a pole of order 2. Indeed, as the generic attractor predicts the values of $n_{\rm s}$ and r at leading order in $1/N$ are the same for these models.

6.3 Analytic predictions of the generic strong attractor model

After this general introduction concerning the different attractor models, we continue with investigating the strong coupling attractor obtained in section 6.2.1. The aim of this section is to explicitly show the robustness of the inflationary potential from an arbitrary number of higher order terms. Consider the frame function as well as the potential to be arbitrary polynomials with the only requirement that the Jordan frame potential and the square of the frame function share the order of their first zero for ϕ; in particular, we require the Jordan frame potential to have a minimum and the frame function to contain a term linear in the Jordan frame field ϕ. We thus make the following ansatz

$$\Omega(\phi) = 1 + \xi \sum_{n=1}^{M_\Omega} a_n \phi^n, \quad V_J(\phi) = \lambda \sum_{m=2}^{M_V} b_m \phi^m \,, \tag{6.20}$$

where

- We have kept the factor λ to be consistent with the original work [204] and will assume it to take a natural value of $\lesssim \mathcal{O}(1)$.
- We assume b_2 and a_1 to be positive in order to ensure a Minkowski minimum at $\phi = 0$ and that χ and ϕ both decrease at the same time ($d\phi/d\chi > 0$) close to the minimum.
- We have introduced $M_{\Omega,V}$ to denote the respective cut-off of both series. These will not play a role in the analytic part; in principle, both polynomials may contain an infinite number of terms.

For the general set-up (6.20), and for now assuming to be in the regime $\phi < 1$, the expression for the number of e-folds of (6.9) obtains corrections as

$$N_* \sim \frac{3}{4}\,\Omega(\phi) - \frac{b_3 \Omega(\phi)^3}{8\, b_2 a_1 \xi} + \mathcal{O}^{(2)}\left(\frac{\Omega(\phi)^2}{\xi}\right), \tag{6.21}$$

which may be understood as an expansion in Ω^2/ξ. From the zeroth-order relation (6.9) for the number of e-folds, we find that the lower bound on the non-minimal coupling strength for generating a sufficient amount of inflation within $\Delta\phi < 1$ is

$$\xi \gtrsim \mathcal{O}(N_e^2). \tag{6.22}$$

We will assume this in what follows.

To obtain a value for ξ that ensures the corrections to be sufficiently far away from the inflaton's minimum and to have inflation matching observations by Planck, it is most useful to study the inflationary observables and their dependence on the infinite tower of higher order terms. To leading order, the expressions for the inflationary observables $n_{\rm s}$ and r of (6.20) are given by

$$n_{\rm s} = 1 - \frac{2}{N_*} + \frac{64}{27}\frac{b_3}{b_2}\left(\frac{N_*}{a_1\xi}\right) + \mathcal{O}^2\left(\frac{1}{N_*}, \frac{N_*}{a_1\xi}\right), \tag{6.23a}$$

$$r = \frac{12}{N_*^2} + \frac{128}{9}\frac{b_3}{b_2}\left(\frac{1}{a_1\xi}\right) + \mathcal{O}^2\left(\frac{N_*}{a_1\xi}\right) + \mathcal{O}^3\left(\frac{1}{N_*}\right), \tag{6.23b}$$

which is in line with Ref. [218]. Expressions (6.23) are expansions in $1/N_*$ and $N_*/(a_1\xi)$. For the spectral index $n_{\rm s}$, the leading order terms are the linear contributions of the $1/N_*$ and the $N_*/(a_1\xi)$ expansions. For the tensor to scalar ratio r, the leading order terms are the quadratic and bilinear expressions of both expansions (note that we only give two of these three terms). Further subleading terms stem from higher order and cross terms in $1/(a_1\xi)$ and $N_*/(a_1\xi)$ and are denoted by $\mathcal{O}^{(n)}$. Note that we have omitted the subleading corrections of Ref. [193], i.e. higher order terms in $\log(N_*)/N_*$, for clarity.

For $n_{\rm s}$ and r to be dominated respectively by the linear and quadratic term in $1/N_*$, i.e. for prolonging the intermediate plateau of the Einstein frame potential, we quickly identify the requirement (6.22), self-consistent with the derivation's starting point. This hence marks the onset of a convergence of the inflationary predictions towards the values measured. Moreover, the next to leading order terms come with the same a_1, b_2, b_3 dependence. This implies that the ratio of the next to leading order terms has a universal form

$$\frac{\delta r}{\delta n_{\rm s}} = \frac{6}{N_*}\,. \tag{6.24}$$

This predicts that in the vicinity of the Starobinsky point in an $n_{\rm s}/r$ scatter plot, there will be deviations to both the bottom left and the top right with a fixed

slope that is independent of the specific coefficients. The former of these have b_3 negative (note that a_1 and b_2 have to be positive to guaranty the positivity of the frame function and the potential around the minimum); these corrections induce a hilltop-like deformation to the plateau. Similarly, the predictions to the top right of Starobinsky arise from positive b_3 corrections, corresponding to an upward curve in the plateau.

Thus we conclude that in the presence of a *generic* non-minimal coupling, to be contrasted to the simpler case satisfying square relation (6.2), we expect the approach to the universal attractor to take place at a later stage (i.e. larger value of ξ) but also in a cleaner manner (i.e. in a straight line). This is nicely confirmed by Fig. 6.4 and 6.1.

Turning to the comparison with observations, for higher order terms not to spoil the value of $n_{\rm s}$ observed by Planck, we consider the 2σ bound by Planck of $\delta n_{\rm s} < 0.008$ at $N_* = 55$ and find, given $a_1, b_2, b_3 \sim \mathcal{O}(1)$,

$$\xi \gtrsim 10^4 \,. \tag{6.25}$$

This hence sets, given order one coefficients, a lower bound on the non-minimal coupling strength ξ to realize observationally viable slow-roll inflation. Remarkably, the value of ξ obtained from the requirement of matching the observed spectral index $n_{\rm s}$ is also similar to the value needed to match the COBE normalization[2] (provided the self-coupling $\lambda \approx 1$). Thus two independent observational indications – in technical terms the spectral index $n_{\rm s}$ and the amplitude $A_{\rm s}$ – hint towards an otherwise ad hoc value of the theory's parameter. The length and the height of the inflationary plateau are correctly set by the single parameter ξ.

The results of Ref. [205] hence nicely carry over to our more general ansatz (6.20): given a scalar field with a minimum and polynomial non-minimal coupling with strength $\xi \gtrsim 10^4$ as required by the COBE normalization and expressions (6.23), plateau inflation with Planck-like observables will be realised.

6.4 Numerical results

We now turn to the numerical body of this work and study the behaviour of ansatz (6.20) given arbitrary coefficients. By choosing random values for a_n, b_m, a Monte Carlo analysis can be performed using a procedure based on section 4.4, but parametrize the potential instead of the Hubble function. Then we use the potential slow roll parameters to compute the flow. We chose the binomial prior distribution for a_n and b_m, thus the intervals $[-1/n!, 1/n!]$, in order to represent a Taylor series with an increasing convergence range for large truncation order[3].

[2] Recalling $A_{\rm s} = (24\pi^2)^{-1} V/\epsilon \sim 10^{-9}$ stemming from the CMB temperature data, it readily follows from Eq. (3.38) that $\xi \sim 10^5 \sqrt{\lambda}$.

[3] We will comment on the omission of the power law priors in section 6.5.

Our numerical model closely follows the approach from section 4.4, with some modifications to incorporate the non-canonical kinetic term. Thus sampling the current model in the Einstein frame (6.3), but without utilizing the canonical normalization (6.7). With a non-canonical kinetic term the first two slow-roll parameters become

$$\epsilon_{\rm V} = \frac{1}{2\,K}\left(\frac{1}{V_J}\frac{\partial V_J}{\partial\phi} - \frac{2}{\Omega}\frac{\partial\Omega}{\partial\phi}\right)^2 , \tag{6.26a}$$

$$\eta_{\rm V} = \frac{\Omega^2}{K\,V_J}\left[\frac{\partial^2}{\partial\phi^2}\left(\frac{V_J}{\Omega^2}\right) - \frac{1}{2\,K}\frac{\partial K}{\partial\phi}\frac{\partial}{\partial\phi}\left(\frac{V_J}{\Omega^2}\right)\right] , \tag{6.26b}$$

in terms of the non-canonical kinetic function

$$K = \frac{1}{\Omega} + \frac{3}{2}\left(\frac{1}{\Omega}\frac{\partial\Omega}{\partial\phi}\right)^2 . \tag{6.27}$$

The number of e-folds then follows as

$$N_* \approx \int \frac{1}{\sqrt{2\epsilon_{\rm V}}} d\chi = \int \frac{\sqrt{K}}{\sqrt{2\epsilon_{\rm V}}} d\phi\,, \tag{6.28}$$

where χ is the canonical Einstein frame and ϕ the non-canonical Jordan frame inflaton. Using these expressions for the slow-roll parameters, the rest of the procedure is similar to the one section 4.4 but using the potential slow roll parameters. This procedure is iterated 10^6 times in all ensembles shown.

We expand $n_{\rm s}$ and r only to first order in slow roll, while the accuracy of the figures will imply that we need higher precision. We do not add higher order terms since our goal is to see the approach towards the general attractor, and not to obtain very precise high order predictions for $n_{\rm s}$ and r in the attractor phase. Moreover, at this moment there is no need to use higher orders of slow roll, since the Planck bounds on $n_{\rm s}$ and r are not precise enough. However, the linear terms in the $1/N_*$ expansion of Eq. (6.5) will not be enough in comparison with the numerical data, and in principle higher order terms have to be included to match the accuracy in the figures. Performing this analysis we obtain that the so-called 'Starobinsky point' will be at $n_{\rm s} = 0.96157, r = 0.004192$ for $N_* = 50$ to first order in slow roll.

One should distinguish different late-time behaviours, listed in section 4.3. In addition to these behaviours, there is a fraction of the configurations with a zero in Ω or V (or both) before inflation starts. Negative potential and frame function are not allowed during inflation, thus we give them the label Ω, V*-negative*. In what follows, we will focus on the non-trivial trajectories.

Secondly, one should worry about the effects of the truncation of the polynomials in (6.20): do the resulting predictions depend on these? Fortunately, at the large ξ values that we are presently interested in, it is computationally possible to include a sufficient number of terms in both the non-minimal coupling and

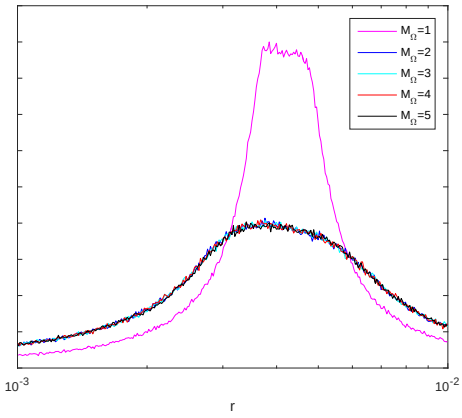

Figure 6.3: *An r density plot, on a linear scale, for different values of M_Ω with $M_V = 10$ and $\xi = 10^4$. For $M_\Omega > 2$ the system is truncation independent.*

the scalar potential to render our results truncation independent. This is illustrated in Fig. 6.3. In what follows, we will consider the specific case of $M_V = 10$ and $M_\Omega = 5$, but none of our results depend on these specific numbers if chosen sufficiently large.

Turning to the numerical results, we start with a scatter plot in Fig. 6.4, comparing the predictions for $\xi = 10^2$ and $\xi = 10^4$ with fixed $M_\Omega = 5$, $M_V = 10$ (and setting $N_* = 50$). In perfect agreement with our analytic results, indeed a clearly visible line is present that goes from bottom left to top right through the Starobinsky point shown with a red star. Around this point, its slope is given by Eq. (6.24). Moreover, this line is much more pronounced for the larger value of ξ.

Studying models close to the Starobinsky point is difficult using scatter plots, since the finite point size blurs too much information regarding the density of points. Therefore, to be able to make any observation regarding the onset of the universal attractor regime, one should consider the density of the spectrum. For this we binned the data in small bins of n_s (r) and counted the number of points within each bin, thereby marginalizing over r (n_s). The resulting curve is a rough measure for the probability distribution of the variable, since the number of points over which is sampled is large. For a true measure of the probability, the spectrum has to be normalized. However, we only calculated the number of points in a bin and divided by the total number of points, which actually depends on the chosen binsize; fortunately, this will not influence our conclusions.

The density plots for n_s and r are shown in Fig. 6.5. In these plots it is clear that for $\xi = 10^2$, the Starobinsky point is not of any importance, and the ensemble is most likely to be found in a hilltop state. When $\xi = 10^4$ a peak is clearly visible

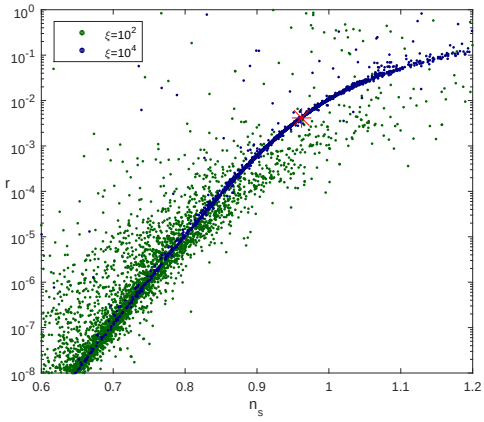

Figure 6.4: *Scatter plot of* 5000 *trajectories from the ensembles with* $M_\Omega = 5$ *and* $M_V = 10$ *for* $\xi = 10^2$ *in green and* $\xi = 10^4$ *in blue. The red star represents the Starobinsky point* $n_s \approx 0.962, r \approx 0.004$.

at the Starobinsky point, and this peak sharpens when ξ increases, just as the analysis in section 6.3 demonstrated. This centering around the Starobinsky point is a continuous process, starting from around $\xi \approx N_*^2$.

There is one final probe we want to present here that shows the emergence of the attractor phase, and that is the percentage of the number of non-trivial outcomes of inflation. As explained before, a random model can have different outcomes of inflation, depending on the shape of the potential and the frame function. However, if the attractor phase is reached at infinite ξ, the outcome becomes independent of the model, and hence all models should be non-trivially ending.

To probe this we plot the percentage of the number of outcomes in Fig. 6.6. The probability that a model ends non-trivially indeed increases when ξ increases, and the number of models with insufficient e-folds to account for the observations and the number of models with negative potential and/or frame function during inflation decrease.

Note that in Fig. 6.6 we observe the maximal increase of the number of non-trivial points around $\xi = 10^4$. Also $\xi = 10^4$ was the location where the peak was first centred around the Starobinsky point. We hence conclude that the lower bound $\xi \gtrsim 10^4$ appears first from CMB normalization arguments and our toy model analysis in subsection 6.3 and follows to be a special value also in the numerical study.

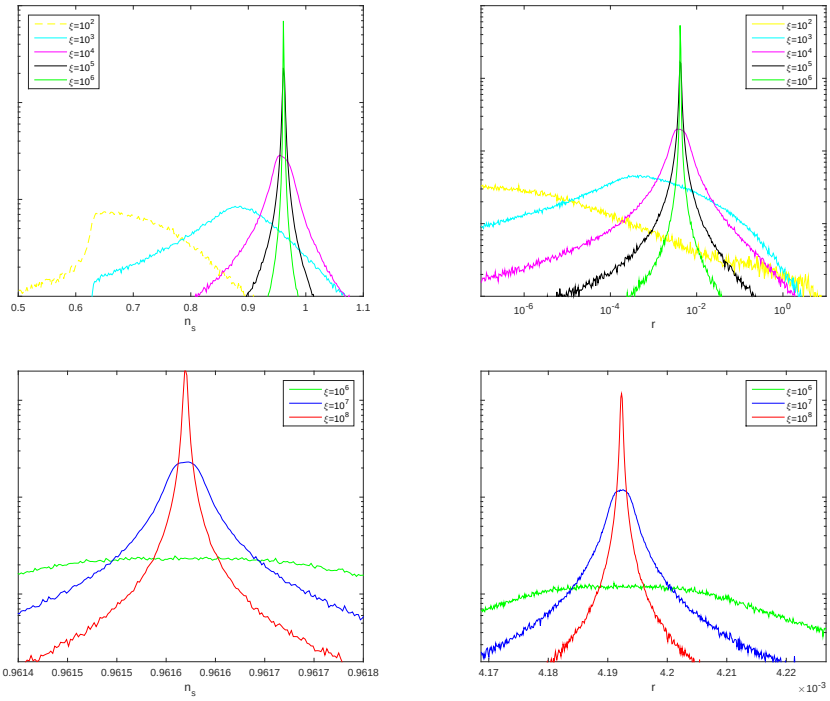

Figure 6.5: *Density profiles (on a log-scale) for different values of ξ. The left frames show the density profile for n_s, while the right frames show the density profile for r. The bottom frames are a zoom in around the Starobinsky point. Both n_s and r peak at the Starobinsky point for $\xi \gtrsim 10^4$.*

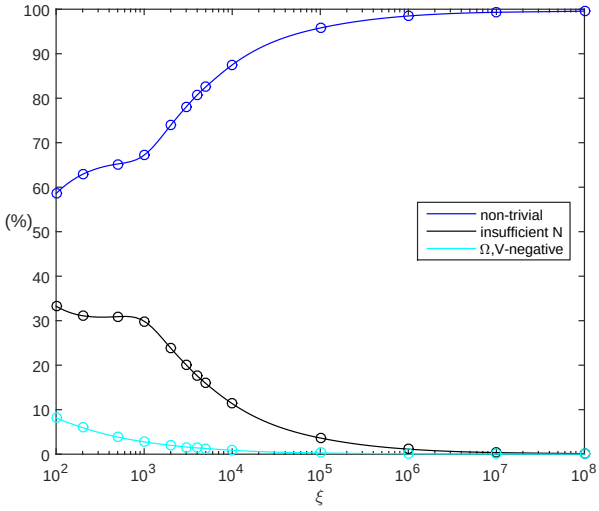

Figure 6.6: *The occurrence of different late-time behaviours as a function of ξ. The circles denote actual data points, the lines are only to guide the eye.*

6.5 Discussion

In this work, we have revisited non-minimally coupled inflation models in the spirit of Refs. [103, 119, 204]. Our interest was whether there exists a value of the non-minimally coupling strength that is preferred not only by matching COBE normalisation.

We first described how the non-minimal coupling ξ may be used to induce an effective shift-symmetry which is protected against a possibly infinite tower of higher order corrections. The size of the non-minimal coupling determines the field range of this Einstein frame shift-symmetry. We identified two distinct regimes:

- $\xi \sim \mathcal{O}(N_e^2)$: In this regime, the Jordan frame field is mostly sub-Planckian during inflation. As a consequence, it is inherently protected from most higher order terms, and may only be affected by a single correction term to the square relation (6.2). Inflation will be driven by an intermediate plateau of hilltop potential generating at least N_* e-folds. The inflationary predictions will therefore be roughly similar to those of Planck.

- $\xi > O(N_e^2)$: For larger values, the Jordan field only takes small values during inflation, and inflation is therefore protected from any higher-order term and is effectively governed the square relation (6.2). Due to the larger non-

minimal coupling, the intermediate plateau is prolonged such that the inflationary observables begin to converge towards the sweet spot of Planck. The predictions will have entered the 2-σ contours of Planck once $\xi \sim \mathcal{O}(10^4)$. This lower bound is in remarkable agreement with the value of ξ required to match the scalar perturbation amplitude $A_{\rm s}$ [219].

In the numerical component of this work, we parametrized non-minimal coupling functions and potentials as arbitrary polynomials. Drawing the coefficients of the polynomials randomly, we examined the resulting Einstein frame potentials to find out whether observationally viable slow-roll inflation occurs. We found that with increasing non-minimal coupling ξ, the number of non-trivial inflationary trajectories increases. Remarkably, this increase is most pronounced in the range $\xi \sim \mathcal{O}(N_*^2)$ to $\xi \sim \mathcal{O}(10^4)$. Furthermore, we found that at $\xi \sim \mathcal{O}(N_*^2)$ there is a transition from a peak at low $n_{\rm s}$ to a peak at the Starobinsky prediction of $n_{\rm s} = 0.962$.

In other words, a non-minimal coupling ξ can induce a shift-symmetry protected against all higher order terms (i.e. length of an inflationary plateau) [210, 220]. The preferred value to match the COBE normalization coincides with the inflationary observables taking Planck-compatible values.

To have a prediction of the implications of the assumption of factorial fall-off of the coefficients we repeated the analysis with the power law prior, using the random interval as $[-1, 1]$ for a_n, b_n in (6.20). Though, as will be explained in appendix B, the low order truncations of this system were different, the truncation independent regime showed the same observations. Thus we conclude that the above analysis is independent of the choice of the prior interval.

Regarding the type of series used, for instance using Fourier series instead of polynomials, we expect that our main finding; that for large ξ all models are located around the Starobinsky point, is still valid. However, the approach towards this point, i.e. the predictions for $\xi \sim \mathcal{O}(N_*^2)$ and $\xi \sim \mathcal{O}(10^4)$, might in general be different as well as how these models approach the Starobinsky point, i.e. Fig 6.4. Studying the model dependence of the predictions is an interesting follow-up analysis.

CHAPTER 7

Supersymmetry and supergravity

Introduction

In section 2.1 the standard model of particle physics was constructed. This model fits extremely well with current experiments, but in section 2.1.1 some theoretical puzzles of the standard model were raised. These were i) the naturalness problem of the Higgs potential, ii) why the running of the standard model gauge parameters does not allow for unification into a singly connected gauge group (a grand unified theory or GUT) and iii) how at energies of the order of the Planck scale $M_{\mathrm{p}} \approx 2.435 \times 10^{18}$ GeV gravitational effects are encoded.

Finding a solution for these problems is simplified when imposing that the standard model is supersymmetric. However, supersymmetry cannot be an explicit symmetry, thus has to be broken spontaneously. If the supersymmetry breaking scale is close to the electroweak scale, the loop terms originating from the supersymmetric partner of the top quark (named stop squark), will cancel loop contributions from the top quark, rendering the Higgs mass stable. In addition, it is possible for such models (even models with a larger supersymmetry breaking scale) to make the standard model couplings converge at the GUT scale. Finally, the most popular model that unifies gravity with the standard model is string theory, which requires supersymmetry for consistency.

To naturally solve the Higgs hierarchy problem, the stop mass has to be roughly in the TeV range. However, no signatures of the stop squark, or other supersymmetric particles, have been observed by experiments at the Large Hadron Collider (LHC) up to roughly a TeV. Therefore, solving the Higgs hierarchy problem with

supersymmetry is becoming difficult. Lifting the requirement of solving the hierarchy problem, grand unification is possible if the masses of the superpartners are below roughly $M_{\mathrm{GUT}} \approx 10^{13}$ TeV. However, it is unfortunate that the energy scale at which supersymmetry is broken is unknown.

Supersymmetry is an interesting symmetry to be considered in combination with inflation since inflation takes place at very large energies, at which supersymmetry might be exact. Moreover, the inflaton field value during inflation can be sufficiently large that some low energy effects of string theory are relevant. The low energy limit of string theory is described by supergravity, which is the quantum field theory invariant under local supersymmetry transformations.

In section 7.1, supersymmetric quantum field theories will be studied, followed in section 7.2 by supersymmetry breaking. Then, in section 7.3, the nonlinear realisation of supersymmetry will be studied using nilpotent superfields. In section 7.4 global supersymmetry will be gauged to build the theory of supergravity. Finally, in section 7.5 supersymmetric theories of inflation will be reviewed, with focus on nilpotent inflation in supergravity. This section closes with a few words on reheating and the gravitino problem.

The following sections on global (or rigid) supersymmetry are based on Refs. [221–223].

7.1 Basics of supersymmetry

7.1.1 Supersymmetric Lagrangians

The defining feature of supersymmetry is a fermionic, hence anticommuting, generator of the symmetry group. This is represented in the supersymmetry algebra [221]

$$\{Q, Q^\dagger\} = 2\sigma^\mu P_\mu, \qquad \{Q, Q\} = \{Q^\dagger, Q^\dagger\} = 0, \qquad [P^\mu, Q] = [P^\mu, Q^\dagger] = 0, \tag{7.1}$$

where Q is the supersymmetry generator, P^μ the operator of four-momentum from the Poincaré algebra and $\sigma^\mu = \{\mathbb{1}, \sigma^i\}$ are the Pauli matrices (σ^i) supplemented with the identity matrix ($\mathbb{1}$). Since the generator of the supersymmetry algebra is fermionic, anticommutators are used in Eq. (7.1) instead of commutators. Here and in the rest of this chapter fermions are represented as Weyl spinors and spinor indices are suppressed.

After having defined the symmetry of a theory the particle content can be chosen as irreducible representations of the symmetry group. However, since the supersymmetry transformation changes a particle into another particle, sets of particles have to be defined that collectively transform under the supersymmetry rules. The anticommuting nature of the supersymmetry generator implies that the number of states related by supersymmetry transformations are given by the number of supersymmetry generators $\mathcal{N}$. In this thesis only $\mathcal{N} = 1$ superalgebras

will be considered, so that every particle has a single supersymmetric partner with a difference in spin of 1/2 [221].

As an example, consider a scalar field ϕ and a fermion ψ that transform under supersymmetry transformations as [221]

$$\delta_\epsilon \phi = \sqrt{2}\epsilon\psi, \qquad \delta_\epsilon \psi = i\sqrt{2}\sigma^\mu \bar{\epsilon}\partial_\mu \phi, \tag{7.2}$$

where the spinor ϵ is the parameter of the variation. Using the equations of motion it can be shown that the algebra is closed on-shell. The Lagrangian of this theory, which is named the massless Wess-Zumino model,

$$\mathcal{L} = \partial_\mu \phi^\star \partial^\mu \phi - i\bar{\psi}\bar{\sigma}^\mu \partial_\mu \psi \tag{7.3}$$

is the Lagrangian of a free scalar field and a free fermion field. Using the supersymmetry transformation (7.2), the action of Eq. (7.3) is invariant since

$$\begin{aligned} \delta S &= \int \mathrm{d}^4x\, \delta\, \mathcal{L}, \\ &= \sqrt{2} \int \mathrm{d}^4x\, \left(\epsilon(\partial_\mu \psi \partial^\mu \phi^* - \sigma^\nu \bar{\sigma}^\mu \partial_\nu \phi^* \partial_\mu \psi) + (\partial_\mu \phi \partial^\mu \bar{\psi} + \bar{\psi}\bar{\sigma}^\mu \sigma^\nu \partial_\mu \partial_\nu \phi)\bar{\epsilon}\right), \\ &= 0, \end{aligned} \tag{7.4}$$

where in the last step the first three term were integrated by parts and the identity $\sigma^\mu \bar{\sigma}^\nu \partial_\mu \partial_\nu \phi = \partial_\mu \partial^\mu \phi$ was used [223].

An important technical detail of the supersymmetry transformations (7.2) is that it is only closed on-shell. This is manifest by counting the number of degrees of freedom [221]. For a symmetry to be exact, the number of degrees of freedom inside the theory should be the same before and after a symmetry transformation. Hence the number of bosonic degrees of freedom should equal the number of fermionic degrees of freedom. On-shell both the (complex) scalar and the fermion have two degrees of freedom, while off-shell the fermion has four degrees of freedom and the scalar only two. To equal the number of degrees of freedom also off-shell, a boson has to be introduced that has two degrees of freedom off-shell and carries no degrees of freedom on-shell. This auxiliary field F, appears in the massless Wess-Zumino model of Eq. (7.2) with only the potential term F^*F and no kinetic term, so its equation of motion is trivial. With this auxiliary field the supersymmetry transformations [221]

$$\delta_\epsilon \phi = \sqrt{2}\epsilon\psi, \tag{7.5a}$$
$$\delta_\epsilon \psi = i\sqrt{2}\sigma^\mu \bar{\epsilon}\partial_\mu \phi + \epsilon F, \tag{7.5b}$$
$$\delta_\epsilon F = -i\bar{\epsilon}\bar{\sigma}^\mu \partial_\mu \psi, \tag{7.5c}$$

close also off-shell, meaning without imposing the equations of motion. This set of fields forms a linear representation of the superalgebra and is therefore called a multiplet.

As the name suggests, adding a mass to the Wess-Zumino model is possible. However, since the momentum operator and the supersymmetry generator Q commute (see Eq. (7.1)), the masses of the particles in the multiplet should be equal [221]. It is also possible to add an extra set of fields and introduce interaction terms, but this is less straightforward since the interactions have to be invariant under supersymmetry transformations. It is possible to build an interacting Wess-Zumino model using the formalism introduced above [221], but it is simpler to use superfields.

7.1.2 Superfields

In the example of Eq. (7.2) the supersymmetry relations were imposed rather straightforwardly using only a minimal number of fields. But it was also recognized that when evaluating multiple fields with interaction terms it is complicated to find a supersymmetric Lagrangian. Therefore it is convenient to combine the multiplets into a single field, named a superfield. Superfields are defined within superspace, which is a space obtained from enlarging the normal space-time coordinates to $\{x^\mu, \theta, \bar{\theta}\}$, where x^μ are the four dimensions of space-time and θ ($\bar{\theta}$) is (the complex conjugate of) an anticommuting (Grassmann) coordinate.

The superfield Φ is defined as a field in superspace. To express the superfield in components, it is Taylor expanded in the Grassmann numbers θ and $\bar{\theta}$ [223]

$$\begin{aligned}\Phi(x,\theta,\bar{\theta}) =&\phi(x) + \theta\eta(x) + \bar{\theta}\bar{\xi}(x) + \theta^2 m(x) + \bar{\theta}^2 n(x) + \theta\sigma^\mu\bar{\theta}A_\mu(x)\\ &+ \theta^2\bar{\theta}\bar{\lambda}(x) + \bar{\theta}^2\theta\psi(x) + \theta^2\bar{\theta}^2 d(x),\end{aligned} \tag{7.6}$$

where $\phi(x)$ and the lower case Latin letters represent scalars, the other Greek letters fermions and A_μ a vector field. This superfield consists of far more components than considered in the previous section and these additional components will appear as auxiliary fields. To reduce the number of auxiliary fields, the chiral superfield is defined by imposing the constraint

$$\bar{D}\Phi = \partial_{\bar{\theta}}\Phi = 0, \tag{7.7}$$

where the covariant derivative (D) is defined such that it anti-commutes with the supersymmetry operator, hence [221]

$$D\Phi^\dagger = \left[\partial_\theta - 2i(\sigma^\mu\theta^\dagger)\partial_{y^\mu}\right]\Phi^\dagger, \tag{7.8}$$

and $y^\mu = x^\mu + i\bar{\theta}\bar{\sigma}^\mu\theta$. The constraint (7.7) on the superfield Φ is solved in the component notation of Eq. (7.6) as [223]

$$\Psi = \phi(y) + \sqrt{2}\theta\psi(y) + \theta^2 F(y), \tag{7.9a}$$

$$\begin{aligned}&= \phi(x) + \sqrt{2}\theta\psi(x) + \theta^2 F(x) - \frac{i}{\sqrt{2}}\theta^2\bar{\theta}\bar{\sigma}^\mu\partial_\mu\psi(x)\\ &\quad + i\bar{\theta}\bar{\sigma}^\mu\theta\partial_\mu\phi(x) + \frac{1}{4}\theta^2\bar{\theta}^2\partial_\mu\partial^\mu\phi(x),\end{aligned} \tag{7.9b}$$

where the auxiliary field F is a combination of the scalars appearing in Eq. (7.6) and in the second line the fields are expanded in x. The matter content of the chiral superfield in (7.9) equals the matter content of the Wess-Zumino model in Eq. (7.5), hence this model of free supersymmetric particles can be obtained from a single chiral superfield.

Describing gauge interactions with a chiral superfield is not possible, since it does not contain a spin-1 gauge boson. For this purpose the vector multiplet (V) was defined as the superfield satisfying the constraint [221]

$$V = V^*. \tag{7.10}$$

This constraint invokes a multiplet with 4 real scalars, 2 fermions and a vector field, of which the full expression can be found in [221]. In addition, the gauge transformations use a complex gauge parameter and the imaginary part of this transformation can be used to gauge some of the fields in the vector multiplet. In this Wess-Zumino gauge, the vector superfield becomes in components [221]

$$V = \theta\sigma^\mu\bar{\theta}A_\mu + \theta^2\bar{\theta}\lambda^\dagger + \bar{\theta}^2\theta\lambda + \frac{1}{2}\theta^2\bar{\theta}^2 d, \tag{7.11}$$

where d is an auxiliary field similar to F in the chiral multiplet (7.9). With these two types of superfields, chiral and vector, supersymmetry invariant actions can be obtained.

7.1.3 Kähler and superpotential

To build a supersymmetry invariant action, we can use that the action

$$S = \int \mathrm{d}^4x\, \mathrm{d}^2\theta\, \mathrm{d}^2\bar{\theta}\, K(\Phi, \Phi^\dagger) + \int \mathrm{d}^4x\, \mathrm{d}^2\theta\, W(\Phi) + \text{c.c.} \tag{7.12}$$

is invariant under supersymmetry transformations, where the real function $K(\Phi, \bar{\Phi})$ is named the Kähler potential and the holomorphic function $W(\Phi)$ the superpotential [222]. The mass dimension of the Kähler potential is 2, and of the superpotential 3.

When considering vector fields, typically a gauge symmetry is considered. For a general (non-Abelian) gauge group the supersymmetric field strength is defined as [221]

$$\mathcal{W}_\alpha \equiv -\frac{1}{4}\bar{D}_{\dot{\alpha}}\bar{D}^{\dot{\alpha}}\left(e^{-V}D_\alpha e^V\right), \tag{7.13}$$

where α is a spinor index and D_α is the SUSY covariant derivative defined in Eq. (7.8). In analogy with non-supersymmetric gauge theories, the field strength can be given a group index using

$$\mathcal{W}_\alpha = 2g_a T^a\, \mathcal{W}^a_\alpha, \tag{7.14}$$

where T^a are the generators of the gauge group. Then the action becomes

$$S = \int \mathrm{d}^4x\, \mathrm{d}^2\theta \left(\frac{1}{4} - i\frac{g_a^2\Theta_a}{32\pi^2}\right) \mathcal{W}^a\, \mathcal{W}^a, \tag{7.15}$$

where Θ is a parameter and the spinor index of $\mathcal{W}$ is again suppressed. When constructing a supersymmetric theory of QCD, the Θ parameter is the same as appearing in Eq. (2.4), in the discussion of the strong CP-problem. Since the field strength is a chiral superfield, this is an F-term.

If the gauge group is Abelian, also a D-term called the Fayet-Iliopoulos term can be written, [221]

$$S = \int \mathrm{d}^4x\, \mathrm{d}^2\theta\, \mathrm{d}^2\bar{\theta}\, (-2\kappa V), \tag{7.16}$$

where κ is a real parameter. If κ is nonzero this D-term can be used for supersymmetry breaking, but this possibility will not be considered in this thesis.

Combining Eqs. (7.12) and (7.15) and neglecting the Fayet-Iliopoulos term, the full action for a supersymmetric gauge theory with chiral superfields Φ_i and gauge fields V_j, where i and j run over the different fields, is

$$\begin{aligned} S = &\int \mathrm{d}^4x\, \mathrm{d}^2\theta\, \mathrm{d}^2\bar{\theta}\, K(\Phi_i, \tilde{\Phi}_i^\dagger) \\ &+ \int \mathrm{d}^4x\, \mathrm{d}^2\theta \left[\left(\frac{1}{4} - i\frac{g_a^2\Theta_a}{32\pi^2}\right) \mathcal{W}^a\, \mathcal{W}^a + W(\Phi_i)\right] + \text{c.c.}, \end{aligned} \tag{7.17}$$

where the fields $\tilde{\Phi}^\dagger \equiv \Phi^\dagger e^V$ are used to make the Kähler potential gauge invariant.

For most inflationary purposes only the scalar part of the action (7.17) is required. Neglecting gauge interactions, the scalar potential is [222]

$$V_s = (K_{i\bar{j}})^{-1}\, W_i \bar{W}_{\bar{j}}, \tag{7.18}$$

where $K_{i\bar{j}} = \partial^2 K/\partial\phi_i \partial\bar{\phi}_{\bar{j}}$ and $W_i = \partial W/\partial\phi_i$. In this expression the scalar components of the superfields should be used.

A feature of supersymmetric field theories are the non-renormalization theorems, which state that terms in the superpotential do not receive perturbative corrections [224]. Hence, in Eq. (7.18) loop terms appear only through the Kähler potential and a general expression for the 1-loop terms can be obtained, in analogy with the Coleman-Weinberg potential in field theory. Assuming that the tree level Kähler potential is canonical, this contribution is [224]

$$K_{\text{1-loop}} = -\frac{1}{32\pi^2}\, \mathrm{tr}\left[M^\dagger M \log\frac{M^\dagger M}{\Lambda^2}\right], \tag{7.19}$$

where Λ is the cut-off scale and $M_{ij} = \langle \partial^2 V/\partial\phi_i \partial\phi_j \rangle$ is the tree level mass matrix. The 1-loop correction to the scalar potential of Eq. (7.18) from the 1-loop

corrections of the Kähler potential are

$$V_{s,\text{1-loop}} = -\frac{1}{64\pi^2}\,\text{Str}\left[(M^\dagger M)^2 \log\frac{M^\dagger M}{\Lambda^2}\right], \tag{7.20}$$

where the supertrace Str was defined as

$$\text{Str}\,A = \sum_j (-1)^{2j}(2j+1)\,\text{tr}\,(A)\,, \tag{7.21}$$

and sum over j corresponds to the sum over all particles with spin j. This equation is relevant for discussing classically flat directions, for instance in the context of the breaking of supersymmetry, as will be explained in section 7.2.

7.1.4 The MSSM

Similar to the construction of the standard model, the minimal supersymmetric standard model (MSSM) is obtained by imposing that the theory is i) invariant under gauge transformations of the group $SU(3)\times SU(2)_L \times U(1)$, ii) is renormalizable and iii) has the minimal matter content necessary to explain the observations. In the MSSM, the standard model fermions are represented by chiral superfields and the standard model gauge fields by vector multiplets. No additional fields except of the superpartners of the standard model fields are introduced, with the exception of the Higgs field which has to be split into two chiral superfields for symmetry reasons, as will be explained below. The full set of particles of the MSSM is shown in Fig. 7.1. For terminology, all scalar superparners have a s- prefix, while the fermionic superparners have an -ino suffix. For example, the scalar superpartner of a quark is named squark and the fermionic superpartner of the gluon is the gluino.

In addition, a new symmetry is introduced in the MSSM to forbid proton decay at tree level. This symmetry, called R-parity, is a Z_2 symmetry for which the standard model particles are even and the superpartners are odd. Hence, there will be no vertices containing an odd number of superpartners. Due to R-parity the lightest supersymmetric particle (LSP) cannot decay, and is a candidate for dark matter. The conditions of R-parity together with the conditions i),ii) and iii) discussed above reduce the Kähler potential to the minimal form $K = \Phi_i^\dagger \Phi_i$ (with i running over all superfields), and the superpotential to [221]

$$W = \tilde{u}^\dagger y_u Q H_u - \tilde{d}^\dagger y_d Q H_d - \tilde{e}^\dagger y_e L H_d + \mu H_u H_d, \tag{7.22}$$

where y_i and μ are parameters. Note that to preserve $SU(2)$ invariance in the holomorphic superpotential an additional Higgs field is introduced.

The R-parity that was imposed in the standard model can be extended to R-symmetry, which is a $U(1)$ symmetry. Under R-symmetry, the superpotential has R-charge 2 while the Kähler potential has a vanishing R-charge. If R-symmetry

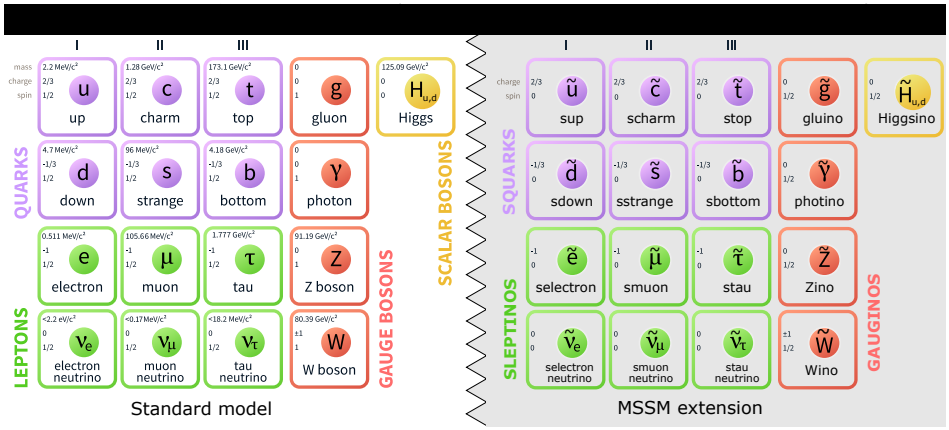

Figure 7.1: *The particle content of the MSSM, on the left the standard model particles from Fig. 2.1, in the grey region the (unobserved) MSSM particles. Note that the Higgs doublet gets doubled into H_u and H_d.*

is exact, quantum corrections will not introduce R-symmetry breaking, while if R-symmetry is broken by a single operator in the theory, the R-symmetry breaking operators will be suppressed by the coefficient of this R-symmetry breaking operator. Hence, this symmetry generates selection rules on the operators that appear in the Lagrangian.

No superpartner of a standard model particle has been observed in experiments, which sets lower bounds on the masses of these particles. Unfortunately, these bounds are strongly model dependent. Therefore, the bounds on the superpartner masses are typically represented as a function of the mass of another superpartner in this so called simplified model setup. For instance, Fig. 7.2 depicts the excluded region for the gluino mass horizontally versus the lightest neutralino vertically using data from the CMS collaboration [225]. The neutralino is a linear combination of the different spin-1/2 neutral particles that appear in the MSSM, thus a combination of the Higgsinos, the Bino and the neutral component of the Wino. In the simplest models of supersymmetry breaking, the neutralino is the LSP[1]. All other superpartners are assumed to be parametrically more massive than the gluino in this analysis. If the gluino is lighter than the neutralino, this decay is kinematically forbidden, so this region of the parameter space is not observed in the analysis used for Fig. 7.2. The results from the ATLAS detector are

[1]If gravity is included, the gravitino is often lower in mass, but the decay width of the neutralino to the gravitino is typically unobservably long at collider scales.

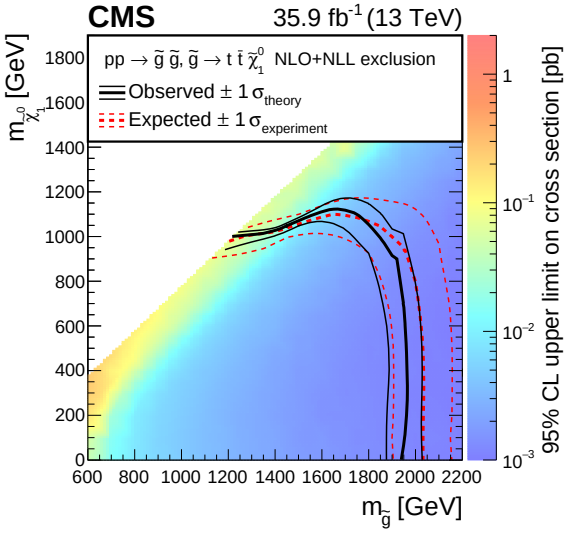

Figure 7.2: *Measured constraints on the mass of the gluino $\tilde{g}$ and neutralino ($\tilde{\chi}_1^0$) in the simplified scenario that the gluino decays fully into a top quark pair and the neutralino. The neutralino is considered the LSP and all other superparticles are assumed to be infinitely massive. Figure from [225] .*

similar [226].

7.2 Supersymmetry breaking

Supersymmetry imposes that the masses of the superpartners are the same as the masses of the particles. If supersymmetry is an exact symmetry of nature, there should be a whole zoo of bosonic superpartners of the standard model fermions. None of these particles are observed, so supersymmetry is not an exact symmetry of nature. This leaves open the possibility that supersymmetry is broken either explicitly or spontaneously at some energy scale. To keep the theory predictive below the supersymmetry breaking scale, spontaneous supersymmetry breaking will be imposed in this thesis [221]. In this section we study how a theory with a supersymmetric Lagrangian can break supersymmetry in the ground state of the theory.

Supersymmetry is broken spontaneously if the ground state does not have zero potential energy, since if the ground state has energy the algebra of Eq. (7.1) can not be fulfilled due to the appearance of the momentum operator [221]. The

potential of a supersymmetric theory is

$$V = \sum_i |F_i|^2 + \sum_j |D_j|^2, \tag{7.23}$$

where the index i and j run over all F and D terms as defined in section 7.1.3. The supersymmetric theory is therefore spontaneously broken if in the vacuum $F \neq 0$ and/or $D \neq 0$. The possibility that $D \neq 0$ can only be obtained if the gauge symmetry is Abelian through the Fayet-Iliopoulos term of (7.16) or if the symmetry is broken. It turns out that a breaking of supersymmetry through the $U(1)_Y$ of the MSSM is impossible, because if a Fayet-Iliopoulos term is added to the action there exists a vacuum in which the gauge symmetries are broken but supersymmetry is not [221]. Hence, for D-term supersymmetry breaking an additional Abelian gauge symmetry has to be introduced. We will not discuss this possibility, but instead use a nonzero F-term to break supersymmetry.

Chiral superfields models with a nonzero F-term in the vacuum are named O'Raifertaigh models. Typically, these models introduce a superfield that has a linear term in the superpotential. If, due to a proper choice of the superpotential, all the F-terms ($F_\Phi = \partial W/\partial\Phi$) cannot simultaneously vanish anywhere in field space, then supersymmetry is spontaneously broken.

The mode with a nonzero F-term contains a massless fermion called the goldstino – which is analogous to the massless bosonic Goldstone mode in theories with a broken bosonic symmetry – and its scalar superpartner the sgoldstino. In spontaneously broken supersymmetric models, there is no a-priori reason for the sgoldstino to be massless. However, in typical examples of O'Raifertaigh models the sgoldstino potential completely vanishes. Since there is no symmetry that protects the sgoldstino mass, a potential appears at loop level through the Coleman-Weinberg term in Eq. (7.20). For this reason the sgoldstino has only a potential at loop level.

A problematic feature of the O'Raifertaigh model is that the supertrace over the masses of all particles satisfies the sum role [221]

$$\mathrm{Str}\left(m_i^2\right) = \sum_j (-1)^{2j}(2j+1)\,\mathrm{tr}\left(m_j^2\right) = 0. \tag{7.24}$$

This implies that there must be scalar degrees of freedom with masses below the mass of the heaviest fermion. If also lepton flavour conservation is considered, the bound becomes $m_{\tilde{e}_1}^2 + m_{\tilde{e}_2}^2 - 2m_e^2 = 0$, where the $\tilde{e}_i$ represent the two (real) selectrons and e the electron. This forces the mass of at least one of the selectrons to be below the electron mass, which is experimentally ruled out [221].

The sum rule (7.24) assumes that the supersymmetry breaking field is directly coupled to the MSSM fields. This is not necessary, it is possible to introduce an additional sector that does not couple to the MSSM at tree level and in which supersymmetry is broken. The supersymmetry breaking is then mediated to the

standard model sector. There are different proposals how to mediate the supersymmetry breaking in the hidden sector to the observable sector. The two most popular scenarios are through gravitational interactions and through messenger particles. In the following both will be shortly explained. In chapter 8 gauge mediated supersymmetry breaking will be used to propagate the supersymmetry breaking.

Gravity couples to all particles identically, hence even if there are some fields completely disconnected from the visible sector, there will always be gravitational interactions between them. Since gravity couples equally to all particles, supergravity will provide new non-renormalizable interactions between the visible and the hidden sectors [221]. From dimensional analysis, the masses introduced for the superpartners are of the order of

$$m_{\text{soft}} \approx \frac{F}{M_{\text{p}}}, \tag{7.25}$$

where F is the size of the F-term that breaks supersymmetry.

Though gravity mediation is the a popular mediation scheme, there are several drawbacks. The first is that there is no guarantee that the sparticle mass matrices will be aligned with the particle mass matrices. The off-diagonal terms in the sparticle mass matrix can generate a breaking of accidental symmetries of the standard model, for instance flavour symmetry, whose breaking leave very clear signatures in experiments. This problem does not exist if the full supergravity (or string) theory suppresses these terms. However, this is the second drawback of using gravity mediation: it is not known how to properly address quantum gravity theories. Note that this is only a technical issue that might be solved in the future. Moreover, since the LHC data pushes the lower bound on the sparticle masses above the TeV scale, the supersymmetry breaking scale might be high enough to prevent the flavour mixing to appear in current experiments.

Another scheme to mediate supersymmetry breaking to the standard model is gauge mediation [227]. In gauge mediation, messenger particles (X) are introduced, which are gauged under the standard model symmetry group and obtain a mass due to a coupling in the superpotential with the goldstino multiplet (S),

$$W \supset ySX\tilde{X}. \tag{7.26}$$

Due to this mass term, the fermion component of X gets a mass from the sgoldstino vacuum expectation value (VEV), while the scalars obtain an additional correction from the F term. Since X and $\tilde{X}$ are charged under the standard model gauge group, supersymmetry breaking is mediated to the MSSM. The mass of the gauginos is generated by 1-loop diagrams, while the gauge bosons are protected by gauge symmetry. The mass splitting of the chiral fields in the MSSM is then obtained at 2-loop order.

A simple model of gauge mediation is to assume that there exists an $SU(5)$ grand unification group. By introducing N_5 messengers X_j (and $\tilde{X}_j$), where the

index j runs from 1 to N_5, in the (anti-)fundamental representation of $SU(5)$, the superpotential of the messenger sector can be written as

$$W_{\text{mess}} = \lambda S X_j \tilde{X}_j, \tag{7.27}$$

where S is the goldstino field and λ a dimensionless coupling. Since the gaugino masses are obtained at 1-loop, there masses will be [221, 227]

$$m_{\lambda_a} = \frac{N_5 \alpha_a}{4\pi} \frac{F}{M}, \tag{7.28}$$

where $M = \lambda \langle S \rangle$ is the mass of the messenger fields and α_a the coupling constant of type a running from 1 to 3. The masses of the sfermions are 2-loop suppressed,

$$m_{\phi_i}^2 = 2N_5 \sum_a C_a(\phi_i) \left(\frac{\alpha_a}{4\pi}\right)^2 \left(\frac{F}{M}\right)^2, \tag{7.29}$$

where the $C_a(\phi_i)$ are the quadratic Casimir invariants. In Eqs. (7.28) and (7.29) the running of the masses between the energy scale of gauge mediation (M) and the LHC scale was neglected. The true masses at the energies of current experiments have to be obtained by properly taking this running into account.

7.3 Constrained superfields

7.3.1 Nilpotent superfields

Similar to spontaneously broken bosonic symmetries, it is possible to construct a non-linear realisation of supersymmetry using constrained superfields. This non-linear realisation of supersymmetry will be used in section 7.5 to simplify the construction of inflationary potentials in supergavity and will be the main subject of chapter 8.

In bosonic theories the study of non-linear realisations of global symmetries is a useful technique to explain the low-energy theory if the symmetry is spontaneously broken, see for instance Ref. [228]. The spontaneous breaking of the global symmetry generates a mass splitting between the different states. The heavy states can be integrated out and only the (mass-less) Goldstone modes are left in the theory. These Goldstone modes transform along each other under the original group, but this symmetry is non-linearly realised.

The same technique can be applied to supersymmetry. In fact, the first supersymmetric action that was constructed by Volkov and Akulov in 1973 [229] used non-linearly realised supersymmetry, which was further developed in Refs. [230, 231]. In Refs. [231–233] was shown that the non-linear realisation of supersymmetry is analogous to a theory of linearly realised supersymmetry if supersymmetry is spontaneously broken. It is expected that at high energies supersymmetry will

be realised linearly, but a non-linear realisation is more elegant in the low-energy limit of the theory.

Supersymmetry is nonlinearly realised by introducing a nilpotent chiral superfield S, which satisfies the constraint

$$S^2 = 0. \tag{7.30}$$

When writing this into components using Eq. (7.9), Eq. (7.30) leads to

$$s = \frac{\psi_s^2}{2F_s} \qquad s\psi_s = 0, \qquad F_s \neq 0 \tag{7.31}$$

where s, ψ_s and F_s are respectively the (complex) scalar part, the fermion part and the F-term of the goldstino superfield S. The third relation in Eq. (7.31) implies that supersymmetry is spontaneously broken. Note that, since fermions are anticommuting, the first condition of (7.31) solves the second, hence only the first condition has to be imposed. In addition, this relation implies that the sgoldstino s is completely determined by the goldstino ψ_s. This will be an important feature of nilpotent models when discussing inflation in section 7.5.

To exemplify the appearance of the constrained superfield in spontaneously broken supersymmetry, consider the toy model [231]

$$K = SS^\dagger - \frac{c}{\Lambda^2}\left(SS^\dagger\right)^2, \qquad W = fS, \tag{7.32}$$

where c and f are positive constants and Λ is the cut-off scale of the effective theory. This cut-off scale originates from the high-energy (UV) physics that generated the second term in the Kähler potential of which the origin will be discussed in chapter 8. Using Eq. (7.18), the sgoldstino mass can be obtained

$$m_s^2 = \frac{4c}{\Lambda^2} f^2. \tag{7.33}$$

Note that this mass is inversely proportional to the cut-off scale of the effective theory. If the theory is evaluated at an energy below the sgoldstino mass, this particle can be integrated out. By computing the full Lagrangian from Eq. (7.6), the equation of motion for the sgoldstino can be obtained. This equation of motion is solved if s satisfies Eq. (7.31), with $\langle F_s \rangle = -f$, hence in the IR this theory resembles a nilpotent theory. Since $\langle F_s \rangle$ is nonzero, supersymmetry is indeed spontaneously broken. The sgoldstino is integrated out, which is a general feature of nilpotent theories. For this reason these theories are also dubbed sgoldstinoless.

7.3.2 Additional constrained superfields

When considering supersymmetric theories in the (IR) limit where supersymmetry is broken, the superfields will include a light particle and its heavy superpartner.

In the IR-theory, the heavy sparticle will be too heavy to interact with other states and can be removed. For this, additional constraints between the nilpotent superfield (S) and other superfields (Y) were introduced in Ref. [231]. Due to these constraints some components in Y are projected out similarly to the removal of the sgoldstino from the nilpotent superfield. There are two reasons for this to be interesting. First, as anticipated above, it can be utilized to obtain a theory with only the standard model and the goldstino [231]. This theory has the full set of couplings between the goldstino and the standard model fields, which is nontrivial to obtain if linear supersymmetry breaking is considered. Secondly, this type of constraints can be used to remove the sinflaton, the complex scalar partner of the inflaton, from the spectrum during inflation, which is useful when building single-field inflation models. For this second reason, we will focus here on the chiral multiplet, however similar constraints can also be defined to remove the gauginos from the vector multiplet [231].

In the MSSM, quarks[2] are represented by the chiral superfield Q, which contains the standard model fermion and the complex scalar superpartner. The scalar field from the fermion superfield can be removed with the constraint

$$Q_{NL}S_{NL} = 0, \tag{7.34}$$

where NL means that the theory is considered in the IR limit in which supersymmetry is nonlinearly realised and S is the nilpotent superfield defined by Eq. (7.30). Writing this constraint in components, the scalar field is mapped into a set of fermions (and F-terms) [231]. Similarly, a superfield with only a scalar can be obtained with

$$S_{NL}\bar{H}_{NL} = \text{chiral} \qquad \text{or} \qquad S_{NL}\left(A_{NL} - \bar{A}_{NL}\right) = 0. \tag{7.35}$$

The first constraint imposes that the superfield H only contains a complex scalar field, while the second constraint imposes that A only contains a real scalar field. The first constraint can be used to define the Higgs doublet in the standard model, while the second is interesting for studying inflation.

Another extension to the nilpotent formalism is to define higher order nilpotency constraints. The nilpotent-n superfield, where n is an integer, is defined as a superfield obeying the constraint [234]

$$S^n = 0, \qquad \text{while} \qquad S^{p<n} \neq 0. \tag{7.36}$$

The nilpotent superfields used so far were nilpotent-2 superfields. Interestingly, the scalar part of a nilpotent-n superfield is completely determined by the fermions, just as in the case of nilpotent-2 superfields, though in this case multiple fermions are necessary. To generate a consistent nilpotent-n theory, $n-1$ superfields are required. The reason is that the nilpotent-n superfield requires a scalar field ϕ with the condition $\phi^n = 0$.

Nilpotent-n fields will not be studied in this thesis.

[2]The leptons can be treated similarly.

7.4 Supergravity

The discussion above focussed on global or rigid supersymmetry. However, an interesting feature of inflation is that it might be a test ground for supergravity, which is obtained by promoting supersymmetry to a local symmetry. Since the supersymmetry algebra in Eq. (7.1) mixes nontrivially with the Pointcarré algebra, gauging supersymmetry implies that also the Pointcarré algebra is gauged. Therefore, local supersymmetry corresponds to a theory of gravity. In this section, a short review on the main supergravity framework will be provided, with the aim to write inflation models embedded in supergravity. Some general reviews on supergravity are Refs. [235, 236], while reviews on supergravity and inflation are Refs. [237, 238].

Given that quantum gravity contains a spin-2 graviton in the spectrum, supergravity should include this graviton and its spin-3/2 superpartner named the gravitino (ψ_μ). To preserve Lorentz invariance, the graviton must be massless, hence if supersymmetry is exact also the gravitino is massless. If supersymmetry is spontaneously broken, a process similar to the Higgs effect happens, named the superhiggs effect [236], and the goldstino is absorbed by the longitudinal component of the gravitino, giving the latter a nonzero mass. This mass is given by the expression

$$m_{3/2}^2 = e^{\frac{K}{M_{\rm p}^2}} \frac{|W|^2}{M_{\rm p}^4}, \tag{7.37}$$

which in the low energy limit $M_{\rm p} \to \infty$ becomes

$$m_{3/2} \approx \frac{|W|}{\sqrt{3} M_{\rm p}^2}. \tag{7.38}$$

For theories with local supersymmetry, the Lagrangian can be split in six parts

$$\mathcal{L} = \mathcal{L}_B^C + \mathcal{L}_{FK}^C + \mathcal{L}_F^C + \mathcal{L}_B^V + \mathcal{L}_{FK}^V + \mathcal{L}_F^V, \tag{7.39}$$

where the subscripts B, FK and F stand for boson, fermion kinetic and fermion interaction terms respectively, and the terms with superscript V contain gauge fields. Complete expressions of the six Lagrangians can be found in [236], but in this thesis only $\mathcal{L}_B^C$ will be used. Assuming in addition – as will be done below as well – that gauge interactions do not play an important role, the bosonic Lagrangian of supergravity becomes

$$\mathcal{L}_B = -\tfrac{1}{2} M_{\rm p}^2 R - G_{i\bar{\jmath}} \partial_\mu \phi_i \partial^\mu \phi_{\bar{\jmath}}^* - e^{\frac{G}{M_{\rm p}^2}} \left[G_i \left(G^{-1} \right)_{i\bar{\jmath}} G_{\bar{\jmath}} - 3 M_{\rm p}^2 \right] M_{\rm p}^2, \tag{7.40}$$

where the superscript C is dropped. The function $G(\phi, \phi^*)$ is defined as

$$G(\phi, \phi^*) = K(\phi, \phi^*) + M_{\rm p}^2 \ln \left| \frac{W(\phi)}{M_{\rm p}^3} \right|^2 \tag{7.41}$$

and a subscript i ($\bar{j}$) implies a derivative with respect to the field ϕ_i ($\phi_{\bar{j}}^*$). Hence, supergravity can be fully represented by a single function[3], $G(\Phi, \Phi^\dagger)$, though in the following this framework will not be used and the Kähler potential and the superpotential will be defined separately. Note that the potential (7.40) is non-renormalizable.

In section 7.3, supersymmetry breaking in rigid supersymmetry was introduced non-linearly using constraint superfields. However, the introduction of superspace in supergravity is subtle since the spinor coordinates θ become part of the local algebra and are called Θ. Let me bypass the subtleties of superspace and move directly to the graviton multiplet which consists of the graviton, the gravitino and some auxiliary fields. From the gravitino a chiral multiplet named the curvature superfield $\mathcal{R}$ is defined which corresponds to covariant perturbations of the metric. This field can be used to define a nilpotent superfield that will nonlinearly break supersymmetry with the constraint [239]

$$\left(\frac{\mathcal{R}}{S_0} - \lambda\right)^2 = 0, \tag{7.42}$$

where λ is a parameter that can be used to set the cosmological constant and S_0 is the chiral compensator field, which is a field used to build supergravity actions but carries no fundamental degrees of freedom [240][4]. The constraint (7.42) can be solved order by order and results indeed in a theory with supersymmetry breaking but without a goldstino. This was expected, since the goldstino is absorbed by the gravitino due to the superhiggs effect.

By using Lagrange multipliers, the action relating the constraint (7.42) can be rewritten with an additional nilpotent-2 field X [241]. The Kähler and superpotential of this theory are simply

$$K = 3|X|^2 \qquad W = W_0 + \lambda X, \tag{7.43}$$

which is what is expected for a nilpotent-2 theory. Therefore, as in rigid supersymmetry, supersymmetry breaking in supergravity can be nonlinearly realised using a nilpotent-2 superfield [239, 241–243].

This can be expanded to a more general case with additional matter multiplets Q_i for which the Kähler and superpotential are, when expanded in the nilpotent-2 field,

$$K = K_0 + (K_1 X + \text{c.c.}) + K_2|X|^2, \qquad W = W_0 + W_1 X, \tag{7.44}$$

where the $K_j(Q_i, Q_i^\dagger)$ and $W_l(Q_i)$ for $j = 1, .., 3$ and $l = 1, 2$ are arbitrary functions. It was shown in Ref. [239] that the specific case $K_1 = K_2 = 0$ leads to the

[3] If gauge interactions are present, also the gauge kinetic function f_{ij} is relevant.

[4] It is similar to the $\phi^2 - \chi^2$ combination in the Lagrangian (6.15). First a conformally invariant supergravity theory is constructed, after which the conformal symmetry is broken by the chiral compensator. See also the discussion around Eq. (6.15).

gravitational nilpotent theory described by Eq. (7.42), with W_0 and λ functions of the fields Q_i.

A similar framework can be used to obtain the Starobinsky model defined in section 3.4.2 [244]. Also, by imposing constraints on combinations of $\mathcal{R}$ and the goldstino X, certain modes in the gravitino multiplet can be opened, generating an interesting new set of models [245]. For instance, it is natural to choose a constraint that will integrate out the auxiliary component of the scalar part of $\mathcal{R}$, which can be accomplished by choosing $X\,\mathcal{R} = 0$ [245].

7.5 Supersymmetric theories of inflation

In general, inflation models can be divided into two types. The first type are the small-field models, for which $\Delta\phi \equiv \phi_* - \phi_{\text{end}} < M_{\text{p}}$, while the large-field models have $\Delta\phi > M_{\text{p}}$. Small-field models often contain multiple fields, for instance many hybrid inflation models belong to this category, while single-field models are typically large-field models[5], as are the models described in section 3.4.

Also small-field inflation typically occurs at large energy scales when compared to current collider scales, hence rigid supersymmetry might be the relevant extension of the standard model at those energies. Since supersymmetric extensions typically contain a large number of scalar fields, there are a plethora of possible inflaton candidates. Typically non-perturbative terms are relevant to obtain small-field inflation (or the model is ruled out by the CMB measurements). Hence, building supersymmetric models with inflation is not trivial, but some progress is reached, for instance in ISS-flation [246, 247] and MSSM inflation [248].

Large-field inflation models, on the contrary, require an understanding of the physics at energy scales where gravitational effects might not be negligible. In this scenario, often supergravity inflation models are considered, but in principle this might not be correct as the inflation model should be fully implemented in string theory. It is possible that certain supergravitity models, especially the models with a mild field excursion $\Delta\phi \approx M_{\text{p}}$, can be described using supergravity. However, it is an open question if this is indeed allowed in string theory [249–254]. Though there are interesting developments in embedding inflation models directly in string theory [255–260], this thesis will consider inflation in supergravity.

In the following subsections, first supergravity inflation will be shortly reviewed, with emphasis on nilpotent inflation and the α-attractor model introduced in section 6.2. Then, in the second subsection, some phenomenological problems of reheating will be explained, mainly the problem of gravitino overproduction. In the following we will be interested in large field models, and will hence try to obtain models of inflation in supergravity.

[5]Note that this is not a general statement and there are small-field models known with only a single inflaton.

7.5.1 Supergravity and inflation

For considering inflation in supergravity, the potential of the scalar field is written as

$$V = e^{\frac{K}{M_{\rm p}^2}} \left[(K^{-1})_{i\bar{j}} \left| W_i + \frac{W K_i}{M_{\rm p}^2} \right|^2 - \frac{3|W|^2}{M_{\rm p}^2} \right], \tag{7.45}$$

as given by Eq. (7.40). Three features of the Lagrangian are problematic for single field inflation to occur. The first is that the scalar components of superfields are complex scalar fields. Thus, even when considering only one superfield, there will be two inflaton candidates. The second feature, known as the η problem, is that a canonical Kähler potential is at least quadratic in the fields, hence $V \propto \exp\left(\phi^2\right)$, where ϕ is the inflaton. This potential is too steep to drive inflation, since $\eta_{\rm V} > 1$. The third undesirable feature of (7.45) is the $-3|W|^2/M_{\rm p}^2$ in the potential, which might render the potential unstable and negative.

In general, the first problem is usually relatively mild. The reason is that a large VEV for the inflaton typically stabilises its superpartner. Solving the second problem is relatively straightforward. The problematic term in the potential is originating from the Kähler potential, hence imposing that the Kähler potential is invariant under the shift symmetry $\varphi \to \varphi + \delta$, where φ is the inflaton, will solve the problem [261]. Hence, if the inflaton is the imaginary part of ϕ, the η problem is solved if $K(\Phi, \Phi^\dagger) = K(\Phi + \Phi^\dagger)$.

Since the potential of a theory with an exact shift symmetric is completely flat, lifting this symmetry of the Kähler to a symmetry of the potential is not possible. If the superpotential breaks the shift symmetry, this breaking will be transmitted to the Kähler potential via quantum corrections. If these quantum corrections are small, these corrections will not reintroduce the η problem. In general, it is also possible to break the shift symmetry directly in the Kähler potential, as long as it is still an approximate symmetry.

The problem that many (large field) inflation models are unbounded from below is more complicated to solve. To illustrate the problem, consider the model [261]

$$K = \tfrac{1}{2}\left(\Phi + \Phi^\dagger\right)^2, \qquad W = m\Phi^2, \tag{7.46}$$

where m is the mass of the inflaton field. To break the shift symmetry only mildly, it sufficies to insistent on $m < M_{\rm p}$. In the rigid limit, this potential resembles a two-field copy of quadratic inflation. However, in supergravity the sinflaton is stabilized to 0 if $\phi \lesssim 3M_{\rm p}$. Integrating out the sinflaton, the inflaton potential becomes

$$V = \frac{1}{4} m^2 \varphi^2 \left(8 - \frac{3\varphi^2}{M_{\rm p}^2} \right), \tag{7.47}$$

where $\varphi = \mathrm{Im}\,\phi$ is the inflaton. This potential is plotted in Fig. 7.3 where it is shown that the potential has a maximum below $\varphi_e = \sqrt{2} M_{\rm p}$ where quadratic inflation ends. Hence, this model is a hilltop inflation model, rather than a quadratic.

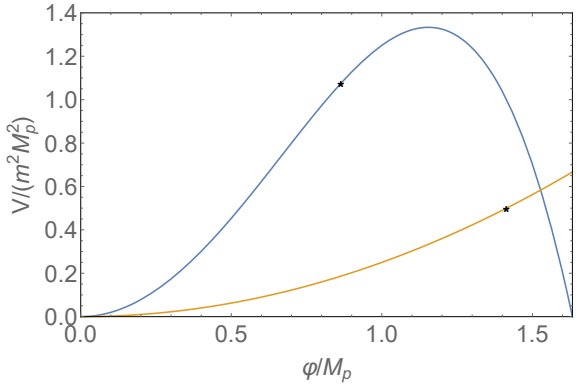

Figure 7.3: *In blue the potential of Eq. (7.47) representing quadratic inflation in supergravity, and in yellow the quadratic potential. The black stars mark the value for φ where inflation ends. In the relevant inflationary regime, on the right of the black star on the orange line, the supergravity model does not inflate towards the minimum at $\phi = 0$.*

In this particular hilltop model the top of the potential is reached in roughly a single e-fold, hence it is not possible to obtain 50 e-folds of inflation to explain the observed CMB anisotropies.

By considering specific Kähler and superpotentials, it is possible to solve the undoundedness problem within the framework of a single superfield, as was done in Refs. [212, 262–266][6]. However, when insisting on single-field, non-hilltop, polynomial potentials this is not possible, since for large inflaton field values the $-|W|^2$ term will always be larger than the derivative terms. A solution is to introduce a stabilizer field S with an interaction of the type

$$K = \tfrac{1}{2}\left(\Phi + \Phi^\dagger\right)^2 + S^\dagger S, \qquad W = \left(f_0 - \frac{m}{2M_\mathrm{p}}\Phi^2\right)(M_\mathrm{p} + \delta S)\,, \tag{7.48}$$

where δ and f_0 are constant parameters. The quadratic potential $\frac{1}{2}m^2\varphi^2$ is obtained when integrating out the scalar component of S and the sinflaton. The stabilizer field S in this model also breaks supersymmetry, since $\langle F_s\rangle = -f_0\delta \neq 0$. Setting $\delta \approx \sqrt{3}$, the vacuum $\Phi = S = 0$ has vanishing potential. Hence, a small deviation from $\delta = \sqrt{3}$ explains the current accelerated expansion[7]. The parameter f_0 defines the supersymmetry breaking scale.

However, by introducing an additional superfield two real scalar fields were added to the theory. To remove these fields from the spectrum, in Ref. [267] was

[6]Though many of these models are hybrid inflation models.

[7]Though this does not explain how δ became this value, so the cosmological constant problem is not really solved.

proposed to constrain the stabilizer S to be a nilpotent-2 superfield, which became an active field of research [239, 268–274]. The important feature of nilpotent superfields is that the scalar fields have a very large mass and can be integrated out in the IR. Then, assuming that inflation is far enough in the IR, the stabilizer field is integrated out and only an inflaton in a quadratic potential is left.

Simply defining the stabilizer field to be a nilpotent-2 superfield solves the problem and in addition provides a natural mechanism for supersymmetry breaking [275], but an interesting question is whether this is theoretically consistent [243, 276, 277]. The nilpotency constraint is a low energy effective description of a theory in which supersymmetry is broken linearly. For supersymmetry to be realised non-linearly by the nilpotent-2 constraint, the operator $-\gamma|S|^4$ in Eq. (7.32), with $\gamma = c/M^2$, should exist in the Kähler potential with the parameter $\gamma \gg 1$. Within a perturbative theory, this operator cannot appear at tree level but it does appear at loop level through the Coleman-Weinberg potential. Expanding Eq. (7.19) for small S, we obtain that $\gamma \approx c/\Lambda^2$, where Λ is the cut-off scale, and c contains the loop factor. Large γ implies either large c, rendering the theory non-perturbative, or small Λ. The energy scale Λ typically refers to the mass of some particles that are integrated out and it is not allowed to integrate out particles with a mass below the energy scale at which the theory is considered. For inflation the typical energy scale is H, hence for the consistency of the effective theory it is required that $\Lambda \gtrsim H$ during inflation. This set of constraints strongly limits the validity range of nilpotent inflation theories, as we will discuss in detail in chapter 8.

For example, Eq. (7.48) can be UV-completed using the O'Raifeartaigh model

$$K = \tfrac{1}{2}(\Phi + \Phi^\dagger)^2 + |S|^2 + |X|^2 + |Y|^2 \tag{7.49}$$

$$W = f(\Phi)(1 + \delta S) + \lambda S X^2 + M X Y, \tag{7.50}$$

where δ and λ are constant parameters, M is the mass of the X and Y fields and $f(\Phi)$ is an arbitrary function of the inflaton. If we consider M large, the X and Y fields can be integrated out and the low energy Kähler potential becomes

$$K_{IR} = \tfrac{1}{2}(\Phi + \Phi^\dagger)^2 + |S|^2 - \frac{\lambda^4}{6(8\pi^2)M^2}|S|^4. \tag{7.51}$$

An interesting analysis, performed by Dudas et al. in Ref. [278], showed that indeed there is a tachyon in the imaginary parts of the scalar components of X and Y if $M^2 < 2\sqrt{3}\lambda m_{3/2} M_{\rm p}$, while the gravitino mass $m_{3/2}$ is roughly at the Hubble scale during inflation. The authors showed that the actual window for M in quadratic inflation is very small and close to the Planck scale. This implies that the sgoldstino mass is never more than a factor 10 larger than the gravitino mass. Hence, for the sgoldstino mass to be sufficiently large so that it can be integrated out during inflation, the gravitino mass has to be large as well. This hints to the fact that consistent nilpotent inflation implies a large supersymmetry breaking scale in the vacuum.

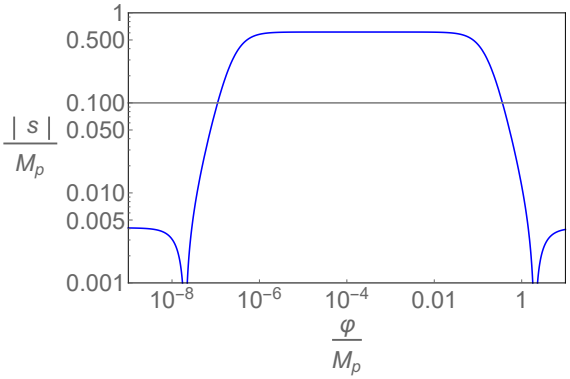

Figure 7.4: *The absolute value of the sgoldstino VEV after inflation in blue, with the cutoff scale of the theory* Λ *in grey, using the model from Ref. [278] with the parameters* $m_{3/2} = 10^4$ *GeV and* $m_s = 10^6$ *GeV. For a large part of the trajectory, the sgoldstino VEV is above the cutoff scale of the theory. The sharp drops are caused by a crossing of the VEV through 0.*

Another problem, which was not analysed in Ref. [278], is that during inflation the sgoldstino acquires a VEV that in this scenario is beyond the Planck scale, as is shown in Fig. 7.4. Due to this large VEV the first order Taylor expansion of the Coleman-Weinberg 1-loop potential used in (7.51) is not sufficient. This renders the analysis of the stability based on the terms in Eq. (7.51) incorrect. Both problems, the large VEV for S and the impossibility to have small supersymmetry breaking, will be studied further in chapter 8, where a model will be introduced that circumvents these issues.

For inflationary model building, additional constraints can be imposed to remove more fields from the theory, as shown for global supersymmetry in section 7.3, which can be applied with minor changes also in supergravity [271, 272]. The strongest constraint, $S(\Phi + \Phi^\dagger) = 0$, can be used to remove all particles from the spectrum, except for the (imaginary) inflaton and the goldstino. Therefore, a possible stabilization of the sinflaton is not necessary in this case and the removal of the fermionic inflatino simplifies reheating [279–281].

Models of the type with $S^2 = S(\Phi + \Phi^\dagger) = 0$ are obtained in a Kähler and superpotential of the form [272]

$$K = SS^\dagger + (\Phi + \Phi^\dagger)^2 h(\Phi - \Phi^\dagger), \qquad W = f(\Phi)S + g(\Phi), \tag{7.52}$$

where f, g and h are arbitrary functions. Note that this additional condition therefore provides an explanation for the shift invariance of the Kähler potential in Eq. (7.45).

Another model that can be made invariant under the two nilpotent constraints described above is the α-attractor models introduced in section 6.2. The T-mode α-attractor can be obtained in supergravity by considering the Kähler potential [208–211, 271, 282]

$$K = -\frac{3M_{\rm p}^2}{2}\alpha \log\left(\frac{\left(M_{\rm p}^4 - \Phi\Phi^\dagger\right)^2}{\left(M_{\rm p}^2 - \Phi^2\right)\left(M_{\rm p}^2 - \left(\Phi^\dagger\right)^2\right)}\right) + SS^\dagger. \tag{7.53}$$

Taking W as in Eq. (7.52) will be consistent with the constraints. Similarly, the E-mode α-attractor is characterized by the Kähler potential [211]

$$K = -\frac{3M_{\rm p}^2}{2}\alpha \log\left(\frac{\left(\Phi + \Phi^\dagger\right)^2}{4\Phi\Phi^\dagger}\right) + SS^\dagger. \tag{7.54}$$

An explicit calculation that these functions can be made consistent with the above nilpotency constraints involving two superfields is given in [271].

In section 6.2 the α-attractor was obtained by considering models with an explicitly broken conformal symmetry. This can be obtained in supergravity with two different approaches, depending on how the gravitino is introduced. The Kähler potential (7.53) leads to a theory with exact conformal symmetry in the kinetic sector of Φ only (the superpotential will break conformal symmetry, as in section 6.2), while the stabilizer field is not conformally invariant. To also include the S field in the superconformal theory, the Kähler and superpotentials [206]

$$K = M_{\rm p}^2 \log\left(\frac{-|X|^2 + |\Phi|^2 + |S|^2}{M_{\rm p}^2}\right), \qquad W = S\left(X^2 - \Phi^2\right) f\left(\frac{\Phi}{X}\right), \tag{7.55}$$

are considered for which the conformal compensator field X, has the wrong kinetic sign [206, 283]. The function f in the superpotential breaks the superconformal symmetry to give a potential to the inflaton. As in section 6.2, different attractors can be found with different gauge choices of the superconformal symmetry. For instance, choosing $X = \bar{X} = \sqrt{3}M_{\rm p}$ leads to

$$\begin{aligned} K &= -3\alpha M_{\rm p}^2 \log\left(1 - \frac{1}{3M_{\rm p}^2}(SS^\dagger + \Phi\Phi^\dagger)\right), \\ W &= Sf\left(\frac{\Phi}{\sqrt{3}}\right)\left(3 - \frac{\Phi^2}{M_{\rm p}^2}\right)^{(3\alpha-1)/2}, \end{aligned} \tag{7.56}$$

which is the T-mode α-attractor.

On closing, note that the combining factor between the different Kähler potentials of (7.53), (7.54) and (7.56) is the logarithmic dependence on the inflaton field [216]. In section 6.2 was explained that the α-attractor originates from a hyperbolic geometry of the field space. This type of logarithmic Kähler potential indeed implies such a conformal (or Poincaré) disk model [216].

7.5.2 Reheating

Supersymmetry can also generate interesting features during the era of reheating. Two important effects will be explained in this section. The first is the possibility that the known evolution of the universe is strongly affected by a large amount of gravitinos. A second effect of supersymmetry on reheating will be the appearance of moduli that might generate another reheating-like era.

The gravitino only interacts gravitationally to the standard model matter. Therefore, if it decays it decays extremely slowly. This has important consequences when a sizeable fraction of gravitinos decay during Big Bang nucleosynthesis, discussed in section 2.5, since then the remnants of the decay will affect the abundance of elements in the universe [153, 284]. If the gravitino is the supersymmetric particle with the lowest mass (LSP), it is stable if R-parity is conserved. Evidently, the gravitino might be the observed cold dark matter if it is stable and produced with exactly the right abundance. However, in many models the gravitino is overproduced, leading to the gravitino overproduction problem. Finally, the decay of the next to lightest supersymmetric particle (NLSP) to the gravitino is strongly suppressed but should not be slower than the time until BBN [284]. Therefore, it is important to study the creation mechanisms of the gravitino.

In the early universe, the gravitino can be produced through several different processes. The standard paradigm for dark matter discussed in section 2.6 is that it is produced through the freeze-out process, but since the gravitino is coupled very weakly to the thermal plasma, it usually does not thermalize and this possibility is not considered in this thesis. In addition, bath particles can decay or scatter into gravitinos. Though both processes can be named freeze-in, gravitino literature uses the name freeze-in only for the decay of bath particles into gravitinos, while the scattering into gravitinos is named thermal production Refs. [285–288].

To compute the gravitino abundance through the decay of bath particles into gravitinos, the theory developed in section 2.6 can be used. The decay widths of particles into gravitinos is universal and only depends on the mass of the decaying particle [227]

$$\Gamma(\tilde{\chi} \to \chi' \tilde{G}) = \frac{\kappa m_{\chi'}^5}{48\pi M_{\mathrm{p}}^2 m_{3/2}^2}\,, \tag{7.57}$$

where $\tilde{\chi}$ is the NLSP and χ' the standard model partner of the NLSP. The constant κ is of order 1, see Ref. [227] for the complete expressions. Using Eq. (2.29), the gravitino yield from freeze-in is [75]

$$Y_{\text{freeze-in}} = \sum_{\tilde{X}} \frac{135\sqrt{90} g_{\tilde{X}}}{8\pi^4 g_*^{3/2}} \frac{\Gamma_{\tilde{X}} M_{\mathrm{p}}}{m_{\tilde{X}}^2} I\,, \tag{7.58}$$

where the sum runs over all the superparticles ($\tilde{X}$) and I was defined in Eq. (2.30).

The thermal production through scatterings of bath particles into gravitinos is rather complicated, since thermal effects have to be taken into account properly.

These contributions were investigated in Refs. [285–288], combining analytical and numerical techniques. These analyses found that if the gravitino mass is below 10 GeV, the reheating temperature is required to be below 10^{10} GeV to not overclose the universe, while for most models of baryogenesis a reheating temperature above 10^{10} GeV is necessary.

Also other solutions exist to solve the gravitino problem. For instance, a late time entropy production can dilute an earlier generated gravitino abundance [289–293]. However, if this entropy insertion produces a large amount of antimatter, this might reintroduce the matter/antimatter asymmetry problem. Another solution is to use either an extremely light gravitino, [294,295] or a very heavy gravitino [296].

Typically, an additional important source of gravitino production comes from direct decay of the inflaton into the gravitino [160,161,297], as explained in section 3.5 for a more general case. The main contribution of this decay is the inflaton decaying into the goldstino, which is the longitudinal component of the gravitino. Though this is often an important component of the gravitino abundance, the computation is highly model dependent.

Finally, gravitinos can be produced in the era of preheating due to resonant processes [279, 285]. In Ref. [298] it was shown that this can be a relevant production process if a stabilizer field is introduced. The precise amount of gravitinos produced during preheating requires a dedicated study and is beyond the content of this thesis.

Another effect of supersymmetry on reheating, and potentially also on inflation, are flat directions. Typical supersymmetric theories contain many directions in the scalar field space that have a potential characterized by the size of supersymmetry breaking only. During inflation the supersymmetry breaking scale is defined by the hight of the potential, which equals H^2 through Eq. (3.6), thus these fields will have a similar mass [299] and can be ignored. However, during reheating these orthogonal states might be relevant.

An example is the Polonyi problem in inflation models with gravity mediated supersymmetry breaking [300–302]. In most inflation models the sgoldstino field is stabilized to $S = 0$ during inflation, while after inflation it acquires a nonzero VEV. The relaxation of the sgoldstino to its VEV is through a process that is very similar to reheating after inflation and the sgoldstino will continue adding energy to the thermal plasma, even if it is not the main contribution to the energy density of that plasma. Since the decay of the sgoldstino in gravity mediated models of supersymmetry breaking $\Gamma_S \propto m_s^3/M_{\rm p}^2$ is often after BBN, this decay will change BBN in an observable manner.

In gauge mediation models the Polonyi problem often does not appear, since in such models $\Gamma_S \propto \langle F \rangle / M_{\rm mess}$ which is much larger, hence the decay time of the sgoldstino is smaller. But also in gauge mediation a similar problem appears if there are moduli in the supersymmetric theory, or originating from string theory, which get displaced from their VEV during inflation and interact very weakly with the other fields in the theory [302].

An interesting observation is that the Polonyi problem pushes the theory towards very large soft masses. Assuming that in gravity mediation all superpartners, including the gravitino and the sgoldstino, have roughly the same mass, the requirement that the sgoldstino field decays before the onset of BBN can be solved if the sgoldstino field is above 10 TeV [301, 303, 304], but even that scenario has severe problems with the decay products [303, 304]. Since no experimental constraints on supersymmetry exist on this energy scale, it would be interesting if this cosmological bound can be lowered. For gauge mediation the moduli problem is less severe, since the sgoldstino decay is much faster and much smaller soft masses can be obtained. A model that solves these issues using gauge mediation was obtained in Ref. [289] and in chapter 8 we will show another example that evades the gravitino problem. In Ref. [289] also the matter-antimatter asymmetry in the universe was solved.

CHAPTER 8

Sgoldstino-less inflation and low energy SUSY breaking

8.1 Introduction

When studying large-field supergravity inflation models in section 7.5, it was shown that it is convenient to use nilpotent multiplets to stabilize the inflaton trajectory. However, the nilpotent inflation model that was considered in this chapter was only consistent in a small window of energy scales for the supersymmetry breaking scale. The reason for this small window is that the nilpotency condition required two opposite regimes for the cut-off scale of the effective theory, which could not always be satisfied.

Additional problems appearing in section 7.5.2 were the Polonyi problem and the gravitino abundance problem. In models with gravity mediation the sgoldstino mode typically has a very long lifetime and the decay of the sgoldstino occurs during BBN, in contrast to observations. Models in which supersymmetry breaking is mediated to the standard model through gauge mediation have the sgoldstino decaying much faster, but for these models the gravitino mass is small and therefore its primordial abundance is typically too large.

In this chapter a model of gauge mediation will be introduced that addresses the two problems mentioned above. In section 8.2 we introduce the generic consistency conditions that nilpotent inflation models should satisfy. In section 8.3 we introduce our model, where the inflationary dynamics is governed by the α-attractor mechanism introduced in section 6.2. We revisit the α-attractor predictions and

we discuss the regime of validity of the effective field theory (EFT) approximation in this concrete example. (Some more details are in Appendix C.) In section 8.4 we introduce a possible UV completion of the model, based on a supersymmetry breaking sector with gauge mediation. We first analyse the consistency conditions of the UV theory and recover bounds compatible with those discussed in the EFT analysis. In section 8.5 we perform a phenomenological analysis of the model. We compute the reheating temperature and implement bounds from the gravitino overabundance problem, Big Bang nucleosynthesis and LHC constraints. Finally, we conclude in section 8.6.

This chapter is based on publication [305].

8.2 Effective field theory for sgoldstino-less inflation

The idea of nilpotency was already introduced in section 7.3, and used for inflation models in section 7.5. These inflation models [213, 239, 241, 256, 257, 259, 267–274, 282] are characterized by the presence of a nilpotent chiral superfield $S^2 = 0$ [229–232, 242], *i.e.* the goldstino superfield, which is responsible for spontaneous supersymmetry breaking, and another chiral superfield Φ whose imaginary component is the inflaton field, which exhibits a shift symmetry in order to make its potential viable for inflation [261]. The nilpotency condition corresponds to the fact that the scalar component of the chiral superfield S, *i.e.* the sgoldstino, has been integrated out. The theory with the nilpotent superfield (and potentially with other constrained superfields) is then interpreted as an effective field theory valid up to the energy scale of the sgoldstino.

In this section, our aim is to take a step back and write an effective field theory (EFT) which includes the sgoldstino, but where we can estimate its mass and follow its decoupling at low energies. As was explained in section 7.2, the tree level potential of the sgoldstino vanishes. However, it gets its mass through non renormalizable operators in the Kähler potential, which can be for instance generated perturbatively in a weakly coupled UV completion. Such physics can be simply captured in a class of models of inflation in supergravity which is characterized by a few arbitrary functions. We take the following Kähler and superpotential

$$K = \mathcal{K}(\Phi, \Phi^\dagger) + SS^\dagger - \frac{(SS^\dagger)^2}{\Lambda_{\rm eff}^2} \tag{8.1a}$$

$$W = f(\Phi)S + M_{\rm p} h(\Phi)\,. \tag{8.1b}$$

In these expressions the Kähler potential for Φ typically respects a shift symmetry which makes it independent of the imaginary component, to be eventually identified with the inflaton field. It can be typically non-canonical with Planck scale corrections, reducing to a canonical form when the lowest component ϕ is small, *i.e.* after inflation. $f(\Phi)$ and $h(\Phi)$ are functions of the inflaton field and

can include higher dimensional operators typically suppressed by the Planck scale. These functions are arbitrary up to the constraint that $h'(0) = f'(0) = 0$, since we demand that S is the only field that breaks supersymmetry. They determine the scalar potential for the inflaton and hence should be chosen properly in order to have viable single-field inflationary dynamics and a (meta)-stable vacuum at the end of inflation. Moreover, these functions have to be tuned in order to obtain a vanishingly small cosmological constant in the vacuum at the end of inflation.

The validity of the sgoldstino-less description is controlled by the sgoldstino mass, which is ϕ dependent

$$m_s^2 = \frac{4|f(\phi)|^2}{\Lambda_{\rm eff}^2} \ . \tag{8.2}$$

The fermionic component of S is the goldstino and it is massless. It is eaten by the gravitino which then acquires the mass given in Eq. (7.38), $m_{3/2} \propto |W|/M_{\rm p}^2$. Note that the sgoldstino mass depends on another scale, which is the scale that sets the validity of this effective theory $\Lambda_{\rm eff}$. By definition of EFT, this scale must be larger than m_s. One should then wonder what is the typical size of $\Lambda_{\rm eff}$ with respect to the Planck scale and how such a non-renormalizable operator is generated in a UV completion of the theory. If $\Lambda_{\rm eff} \sim M_{\rm p}$ the simplest interpretation is that this quartic operator arises from Planck scale physics. If instead $\Lambda_{\rm eff} \ll M_{\rm p}$ then one is necessarily integrating over some physics below the Planck scale and the operator leading to the sgoldstino mass can be typically interpreted as the leading term in a series of higher dimensional corrections to the Kähler potential suppressed by powers of $\Lambda_{\rm eff}$.

In the first case, the sgoldstino mass at the end of inflation will scale as $\frac{f_0}{M_{\rm p}}$, where $f_0 \equiv f(0)$. In order for this scalar to be decoupled from SM physics we should demand its mass to be larger than roughly a TeV. This automatically sets f_0, the scale of supersymmetry breaking at the end of inflation, to be large, and poses the model in a scenario where the gravity mediated contribution to the MSSM soft terms, also scaling as $\frac{f_0}{M_{\rm p}}$, are sizeable. Actually, if $\Lambda_{\rm eff} \sim M_{\rm p}$, in the vacuum the gravitino mass turns out to be of the same size as m_s.

In the second case, the sgoldstino mass is given by $\frac{f_0}{\Lambda_{\rm eff}} \gg \frac{f_0}{M_{\rm p}}$. Then f_0 can be small keeping m_s sizeable, and SUSY breaking can be mediated to the MSSM via gauge interactions, with gravity mediated effects subleading. In this paper we are interested in the second case, and hence we are immediately facing questions associated to the validity of the effective theory at very high scales and the role played by $\Lambda_{\rm eff}$. As reviewed in section 7.5, requires a viable UV-completion of sgoldstino-less inflation models an effective scale $\Lambda_{\rm eff}$ of at most one order of magnitude smaller than the Planck scale, see also Ref. [278]. Here we discuss systematically the consistency conditions that we expect the effective theory to satisfy, and we propose a strategy to realize models of inflation with low supersymmetry breaking scale at the end of inflation.

8.2.1 Consistency conditions

Let us start with identifying the consistency conditions that the effective theory in (8.1a) should satisfy. The idea is, again, that the EFT should be in its regime of validity at the energy scales of the physics that one is describing, that is during and after inflation. Hence, these conditions must be satisfied along the entire inflaton trajectory, from Planckian values to the origin:

$$m_s^2 \ll \Lambda_{\rm eff}^2 \ , \qquad \langle s \rangle \ll \Lambda_{\rm eff} \ . \tag{8.3}$$

These two conditions are necessary to have a well defined effective theory for S. Observe that all quantities appearing in these conditions should be intended as functions of the value of the inflaton field. The first condition in (8.3) is easily translated into the constraint

$$f(\phi) \ll \Lambda_{\rm eff}^2 \ . \tag{8.4}$$

The second condition in (8.3) is involved and requires the study of the sgoldstino vacuum expectation value (VEV) along the entire inflaton trajectory.

Note that strictly speaking, an EFT such as (8.1a) treats differently Φ and S, in the sense that integrating out the physics at $\Lambda_{\rm eff}$ affects the Kähler potential of S, while the one of Φ is more generally determined by Planck scale physics. Nevertheless, we can conservatively ask that also the degrees of freedom of Φ, at least after inflation, are within the regime of validity of the EFT of S:

$$m_\phi^2 \ll \Lambda_{\rm eff}^2 \ . \tag{8.5}$$

Besides these consistency conditions, in order to guarantee that inflation is driven by a single field (or equivalently, that the goldstino superfield is nilpotent at that time), we should demand that during inflation the sgoldstino is heavier than the typical scale, *i.e.* the Hubble scale, hence

$$m_s^2\big|_{\rm infl} \gg H^2\big|_{\rm infl} \ . \tag{8.6}$$

On the other hand this translates simply to

$$\Lambda_{\rm eff} \ll M_{\rm p} \ , \tag{8.7}$$

where we assume a potential dominated by $|f(\phi)|^2$. We thus see that having a scale for new physics lower than the Planck scale is actually a requirement for contemplating the decoupling of the sgoldstino from inflation.

Note that generically the effective scale $\Lambda_{\rm eff}$ can be a function of the inflaton field, varying along the inflationary trajectory. This is a promising possibility since a function $\Lambda_{\rm eff}(\phi)$ increasing with ϕ implies that the validity threshold of the effective theory grows with increasing ϕ. Note that a ϕ dependent $\Lambda_{\rm eff}$ would introduce a new source of shift symmetry breaking, which should be controlled by a small parameter.

In the next section we will study the implications of the consistency conditions on the effective field theory with dynamical $\Lambda_{\rm eff}(\Phi)$ in a simple model. We will then provide a UV completion which generates such an effective theory.

8.3 An illustrative model

8.3.1 Definition of the model

The Lagrangian we will consider in this section is of the form

$$\begin{aligned} K &= -\frac{3\alpha}{2} M_{\rm p}^2 \log\left(\frac{(M_{\rm p}^2-\Phi\Phi^\dagger)^2}{(M_{\rm p}^2+\Phi^2)(M_{\rm p}^2+\Phi^{\dagger 2})}\right) + SS^\dagger - \frac{(SS^\dagger)^2}{\Lambda_{\rm eff}(\Phi)^2}\,, \\ W &= f(\Phi)S + M_{\rm p} h(\Phi)\,, \end{aligned} \tag{8.8}$$

where the scale $\Lambda_{\rm eff}$ is, as announced above, promoted to be a function of the inflaton field value during inflation. The choice of a non-minimal form for the Kähler potential resembles the α-attractor Kähler potential already discussed in section 7.5 (compare with Eq. (7.53)). It allows us to reach much better observables while keeping polynomial and independent the functions f and h.

The three different functions introduced above will be taken of the form

$$f(\Phi) = f_0 - \frac{m_f}{M_{\rm p}}\Phi^2\,, \quad h(\Phi) = h_0 - \frac{m_h}{M_{\rm p}}\Phi^2\,, \tag{8.9}$$

and

$$\Lambda_{\rm eff}^2(\Phi) = |\Lambda_0 + g\Phi|^2\,. \tag{8.10}$$

In this situation, $\Lambda_{\rm eff}^2(\Phi)$ will take large values during inflation (where $\mathrm{Im}(\Phi) \sim M_{\rm p}$) and fall down to lower values when Φ rolls down its potential.

Several remarks should be made about the structure of the Kähler potential in (8.8). For field values much smaller than the Planck scale, the α-attractor Kähler potential is a canonical one (for $\alpha = 1/3$) exhibiting a shift symmetry for $\mathrm{Im}(\Phi)$. The non-renormalizable term for S suppressed by $\Lambda_{\rm eff}(\Phi)$ is instead a non-canonical term, whose Φ dependence introduces an extra source of breaking of the shift symmetry. Henceforth we consider $g \ll 1$ such that the breaking of the shift symmetry is small. Moreover, the scale $\Lambda_{\rm eff}(\Phi)$ represents the mass scale where we expect new physical states. Hence we observe that we cannot explore regions where $\mathrm{Re}(\Phi) = -\frac{\Lambda_0}{g}$ since in this locus the Kähler potential becomes singular, corresponding to some states in the UV completion of the model that become massless.

As already stated, in taking into account corrections to the Kähler potential in Eq. (8.8), somehow we are considering on different footing the inflaton superfield and the sgoldstino superfield. The assumption is that the α-attractor type potential is set by Planck scale physics, while the corrections to the sgoldstino are generated at a much smaller scale. This assumption is valid as soon as $\Lambda_{\rm eff}(\Phi) \ll M_p$,

which we ensure by demanding $\Lambda_0 \ll M_p$ and $g \ll 1$. Note that $g \ll 1$ also ensures that condition (8.6) is satisfied.

The states at the scale $\Lambda_{\rm eff}(\Phi)$ will also generically generate Kähler corrections for the field Φ, possibly mixing Φ and S. However, we keep only the corrections to the field S since the sgoldstino would be massless at tree level if not for such corrections, which are the leading terms generating a sgoldstino mass. In the case of the inflaton field Φ, possible Kähler corrections to its mass from physics at the scale $\Lambda_{\rm eff}(\Phi)$ will be proportional to g and subleading with respect to the tree level terms. We will see how to generate the corrections to the Kähler potential in a UV complete theory in the next section, where also other terms (allowed by the symmetries) will be present, but will not change qualitatively the analysis of this section.

8.3.2 EFT validity analysis

We now proceed with the analysis of the scalar potential and the consistency conditions of the EFT description. Going to a real basis, one can define

$$\phi \equiv \frac{\chi + i\varphi}{\sqrt{2}}, \quad S \equiv \frac{s + i\sigma}{\sqrt{2}}, \tag{8.11}$$

where due to the structure of the Kähler potential, φ will play the role of the inflaton in what follows. The absence of linear terms in a small field expansion in χ guarantees that the sinflaton (χ) is stabilized to zero VEV during the whole inflationary trajectory.

Assuming the validity of the effective formulation and that the stabilizer S acquires a sufficient mass during inflation, which will be checked a posteriori, one can derive the inflaton-dependent vev of the scalar s to be

$$\langle s \rangle = M_{\rm p} \frac{(\varphi^2 - 2M_{\rm p}^2)^2 f' h' + 24\alpha f h M_{\rm p}^2}{6\sqrt{2}\alpha \left(-\frac{(\varphi^2 - 2M_{\rm p}^2)^2}{12\alpha}(f'^2 + h'^2) + \frac{4f^2 M_{\rm p}^4}{\Lambda_{\rm eff}^2} - 2h^2 M_{\rm p}^2 \right)}, \tag{8.12}$$

where a prime denotes a derivative with respect to the complex field Φ in (8.9), and the functions f, h and $\Lambda_{\rm eff}$ are all dependent on $\Phi = i\frac{\varphi}{\sqrt{2}}$ during inflation.

In the vacuum at the end of inflation, where $\Phi = 0$, the cosmological constant can be removed by imposing that

$$V(\varphi = 0) = 0, \tag{8.13}$$

which is equivalent to fixing

$$h_0^2 = \frac{f_0^2}{3}\left[1 + \mathcal{O}\left(\frac{\Lambda_0^2}{M_{\rm p}^2}\right)\right]. \tag{8.14}$$

Note that in this vacuum $\langle s \rangle \propto \Lambda_0^2/M_{\rm p}$, *i.e.* it is of the same order as the corrections to the above relation. In addition, the physical mass of the inflaton m_φ is given

by the parameter $2m_h$, whereas the gravitino mass (7.38) will fall down at the end of inflation to $f_0/\sqrt{3}M_{\rm p}$.

The vacuum at vanishing Φ is not a global minimum. Indeed, there is a supersymmetric vacuum in field space where the sinflaton gets a VEV of order $\sqrt{\frac{f_0 M_{\rm p}}{m_f}}$. One therefore has to ensure that there are no tachyonic directions about the extremum. We find that the stability of the non-supersymmetric vacuum in the sinflaton direction imposes the constraint[1]

$$m_h^2 > \frac{3\alpha f_0 m_f}{2M_{\rm p}} \ . \tag{8.15}$$

The inflationary trajectory spans the space of $\mathrm{Im}(\Phi)$ with $\mathrm{Re}(\Phi) = \mathrm{Im}(S) = 0$ while the real part of the sgoldstino is given by equation (8.12). We should follow the inflationary trajectory in the $\varphi - s$ space in order to verify that the conditions listed in the previous sections (and the absence of tachyons) are satisfied.

The simple conditions (8.4) and (8.5) are translated in the following constraints

$$f_0 < \Lambda_0^2 \ , \qquad \frac{m_f}{M_{\rm p}} < g^2 \ , \qquad m_h < \Lambda_0 \ . \tag{8.16}$$

We note that the coupling g is crucial to keep the sgoldstino mass within the validity of the effective theory. We will see how these bounds correspond typically to no-tachyon conditions in explicit UV completions of the model.

The third condition advocated in section 8.2 is

$$\langle s \rangle \ll \Lambda_{\rm eff}(\Phi) \tag{8.17}$$

and it is quite involved to solve analytically given the different terms entering into the expression for the sgoldstino VEV (8.12). In Appendix C we perform a simplified analysis of this VEV and we find that imposing the following inequalities

$$f_0 \ll \frac{\Lambda_0^2 m_f}{M_{\rm p}} \ , \qquad \frac{\Lambda_0^2}{M_{\rm p}^2} \ll \frac{m_h}{m_f} \ , \qquad \frac{\Lambda_0}{M_{\rm p}} \gg \frac{m_h}{m_f} \ , \tag{8.18}$$

one is guaranteed that the sgoldstino VEV is within the validity of the EFT along the whole inflationary trajectory[2].

To conclude, we find that in the model (8.8) the EFT is consistent all along inflation if the conditions (8.15), (8.16) and (8.18) are satisfied. Note that the last condition in (8.18) leads automatically to $m_h \ll m_f$. This implies that during inflation, when the inflaton takes field values of order $M_{\rm p}$, the parameter m_f

[1] Using the approximate formula $S_{\rm bounce} \propto (\Delta\phi)^4/\Delta V$, a qualitative estimate of the tunnelling rate into the SUSY vacuum indicates that the metastable vacuum is sufficiently long-lived for the typical range of parameters that we will consider.

[2] Other valid regions in parameter space exist, but we found that this is the only one that survives the more stringent bounds of the weakly coupled UV completion that we will consider in the next section.

dominates the scalar potential and hence sets the scale of inflation. The mass of the inflaton at the end of inflation is instead controlled by m_h, which is a different (and much smaller) scale.

8.3.3 α-attractor inflation

During inflation, the potential will be dominated by the mass scale m_f which will be fixed by the cosmological observables. Indeed, in an expansion for small parameters f_0, m_h and Λ_0, the effective potential during inflation is, at leading order

$$V_{\rm inf} \approx \frac{m_f^2}{4M_{\rm p}^2}\varphi^4 \,. \tag{8.19}$$

However, due to the non-canonical Kähler potential, we have to normalize the inflaton using Eq. (6.13). This follows the α-attractor scenario, as discussed in section 6.2.2. In this chapter, we will use the scenario of small α, since large α is observationally unsatisfactory. Note also that the only parameters appearing in the potential are from the ϕ part, there is no mixing with the additional fields in the theory. This is a generic feature of α-attractors, as was shown in Ref. [213]. Due to the particular structure of the kinetic term, the couplings with other fields get suppressed. In addition, in Ref. [220] was shown that the next-to-leading order terms in the perturbation series do not modify the inflationary predictions.

The COBE normalization and the slow roll conditions can be used to extract the values of $n_{\rm s}$, r and m_f as a function of α and the number of e-folds. We here focus on the case of the quartic power potential as in Eq. (8.19). Moreover, in order to provide analytic expressions, we can consider N to be large and expand the relevant quantities in powers of $1/N$.

The inflation observables $n_{\rm s}$ and r at second order in this expansion and in slow roll are given in Eq. (6.14). Moreover, the COBE normalisation $A_{\rm s} = (24\pi^2 M_{\rm p}^4)^{-1} V/\epsilon_* \approx 2.2 \cdot 10^{-9}$ can be used to fix

$$m_f^2 = A_{\rm s}\frac{18\alpha\pi^2}{N^2}M_{\rm p}^2, \tag{8.20}$$

where we expanded m_f only to first order in $1/N$ since we do not require additional accuracy.

The predictions for the α-attractor model with quartic potential is displayed in Fig. 8.1 for different choices of α and of the number of e-folds N. In section 8.5, once we will have specified the UV completion, we will compute the reheating temperature and derive the expected number of e-folds. One can observe that anyway the required values of m_f stand between $10^{-6}M_{\rm p}$ and $10^{-4}M_{\rm p}$, the lowest values being favoured for $\alpha = 1/3$.

Note that generically for small numbers of e-folds one can obtain from the α-attractor models values of $n_{\rm s}$ which are in the low-end region of the allowed Planck contours.

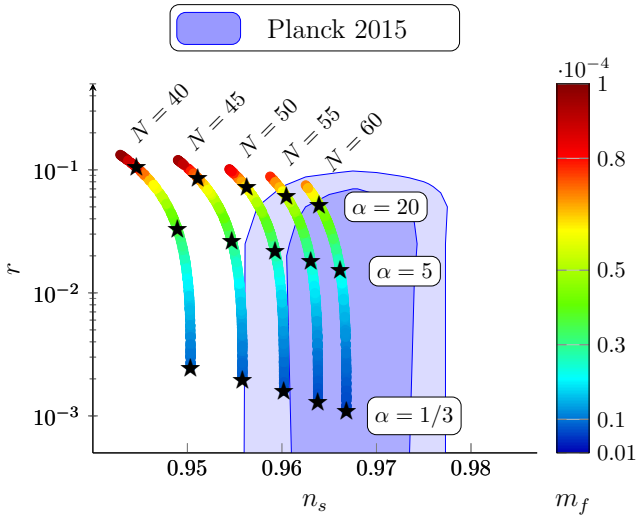

Figure 8.1: *Inflation observables for α-attractor models using different values of the α parameter and number of e-folds. The color bar indicates the value of m_f (in units of $M_{\rm p}$) required for satisfying the COBE normalization measurement. The shaded region indicates the values favoured by the Planck collaboration at 1 and 2 σ [14].*

8.3.4 Remarks on quadratic inflation

Before proceeding to analyse a UV completion of this model, we would like to make a few remarks about the consequences of the consistency conditions identified in this section for other inflation models. In particular we would like to assess if nilpotent quadratic inflation (described in section 3.4) can be consistently realized since, even if it is disfavoured by recent measurements of the tensor-to-scalar ratio r [14, 16, 17], it could represent a minimal application of the nilpotent paradigm.

The most economical possibility would be to consider a shift symmetric Kähler potential $\mathcal{K} = \frac{1}{2}(\Phi + \Phi^\dagger)^2$ and a quadratic expression for $h(\Phi)$, with $h''(\Phi)$ setting the scale of inflation. In order for the stabilization of the scalar potential to be effective at large field values, one should choose $f(\Phi)$ properly. For instance, further requiring the cosmological constant in the vacuum to be zero restricts to the choice $f(\Phi) = \sqrt{3}h(\Phi)$ [268, 306, 307].

This immediately leads to two important issues. First consider the case in which $\Lambda_{\rm eff}$ is a constant independent on the inflaton VEV. Then the requirement $f(\phi) \ll \Lambda_{\rm eff}^2$ already puts strong constraints on the allowed values for $\Lambda_{\rm eff}$. For instance, if $f(\phi)$ is a quadratic function, *i.e.* $f(\phi) = f_0 - \frac{m_f}{M_{\rm p}}\phi^2$, then we auto-

matically obtain $\frac{m_f}{M_\mathrm{p}}\phi^2 \ll \Lambda_\mathrm{eff}^2$. For quadratic inflation, which needs large m_f and reaches transplanckian values of ϕ, this implies a severe lower bound for Λ_eff, as explained in [278].

Second, one can consider the possibility of a dynamical Λ_eff, as we assumed in our illustrative model. Note that the derivation of the sgoldstino VEV and the EFT analysis would be only mildly changed, since the Kähler attractor potential reduces to the canonical shift symmetric one for small values of ϕ and $\alpha = 1/3$. In particular, the conditions (8.18) should still be fulfilled. If $m_h \sim m_f$ the third condition in (8.18) would imply $\Lambda_0 \gg M_p$ which is not possible. Said differently, the sgoldstino VEV would exceed the limit of the EFT validity if $m_h \sim m_f$, rendering the EFT description, with its truncation at quartic order in S, inconsistent. Indeed, the same conclusion was reached in section 7.5.

A very careful different choice of the functions $f(\Phi)$, $h(\Phi)$ and $\Lambda_\mathrm{eff}(\Phi)$ could possibly overcome these issues, however we consider them as a sufficient motivation to forgo quadratic inflation and prefer to work with the α-attractor scenario.

8.4 UV completion and mediation of SUSY breaking

We now consider a UV completion of the effective model whose aim is two-fold. We add extra fields which, upon integrating them out, produce the effective quartic term in S, and at the same time act as mediators of supersymmetry breaking to the standard model. As our goal is to achieve scales of SUSY breaking which are rather low, we use the gauge mediation scenario of supersymmetry breaking (GMSB) discussed in section 7.2, so that the extra fields can be taken to be the usual messengers, charged under the SM gauge group.

As is customary in GMSB, it is better to actually take the messengers to be in representations of a grand unified group, $SU(5)$ being the minimal choice. Messengers come in vectorial representations, and the simplest option is to have one or more copies of $\mathbf{5} \oplus \bar{\mathbf{5}}$.

We thus introduce the fields X and Y in the $\mathbf{5}$, and $\tilde{X}$ and $\tilde{Y}$ in the $\bar{\mathbf{5}}$, and we consider a generalized O'Raifeartaigh model which is equivalent to the effective IR description of the theory considered in [308].

In the rigid limit $M_\mathrm{p} \to \infty$, we assume a canonical Kähler potential for all the fields (inflaton Φ included, which is indeed what one gets in this limit from Eq. (8.8) for $\alpha = 1/3$), and a superpotential

$$W = -m_h\Phi^2 + f_0 S - \lambda_f S\Phi^2 + \lambda S X\tilde{X} + (M + g_f\Phi)(X\tilde{Y} + Y\tilde{X}) + m_y Y\tilde{Y} \ . \quad (8.21)$$

Let us comment on the various terms. If we set $\Phi = 0$ and $m_y = 0$, we have a complexified version of the usual O'Raifeartaigh model, with S playing the role of the superfield with a non-vanishing F-term, a classical flat direction and the

goldstino as fermionic component. Its coupling to the messengers λ can be taken to be typically $\mathcal{O}(1)$. Turning on the term with m_y breaks R-symmetry and thus allows for gauge mediation to generate non-zero gaugino masses, as shown in [308].

Bringing now the inflaton into the game, the crucial term is the one with g_f, which couples Φ to all the messengers and, more importantly, makes their mass inflaton-dependent. The last two terms involving m_h and $\lambda_f = m_f/M_{\rm p}$ will not be important for the physics of SUSY breaking. Note that, if we assume that the term with m_h preserves R-symmetry, then both g_f and λ_f break it, and should be taken to be small. Indeed, λ_f can be assumed to take its value between 10^{-6} and 10^{-4} as in the previous section[3].

Since W breaks R-symmetry for generic couplings, we expect to have SUSY vacua. However, if the R-symmetry breaking terms are small enough, we also expect the SUSY breaking vacuum near the origin to survive as a long-lived metastable state. We anticipate that the latter state will be obtained as follows: one sets all the messenger fields and the inflaton to zero, and then computes the effective potential for S. There is generically a local minimum near the origin which becomes a global minimum if one takes $m_y, g_f, \lambda_f \to 0$. The SUSY vacua (*i.e.* solutions to the F-term equations descending from W above) occur either for parametrically large non-zero values of the messenger fields, *i.e.* outside the domain of validity of the effective low-energy theory where the messengers have been integrated out, or for large sinflaton VEVs. It is indeed possible to check that the SUSY vacua are far enough from the inflationary trajectory in the $\Phi - S$ plane.

8.4.1 No tachyons in the messenger sector

First, we discuss the conditions for which there are no tachyons in the messenger sector, along the inflationary trajectory, *i.e.* around zero values of X, Y, $\tilde{X}$ and $\tilde{Y}$. The potential, given by the sum of squared F-terms, is

$$\begin{aligned} V =& |-2m_h\Phi - 2\lambda_f S\Phi + g_f(X\tilde{Y} + Y\tilde{X})|^2 + |f_0 - \lambda_f\Phi^2 - \lambda X\tilde{X}|^2 \\ &+ |\lambda SX + (M + g_f\Phi)Y|^2 + |\lambda S\tilde{X} + (M + g_f\Phi)\tilde{Y}|^2 \\ &+ |(M + g_f\Phi)X + m_y Y|^2 + |(M + g_f\Phi)\tilde{X} + m_y\tilde{Y}|^2 \ . \end{aligned} \tag{8.22}$$

[3]At this point, note that W has also several terms that break the shift symmetry of the inflaton (*i.e.* the imaginary part of Φ). The only one specific to the UV completion is the one proportional to g_f, which then cannot take too large values.

Expanded to quadratic order in the messenger fields (but to any order in S and Φ), we get

$$\begin{aligned} V = &- 2g_f\Phi^*(m_h + \lambda_f S^*)(X\tilde{Y} + Y\tilde{X}) - 2g_f\Phi(m_h + \lambda_f S)(X^*\tilde{Y}^* + Y^*\tilde{X}^*) \\ &- \lambda(f_0 - \lambda_f\Phi^{*2})X\tilde{X} - \lambda(f_0 - \lambda_f\Phi^2)X^*\tilde{X}^* + \lambda^2|S|^2(|X|^2 + |\tilde{X}|^2) \\ &+ |M + g_f\Phi|^2(|X|^2 + |\tilde{X}|^2 + |Y|^2 + |\tilde{Y}|^2) + m_y^2(|Y|^2 + |\tilde{Y}|^2) \\ &+ \lambda S(M + g_f\Phi^*)(XY^* + \tilde{X}\tilde{Y}^*) + \lambda S^*(M + g_f\Phi)(X^*Y + \tilde{X}^*\tilde{Y}) \\ &+ m_y(M + g_f\Phi)(XY^* + \tilde{X}\tilde{Y}^*) + m_y(M + g_f\Phi^*)(X^*Y + \tilde{X}^*\tilde{Y})\,. \end{aligned} \tag{8.23}$$

If we are to safely integrate out the messengers, we need to make sure that their squared mass matrix does not have negative eigenvalues, *i.e.* there are no tachyonic directions. When this is ensured, we will assume that the mass eigenvalues are dominated by the diagonal values (the last term in the second line and the terms in the third line in Eq. (8.23))[4]. Thus in order to get a flavour of when tachyons could possibly arise, one can simply compare the off-diagonal terms to the diagonal ones.

First of all, we must exclude tachyons near the origin, that is for values of S and Φ subleading to any other scale. This is as in usual minimal GMSB, and we find

$$M^2 \gtrsim |\lambda f_0|\ , \tag{8.24}$$

where we have also assumed that m_y is at most of the order of M (this is necessary in order not to bring the SUSY vacua too close to the origin in the messenger directions).

Going now to early times, at the beginning of the inflationary trajectory, we can assume $g_f\Phi \gg M$. In this regime the diagonal terms are all of the order of $g_f^2\Phi^2$, while the off-diagonal terms are respectively of order $g_f\Phi(m_h + \lambda_f S)$, $\lambda\lambda_f\Phi^2$, $\lambda S g_f\Phi$ and $m_y g_f\Phi$. The new conditions are

$$g_f^2 \gtrsim \lambda\lambda_f\ , \qquad g_f\Phi \gtrsim \lambda S\ , \qquad g_f\Phi \gtrsim m_h\ , \tag{8.25}$$

where we have already simplified some redundant conditions by taking into account that $m_y \lesssim M$ and $\lambda_f \ll \lambda$.

Finally taking values of Φ which are such that $g_f\Phi \lesssim M$, the same rule of thumb that off-diagonal terms should be less than M^2 gives the only additional conditions

$$g_f\Phi \lesssim \frac{M^2}{m_h}\ , \qquad \lambda S \lesssim M\ . \tag{8.26}$$

The two conditions $g_f\Phi \gtrsim m_h$ and $g_f\Phi \lesssim M^2/m_h$ together imply that the inflationary trajectory does not cross a tachyonic region only if

$$M \gtrsim m_h\ . \tag{8.27}$$

[4]More specifically we can further assume that the diagonal terms are dominated by the term $|M + g_f\Phi|^2$. We can then distinguish two regimes, when $\Phi \gg M/g_f$ and when $\Phi \ll M/g_f$.

Note that this condition implies that the mass of the inflaton after inflation lies within the regime of validity of the effective theory where the messengers have been integrated out.

All in all the no-tachyon constraints are

$$M \gtrsim m_h \ , \qquad \lambda S \lesssim M + g_f \Phi \ , \qquad g_f^2 \gtrsim \lambda \lambda_f \ , \qquad M^2 \gtrsim |\lambda f_0| \ . \tag{8.28}$$

These are indeed the conditions we had been imposing on the EFT of the previous section, once the UV parameters are matched to the effective theory, as we will see in the next subsection.

8.4.2 Integrating out the messengers

We now integrate out the messengers in order to make contact with the low-energy effective theory discussed in the previous section. Assuming that we are far away from the tachyonic regions, we can integrate out the messenger in a SUSY fashion, obtaining the one-loop Kähler potential directly [309, 310]. This can be further simplified by treating the terms proportional to λS and m_y as perturbations with respect to the dominant mass term proportional to $M + g_f \Phi$. The one-loop Kähler potential thus involves, when expanded in S, the following terms

$$\begin{aligned} K_{1-\text{loop}} = & -\frac{N_m \lambda^4 (S S^\dagger)^2}{12(8\pi^2)|M + g_f \Phi|^2} - \frac{N_m \lambda^2}{2(8\pi^2)} S S^\dagger \log[\frac{|M + g_f \Phi|^2}{M_{\rm p}^2}] \\ & - \frac{N_m \lambda m_y}{2(8\pi^2)} \left(\frac{S^\dagger (M + g_f \Phi)^2 + h.c.}{|M + g_f \Phi|^2} \right) \\ & + \frac{N_m m_y \lambda^3}{12(8\pi^2)} S S^\dagger \left(\frac{S}{(M + g_f \Phi)^2} + h.c. \right) \end{aligned} \tag{8.29}$$

where N_m is the number of copies of the system composed of the $X, \tilde{X}, Y$ and $\tilde{Y}$ superfields. We actually have $N_m = 5 N_5$, taking into account that the messengers come in representations 5 and $\bar{5}$. Note that there are also one-loop terms dependent only on S or only on Φ, that we omitted since they just represent loop-suppressed corrections to the canonical terms. The expression is expanded at first order in $m_y/(M + g_f \Phi)$.

The first term in (8.29) corresponds to the higher dimensional correction that we considered in the EFT description (see Eq. (8.8)) and is the one giving a mass to the sgoldstino. The other terms are other one-loop corrections which are allowed by symmetries and indeed can be generically added to the effective Kähler potential in (8.8). The second term in the first line is simply a sub-leading correction to the canonical kinetic term for the sgoldstino, which depends on the inflaton φ only at order $O(g_f^2)$.

The second and third line are suppressed by a factor of m_y/M and as soon as $m_y < M$ it is not relevant for the inflaton trajectory. However, these terms include the leading order operator that determines the decay of the inflaton in the

sgoldstino, and are hence important later on in our analysis. Moreover, they lead to a VEV for the sgoldstino also in the non-SUSY vacuum of the (rigid) theory at the end of inflation, which scales as $\langle s \rangle \sim \frac{m_y}{\sqrt{2}\lambda}$. Note that for m_y close to M, which will be needed in order to have sizeable gluino masses, the sgoldstino VEV could become a relevant contribution to the inflaton mass which is now $m_\varphi \simeq 2m_h + 2\lambda_f \langle S \rangle$. We will comment later about this fact and we will show that in the interesting region of the parameter space this contribution is always negligible so that we can simply take $m_\varphi \simeq 2m_h$, as in the discussion of section 8.3.2.

As a consistency check, we verified numerically on the benchmarks considered in the following analysis, that these extra Kähler corrections play a negligible role in the determination of the inflaton trajectory in the $S - \Phi$ plane, and the first term in (8.29) is enough to capture the main features.

Comparing (8.29) with (8.8), we see that we can identify

$$\Lambda_0 + g\Phi = \frac{\sqrt{6}(4\pi)}{\sqrt{N_m}\lambda^2}(M + g_f\Phi) \ . \tag{8.30}$$

As a consequence, the effective theory parameters Λ_0 and g are related to the UV messenger theory parameters M and g_f by

$$\Lambda_0 = \frac{\sqrt{6}(4\pi)}{\sqrt{N_m}\lambda^2}M \ , \qquad g = \frac{\sqrt{6}(4\pi)}{\sqrt{N_m}\lambda^2}g_f \ . \tag{8.31}$$

We see that, as it is usually the case, the UV scale of the effective theory, and its coupling g, are somewhat larger than the messenger masses, and their coupling to the inflaton, respectively. This has to be taken into account when comparing the inequalities keeping us within the validity of the effective theory, to the ones keeping us away from the tachyonic domain of the UV theory. In particular, if we use the matching (8.31) to compare the inequalities that we have obtained in the EFT analysis in section 8.3 (Eq. (8.16) and Eq. (8.17)) and the ones that we have obtained by demanding absence of tachyons in the UV theory in section 8.4.1 (Eq. (8.28)), we find that the former are typically weaker. Hence in the following we will consider the dynamics of the UV completed model and we will apply the conditions (8.28).

8.4.3 Low-energy spectrum and gauge mediation

We now discuss the spectrum of the model, both during inflation and at the end of it. This will help setting the scale of some of the parameters of the model. From the inflationary sector we have the inflaton, together with its bosonic and fermionic partners. In the SUSY breaking sector, we have the gravitino and the sgoldstino. Eventually, we have the visible sector: we no longer consider the messengers, however their mass scale affects the visible sector soft masses through gauge mediation.

Let us start with the inflationary sector. We concentrate here on the spectrum after inflation, which determines how much this sector could be relevant also to collider physics. Near the origin of Φ, the SUSY mass of all its components is controlled by m_h. The SUSY breaking splittings are given by $\lambda_f f_0$, which is smaller than m_h^2 by virtue of the condition (8.15) to avoid tachyons in this sector.

In the S sector, we can consider the mass of the gravitino and the mass of the sgoldstino. Note that the splitting between the latter two masses is all important for the viability of a sgoldstino-less description of inflation in supergravity. Indeed, we need to find the existence of a regime in which the gravitino is well below the scale of inflation (so that a supergravity description is justified) while the sgoldstino is above that scale, so that it makes sense to integrate it out (using a nilpotent superfield from the outset, for instance).

The mass of the gravitino can be obtained from the standard SUGRA expression given in Eq. (7.37) as

$$m_{3/2}^2 = e^{\frac{K}{M_{\rm p}^2}} \frac{|W|^2}{M_{\rm p}^4} \simeq \left| \frac{h_0}{M_{\rm p}} - m_h \frac{\Phi^2}{M_{\rm p}^2} \right|^2 \ , \tag{8.32}$$

where we have used the fact that in all regimes $h(\Phi) \gg Sf(\Phi)/M_{\rm p}$. (In the large Φ regime, one uses (8.12) to obtain $S \sim M_{\rm p} \frac{g^2 m_h}{m_f}$, under the only assumption $m_f \gg m_h$). During inflation, the Φ-dependent term will dominate, but given that Φ is Planckian at most, we will have $m_{3/2} \lesssim m_h$, indeed smaller than the scale of inflation which is determined by m_f. At the end of inflation, the gravitino mass is given as usual by

$$m_{3/2} \simeq \frac{f_0}{\sqrt{3} M_{\rm p}} \ . \tag{8.33}$$

In low scale SUSY breaking models, this will be the smallest scale.

The sgoldstino mass is controlled by the quartic term in the Kähler potential (8.29). It gives a mass

$$m_s^2 = \frac{N_m \lambda^4 |f_0 - \lambda_f \Phi^2|^2}{3(8\pi^2)|M + g_f \Phi|^2} \ . \tag{8.34}$$

During inflation, *i.e.* for large Φ, we have

$$m_s \simeq \frac{\sqrt{N_m} \lambda^2 \lambda_f \Phi}{\sqrt{6}(2\pi) g_f} = 2 m_f \frac{\Phi}{g M_{\rm p}} \ . \tag{8.35}$$

Thus as long as $\Phi > g M_{\rm p}$ the sgoldstino mass is larger than the scale of inflation, allowing to integrate it out (as in a nilpotent formulation). However we also see that by no means it decouples entirely from the spectrum, its effective mass soon plunging below m_f. Indeed, at the end of inflation the sgoldstino mass is

$$m_s \simeq \frac{\sqrt{N_m} \lambda^2 f_0}{\sqrt{6}(2\pi) M} \ . \tag{8.36}$$

As we will see instantly, this is at a scale just an order of magnitude larger than the soft masses of the visible sector.

Assuming gauge mediation of SUSY breaking to be exclusively operated through the messengers which also couple to the inflaton, the soft masses of the visible sector can be completely determined using Eqs. (7.28) and (7.29). We note that the expressions are complicated by the presence of several parameters, such as m_y which is necessary to obtain non-zero gaugino masses [308]. The gaugino and sfermion masses scale similarly to the sgoldstino mass, where however the loop suppression is due to SM gauge couplings, and where the gaugino suffers from an extra suppression in power of m_y/M because of R-symmetry

$$m^2_{\text{sfermions}} \simeq \sum_i \frac{2N_5 C_2^i g^4_{SM(i)} \lambda^2 |f_0 - \lambda_f \Phi^2|^2}{(4\pi)^4 |M + g_f \Phi|^2} \ , \tag{8.37a}$$

$$m^{(i)}_{\text{gaugino}} \simeq \frac{N_5 g^2_{SM(i)} \lambda m_y |f_0 - \lambda_f \Phi^2|}{(4\pi)^2 |M + g_f \Phi|^2} \ . \tag{8.37b}$$

In particular the sfermion masses are quite large during inflation, but eventually reduce to the usual value [308] after settling in the vacuum[5]:

$$m^2_{\text{sfermions}} \simeq \sum_i \frac{2N_5 C_2^i g^4_{SM(i)} \lambda^2 f_0^2}{(4\pi)^4 M^2} \ , \qquad m^{(i)}_{\text{gaugino}} \simeq \frac{N_5 g^2_{SM(i)} \lambda m_y f_0}{(4\pi)^2 M^2} \ , \tag{8.38}$$

where C_2^i are the quadratic Casimir of the sfermions and i runs over the SM gauge groups. These are the values that we will use in the phenomenological analysis in section 8.5.

8.4.4 Analysis of the allowed parameter space

We can now combine all the consistency conditions in order to identify the allowed regions of parameter space and determine what are the typical mass scales of the relevant particles entering into the model, *i.e.* the inflaton, the sgoldstino, and the superpartners (we will consider as reference the gluino).

The model depends on many parameters, but eventually only few of them determine a qualitative difference in the physics outcome. We summarize here the relevant constraints on the parameters that we have encountered along our analysis:

- No tachyon condition in the UV model, arising from the analysis of the messenger mass matrix:

$$M \gtrsim m_h \ , \qquad \lambda S \lesssim M + g_f \Phi \ , \qquad g_f^2 \gtrsim \lambda \frac{m_f}{M_{\text{p}}} \ , \qquad M^2 \gtrsim |\lambda f_0| \ . \tag{8.39}$$

[5] We neglect RG running effects.

The condition on the sgoldstino VEV along the entire trajectory can be analyzed as we did for the EFT in Eq. (8.18) (see Appendix C), yielding

$$\lambda S \lesssim M + g_f \Phi \quad \Rightarrow \quad \left\{ f_0 \lesssim \frac{m_f}{\kappa M_{\rm p}} M^2 \,,\; \frac{M^2}{\kappa M_{\rm p}^2} \lesssim \frac{m_h}{m_f} \,,\; \frac{M}{M_{\rm p}} \gtrsim \lambda \frac{m_h}{m_f} \right\} \,, \tag{8.40}$$

where $\kappa = \frac{N_m \lambda^4}{12(8\pi^2)}$. In practice, these conditions can be circumvented taking a strongly coupled hidden and messenger sector, for which no perturbative analysis can be done, leaving us with the EFT treatment of the previous section.

- No tachyons in the effective theory, *i.e.* the inflaton sector:

$$m_h^2 > \frac{3\alpha f_0 m_f}{2M_{\rm p}} \,. \tag{8.41}$$

It is not straightforward to extract from this set of inequalities what is the allowed volume in the parameter space. So, in order to investigate the allowed region, we can proceed by fixing some parameters to typical values and plot the resulting region. Once we fix the dimensionless quantities $(\lambda, g_f, N_5, \frac{m_y}{M})$ and we take $m_f \sim 10^{-5} M_{\rm p}$ as suggested by the analysis in Fig. 8.1, we are left with only 3 independent parameters, *i.e.* $\{f_0, M, m_h\}$. We can trade two of these parameters with physical masses to conclude that our parameter space is a region in the three dimensional space spanned by $\{m_\lambda, m_{3/2}, m_h\}$, where we indicated with m_λ the gluino mass.

The allowed region of parameter space can then be easily displayed in the $\{m_{3/2}, m_h\}$ plane by fixing m_λ to some phenomenologically interesting value, as we do in Fig. 8.2. We considered as upper limit for the gravitino mass the value of 1 GeV since we want to focus on the case where the gauge mediated contributions to the soft masses dominate the gravity contributions[6].

As we can observe, the allowed region in the $\{m_{3/2}, m_h\}$ plane gets smaller as we increase the gluino mass, disappearing completely (in the $m_{3/2} \leq 1$ GeV region) for $m_\lambda \geq 20$ TeV on the selected benchmark. Note that the two boundaries are set by the two conditions (where we have reinstated the exact numerical prefactor for added precision):

$$\frac{M}{M_{\rm p}} > \lambda \sqrt{2} \frac{m_h}{m_f} \qquad \Longrightarrow \qquad \text{Upper border} \,, \tag{8.42a}$$

$$m_h^2 > \frac{3\alpha f_0 m_f}{2M_{\rm p}} \qquad \Longrightarrow \qquad \text{Lower border} \,. \tag{8.42b}$$

We can saturate these inequalities to find the expressions $m_h^{(up)}$ and $m_h^{(low)}$ which determine the upper and lower lines of the triangle shaped allowed regions in Fig. 8.42b.

[6] In producing the plot, we also imposed $M \leq 10^{15}$GeV.

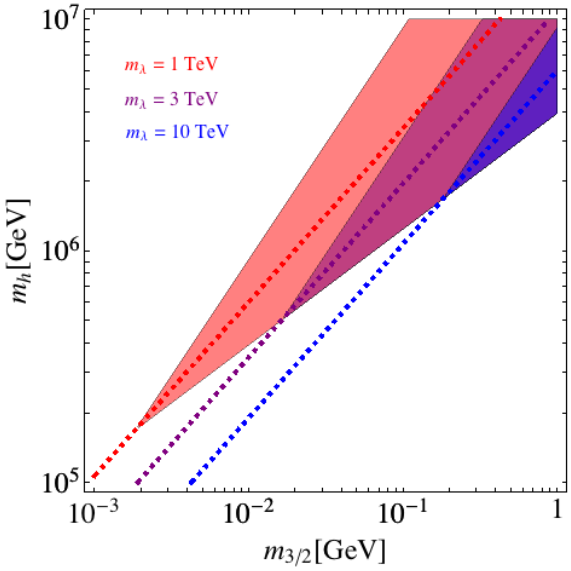

Figure 8.2: *Allowed region of parameter space in the* $\{m_{3/2}, m_h\}$ *plane by fixing* $m_\lambda = 1, 3, 10$ *TeV respectively for the light red, purple, blue region. The dashed lines represent the line defined in equation (8.47) for the different gluino masses. The other parameters are fixed as* $\{\frac{m_y}{M} = 0.15, \lambda = 0.25, N_5 = 3, g_f = 2\times10^{-3}, \alpha = 1/3, m_f = 7.3 \times 10^{-6} M_{\rm p}\}$.

It is instructive to consider the tip of the triangles, giving the lowest allowed values for the gravitino mass (and the inflaton mass), for a given gluino mass. It is simply obtained by saturating the two inequalities above. Using (8.33) and (8.38) we get:

$$m_{3/2}^{\rm tip} = \sqrt{3}\alpha \left(\frac{(4\pi)^2}{N_5 g_{SM}^2}\right)^2 \left(\frac{M}{m_y}\right)^2 \frac{m_\lambda^2}{m_f} \ . \tag{8.43}$$

This is to be confronted with the lowest gravitino mass that one could obtain in our gauge mediated model, considered on its own, given by the bound (8.24):

$$m_{3/2}^{\rm lowest,GMSB} = \frac{1}{\sqrt{3}\lambda} \left(\frac{(4\pi)^2}{N_5 g_{SM}^2}\right)^2 \left(\frac{M}{m_y}\right)^2 \frac{m_\lambda^2}{M_{\rm p}} \ . \tag{8.44}$$

We thus see that

$$m_{3/2}^{\rm tip} = 3\alpha\lambda \frac{M_{\rm p}}{m_f} m_{3/2}^{\rm lowest,GMSB} \ , \tag{8.45}$$

that is roughly 5 orders of magnitude above the lowest gravitino masses generically

allowed by GMSB[7]. In other words, the scale of supersymmetry breaking cannot be as low as we could hope in a GMSB scenario. Putting numbers, and using the benchmark point of Fig. 8.2, we get

$$m_{3/2}^{\text{tip}} \simeq 2 \text{ MeV} \left(\frac{m_\lambda}{1 \text{ TeV}}\right)^2 . \tag{8.46}$$

Thus we see that, for reasonable gluino masses, the gravitino cannot be lighter than a few MeV. This translates into a lowest supersymmetry breaking scale of the order of $\sqrt{f_0} \sim 10^8$ GeV, showing that for this class of weakly coupled models the scale of SUSY breaking cannot be arbitrarily small and compatible with sgoldstino-less inflation.

8.5 Phenomenological analysis

In order to simplify our analysis, from now on we will focus on the dashed lines in the middle of the triangles in Fig. 8.2, which is the average mean defined as

$$m_h^* = \sqrt{m_h^{(up)} m_h^{(low)}} , \tag{8.47}$$

which determines m_h for a given value of the other parameters. In this way we are reduced to a two dimensional parameter space spanned by $\{m_{3/2}, m_\lambda\}$, in which we will present our phenomenological analysis.

Given that the model we have considered in the previous section includes predictions both for cosmology as well as for particle physics, we can constrain the parameter space using inflation observables, considerations about the reheating temperature, gravitino dark matter abundance, Big Bang nucleosynthesis (BBN), as well as LHC constraints. We discuss all these aspects in the next subsections under some simplifying assumptions. In particular, we do not take into account the extended Higgs sector and its possible effects on the phenomenology. In our model, the NLSP is a neutralino, thus a combination of the Bino, Zino and Higgsinos, as discussed in section 7.1.4. We consider this NLSP to be predominantly Bino, assuming that the μ parameter is such that the Higgsino is significantly heavier, and consistent with the estimates of the soft terms done previously (8.38). At the end of the section, we will comment on how our analysis would be affected if instead the NLSP neutralino is a mixture of Bino-Higgsino.

We will present all the phenomenological characterization in the $\{m_{3/2}, m_\lambda\}$ plane, restricting to the line (8.47) as just mentioned. We verified that exploring other areas of the allowed region in Fig. 8.2 does not change qualitatively our conclusions.

[7]We can actually trace back this bound to one of the conditions in Eqs. (8.40), specifically the one giving an upper bound to f_0/M^2 proportional to m_f/M_{P}.

Our investigation will show that, once we consider all bounds together, the remaining allowed parameter space gets significantly reduced. In particular our results highlight the complementarity of the different phenomenological constraints, suggesting that a broad approach to inflation models, including analysis of the reheating epoch as well as the connection to particle physics, is needed in order to extract robust conclusions and predictions.

8.5.1 Reheating temperature and $n_{\rm s}$

Since in our model the couplings between the inflaton and the MSSM particles are well defined (up to the Higgs sector, that we do not specify), we can estimate the inflaton decay modes and the reheating temperature, as was explained in section 3.5. This is relevant since the inflaton decays via messenger loops to MSSM particles and thus the reheating temperature will be low. A low reheating temperature corresponds to a relatively small number of e-folds during inflation, hence a sizeable shift if compared to the usual estimate of 60 e-folds, as in Refs. [214, 311]. In addition, the gravitino problem is simpler to solve with a low reheating temperature [288, 312].

The reheating temperature can be found from the energy density at which the Hubble rate ($H_{\rm reh}$) equals the decay width of the inflaton (Γ_ϕ) [152], combining Eqs. (2.19), (3.61), (3.60) and (2.17)

$$\rho_{\rm reh} = \frac{\pi^2 g_*}{30} T_{\rm reh}^4 = 3H_{\rm reh}^2 M_{\rm p}^2 = 3\Gamma_\phi^2 M_{\rm p}^2 = \rho_{\rm end} e^{-3N_{\rm reh}(1+\bar{w}_{\rm reh})}, \tag{8.48}$$

where $H_{\rm reh}$ is the Hubble rate at the end of reheating, $g_* \sim 220$ is the number of relativistic degrees of freedom at reheating, $\bar{w}_{\rm reh}$ is defined in Eq. (3.58) and $\rho_{\rm end}$ is the energy density at the end of inflation. The first equality defines the temperature $T_{\rm reh}$ and the last equality the number of e-folds during reheating ($N_{\rm reh}$). Though the thermalization after the inflaton decay might take time and result in a lower reheating temperature, we will in the following stick to this upper bound. Finally, from Eq. (3.59) follows that $\bar{w}_{\rm reh} = 0$, since our potential is quadratic around the minimum [151].

Given a certain reheating temperature, the number of e-folds between the end of inflation and the moment a mode with $k_* = 0.002{\rm Mpc}^{-1}$ left the horizon can be obtained using Eqs. (3.63) and (3.64). Note that this is an implicit equation since r depends on N, as shown in Eq. (6.14). This relation can be solved for the reheating temperature, resulting in

$$T_{\rm reh} = \frac{495\sqrt{3}e^{3N}}{43\pi^2\sqrt{2A_{\rm s}\alpha}} M_{\rm p} \left(\frac{k}{a_0 T_0}\right)^3 \left(\frac{4+\sqrt{16+3\alpha}-\sqrt{3\alpha}}{4+\sqrt{16+3\alpha}+\sqrt{3\alpha}}\right)^4 \left(N + \mathcal{O}\left(N^0\right)\right), \tag{8.49}$$

where again we used the $1/N$ expansion. A more careful analysis, keeping higher orders in N showed that in our model corrections to this equation are of the order

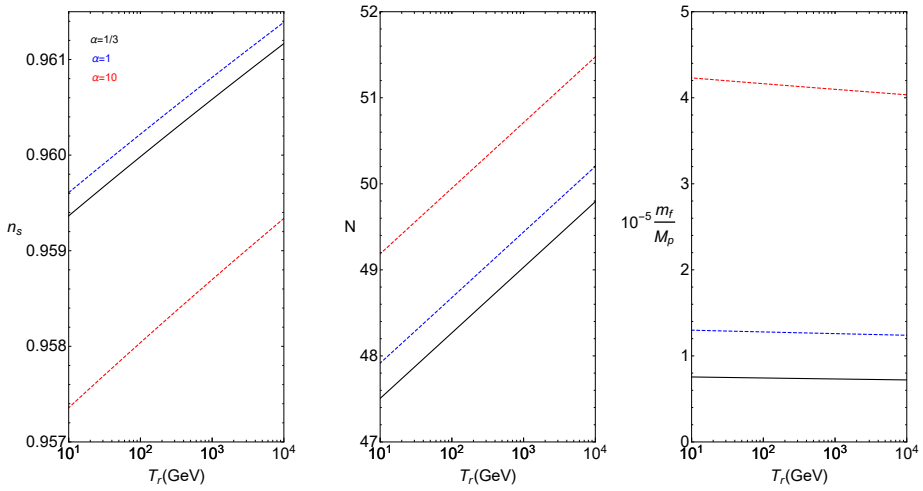

Figure 8.3: *From left to right, the dependence on the reheating temperature of* n_s, N *and* m_f *for different values of* α. *The straight black line represents our scenario with* $\alpha = 1/3$, *while the blue and red dotted lines represent resp.* $\alpha = 1, 10$.

of a percent. However, due to the exponential behaviour on the number of e-folds, a small deviation in N changes the reheating temperature considerably.

In our model the reheating temperature can be computed from the inflaton decay width, and we use Eq. (3.63) to extract the expected number of e-folds. Then we plug this result in Eq. (6.14) and Eq. (8.20) to obtain precise predictions for n_s, r and m_f as a function of the reheating temperature. The results of this procedure are plotted in Fig. 8.3 for N, n_s and m_f. The tensor to scalar ratio, being $1/N^2$ suppressed, is roughly 0.002, far below the current experimental constraints.

We now discuss the most relevant decay modes of the inflaton and estimate its decay width to obtain the expected reheating temperature. The mass of the inflaton is taken to be $m_\varphi = 2m_h$, neglecting possible contributions from the sgoldstino VEV. We will verify that this is consistent on the considered region of the parameter space.

In the complete model there is no tree-level coupling between the inflaton and MSSM fields and the decay channels are loop suppressed. The leading decay mode arises from the following operator generated at one-loop (together with the operator responsible for the gluino masses)

$$W \supset \int d^2\theta \frac{\alpha_s N_5}{4\pi} \frac{g_f}{M} \Phi \, \mathcal{W}_\alpha \mathcal{W}^\alpha \,, \tag{8.50}$$

and it gives the following decay modes into gluons and gluinos

$$\Gamma_\phi \approx \Gamma_{\phi gg} + \Gamma_{\phi \tilde{g}\tilde{g}} = \frac{\alpha_s^2 N_5^2 g_f^2}{\pi^3 M^2} m_h^3 \ . \tag{8.51}$$

These are the dominant decay modes of the inflaton[8] and we approximate with this value the total decay width of the inflaton. Because of the one-loop suppression of this decay width the reheating temperature is rather low in our parameter space, of the order of the TeV scale,

$$T_{\rm reh} \simeq 900 \text{ GeV} \left(\frac{m_h}{200 \text{ TeV}}\right)^{3/2} \left(\frac{m_\lambda}{1 \text{ TeV}}\right) \left(\frac{20 \text{ MeV}}{m_{3/2}}\right) \tag{8.52}$$

where the numerical values of the parameters has been fixed as in Fig. 8.2. Then, from Fig. 8.3 we see that for $\alpha = 1/3$ the number of e-folds is about $48 - 49$, and hence that $n_{\rm s}$ is rather small. We also note that the value of m_f is around $8 \times 10^{-6} M_{\rm p}$, as the benchmark point we have chosen in the previous section.

8.5.2 Gravitino abundance

In this model the gravitino is the LSP and can be a viable dark matter candidate if $\Omega_{3/2} h^2 \simeq \Omega_{DM} h^2 = 0.12$ (see e.g. [296, 313–315] for recent developments on gravitino dark matter). Neglecting possible dilution factors, we conservatively demand that the gravitino abundance does not overclose the universe by imposing $\Omega_{3/2} h^2 \leq \Omega_{DM} h^2$. Gravitino relics can be obtained with several mechanisms, as was explained in section 7.5.2. These mechanisms are i) thermal production; ii) freeze-in production through the superparticle decays; iii) production through inflaton decays; iv) decay of the NLSP, that here is assumed to be the Bino.

In the following we study these production mechanisms and we find the constraints they impose on the parameter space of the model:

i) The reheating temperature for our range of parameters is at most of O(TeV), with gravitino at least of MeV mass, and hence the thermal production of gravitino is not significant [286, 288, 312]. We verified this explicitly in our numerical analysis.

ii) The freeze-in scenario for gravitino dark matter has been proposed as a mechanism to obtain the correct gravitino relic abundance through the decay of the MSSM superparticles [75, 286, 316, 317]. In our case the abundance of the heavy superparticles is suppressed by a Boltzmann factor, due to the low reheating temperature[9], and hence we have to use Eq. (7.58). The

[8] The ones into sfermions are loop suppressed and the ones in other gauge bosons and gauginos are coupling suppressed.

[9] In the period between the end of inflation and before the radiation dominated era, the temperature can be higher, and hence also the freeze-in contribution. However, the produced gravitinos get diluted before radiation starts dominating [163, 318, 319]. As a crude approximation, we neglect these two compensating effects.

superparticle masses are much heavier than the current temperature of the universe, so the upper bound of the integral I in Eq. (7.58) is taken as $x_{\max} = \infty$, however we cannot ignore the low reheating temperature, so $x_{\min} = m_{\tilde{X}}/T_{\rm reh}$. We numerically perform this integral, and demand this abundance to not exceed the dark matter one.

iii) The decay of the inflaton into gravitinos, or into supersymmetric particles eventually decaying into gravitinos, can give a large contribution to the gravitino relic abundance. In these processes the goldstino component of the gravitino is the one setting the relevant interactions.

The inflaton can decay directly into goldstinos or sgoldstinos through the interactions induced by the third line of Eq. (8.29), which determines the direct decay into goldstinos as

$$\Gamma_{\varphi\to GG} = \frac{1}{4\pi}\left(\frac{N_m g_f \lambda^3 m_y}{48\pi^2 M^3\sqrt{2}} f_0\right)^2 m_\varphi \ , \tag{8.53}$$

where $m_\varphi = 2m_h$ is the mass of the inflaton. This decay is very much suppressed compared to (8.51) but can nevertheless lead to an overabundance of gravitinos. Moreover, another relevant channel is the decay into sgoldstino, since in our parameter space we have $m_\varphi > m_s$. This decay mode has the same partial width as the one above, hence it can be important since the sgoldstino will decay mainly into goldstinos.

Using Eq. (3.65), we estimate the abundance of gravitinos arising from these processes, assuming conservatively that the sgoldstino decays with 100% BR into two gravitinos, as

$$Y_{3/2}^{\rm decay} \simeq \frac{3T_{\rm reh}}{4m_\varphi}\left(2{\rm BR}_{\varphi\to GG} + 4{\rm BR}_{\varphi\to s\sigma}\right) \ , \tag{8.54}$$

where we included multiplicity factors. We impose that this abundance does not exceed the dark matter abundance.

Furthermore, decays of the inflaton into MSSM particles and eventually into the NLSP have sizeable branching ratios. However, if the NLSP is in thermal equilibrium, its abundance will be set by the thermal bath dynamics. In order for the NSLP to be in thermal equilibrium we demand that the reheating temperature is larger than the NLSP mass, *i.e.* the Bino mass

$$T_{\rm reh} \gtrsim m_{\tilde{B}} \ . \tag{8.55}$$

iv) The abundance of the Bino in the case in which the other sparticles are very heavy has been computed in [320–322] and it depends on the slepton masses

$m_{\tilde{l}}$, which we estimate in Eq. (8.38), and reads

$$\Omega_{\tilde{B}}h^2 = \frac{\left(m_{\tilde{B}}^2 + m_{\tilde{l}}^2\right)^4}{(460\text{GeV})^2\sqrt{g_*}m_{\tilde{B}}^2\left(m_{\tilde{B}}^4 + m_{\tilde{l}}^4\right)} \ . \tag{8.56}$$

The abundance of the Bino will set the gravitino abundance obtained via Bino decay as

$$\Omega_{3/2}^{\tilde{B}}h^2 = \frac{m_{3/2}}{m_{\tilde{B}}}\Omega_{\tilde{B}}h^2 \ . \tag{8.57}$$

In our analysis we will demand that $\Omega_{3/2}^{\tilde{B}}h^2 \lesssim \Omega_{DM}h^2$.

The gravitinos produced by any of the aforementioned processes could potentially carry a large energy (at most $m_\varphi/2$). A too high free-streaming length of the gravitino could thus destroy small scale structures and is experimentally constrained [161, 323]. Since in our model the inflaton mass is very low (compared to other inflation models), we find, using Eq. (3.67) that this does not constrain our parameter space.

8.5.3 BBN

Late decay of the NLSP into gravitinos can spoil BBN if the decay time is larger than ~ 0.1s [153, 284]. This poses an absolute lower bound in the $(m_{3/2}, m_\lambda)$ plane given by the requirement that

$$\tau_{\tilde{B}} \simeq \Gamma^{-1}_{\tilde{B}\to\gamma/Z+G} \simeq \frac{48\pi m_{3/2}^2 M_p^2}{m_{\tilde{B}}^5} \simeq 0.1 \text{ sec}\left(\frac{m_{3/2}}{10\,\text{MeV}}\right)^2\left(\frac{225\,\text{GeV}}{m_{\tilde{B}}}\right)^5 \tag{8.58}$$

should be less than 0.1 seconds.

8.5.4 Combination of the cosmological and LHC constraints

We can now combine the constraints listed above in one single plot which highlights the viable region in the parameter space of the model in the $(m_{3/2}, m_\lambda)$ plane. As mentioned, we restrict to the dashed line in Fig. 8.2 for definiteness (cfr. Eq. (8.47)).

In Fig. 8.4 we show our results for a representative choice of the numerical parameters, which however does not influence the qualitative features of the conclusions[10]. The black region is excluded because of tachyons in the spectrum, and corresponds in the plot of Fig. 8.2 to going beyond the tip of the allowed conical region along the dashed lines. The purple region is excluded because of the

[10] One can verify numerically that in the explored region the inflaton mass is always given predominantly by $2m_h$, corroborating the previous statements.

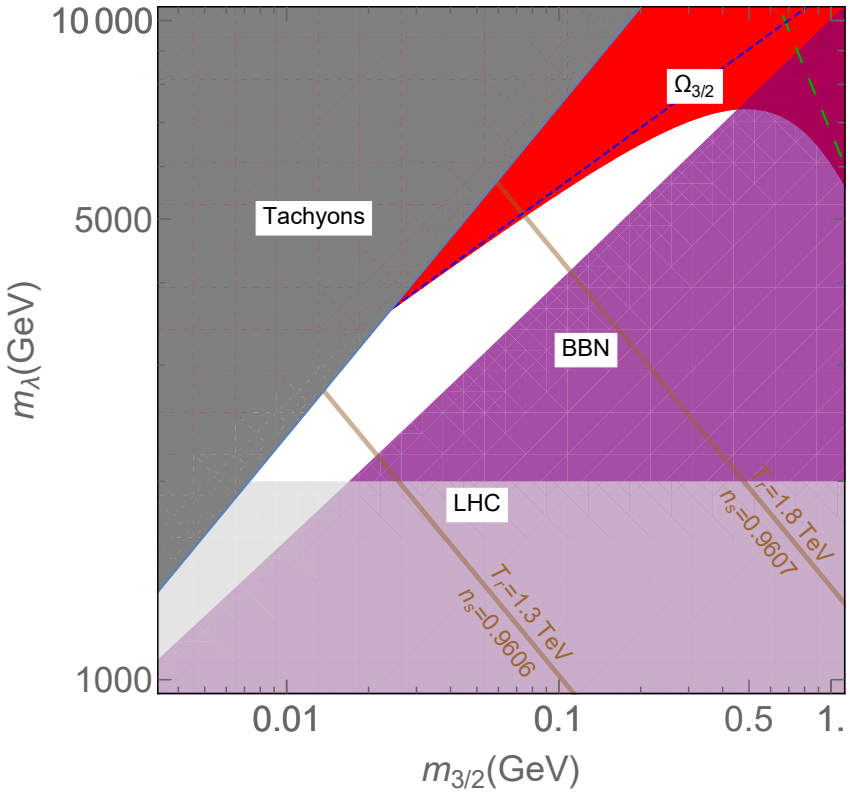

Figure 8.4: *Phenomenological constraints on the parameter space in the* $\{m_{3/2}, m_\lambda\}$ *plane by fixing* m_h *with the relation (8.47). The other parameters are fixed to the same numerical values as in Fig. 8.2. The white region is the one satisfying all the constraints explained in the text. The black region is excluded because of tachyon conditions. The red and purple regions are not viable because of phenomenological constraints on gravitino abundance or BBN, respectively. In the light blue region the gluino mass is lower than 2 TeV, the current LHC bound [225, 226]. The contours denote the spectral tilt* n_s *and the reheating temperature.*

BBN constraint on the Bino decay time in Eq. (8.58). The red region is excluded since the gravitino abundance exceeds the one expected for dark matter because of inflaton decay (above the dashed blue line), because of Bino decay (the region on the right of the dashed green line), or because of a combination of these two mechanisms. The freeze-in contribution to gravitino abundance, instead, turns out not to be relevant on the explored parameter space.

The allowed region passing all the constraints is the white spiky region. On the border between the white and the red regions the gravitino has the correct relic abundance to be the dark matter of the universe. In the rest of the white region dark matter can be constituted by some other particle in the hidden sector, e.g. as in [324].

We note that the gluino mass is bounded from above in the allowed region, and should be smaller than around 7 TeV for the choice of parameters in the plot. In the blue region the gluino mass is below 2 TeV, and hence excluded by the LHC bound[11]. Similarly, also the gravitino mass has both a lower and an upper bound, spanning between a few MeV and half a GeV. In particular, it is interesting to see that the upper bounds on m_λ and $m_{3/2}$ are generated by a combination of the constraints from gravitino overabundance and BBN.

In Fig. 8.4 we also show the contours of the inflation observable n_s, obtained after computing the reheating temperature and using the results of Fig. 8.3. Since a larger n_s (hence larger reheating temperature) is favoured by the Planck data, it is interesting that both Planck and the LHC prefer the same region of parameter space, with larger gluino and gravitino mass. This is clearly a specific feature of the model considered, but it is appealing that two experiments probing completely different physics can provide indications on the same BSM theory.

Our results should be considered as a preliminary analysis of an illustrative model which combines inflation and particle physics predictions, and it emphasizes the interplay between these two sets of physical requirements in shaping viable scenarios.

Further remarks. There are several aspects that we did not consider in our analysis and could be improved. First, in our model besides the inflaton there is another scalar field, the sgoldstino, that could potentially dominate the energy density of the universe at some stage of the cosmological evolution. This would be problematic given that the sgoldstino decays significantly into gravitinos, eventually leading to an overabundance of the latter. However we argue that this should not happen in the parameter space we explored for the following reasons, leaving a detailed analysis to future work. The scenario is very similar to curvaton models [137, 325, 326], with the sgoldstino playing the role of the curvaton. First, as one can check explicitly, the decay width of the sgoldstino is of similar order of magnitude of the decay width of the inflaton for our numerical values used for

[11] This estimate is very conservative since the actual bound depends on the decay mode of the gluino and on the rest of the SUSY spectrum, see section 7.1.4.

Fig. 8.4. Moreover, the field excursion of the sgoldstino VEV is much smaller than the inflaton one, being constrained to be smaller than $M + g_f \phi$ to avoid tachyons, and being concretely always smaller than M along the entire inflaton trajectory (which can be inferred from formula (C.1) and condition (C.4) in Appendix C). These two observations can be confronted with the results of Ref. [327] which consider the contribution to post-inflationary evolution of simple curvaton models for a range of parameters. Our sgoldstino scenario can be argued to map to one where the curvaton never dominates the energy of the universe, though this question deserves clearly further dedicated study.

As already mentioned, we did not include possible effects from the extended SUSY Higgs sector and from the Higgsino, and we further assumed the Bino to be the NLSP. Note that if the neutralino NLSP would be instead mostly Higgsino-like the bounds from BBN (purple region) and from NLSP decay (the part of the red region on the right of the dashed green line) would be considerably softened since the abundance of the Higgsino-like neutralino is suppressed compared to the one of the Bino.

Concerning the gravitino abundance, we did not consider possible non-thermal production arising during preheating [285]. The results of Ref. [298] seem to indicate that our model, where $h(\Phi)$ is a quadratic function, should not be hindered by such effects, but a dedicated analysis should be performed to reach a definite conclusion. Generically, there can be other effects during the cosmological history of the universe, in particular in the (p)reheating epoch, that would eventually lead to additional gravitino production mechanisms which would impact significantly the outcome of our analysis. We leave for future studies a more thorough study of the gravitino problem. However, we argue that our results already hint at the possibility that the gravitino problem can be more easily circumvented in this class of models, due to the low reheating temperature, which is an intrinsic property of our model, in particular of the coupling of the inflaton to the supersymmetry breaking mechanism.

8.6 Discussion

In this paper we have addressed the issue of the compatibility of nilpotent inflation with low-scale SUSY breaking. The nilpotent approach simplifies many aspects of the supergravity embedding of inflation since the sgoldstino is taken to be integrated out and its dynamics can be neglected.

We consider a class of models in which the sgoldstino is present but has a mass, given by a higher dimensional effective operator, and we have investigated under which conditions this massive sgoldstino is always effectively decoupled from the physics of inflation. Specializing to a field theoretic weakly coupled UV completion of the SUSY breaking sector, which we take to have a non-trivial coupling to the inflaton, we find that the scale of SUSY breaking cannot be as low as one could

expect, for instance, in gauge mediated models. This can be intuitively understood as follows: low SUSY breaking scales lead generically to a light sgoldstino, and it becomes more difficult to decouple the latter from inflation physics. The constraints are in practice more complicated, but they can be nicely summarized as in Fig. 8.2.

An important remark concerns the implications of our results on the regime of validity of generic nilpotent inflation models. These can encompass various different choices, concerning on one side the inflationary supergravity model, and on the other the type of SUSY breaking dynamics and mediation. Most notably the coupling between two physical set-ups will be important, as in our model. Indeed, in Ref. [278] a variety of models were considered, both for inflation and for SUSY breaking, but no inflaton-dependence was contemplated in the operator giving the sgoldstino its mass. This resulted in very stringent bounds on the scale of SUSY breaking. Our findings relax these bounds, but nevertheless we cannot explore all of the potential parameter space of the SUSY breaking and mediation scales while staying at weak coupling.

It may well be that generalizing even more the types of models we can push further down the bounds on the gravitino mass and the SUSY breaking scale. Note however that our choice of inflationary sector, the α-attractor, is already very flexible in itself. As for the SUSY breaking sector, its effective parametrization as in section 8.3 allowed us to derive a crude approximation of the bounds, that we found using the increased precision of the weakly coupled UV complete model for definiteness. One way to try to overcome these bounds is to take strongly coupled SUSY breaking and messenger sectors. Here we could hope to explore the other valid regions of parameter space that open up in the EFT.

The specification of the UV model, and in particular of the couplings between the inflaton and fields involved in SUSY breaking, has a positive side. It has allowed us to discuss in some detail the physics of inflation, including reheating and dark matter abundance bounds, and confront it with collider bounds on superpartner masses. The complementarity of these bounds is manifest in Fig. 8.4. The result is actually that our model is quite predictive, both for inflation observables (low spectral tilt n_s and reheating temperature) and for collider ones (upper and lower bounds on the gluino and gravitino masses). A different UV completion would certainly change the details, and the outcome of the analysis. We believe however that we have shown how to proceed in such a task.

To conclude, we would like to convey the message that nilpotent inflation can be compatible with low scales of SUSY breaking only with an increasing number of conditions on its UV completion. We do not seem to reasonably expect it to allow for arbitrarily low scales, *i.e.* as for a GMSB scenario with eV-scale gravitino. On the other hand, once a UV completion is specified, such models lead to a complete and complementary characterization of cosmological and collider observables, thus confirming the expectation that inflation and SUSY breaking are intimately tied together.

CHAPTER 9

Conclusions

In this thesis two approaches were studied to elucidate the era of inflation. In chapters 4 – 6 we considered several models for the inflaton potential, and showed that observationally a potential with an asymptotic plateau is preferred by the data. The Starobinsky inflation model, the strong coupling attractor model and the α-attractor model were reviewed and extended. Then, in chapters 7 and 8, we studied the embedding of a specific model, the α-attractor, in a supergravity framework where supersymmetry was realised non-linearly. The non-linear realisation of supersymmetry can be represented with nilpotent superfields, but, as explained in section 7.5, there are non-trivial consistency criteria that a high-energy completion of nilpotent inflation has to satisfy. We analysed such a high energy completion of nilpotent inflation and showed that it is internally consistent. Furthermore, we considered the various predictions of the model, regarding inflation, dark matter and the particle spectrum, and obtained the parameter space where these predictions were consistent with the observations.

In this chapter we will present a summary of the main results in this thesis and point to some directions of future research. We finish with some general remarks concerning the future of inflationary research.

Generic predictions for inflation. In chapters 4 and 5, the generic inflationary predictions for different parametrizations of the Hubble function were studied. The general method used in the community was the horizon flow code, which was reviewed in section 4.3. An important feature of this code is that it parametrizes the Hubble function as a polynomial, which leads to a polynomial potential. This prescription was subsequently used to find the generic features of inflation models

and to obtain the inflaton potential that has the best fit with the observational data.

In section 4.4 we improved the inflationary flow code, such that instead of numerically solving the flow equations (4.3) it used a root-finder for $\epsilon_{\rm H}$. This new procedure, originally proposed by Ramirez and Liddle in Refs. [171, 172], allowed us to systematically study the prior dependence of the algorithm. Using either of the two codes, we concluded that using a polynomial expansion of the Hubble function renders $n_{\rm s}$ too small and r too large. Though this result was already obtained in the literature, only Ref. [172] explicitly investigated the dependence on the prior choice of the algorithm. However, the prior choices investigated by these authors still assumed polynomial inflation models.

A polynomial expansion of the potential implies an 'oversampling' of convex (exponential like) or concave (hilltop like) potentials, which indeed generically have a too large r or a too small $n_{\rm s}$. Models that are known to be more compatible with the CMB data are plateau-like models, which are typically not well captured by the polynomial approximation used in the horizon flow code. Therefore, in this thesis we considered two alternative parametrizations, i) where the Hubble function is expanded as a ratio of polynomials (a Padé approximant) and ii) where the inflaton action represents a strong coupling attractor. These alternative parametrizations showed that the numerical procedure is indeed strongly model dependent.

In addition to the numerical approach introduced above, chapter 5 analytically studied the difference between the predictions of inflation models by solving the flow equations for a quadratic Hubble function and a Hubble function parametrized as a ratio of two linear polynomials ([1,1] Padé approximant). For this analytical result we used that the Hubble functions were symmetric under shifts of $\phi \to \phi+\delta\phi$. This symmetry allowed us to analytically solve all the flow equations except one and in the studied cases the remaining flow equation could be integrated. Using this approach to integrate the flow equations, we showed that the Hubble function parametrized as a [1,1] Padé approximant was consistent with the experimental data from the Planck satellite, while the quadratic Hubble function was not. The reason is that the Padé approximant naturally incorporates plateau-like models, while polynomials do not.

Indeed, the study in chapter 5 of the generic predictions of inflation concluded that a Hubble function expanded as a ratio of polynomials better resembles the inflationary data than a Hubble function expanded with a single polynomial. This confirmed the hypothesis that models with a plateau at a large inflaton field value agree much better with the observables than models with an exponential like or hilltop like potential. This also implies that generic predictions for inflation that use a random scan over inflation models cannot be regarded independently of the space of models under consideration. However, this method can be used to investigate which potential shapes are compatible with observations and which ones are not. This technique therefore explores the space of viable potential shapes, instead of the viable inflationary parameters.

In chapter 6 inflation models were investigated with a non-minimal coupling to gravity. Such models were originally considered with only certain specific potentials and frame functions, where it was realised that for sufficiently large non-minimal coupling ξ the model resembles the Starobinsky model, a plateau inflation model that fits the data extremely well. However, it was not investigated if the attractor also worked for models in which the potential and frame function, the function relating the non-minimal coupling of the inflaton to gravity, were completely arbitrary.

We showed, both analytically and numerically, that for arbitrary potentials and frame functions, if the non-minimal coupling ξ is sufficiently large, the inflation model generically agrees with the observational data. We observed in both the analytical and the numerical procedures that the attractor behaviour appears if $\xi \gtrsim \mathcal{O}\left(N_*^2\right)$ (where N_* is the number of e-folds at horizon exit). Interestingly, compatibility with the COBE normalization $A_s = (2.14 \pm 0.05) \cdot 10^{-9}$ requires a similar value for ξ. We showed that $\xi \approx 10^4$ is sufficient to have generically the inflation model in excellent agreement with the data, and simultaneously being in agreement with the COBE normalisation.

The analyses of chapters 4 – 6 show that inflation is best parametrized with an asymptotically flat potential. Interestingly, this seems to imply that the inflaton potential for very large inflaton field values has to be flat. This flatness of the potential could be naturally obtained if conformal symmetry is restored at these large field values. This asymptotic symmetry also has the advantage that quantum corrections are suppressed, since in the symmetric limit these corrections are absent [220]. Therefore, the smallness of the slow roll parameters can be explained by originating from a breaking of conformal symmetry.

This explains the importance of attractor theories for inflation, since the known attractor models implement this conformal symmetry at large field values. Even if the plateau originating from the attractor model is broken, as in the models studied in chapter 6, the nice plateau-like features can appear if the observable part of inflation only considers the plateau part of the model. This explains why a sufficiently large ξ was required for the strong coupling attractor models to converge, even if the inflaton potential was not asymptotically flat.

Considering the effects of quantum corrections on potentials that are expanded as a Padé approximant, is difficult, since perturbation theory assumes the potential to be polynomial. Within quantum field theory, the perturbation theory will always break the generated plateau, and the generic results presented in chapter 5 will change strongly. However, perturbation theory is probably incorrect for two reasons. First, there is no reason that quantum corrections only generates corrections in the numerator, while leaving the coefficients in the denominator untouched. If the corrections also change the denominator, the plateau at large field values can stay intact and the generic predictions obtained in chapter 5 hold. Secondly, it can be understood from the analysis of chapter 6 that these corrections will be irrelevant if they break the flatness of the plateau only at large field values,

which are not visible in the CMB. A more complete analysis of the quantum corrections in Padé inflation models has not performed and would be an important extension to our analysis.

Another interesting path for future research is to study other parametrizations for inflation models which generically agree with the Planck data. An example of such a theory was introduced in section 4.5, where the Hubble function was parametrized as a function in $1/N$ (where N is the number of e-folds). The reason for considering this model is that it is fully characterized by geometric quantities, without the notion of an inflaton field. It might be of interest to study the generic predictions of theories polynomially expanded in $1/N$, but also to consider again Padé expansions. This analysis can be extended by finding the inflation potentials that correspond to these $1/N$ predictions and search for possible underlying symmetries.

Generally, it is interesting to study different parametrizations for inflation models to understand what type of inflation is allowed by the current data. Examples of such parametrizations might be inflation with an arbitrary kinetic function (with and without an additional non-minimal coupling to gravity) or inflation with a potential expanded in goniometric functions (i.e. Fourier expanded). The former is a generalization of attractors of section 6.2 and the $1/N$ parametrization of the Hubble function, as explained in section 4.5, while the latter is a generalization of natural inflation. A Fourier expanded potential can also be obtained if the high-energy completion of inflation is shift-symmetric under a discrete shift symmetry (while the theories in chapter 8 were shift-symmetric under arbitrary shift symmetries).

Another possibility is to study multi-field inflation models using this flow analysis. Though it is possible to expand the flow code to an inflation model with a few additional inflaton fields [328], this is not trivial. Moreover, the number of arbitrary coefficients that has to be fixed increases quickly. But, studying such models could uncover interesting multi-field features. For inflation with a very large set of fields this method will probably be very slow due the large number of relevant parameters and for such a scenario random matrix theory is more applicable Refs. [142, 143, 329]. However, these studies only considered polynomially expanded potentials, and though the results are less constrained than those of the Hubble flow code, considering these inflation models with attractor-like inflation models might be an interesting scenario.

UV completing nilpotent inflation. Another approach to inflationary model building is to choose a particular inflation model and check if it can be consistently embedded in a theory that represents the full standard model. This approach is interesting since it not only gives insights into which inflation theories are possible and which ones not, but also gives useful hints for how the standard model of particle physics can be extended to higher energies. This last constraint is relevant since inflation is taking place at extremely large energy scales, far beyond the

energy scales of current colliders. Thus, inflation provides a test ground for high energy physics.

An example of such a high-energy extension of the standard model of particle physics is supersymmetry, which for large energy scales can be extended to supergravity. However, as explained in section 7.5, supergravity realisations of single field inflation models often suffer from several problems. Among these, the most severe one is typically the unboundedness of the potential. A popular solution to this problem is to introduce the stabilizer superfield (S) in addition to the inflaton superfield, which stabilizes the inflaton trajectory. However, the scalar components of the stabilizer superfield can change the inflationary predictions. To insist on single field inflation models it is interesting to project out the scalar component of the stabilizer superfield. This can happen if supersymmetry is spontaneously broken and appearing in the low-energy limit non-linearly through a nilpotent superfield, which satisfies the condition $S^2 = 0$. Insisting that the stabilizer superfield is nilpotent projects out the scalar part of this field, as required for single field inflation.

However, nilpotent inflation requires two opposite regimes for the cut-off scale of the high-energy theory, so a-priori it is not clear if nilpotent inflation is possible. Firstly, the cut-off scale should be above the energy scale of inflation, otherwise inflation cannot be described independently of the UV-effects. However, for the nilpotent framework to work the mass of the sgoldstino (the superpartner of the goldstino) should be large, which is inversely proportional to this cut-off scale and proportional to the scale of supersymmetry breaking. In section 7.5 was shown that for the considered high-energy model the bounds were sufficiently strong that the cut-off scale of the effective theory had to be close to the Planck scale. In addition, the supersymmetry breaking scale, and therefore the gravitino mass ($m_{3/2}$), had to be very large. Therefore, a relevant question for particle physics was whether nilpotent inflation could be realised with a low supersymmetry breaking scale.

In chapter 8 we studied a novel nilpotent inflation model in which this problem is, at least partially, solved. The method we chose was to add a coupling between the inflaton and the messenger fields, which transmits the supersymmetry breaking to the standard model sector of the theory. Due to this coupling, the effective cut-off scale was parametrically larger during inflation than in the (non-inflating) vacuum. The gravitino mass in our model had a lower bound $m_{3/2} \gtrsim \mathcal{O}(\text{ MeV})$ and with such a small gravitino mass it is possible to propagate supersymmetry breaking from a hidden sector to the standard model via gauge mediation.

We therefore introduced an explicit high-energy model for which during inflation the goldstino superfield was nilpotent and inflation was realised using the α-attractor formalism, while in the vacuum supersymmetry breaking was mediated to the standard model of particle physics using gauge mediation. Hence, the superpartner masses could be computed and tested with the results from the LHC experiments. In addition, since also the inflaton coupling to the standard model of particle physics was known, the reheating temperature was computed and in-

formation from the reheating phase compared with the data. Precise predictions for n_s and r could be computed, which were in agreement with the Planck data. In addition, the gravitino is in our model a possible dark matter candidate and its abundance strongly constrains the available parameter space. Putting everything together, we were able to test the inflation model with a combination of inflationary, nucleosynthesis, dark matter and LHC observations. These combined constraints rendered the model very predictive.

Several improvements can be made on the above investigation. For instance, the high energy completion of the above model was rather specific. It is therefore interesting to consider the constraints of the supersymmetry breaking scale for other models. In the above inflation model the α-attractor was realised using a no-scale Kähler function for the inflaton, while the other fields in the theory were considered canonical. Evidently, it is interesting to study the importance of this assumption, *i.e.* if the validity of the effective theory changes if also the goldstino and messenger multiplets are considered in a no-scale framework. This will not change the effective theory, since the messenger fields are integrated out and the nilpotent condition on the goldstino implies no difference if written canonical or no-scale. However, there might be important new constraints for the validity of this effective theory.

Another extension of this work is to investigate the corrections to superfields which are constrained in combination with the goldstino. An interesting constraint for inflation is $\Phi S = \Phi^\dagger S$, which removes the imaginary and the fermionic partner of the inflaton superfield Φ. This is beneficial, since the imaginary partner of the inflaton can generate multi-field behaviour if it is light and the fermionic partner of the inflaton can create a large gravitino abundance during preheating. Another example is to impose the nilpotent-3 condition $S^3 = 0$ instead of $S^2 = 0$. The nilpotent-3 condition requires two superfields, which will both have their scalar component integrated out. Since both fields can act as a stabilizer without introducing new inflaton candidates, it is interesting to study if new effects emerge in such a model.

The reheating study, performed in section 8.5, did not take into account all possible phenomena that could occur during this phase. For instance, no non-perturbative effects were treated and neither the nonzero velocity of the inflaton field or possible thermal effects were taken into account. We also noted in our analysis that the coupling between the sgoldstino field and the inflaton field might induce additional sgoldstino oscillations. We interpreted this effect as the possibility that the oscillations of the inflaton acted as a driving force for the sgoldstino oscillations. If this driving force oscillates with the resonance frequency of the sgoldstino field, this field might be excited extremely efficiently. This would introduce large displacement of the sgoldstino field value, even if during inflation it is stabilized to its vacuum expectation value. It would be interesting to further investigate this potential issue.

Final general remarks. Cosmology is currently an active field of research and many observatories aim to analyse possible signals that describe the universe. Several experiments plan to measure primordial B-mode polarization in the CMB. If this does not result in a measurement of r, the bounds might be sufficiently strong to rule out important inflation models. Extremely interesting is the possibility to constrain $r \gtrsim 10^{-3}$ in future B-mode experiments [330–332], which is sufficient to rule out Starobinsky and Higgs inflation (with $r \approx 4 \cdot 10^{-3}$). Since this also rules out most of the models considered in this thesis, it would be extremely interesting to find the right parametrization for the inflation potential.

Another very interesting possible future measurement is the bispectrum, f_{NL}, since a measurement of this quantity signals effects from deviations of the single field setup. Such a measurement would indicate that the inflationary epoch was driven by multiple fields, or that the inflation had higher-derivative interactions. Moreover, with the bispectrum it is possible to distinguish between these different possibilities. Though f_{NL} can be inferred from the CMB, it is more promising to consider large scale structure surveys. The main problem of this search is that observing directly the matter density of the universe is very difficult, since only 20% interacts with light. Most tracers of the matter distribution therefore use galaxies, galaxy clusters or spectral lines (*i.e.* 21 cm) [333], which are all biased tracers of the total matter density profile. Hence, obtaining a good statistic for quantities such as f_{NL} is non-trivial. The current predictions are that within the near future $f_{\text{NL}} > 1$ will be observable [333–335], which will have a huge impact on multi-field inflation.

Another important aim for future observatories is to strengthen the measurement of the local Hubble constant, to investigate if the tension with the Hubble constant measured by the CMB experiments is fundamental or due to some unknown measurement effect. If this discrepancy becomes statistically significant, it might be that the resolution will point towards a certain model of dark energy. This would finally shed some light on this very dark corner of cosmology.

Given the current knowledge, the right model of inflation cannot be easily identified. An important future direction of study is therefore to further investigate the predictions that different inflation models make while the cosmological data improves. This is of particular interest since inflation takes place at extremely high energies and therefore provides valuable hints to how the standard model of particle physics has to be extended to high energy scales. A compelling possibility is that inflation provides a portal to string theory, which is difficult to access by other probes. Therefore, a promising direction in current and future inflationary research is the embedding of inflation in string theory and supergravity. In addition, it is also important to consider possible implementations of inflation in particle physics beyond the standard model, as the Higgs and MSSM inflation scenarios.

Finally, in chapter 8 was shown that another important era for cosmological investigations is the reheating era. Though often neglected, the inflaton cannot be a stand-alone particle without any interactions with the standard model of

particle physics. Instead, a proper understanding of the current universe requires an understanding of the couplings between the inflaton and the standard model particles. Given the sensitivity to the inflationary parameters of the proposed experiments, reheating soon will become a relevant era for consistent inflationary results [150]. Therefore, a classification of what type of dynamics translates to which reheating physics will be extremely useful.

APPENDIX A

The inverse Taylor expansion

In order to further illustrate the analytical method to solve the flow equations depicted in section 5.1, in this appendix, we apply it to the case where the inverse Hubble function is Taylor expanded at second order,

$$\frac{H}{H_0} = \frac{1}{1 + a\phi + b\phi^2}\,. \tag{A.1}$$

The two first slow-roll parameters can be read off from Eqs. (4.5), and one has

$$\epsilon_1 = \frac{2\left(a + 2b\phi\right)^2}{\left(1 + a\phi + b\phi^2\right)^2}\,, \quad \epsilon_2 = -4\frac{2b^2\phi^2 + 2ab\phi + a^2 - 2b}{\left(1 + a\phi + b\phi^2\right)^2}\,. \tag{A.2}$$

Then, under shift transformations $\phi \to \phi + \delta\phi$, the functional form (A.1) is unchanged provided

$$a \to \frac{a + 2b\delta\phi}{1 + a\delta\phi + b\delta\phi^2}\,, \quad b \to \frac{b}{1 + a\delta\phi + b\delta\phi^2}\,, \tag{A.3}$$

where H_0 is also rescaled according to $H_0 \to H_0/(1 + a\delta\phi + b\delta\phi^2)$. These gauge transformations are, for obvious reasons, the same as for the second order Taylor case studied in section 5.2.1, which implies that

$$\gamma = \frac{32b^2}{4b - a^2} = \frac{\left(2\epsilon_1 + \epsilon_2\right)^2}{\epsilon_1 + \epsilon_2} \tag{A.4}$$

is a constant of motion and can be used to label the different trajectories.

Let us now derive the dynamical system associated to this parametrization of the Hubble function. Making use of the same procedure as in section 5.2, we find that Eq. (A.1) implies that $H''' = 6HH'H''/H^2$, and Eqs. (4.5) then gives rise to

$$\epsilon_3 = \epsilon_1 \left(3 + 2\frac{\epsilon_1}{\epsilon_2}\right) . \tag{A.5}$$

This truncates the dynamical system to a closed set of differential equations for (ϵ_1, ϵ_2), given by

$$\frac{\mathrm{d}\epsilon_1}{\mathrm{d}N} = -\epsilon_1\epsilon_2 , \qquad \frac{\mathrm{d}\epsilon_2}{\mathrm{d}N} = \epsilon_1 \left(3\epsilon_2 + 2\epsilon_1\right) . \tag{A.6}$$

In particular, one can check that the combination γ defined in Eq. (A.4) is left invariant. The integrated flow lines of the above system are displayed in Fig. A.1.

Let us now see how this system can be integrated analytically. By inverting Eq. (A.4), one can express ϵ_2 as a function of ϵ_1,

$$\epsilon_2 = -2\epsilon_1 + \frac{\gamma}{2} + \frac{\xi}{2}\sqrt{\gamma^2 - 4\gamma\epsilon_1} , \tag{A.7}$$

where[1] $\xi = \pm 1 = \mathrm{sign}\left[\frac{\epsilon_2(2\epsilon_1+\epsilon_2)}{\epsilon_1+\epsilon_2}\right]$. As before, by inserting Eq. (A.7) into Eqs. (A.6) we obtain a first order differential equation for $\epsilon_1(N)$ that can be solved, and one obtains $\Delta N_* = N(\epsilon_{1,\mathrm{end}}) - N(\epsilon_{1*})$, where $\epsilon_{1,\mathrm{end}} = 1$ and

$$N\left(\epsilon_1\right) = \frac{2}{\xi\sqrt{\gamma^2 - 4\gamma\epsilon_1} - \gamma} + \frac{\xi}{2\gamma}\log\left|\frac{\sqrt{\gamma^2 - 4\gamma\epsilon_1} + \gamma}{\sqrt{\gamma^2 - 4\gamma\epsilon_1} - \gamma}\right| . \tag{A.8}$$

As in the case of the Taylor parametrization, Eq. (A.8) can be inverted,

$$\epsilon_1(N) = \frac{-4W_\chi\left(-e^{-\gamma\Delta N - 1}\right)}{\left[1 + W_\chi\left(-e^{-\gamma\Delta N - 1}\right)\right]^2} , \quad \chi = \begin{cases} 0 \text{ if } \gamma(2\epsilon_1 + \epsilon_2) > 0 \\ -1 \text{ if } \gamma(2\epsilon_1 + \epsilon_2) < 0 \end{cases} , \tag{A.9}$$

where χ determines the branch of the Lambert function W_χ. It is easy to show that χ does not change along a given trajectory.

Let us now discuss the structure of the phase space diagram plotted in Fig. A.1. According to the type of Hubble function one is dealing with, two possibilities must be distinguished:

[1] This sign does not change for trajectories for which ϵ_1 always decreases with time (regions I in the classification introduced below). However, for trajectories for which ϵ_1 first increases, reaches a maximum and then decreases, it is positive before reaching the maximum and negative afterwards (region II).

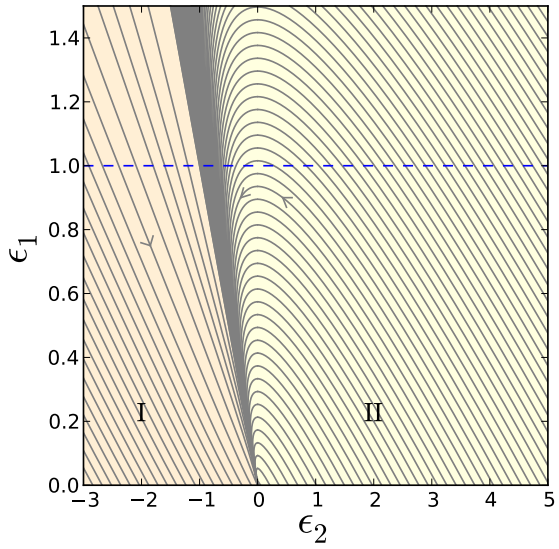

Figure A.1: *Inverse second order Taylor expansion for the Hubble function: flow lines of the system (A.6) in the plane* (ϵ_1, ϵ_2)*. The arrows indicate in which direction inflation proceeds. The blue dashed line corresponds to* $\epsilon_1 = 1$ *where inflation stops. The two regions* I *and* II *refer to the discussion in the main text.*

- In regime I, $\epsilon_2 < -\epsilon_1$, ϵ_1 decreases and ϵ_2 increases as inflation proceeds, reaching one of the (attractive) fixed point $(\epsilon_1 = 0, \epsilon_2 < 0)$ in the asymptotic future. The corresponding Hubble function has a convex shape with a positive minimum. In this case, $\gamma < 0$.

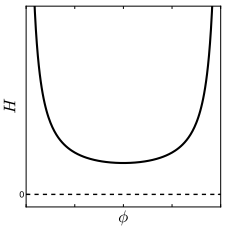

- In regime II, $\epsilon_2 > -\epsilon_1$, ϵ_2 decreases as inflation proceeds while ϵ_1 first increases, crosses a maximum and then decreases, reaching the (attractive) fixed point $(\epsilon_1 = 0, \epsilon_2 = 0)$ in the asymptotic future. The corresponding Hubble function is concave and vanishes at infinity. In this case, $\gamma > 0$.

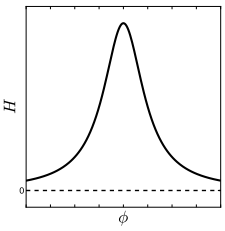

One should note that thanks to the conservation of the sign of γ defined in Eq. (A.4), a given inflationary trajectory never changes region. Amongst the second category, one can distinguish two cases. If the maximum value of ϵ_1 is smaller than one, inflation never ends and reaches the fixed point $(\epsilon_1 = 0, \epsilon_2 = 0)$.

If, on the other hand, the maximum value of ϵ_1 is larger than one, and if one starts inflating with $\epsilon_2 > 0$, then inflation ends naturally when $\epsilon_1 = 1$. This happens when $\gamma > 4$. In this case, one can check that the function $N(\epsilon_1)$ defined in Eq. (A.8) goes to infinity when ϵ_1 goes to 0 which means that a sufficient number of e-folds can always be realized.

However, this requires ϵ_{1*} to be sufficiently small. If one parametrizes a given trajectory within region II by $\epsilon_{2,\mathrm{end}} = -2 + (\gamma + \sqrt{\gamma^2 - 4\gamma})/2$, the value of the second flow parameter at the end of inflation, in the $\epsilon_{1*} \ll 1$ limit one has

$$\epsilon_{1*} \simeq \left(\frac{2 + \epsilon_{2\mathrm{end}}}{1 + \epsilon_{2\mathrm{end}}}\right)^2 \exp\left[\frac{1 - (2 + \epsilon_{2\mathrm{end}})^2 \, \Delta N_*}{1 + \epsilon_{2\mathrm{end}}}\right]. \tag{A.10}$$

Since $\epsilon_{2*} > \epsilon_{2\mathrm{end}}$, $\epsilon_{2*} < 1$ implies that $\epsilon_{2\mathrm{end}} < 1$ hence $\epsilon_{1*} < 10^{-104}$ if $\Delta N_* = 60$. So essentially, $r \simeq 0$ in these models. Making use of Eq. (A.7), one then has

$$\epsilon_{2*} \simeq \frac{(2 + \epsilon_{2\mathrm{end}})^2}{1 + \epsilon_{2\mathrm{end}}}. \tag{A.11}$$

Because $\epsilon_{2\mathrm{end}} > 0$ in those branches where inflation ends naturally, this means that $\epsilon_{2*} > 4$, which is of course completely excluded by CMB observations. As a conclusion, the only trajectories compatible with observations are those that reach the fixed points ($\epsilon_1 = 0, \epsilon_2 < 0$) such that ϵ_2 gives the correct value of n_{s}. However, these are rather fine-tuned situations that moreover require to invoke an extra mechanism to end inflation.

APPENDIX B

Random non-minimal coupling: Higher order terms

The analysis of chapter 6 demonstrated that given $a_1, b_2, b_3 \sim \mathcal{O}(1)$ and $\xi > \mathcal{O}(N_e^2)$, inflation occurs with a leading order Starobinsky (or Hilltop) signature and a value of $\xi \gtrsim \mathcal{O}(10^4)$ can serve to push *all* higher order corrections sufficiently far away in field space to arrive at an observationally viable model. We hence find an inflationary regime independent of the truncation of either series in (6.20).

However, due to the randomness of the coefficients a_n, b_m, it could in principle happen that terms $b_m\phi^m, m > 2$ in the potential evade the ξ-induced flattening and influence the inflationary dynamics. Changing our set-up to the power law prior $a_n, b_m \in [-1, 1]$, we now examine whether or not the set-up remains truncation independent when the coefficients are drawn such that terms $b_m\phi^m$ for $m > 2$ are important, i.e. greater than unity, during inflation; in other words, the Jordan frame field ϕ is trans-Planckian to maintain the required amount of e-folds.

In what follows, we study the case $a_n, b_m \in [-1, 1]$ and $\phi \gtrsim \mathcal{O}(1)$ but the argument readily extends to the scenario $a_n, b_m \in [-1/n!, 1/n!]$ and $\phi \gtrsim \mathcal{O}(M)$. Consider

$$\Omega(\phi) = 1 + \xi \sum_{n=1}^{M} a_n \phi^n, \quad V_J(\phi) = \lambda \sum_{m=2}^{2M+\Delta} b_m \phi^m, \tag{B.1}$$

where Δ is a positive integer and hence parametrizes how much the highest order term of the Jordan frame potential departs from a square relation with the highest order term in the non-minimal coupling function Ω. When $\phi > 1$, we obtain the

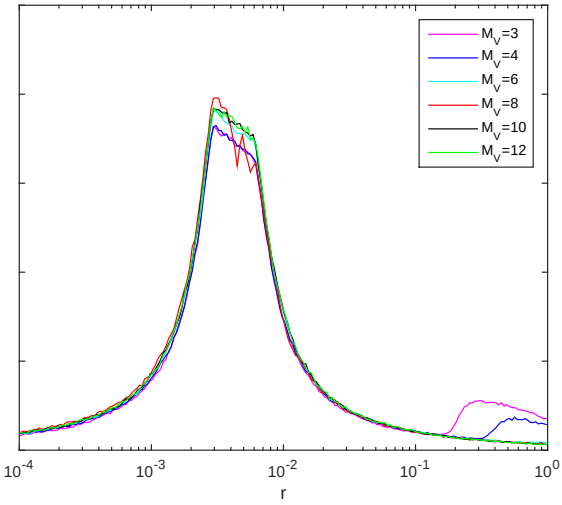

Figure B.1: *Density profile for r with $\xi = 10^4$, $M_\Omega = 1$ and with coefficients b_m that are not factorially suppressed.*

effective potential

$$V_E(\phi) \sim \frac{\lambda}{a_M^2 \xi^2} \left[b_{2M} + \sum_{k=1}^{\Delta} b_{2M+k} \left(\frac{\Omega(\phi)}{a_M \xi} \right)^{\frac{k}{M}} \right]. \tag{B.2}$$

If the potential departs from the square relation between potential and frame function at highest order, the Einstein frame potential in principle feels this effect. While also this effect can be made negligible by tuning Δ or simply pushing it away in field space by enlarging ξ, it could as such play an important role when the coefficients b_m are drawn such that terms of the order $> 2M$ become dominant in the inflationary region of the Einstein frame potential.

As coefficients $b_{m>2M}$ may have either sign, the effect of these higher order terms on the inflationary dynamics can be to curve the potential upwards and hence increase the number of chaotic signatures in the n_s, r plot or to induce a hilltop and thus to enlarge the number of signatures with redder n_s and very small r. We conjecture that a large Δ will increase the number of hilltop signatures while chaotic signatures may only be visible when $\Delta \sim \mathcal{O}(1)$ and M is not too large. This is because a large Δ will allow for an interplay of coefficients $b_{m>2M}$ with possibly different signs such that hilltops occur whereas if there exists just one or two higher order terms, a positive highest order coefficient could be sufficient to steepen the potential before lower order terms will have induced a hilltop. The

phenomenology of this analysis is depicted in Fig. B.1. This shows how chaotic signatures are only visible for $\Delta \sim \mathcal{O}(1)$.

We thus find that once sufficiently large $\xi \gtrsim \mathcal{O}(N_*^2)$ drives the non-canonical field displacement sub-Planckian, the form of the higher order coefficients is mostly irrelevant for the inflationary predictions.

APPENDIX C

Analysis of sgoldstino VEV and EFT validity

In this appendix we give more details on the analysis of the constraint on the sgoldstino VEV performed in chapter 8. As explained in section 8.3, the inflationary trajectory spans the space of $\mathrm{Im}(\Phi)$ with $\mathrm{Re}(\Phi) = \mathrm{Im}(S) = 0$ while the real part of the sgoldstino is given by Eq. (8.12). The condition $\langle S \rangle \ll \Lambda_{\mathrm{eff}}(\Phi)$ is quite involved to solve analytically given the different terms entering into the expression for the sgoldstino VEV (8.12). We will discuss various limits for this expression to extract the relevant inequalities such that the validity of the effective theory is guaranteed along the entire inflationary trajectory. We first analyse the two extrema of the inflaton trajectory. For small φ the sgoldstino VEV is Planck suppressed and scales as $\langle s \rangle \sim \frac{\Lambda_0^2}{M_{\mathrm{p}}}$, hence the EFT condition is trivially satisfied[1]. For very large inflaton, when $\varphi \sim M_{\mathrm{p}}$, the sgoldstino VEV scales as $\langle s \rangle \sim \frac{m_h}{m_f} g^2 M_{\mathrm{p}}$. Here we have assumed that $m_h \ll m_f$, since we have indeed the freedom to decouple the scale of the inflaton mass from the scale of inflation itself. We will see instantly that this hierarchy is actually a requirement. The condition $\langle s \rangle \ll g\varphi \sim g M_{\mathrm{p}}$ hence gives $g \ll \frac{m_f}{m_h}$ which is trivially satisfied. The two extrema of the φ excursion are hence within the EFT validity range.

We now have to investigate the rest of the φ trajectory. A good estimate to understand the possible regimes of validity and the constraints on the parameters can be obtained by expanding both numerator and denominator in Eq. (8.12) in

[1] Here we neglect corrections due to a non-zero m_y in the UV theory, which are in any case relevant only at the end of the trajectory.

some approximation. The largest scale of the model is m_f that will set the energy scale of inflation, as illustrated in section 8.3. We then expand the sgoldstino VEV at leading order in $\frac{\rho}{M_{\rm P}}$, where ρ is any dimensionfull parameter except m_f, and at second order in $\frac{m_f}{M_{\rm P}}$[2], getting

$$\langle s\rangle = \frac{\frac{2\sqrt{6}f_0^2}{3M_{\rm P}} - \frac{2\sqrt{2}m_f m_h\varphi^2}{3\alpha M_{\rm P}}}{\frac{2m_f^2\varphi^2}{3\alpha M_{\rm P}^2} + \frac{(2f_0+\frac{m_f\varphi^2}{M_{\rm P}})^2}{\Lambda_0^2+\frac{g^2}{2}\varphi^2}} \ . \tag{C.1}$$

We should compare this VEV with the scale giving the upper bound on the validity of the effective theory, *i.e.* $\sqrt{\Lambda_0^2+\frac{g^2}{2}\varphi^2}$. From now on we omit any numerical $O(1)$ coefficient (including α) for simplicity of the discussion; they can be reinserted easily by inspecting the expression (C.1).

There are several critical values along the inflaton trajectory where the sgoldstino VEV changes behavior as a function of φ. These are the values where the different terms in (C.1) change from subleading to dominant, which are

$$\varphi^2 \quad \sim \quad \frac{f_0^2}{m_f m_h} \quad , \quad \frac{f_0^2 M_{\rm P}^2}{\Lambda_0^2 m_f^2} \quad , \quad \frac{f_0 M_{\rm P}}{m_f} \quad , \quad \frac{\Lambda_0^2}{g^2} \ , \tag{C.2}$$

where the last one determines also a change in the EFT validity scale. In determining these critical values we have made the crucial assumption that they are ordered as in Eq. (C.2) in increasing size. Indeed the assumption $\frac{\Lambda_0^2}{g^2} \gg \frac{f_0 M_{\rm P}}{m_f}$ implies that the next relevant scale for the behaviour in the denominator is $\frac{f_0^2 M_{\rm P}^2}{\Lambda_0^2 m_f^2}$. This is smaller than $\frac{f_0 M_{\rm P}}{m_f}$ if we further impose $f_0 \ll \frac{m_f\Lambda_0^2}{M_{\rm P}}$. The first ordering on the left in Eq. (C.2) also requires a further assumption. All in all the choice of ordering of the critical values in Eq. (C.2) leads to the following inequalities

$$f_0 \ll \frac{m_f}{M_{\rm P}}\Lambda_0^2 \ , \qquad \frac{\Lambda_0^2}{M_{\rm P}^2} \ll \frac{m_h}{m_f} \ . \tag{C.3}$$

Now we can proceed identifying the inequalities that the parameters should satisfy in order for the sgoldstino VEV to be within the EFT validity regime, in all the five intervals defined by the critical values in Eq. (C.2) from $\varphi \sim 0$ to $\varphi \sim M_{\rm P}$.

Analysing all the intervals one finds that the complete set of inequalities is[3]

$$f_0 \ll \frac{\Lambda_0^2 m_f}{M_{\rm P}} \ , \qquad \frac{\Lambda_0^2}{M_{\rm P}^2} \ll \frac{m_h}{m_f} \ , \qquad \frac{\Lambda_0}{M_{\rm P}} \gg \frac{m_h}{m_f} \ . \tag{C.4}$$

[2]This is equivalent to assuming that the expansion parameter is $\epsilon \sim \frac{\rho}{M_{\rm P}} \sim \frac{m_f^2}{M_{\rm P}^2}$.

[3]We always assume $g \ll 1$.

In particular the last inequality is the one emerging from the analysis of the regimes of validity in the various intervals. Note that it imposes an upper bound on the size of the quadratic term of the inflaton potential, resulting in an upper bound on the inflaton mass at the end of inflation, that will have important consequences for the phenomenology. Moreover, since $\Lambda_0 \ll M_{\rm p}$, it also confirms that $m_h \ll m_f$.

We conclude by observing that by changing the assumptions on the ordering of the various turning points in Eq. (C.1), one can extend to other regions of parameter space where the EFT is still valid. This has indeed also been checked by randomly scanning over the various parameters. However, we have observed that restricting the scan to EFT parameters compatible with a weakly coupled UV completion as in section 8.4, the parameter space is cut out to the UV version of Eq. (C.4), that is Eq. (8.40). Hence our focus on this region.

BIJLAGE D

Samenvatting

Natuurverschijnselen worden bestudeerd op verschillende afstandsschalen. Op zeer grote schaal wordt het universum als geheel bestudeerd, terwijl op kleine schaal de fysica van de elementaire deeltjes onderzocht wordt met de Large Hadron Collider (LHC). De fenomenen die bestudeerd worden met deze verschillende instrumenten zijn zeer verschillend. De fysica van de elementaire deeltjes wordt gekarakteriseerd door het standaardmodel van de deeltjesfysica, deze beschrijft drie van de vier fundamentele krachten: de sterke en zwakke kernkracht en de elektromagnetische kracht. De vierde kracht, de zwaartekracht, wordt niet beschreven in het standaardmodel. Maar deze kracht, beschreven door de algemene relativiteitstheorie, is de belangrijkste kracht voor observaties van het universum.

Het combineren van de twee modellen, het standaardmodel der elementaire deeltjes en de algemene relativiteitstheorie, levert theoretische problemen op. Het belangrijkste probleem is dat het moeilijk blijkt een kwantummechanische beschrijving van de algemene relativiteitstheorie te formuleren. Dit wordt vergemakkelijkt indien een extra ingrediënt wordt toegevoegd aan deze modellen, namelijk supersymmetrie. Met supersymmetrie kunnen modellen als supergravitatie en de snaartheorie worden afgeleid, die inderdaad de mogelijkheid bieden zowel het standaardmodel als de zwaartekracht te beschrijven. Het blijkt echter dat deze theorieën slechts relevant worden als de energieschaal van het bestudeerde proces zeer hoog is. Dit betekent dat experimenten zoals de LHC niet gebruikt kunnen worden voor de validatie van supergravitatie en snaartheorie, hoewel het mogelijk is dat supersymmetrie wel te vinden is met dergelijke experimenten. Het is daarom van belang om andere mogelijkheden te zoeken om deze theorieën te testen. Deze mogelijkheden liggen in het onderzoeken van de oorsprong van het universum.

Er bestaan verschillende kosmologische observaties die niet verklaard kunnen worden met de huidige kosmologische modellen, die beschreven zijn met de algemene relativiteitstheorie en het standaardmodel van de deeltjesfysica. Het is mogelijk om met aanpassingen van de laatste deze observaties te beschrijven, maar volledige duidelijkheid daarover is er nog niet. Voor deze thesis zijn twee observaties van belang

Ten eerste is bij waarnemingen van ons universum significant meer massa waargenomen dan verklaard kan worden door de deeltjes van het standaardmodel van de elementaire deeltjes. Deze nieuwe deeltjes worden niet rechtstreeks waargenomen, hetgeen betekent dat zij niet gekoppeld zijn aan licht. Om deze reden wordt deze nieuwe vorm van materie donkere materie genoemd. De oorsprong van deze donkere materie is onbekend.

Ten tweede blijkt uit waarnemingen dat het vroege universum (en daarmee ook het huidige universum) uiterst isotroop was, hetgeen betekent dat elk punt dat wij waarnemen in het vroege universum er identiek uitziet. Door de eindige snelheid van het licht is het vroege universum opgedeeld in stukjes die causaal met elkaar in verband hebben gestaan, en dus informatie uitgewisseld kunnen hebben. Door de uitdijing van het universum zien wij tegenwoordig vele van dergelijke stukjes universum, door de uitdijing is het plaatje van het universum als het ware uitvergroot. Omdat die verschillende stukjes universum geen informatie konden uitwisselen, zou men verwachten dat zij verschillende eigenschappen hebben, ze hebben immers geen mogelijkheid gehad om 'af te stemmen'. Maar zoals gezegd is het universum uiterst isotroop. Dit probleem, dat te maken heeft met de causale horizon, wordt het horizonprobleem genoemd.

Het horizonprobleem neemt aan dat er in het vroege universum enkel deeltjes bestonden uit het standaardmodel. Het is echter mogelijk om dit probleem op te lossen door een nieuw deeltje te introduceren die een nieuwe fase van versnelde expansie doet plaatsvinden in het zeer vroege universum. Deze periode wordt inflatie genoemd. Zoals gezegd blijkt het niet mogelijk om inflatie te beschrijven binnen het standaardmodel (hoewel er een model bestaat met het Brout-Englert-Higgs boson, maar dit model vereist een aanpassing van de koppeling tussen dit deeltje en gravitatie). Omdat inflatie plaatsvindt op zeer hoge energieën en het standaardmodel daar nog niet is getest is inflatie feitelijk een mogelijkheid om het zeer-hoge energie limiet van het standaardmodel te onderzoeken. Inflatie kan daarom gebruikt worden als een proefgebied om de correcte beschrijving van supergravitatie en snaartheorie te onderzoeken.

De belangrijkste observatie die naar het horizonprobleem leidde was de kosmische achtergrondstraling. Deze straling ontstond toen het vroege universum afkoelde (het universum koelt af omdat het uitdijt) en licht er plotseling (nagenoeg) ongelimiteerd doorheen kon gaan. Dit licht wordt tegenwoordig waargenomen door speciale observatoria, waarvan de laatste (en nauwkeurigste) de Planck satelliet en de BICEP/KECK-telescopen zijn. Door inflatie was het vroege universum zeer isotroop, hetgeen betekent dat de kosmische achtergrondstraling dezelfde

temperatuur had voor elke richting waarin we ernaar kijken. Feitelijk is dit de belangrijkste observatie van het horizonprobleem, dat dus opgelost wordt door een periode van inflatie.

Echter, de kosmische achtergrondstraling is niet perfect isotroop maar er zijn zeer kleine fluctuaties van de temperatuur. Het bestuderen van deze fluctuaties was het belangrijkste doel van de Planck satelliet (hoewel de fluctuaties zelf al gemeten waren door de COBE-satelliet). De Plank satelliet vond niet alleen de fluctuaties zelf, maar toonde ook aan dat ze niet zogeheten schaal-invariant waren, uitgedrukt in de parameter n_s.

Inflatie voorspelt het bestaan van deze schaal-invariante fluctuaties in de kosmische achtergrondstraling. De reden is als volgt. De periode van inflatie wordt gegenereerd door een scalair veld dat in een potentiaal naar beneden rolt. Als dit veld, het inflaton genaamd, langzaam rolt zal het universum versneld uitdijen. Door kwantumfluctuaties ontstaan echter kleine verschillen in delen van het universum en ontstaan uiteindelijk zeer kleine variaties in de dichtheid van het universum op het moment dat de kosmische achtergrondstraling uitgezonden wordt. Deze kleine dichtheidsveranderingen veroorzaken vervolgens de waargenomen temperatuurfluctuaties.

Tijdens inflatie ontstonden behalve dichtheidsfluctuaties ook zwaartekrachtgolven. Deze zwaartekrachtgolven zijn niet rechtstreeks waarneembaar, in tegenstelling tot de golven waargenomen door de LIGO/VIRGO-collaboratie, maar hebben wel effect op de polarisatie van de kosmische achtergrondstraling. Deze polarisatie wordt gemeten in de Planck satelliet en de BICEP/KECK-telescoop. Helaas zijn de effecten van de zwaartekrachtgolven nog niet gemeten, maar er is wel een zeer strikte bovengrens. Deze bovengrens wordt uitgedrukt als een maximale waarde die een parameter genaamd r kan bereiken.

De meting van n_s en de bovengrens op r zijn dermate strikt dat al verscheidene modellen zijn uitgesloten door deze observaties. Echter ook vele modellen zijn nog toegestaan. Het is daarom van belang om te onderzoeken welke modellen wel overeenstemmen met de data en welke niet. Vandaar de focus in dit proefschrift om verscheidene inflatiemodellen te testen met de waarnemingen van n_s en r.

Het eerste deel van de thesis vergelijkt de voorspellingen van verschillende parametrisaties van inflatie met de meting van n_s en de bovengrens op r. Er zijn verschillende manieren om dit te bestuderen, waarvan er twee worden gebruikt in dit proefschrift. De eerste methode is door verschillende potentialen te parametriseren en vervolgens een numerieke scan te doen over deze parameters. De tweede methode is door het bestuderen van zogenaamde attractoren in inflatie.

Voor de numerieke studie naar generieke voorspellingen van inflatie worden drie parametrisaties vergeleken. De eerste parametrisatie was de polynomisch geëxpandeerde potentiaal. Deze parametrisatie was de standaard in de literatuur, maar de generieke voorspelling van deze parametrisatie had een te kleine waarde van n_s. De reden is dat een polynoom over het algemeen een vrij sterk gebogen potentiaal oplevert. Het is bekend dat over het algemeen vlakke potentialen beter

overeenkomen met de observaties, dus is het aannemelijk dat een parametrisatie die over het algemeen een vlakke potentiaal heeft betere voorspellingen zou doen.

Vervolgens worden in het proefschrift modellen onderzocht met vlakke potentialen door de potentiaal te parametriseren als een ratio van polynomen. Deze parametrisatie heeft meestal een vlakke potentiaal voor hoge waarden van het inflaton veld, dus als het inflaton veld deze waarden bereikt zal inflatie beter overeenstemmen met de observaties. Inderdaad bleek uit de numerieke simulaties dat deze parametrisatie veel beter overeenkwam met de data van de kosmische achtergrondstraling.

Om deze claim te versterken werd een nieuwe methode ontwikkeld om een analytische oplossing te verkrijgen voor de differentiaalvergelijkingen die inflatie karakteriseren. De analytische studie gaf hetzelfde beeld als de numerieke, dus een ratio van polynomen voldoet beter dan een enkele polynoom.

Tot slot wordt een algemene versie van het sterke-koppeling attractormodel zowel analytisch als numeriek bestudeerd. Dit attractormodel maakt gebruik van een niet-minimale koppeling tussen het inflaton en gravitatie. Deze koppeling wordt geparametriseerd door een parameter (ξ) en in dit werk vonden we dat als ξ groot genoeg wordt gekozen (van de orde 10^5) inflatie doorgaans voldoet aan de observaties. De reden is dat voor een grote waarde van ξ een plateau ontstaat voor grote waarden voor het inflaton veld, terwijl voor kleine waarden van ξ het plateau te ver weg ligt om effect te hebben op de CMB.

Bovenstaande modellen waren allemaar valide inflatiemodellen, maar zij voorspelden enkel inflatie en niet de daaropvolgende evolutie van het universum. De reden is dat zij niet gekoppeld zijn aan het standaardmodel van de deeltjesfysica. Het tweede deel van dit proefschrift is gewijd aan het verbinden van inflatie met de deeltjesfysica. In dit werk onderzochten we een supergravitatiemodel voor inflatie genaamd 'nilpotente inflatie'. Ons belangrijkste resultaat in dit werk was dat wij het deel van de parameterruimte van het model identificeerden waarin inflatie mogelijk was.

Een interessant bijkomend onderdeel van dit supergravitatiemodel was dat het consistent kon worden gemaakt met het standaardmodel van de deeltjesfysica. Omdat dit model gebaseerd is op supersymmetrie, voorspeldt het een set nieuwe deeltjes, zogenaamde superpartners. De massaś van deze superparners kunnen berekend worden in ons model en vergeleken met de bovengrensen voor de massa's van de LHC, dat deze deeltjes niet hebben waargenomen.

Naast deze massa's, kan in ons model ook de volledige evolutie van het universum worden beschreven. De reden dat dit niet bekend is bij effectieve inflatiemodellen, zoals de modellen die in het eerste deel van het proefschrift beschreven werden, is dat deze modellen het verval van het inflaton in standaardmodeldeeltjes niet meenemen. Voor de periode van inflatie is dit niet relevant, maar na inflatie moet het inflaton uit het universum verdwijnen door te vervallen naar standaardmodeldeeltjes.

Omdat ons model de interacties tussen het inflaton en het standaardmodel

van de deeltjesfysica beschrijft kan deze periode beschreven worden in ons model. Dit betekent dat niet alleen precieze voorspellingen van n_{s} en r gemaakt kunnen worden en dat we de massa's van de superpartners kunnen vinden, maar ook dat we een mogelijke kandidaat hebben voor donkere materie. Derhalve behandelt het laatste deel van de thesis een model met scherpe voorspellingen voor normaal gezien ongerelateerde gebeurtenissen in het universum.

BIJLAGE E

Acknowledgments

It is impossible to finish a PhD without the help and support of many people. Since I stayed half my PhD abroad in Brussels, I had the occasion of meeting many people (roughly twice as many, I guess). I want to express my gratitude to everyone that made my stay in both cities so enjoyable. In the remainder of this section, I would like to thank a number of people in particular.

First, I would like to start with thanking my supervisors Diederik Roest, Alberto Mariotti and Ben Craps. Diederik, thanks for leading me into the interesting world of inflation and that you gave me the opportunity to follow my own path in research. Alberto, I am very happy to have worked with you and that you always found time for detailed explanations concerning particle physics. Ben, I am extremely grateful that you told me to look around at the VUB when I moved to Belgium, so that I could follow the path that interested me most. Even though this meant we did not really work together. I would also like to thank Elisabetta Palante here. As the supervisor of my bachelor and master theses, you made me interested in starting a PhD. Moreover, though I researched a different branch of physics, you shaped the way I think about physics more than anyone else.

Second, I would like to thank Ana Achúcarro, Wilfried Buchmüller, Elisabetta Pallante and Alexander Sevrin for being part of my reading committee. This thesis is not a short one, so I am very happy you found time to read it.

I also thank Tijn and Jan-Willem for being so very kind to take the important task to be my paranymphs. In addition, I would like to thank Douglas Burns and Matthias Vereecken for being so kind to read (part of) my thesis and provide valuable comments.

One does not perform research alone, rather it is the result of open discussions

with collaborators and colleagues. In this regard, I want to thank my collaborators Vincent Vennin, Benedict Broy, Riccardo Argurio and Lucien Heurtier. It has been a pleasure to work with you.

As said above, my work in Groningen and Brussels could not have been possible without all my colleagues at the Van Swinderen institute, IIHE and TENA. Without the nice atmosphere at these institutes the PhD would have been a lot less fun. I had the pleasure to have many conversations with you, of which I learned a lot. I am especially grateful to the PhDs and staff members working on the experimental physics research at the IIHE, that I could always ask questions regarding experiments. Special thanks goes to my office mates Tiago, Julian Karen, Matthias and Ivan for many discussions about roughly anything, including physics. Finally, I would like to thank the secretaries at the three institutes: Annelien, Iris, Marleen and Merel. Without you nothing would have been working, since you are always at the heart of the events.

Learning about physics merely from books and research papers is complicated, if not close to impossible. Therefore, it is important to attend meetings, like seminars and journal clubs that were organised at the institutes, but also on more national scales. Thus I want to thank all the organisers of these seminars. Specifically, I would like tot thank the phenomenology group of the ULB for giving me the opportunity to attend their seminars and journal clubs.

In the current universe, there exists more than only physics (though everything is described by physics). Therefore did I not devote all my time to physics alone and I would like to thank those I had the pleasure of meeting in these activities. Firstly, I would like to thank everyone that I met while played the recorder: of coarse my recorder teachers, Jankees, Aline and Ine. Moreover, playing an instrument alone is rather boring, and I would like to thank the ensembles in which I played, being the recorder ensembles of the Muziekscholen van Groningen and Jette, Ballo dei Folli, the 'Gent' ensemble (with Karen and Gertjan) and the many people I met while playing Irish/Scottish folk music.

It the same spirit I want to thank everyone I met when singing with Bragi and Café latte and dancing with Plaisir Courtois. I would advise everyone to follow the 'German trick' when moving abroad: search for a choir. It is a very easy way to get to know many new people beyond those you meet at your work.

Last, but certainly not least, I want to thank my family for all the support and time we had together.

Bibliografie

[1] **Planck** Collaboration, R. Adam et al., *Planck 2015 results. I. Overview of products and scientific results*, arXiv:1502.01582.

[2] **BICEP2, Keck Array** Collaboration, P. A. R. Ade et al., *BICEP2 / Keck Array VIII: Measurement of gravitational lensing from large-scale B-mode polarization*, *Astrophys. J.* **833** (2016), no. 2 228, [arXiv:1606.01968].

[3] B. Ryden, *Introduction to cosmology*. Cambridge University Press, 2016.

[4] Retrieved from https://commons.wikimedia.org/wiki/File:CMB_Timeline300_no_WMAP.jpg. on December 31, 2017.

[5] A. A. Penzias and R. W. Wilson, *A Measurement of Excess Antenna Temperature at 4080 Mc/s.*, *Astrophysical Journal* **142** (July, 1965) 419–421.

[6] R. H. Dicke, P. J. E. Peebles, P. G. Roll, and D. T. Wilkinson, *Cosmic Black-Body Radiation*, *Astrophys. J.* **142** (1965) 414–419.

[7] D. J. Fixsen, *The Temperature of the Cosmic Microwave Background*, *Astrophys. J.* **707** (2009) 916–920, [arXiv:0911.1955].

[8] S. Weinberg, *Cosmology*. Oxford University Press, 2008.

[9] **COBE** Collaboration, G. F. Smoot et al., *Structure in the COBE differential microwave radiometer first year maps*, *Astrophys. J.* **396** (1992) L1–L5.

[10] R. S. Gonçalves, G. C. Carvalho, C. A. P. Bengaly, J. C. Carvalho, A. Bernui, J. S. Alcaniz, and R. Maartens, *Cosmic homogeneity: a spectroscopic and model-independent measurement*, arXiv:1710.02496.

[11] A. H. Guth, *The Inflationary Universe: A Possible Solution to the Horizon and Flatness Problems*, *Phys. Rev.* **D23** (1981) 347–356.

[12] **Planck** Collaboration, P. A. R. Ade et al., *Planck 2015 results. XIII. Cosmological parameters*, *Astron. Astrophys.* **594** (2016) A13, [arXiv:1502.01589].

[13] **Planck** Collaboration, P. A. R. Ade et al., *Planck 2013 results. XXII. Constraints on inflation*, *Astron. Astrophys.* **571** (2014) A22, [arXiv:1303.5082].

[14] **Planck** Collaboration, P. A. R. Ade et al., *Planck 2015 results. XX. Constraints on inflation*, *Astron. Astrophys.* **594** (2016) A20, [arXiv:1502.02114].

[15] **Virgo, LIGO Scientific** Collaboration, B. P. Abbott et al., *Observation of Gravitational Waves from a Binary Black Hole Merger*, *Phys. Rev. Lett.* **116** (2016), no. 6 061102, [arXiv:1602.03837].

[16] **BICEP2, Keck Array** Collaboration, P. A. R. Ade et al., *Improved Constraints on Cosmology and Foregrounds from BICEP2 and Keck Array Cosmic Microwave Background Data with Inclusion of 95 GHz Band*, *Phys. Rev. Lett.* **116** (2016) 031302, [arXiv:1510.09217].

[17] **BICEP2, Planck** Collaboration, P. A. R. Ade et al., *Joint Analysis of BICEP2/Keck?Array and Planck Data*, *Phys. Rev. Lett.* **114** (2015) 101301, [arXiv:1502.00612].

[18] A. R. Liddle, *An introduction to modern cosmology*. Wiley, 1998.

[19] S. Dodelson, *Modern Cosmology*. Academic Press, Amsterdam, 2003.

[20] E. W. Kolb and M. S. Turner, *The Early Universe*, *Front. Phys.* **69** (1990) 1–547.

[21] W. N. Cottingham and D. A. Greenwood, *An introduction to the standard model of particle physics*. Cambridge University Press, 2007.

[22] M. E. Peskin and D. V. Schroeder, *An Introduction to quantum field theory*. Addison-Wesley, Reading, USA, 1995.

[23] M. Thomson, *Modern particle physics*. Cambridge University Press, New York, 2013.

[24] C. P. Burgess and G. D. Moore, *The standard model: A primer*. Cambridge University Press, 2006.

[25] Retrieved from https://commons.wikimedia.org/wiki/File:Standard_Model_of_Elementary_Particles.svg. on September 5, 2017.

[26] **Particle Data Group** Collaboration, C. Patrignani et al., *Review of Particle Physics*, *Chin. Phys.* **C40** (2016), no. 10 100001.

[27] F. Englert and R. Brout, *Broken Symmetry and the Mass of Gauge Vector Mesons*, *Phys. Rev. Lett.* **13** (1964) 321–323.

[28] P. W. Higgs, *Broken Symmetries and the Masses of Gauge Bosons*, *Phys. Rev. Lett.* **13** (1964) 508–509.

[29] G. 't Hooft, *Naturalness, chiral symmetry, and spontaneous chiral symmetry breaking*, *NATO Sci. Ser. B* **59** (1980) 135–157.

[30] M. Piai, *Lectures on walking technicolor, holography and gauge/gravity dualities*, *Adv. High Energy Phys.* **2010** (2010) 464302, [arXiv:1004.0176].

[31] M. Quiros, *New ideas in symmetry breaking*, in *Summer Institute 2002 (SI 2002) Fuji-Yoshida, Japan, August 13-20, 2002*, pp. 549–601, 2003. hep-ph/0302189.

[32] P. W. Graham, D. E. Kaplan, and S. Rajendran, *Cosmological Relaxation of the Electroweak Scale*, *Phys. Rev. Lett.* **115** (2015), no. 22 221801, [arXiv:1504.07551].

[33] M. Farina, D. Pappadopulo, and A. Strumia, *A modified naturalness principle and its experimental tests*, *JHEP* **08** (2013) 022, [arXiv:1303.7244].

[34] M. Dine, *Naturalness Under Stress*, *Ann. Rev. Nucl. Part. Sci.* **65** (2015) 43–62, [arXiv:1501.01035].

[35] G. Degrassi, S. Di Vita, J. Elias-Miro, J. R. Espinosa, G. F. Giudice, G. Isidori, and A. Strumia, *Higgs mass and vacuum stability in the Standard Model at NNLO*, *JHEP* **08** (2012) 098, [arXiv:1205.6497].

[36] G. W. Anderson, *New Cosmological Constraints on the Higgs Boson and Top Quark Masses*, *Phys. Lett.* **B243** (1990) 265–270.

[37] F. Bezrukov, J. Rubio, and M. Shaposhnikov, *Living beyond the edge: Higgs inflation and vacuum metastability*, *Phys. Rev.* **D92** (2015), no. 8 083512, [arXiv:1412.3811].

[38] A. A. Anselm and A. A. Johansen, *Can electroweak theta term be observable?*, *Nucl. Phys.* **B412** (1994) 553–573, [hep-ph/9305271].

[39] M. Dine, *TASI lectures on the strong CP problem*, in *Flavor physics for the millennium. Proceedings, Theoretical Advanced Study Institute in elementary particle physics, TASI 2000, Boulder, USA, June 4-30, 2000*, pp. 349–369, 2000. hep-ph/0011376.

[40] **Super-Kamiokande** Collaboration, Y. Fukuda et al., *Evidence for oscillation of atmospheric neutrinos*, *Phys. Rev. Lett.* **81** (1998) 1562–1567, [hep-ex/9807003].

[41] **SNO** Collaboration, Q. R. Ahmad et al., *Direct evidence for neutrino flavor transformation from neutral current interactions in the Sudbury Neutrino Observatory*, *Phys. Rev. Lett.* **89** (2002) 011301, [nucl-ex/0204008].

[42] S. F. King, *Neutrino mass models*, *Rept. Prog. Phys.* **67** (2004) 107–158, [hep-ph/0310204].

[43] A. Salvio and A. Strumia, *Agravity*, *JHEP* **06** (2014) 080, [arXiv:1403.4226].

[44] S. Raby, *Grand Unified Theories*, in *2nd World Summit: Physics Beyond the Standard Model Galapagos, Islands, Ecuador, June 22-25, 2006*, 2006. hep-ph/0608183.

[45] D. Baumann, *Inflation*, in *Physics of the large and the small, TASI 09, proceedings of the Theoretical Advanced Study Institute in Elementary Particle Physics, Boulder, Colorado, USA, 1-26 June 2009*, pp. 523–686, 2011. arXiv:0907.5424.

[46] E. Hubble, *A relation between distance and radial velocity among extra-galactic nebulae*, *Proc. Nat. Acad. Sci.* **15** (1929) 168–173.

[47] A. G. Riess et al., *A 2.4% Determination of the Local Value of the Hubble Constant*, *Astrophys. J.* **826** (2016), no. 1 56, [arXiv:1604.01424].

[48] W. Lin and M. Ishak, *Cosmological discordances II: Hubble constant, Planck and large-scale-structure data sets*, *Phys. Rev.* **D96** (2017), no. 8 083532, [arXiv:1708.09813].

[49] **LIGO Scientific, VINROUGE, Las Cumbres Observatory, DES, DLT40, Virgo, 1M2H, Dark Energy Camera GW-E, MASTER** Collaboration, B. P. Abbott et al., *A gravitational-wave standard siren measurement of the Hubble constant*, *Nature* **551** (2017), no. 7678 85–88, [arXiv:1710.05835].

[50] W. Rindler, *Visual horizons in world-models*, *Gen. Rel. Grav.* **34** (2002) 133–153. [Mon. Not. Roy. Astron. Soc.116,662(1956)].

[51] T. M. Davis and C. H. Lineweaver, *Expanding confusion: common misconceptions of cosmological horizons and the superluminal expansion of the universe*, *Proc. Astron. Soc. Austral.* (2003) [astro-ph/0310808]. [Publ. Astron. Soc. Austral.21,97(2004)].

[52] **Supernova Search Team** Collaboration, A. G. Riess et al., *Observational evidence from supernovae for an accelerating universe and a cosmological constant*, *Astron. J.* **116** (1998) 1009–1038, [astro-ph/9805201].

[53] **Supernova Cosmology Project** Collaboration, S. Perlmutter et al., *Measurements of Omega and Lambda from 42 high redshift supernovae*, *Astrophys. J.* **517** (1999) 565–586, [astro-ph/9812133].

[54] P. van Oirschot, J. Kwan, and G. F. Lewis, *Another coincidence problem for ΛCDM?*, in *Proceedings, 13th Marcel Grossmann Meeting on Recent Developments in Theoretical and Experimental General Relativity, Astrophysics, and Relativistic Field Theories (MG13): Stockholm, Sweden, July 1-7, 2012*, pp. 1567–1569, 2015. arXiv:1409.0901.

[55] S. Weinberg, *Anthropic Bound on the Cosmological Constant*, *Phys. Rev. Lett.* **59** (1987) 2607.

[56] A. Vilenkin, *Predictions from quantum cosmology*, *Phys. Rev. Lett.* **74** (1995) 846–849, [gr-qc/9406010].

[57] **Planck** Collaboration, P. A. R. Ade et al., *Planck 2015 results. XVII. Constraints on primordial non-Gaussianity*, *Astron. Astrophys.* **594** (2016) A17, [arXiv:1502.01592].

[58] J. Rich, *Fundamentals of cosmology*. Berlin, Germany: Springer (2001) 302 p, 2001.

[59] J. Lesgourgues and S. Pastor, *Neutrino mass from Cosmology*, *Adv. High Energy Phys.* **2012** (2012) 608515, [arXiv:1212.6154].

[60] J. M. Cline, *Baryogenesis*, in *Les Houches Summer School - Session 86: Particle Physics and Cosmology: The Fabric of Spacetime Les Houches, France, July 31-August 25, 2006*, 2006. hep-ph/0609145.

[61] A. De Felice and S. Tsujikawa, *f(R) theories*, *Living Rev. Rel.* **13** (2010) 3, [arXiv:1002.4928].

[62] E. P. Verlinde, *Emergent Gravity and the Dark Universe*, *SciPost Phys.* **2** (2017), no. 3 016, [arXiv:1611.02269].

[63] S. M. Carroll, V. Duvvuri, M. Trodden, and M. S. Turner, *Is cosmic speed - up due to new gravitational physics?*, *Phys. Rev.* **D70** (2004) 043528, [astro-ph/0306438].

[64] S. Nojiri and S. D. Odintsov, *Unifying phantom inflation with late-time acceleration: Scalar phantom-non-phantom transition model and generalized holographic dark energy*, *Gen. Rel. Grav.* **38** (2006) 1285–1304, [hep-th/0506212].

[65] J. De Haro and L. Aresté Saló, *Reheating constraints in quintessential inflation*, *Phys. Rev.* **D95** (2017), no. 12 123501, [arXiv:1702.04212].

[66] K. Garrett and G. Duda, *Dark Matter: A Primer*, *Adv. Astron.* **2011** (2011) 968283, [arXiv:1006.2483].

[67] M. Markevitch, A. H. Gonzalez, D. Clowe, A. Vikhlinin, L. David, W. Forman, C. Jones, S. Murray, and W. Tucker, *Direct constraints on the dark matter self-interaction cross-section from the merging galaxy cluster 1E0657-56*, *Astrophys. J.* **606** (2004) 819–824, [astro-ph/0309303].

[68] V. Iršič et al., *New Constraints on the free-streaming of warm dark matter from intermediate and small scale Lyman-α forest data*, *Phys. Rev.* **D96** (2017), no. 2 023522, [arXiv:1702.01764].

[69] A. Merle, *keV sterile neutrino Dark Matter*, *PoS* **NOW2016** (2017) 082, [arXiv:1702.08430].

[70] D. Baumann, "Lecture notes: The physics of inflation." Retrieved from http://www.damtp.cam.ac.uk/user/db275/TEACHING/INFLATION/Lectures.pdf.

[71] O. Buchmueller, C. Doglioni, and L. T. Wang, *Search for dark matter at colliders*, *Nature Phys.* **13** (2017), no. 3 217–223.

[72] J. Liu, X. Chen, and X. Ji, *Current status of direct dark matter detection experiments*, *Nature Phys.* **13** (2017), no. 3 212–216, [arXiv:1709.00688].

[73] E. Bulbul, M. Markevitch, A. Foster, R. K. Smith, M. Loewenstein, and S. W. Randall, *Detection of An Unidentified Emission Line in the Stacked X-ray spectrum of Galaxy Clusters*, *Astrophys. J.* **789** (2014) 13, [arXiv:1402.2301].

[74] T. R. Slatyer, *TASI Lectures on Indirect Detection of Dark Matter*, in *Theoretical Advanced Study Institute in Elementary Particle Physics: Anticipating the Next Discoveries in Particle Physics (TASI 2016) Boulder, CO, USA, June 6-July 1, 2016*, 2017. arXiv:1710.05137.

[75] L. J. Hall, K. Jedamzik, J. March-Russell, and S. M. West, *Freeze-In Production of FIMP Dark Matter*, *JHEP* **03** (2010) 080, [arXiv:0911.1120].

[76] C. Cheung, G. Elor, L. J. Hall, and P. Kumar, *Origins of Hidden Sector Dark Matter I: Cosmology*, *JHEP* **03** (2011) 042, [arXiv:1010.0022].

[77] B. Famaey and J. Binney, *Modified Newtonian dynamics in the Milky Way*, *Mon. Not. Roy. Astron. Soc.* **363** (2005) 603–608, [astro-ph/0506723].

[78] P. J. Steinhardt, N. Turok, and N. Turok, *A Cyclic model of the universe*, *Science* **296** (2002) 1436–1439, [hep-th/0111030].

[79] A. R. Liddle, *An Introduction to cosmological inflation*, in *Proceedings, Summer School in High-energy physics and cosmology: Trieste, Italy, June 29-July 17, 1998*, pp. 260–295, 1999. astro-ph/9901124.

[80] A. Albrecht and P. J. Steinhardt, *Cosmology for Grand Unified Theories with Radiatively Induced Symmetry Breaking*, *Phys. Rev. Lett.* **48** (1982) 1220–1223.

[81] A. D. Linde, *A New Inflationary Universe Scenario: A Possible Solution of the Horizon, Flatness, Homogeneity, Isotropy and Primordial Monopole Problems*, *Phys. Lett.* **B108** (1982) 389–393.

[82] A. D. Linde, *Chaotic Inflation*, *Phys. Lett.* **B129** (1983) 177–181.

[83] A. R. Liddle, P. Parsons, and J. D. Barrow, *Formalizing the slow roll approximation in inflation*, *Phys.Rev.* **D50** (1994) 7222–7232, [astro-ph/9408015].

[84] E. J. Copeland, E. W. Kolb, A. R. Liddle, and J. E. Lidsey, *Reconstructing the inflation potential, in principle and in practice*, *Phys. Rev.* **D48** (1993) 2529–2547, [hep-ph/9303288].

[85] W. H. Kinney, *Horizon crossing and inflation with large eta*, *Phys. Rev.* **D72** (2005) 023515, [gr-qc/0503017].

[86] P. J. Steinhardt and M. S. Turner, *A Prescription for Successful New Inflation*, *Phys. Rev.* **D29** (1984) 2162–2171.

[87] V. Vennin, *Horizon-Flow off-track for Inflation*, *Phys.Rev.* **D89** (2014) 083526, [arXiv:1401.2926].

[88] N. J. Cornish and J. J. Levin, *Chaos, fractals, and inflation*, *Phys. Rev.* **D53** (1996) 3022–3032, [astro-ph/9510010].

[89] M. B. Hoffman and M. S. Turner, *Kinematic constraints to the key inflationary observables*, *Phys.Rev.* **D64** (2001) 023506, [astro-ph/0006321].

[90] G. N. Remmen and S. M. Carroll, *Attractor Solutions in Scalar-Field Cosmology*, *Phys.Rev.* **D88** (2013) 083518, [arXiv:1309.2611].

[91] W. H. Kinney and K. Freese, *Negative running can prevent eternal inflation*, *JCAP* **1501** (2015), no. 01 040, [arXiv:1404.4614].

[92] V. Mukhanov, *Inflation without Selfreproduction*, *Fortsch. Phys.* **63** (2015) 36–41, [arXiv:1409.2335].

[93] A. D. Linde, *ETERNALLY EXISTING SELFREPRODUCING INFLATIONARY UNIVERSE*, *Phys. Scripta* **T15** (1987) 169.

[94] V. F. Mukhanov and G. Chibisov, *Quantum Fluctuation and Nonsingular Universe. (In Russian)*, *JETP Lett.* **33** (1981) 532–535.

[95] A. H. Guth and S. Y. Pi, *Fluctuations in the New Inflationary Universe*, *Phys. Rev. Lett.* **49** (1982) 1110–1113.

[96] A. A. Starobinsky, *Spectrum of relict gravitational radiation and the early state of the universe*, *JETP Lett.* **30** (1979) 682–685.

[97] S. Hawking, *The Development of Irregularities in a Single Bubble Inflationary Universe*, *Phys. Lett.* **B115** (1982) 295. Revised version.

[98] J. M. Bardeen, P. J. Steinhardt, and M. S. Turner, *Spontaneous Creation of Almost Scale - Free Density Perturbations in an Inflationary Universe*, *Phys. Rev.* **D28** (1983) 679.

[99] A. A. Starobinsky, *Dynamics of Phase Transition in the New Inflationary Universe Scenario and Generation of Perturbations*, *Phys. Lett.* **B117** (1982) 175–178.

[100] M. J. Rees, *Polarization and Spectrum of the Primeval Radiation in an Anisotropic Universe*, *Astrophys. J.* **153** (1968) L1.

[101] J. Kaplan, J. Delabrouille, P. Fosalba, and C. Rosset, *Cmb polarization as complementary information to anisotropies*, *Comptes Rendus Physique* **4** (2003) 917, [astro-ph/0310650].

[102] E. M. Leitch, J. M. Kovac, C. Pryke, B. Reddall, E. S. Sandberg, M. Dragovan, J. E. Carlstrom, N. W. Halverson, and W. L. Holzapfel, *Measuring polarization with DASI*, *Nature* **420** (2002) 763–771, [astro-ph/0209476].

[103] D. S. Salopek, J. R. Bond, and J. M. Bardeen, *Designing Density Fluctuation Spectra in Inflation*, *Phys. Rev.* **D40** (1989) 1753.

[104] V. F. Mukhanov, H. Feldman, and R. H. Brandenberger, *Theory of cosmological perturbations. Part 1. Classical perturbations. Part 2. Quantum theory of perturbations. Part 3. Extensions*, *Phys.Rep.* **215** (1992) 203–333.

[105] **BICEP2, Keck Array** Collaboration, P. A. R. Ade et al., *BICEP2 / Keck Array V: Measurements of B-mode Polarization at Degree Angular Scales and 150 GHz by the Keck Array*, *Astrophys. J.* **811** (2015) 126, [arXiv:1502.00643].

[106] T. Pereira and C. Pitrou, *Isotropization of the universe during inflation*, *Comptes Rendus Physique* **16** (2015) 1027–1037, [arXiv:1509.09166].

[107] B. Bonga, B. Gupt, and N. Yokomizo, *Inflation in the closed FLRW model and the CMB*, *JCAP* **1610** (2016), no. 10 031, [arXiv:1605.07556].

[108] Y. Cai, Y.-T. Wang, J.-Y. Zhao, and Y.-S. Piao, *Primordial perturbations with pre-inflationary bounce*, arXiv:1709.07464.

[109] S. Dodelson, *Coherent phase argument for inflation*, *AIP Conf. Proc.* **689** (2003) 184–196, [hep-ph/0309057].

[110] J. Martin, C. Ringeval, and V. Vennin, *Encyclopædia Inflationaris*, *Phys.Dark Univ.* **5-6** (2014) 75–235, [arXiv:1303.3787].

[111] A. B. Goncharov and A. D. Linde, *Chaotic Inflation in Supergravity*, *Phys. Lett.* **139B** (1984) 27–30.

[112] A. D. Linde, *Particle physics and inflationary cosmology*, *Contemp. Concepts Phys.* **5** (1990) 1–362, [hep-th/0503203].

[113] A. A. Starobinsky, *A new type of isotropic cosmological models without singularity*, *Phys. Lett.* **B91** (1980) 99–102.

[114] B. Whitt, *Fourth Order Gravity as General Relativity Plus Matter*, *Phys. Lett.* **145B** (1984) 176–178.

[115] J. D. Barrow, *The Premature Recollapse Problem in Closed Inflationary Universes*, *Nucl. Phys.* **B296** (1988) 697–709.

[116] S. Nojiri and S. D. Odintsov, *Modified gravity with negative and positive powers of the curvature: Unification of the inflation and of the cosmic acceleration*, *Phys. Rev.* **D68** (2003) 123512, [hep-th/0307288].

[117] H. Motohashi, *Consistency relation for R^p inflation*, *Phys. Rev.* **D91** (2015) 064016, [arXiv:1411.2972].

[118] F. Bezrukov, M. Yu. Kalmykov, B. A. Kniehl, and M. Shaposhnikov, *Higgs Boson Mass and New Physics*, *JHEP* **10** (2012) 140, [arXiv:1205.2893].

[119] F. Bezrukov and M. Shaposhnikov, *The Standard Model Higgs boson as the inflaton*, *Phys.Lett.* **B659** (2008) 703–706, [arXiv:0710.3755].

[120] C. P. Burgess, H. M. Lee, and M. Trott, *Power-counting and the Validity of the Classical Approximation During Inflation*, *JHEP* **09** (2009) 103, [arXiv:0902.4465].

[121] J. L. F. Barbon and J. R. Espinosa, *On the Naturalness of Higgs Inflation*, *Phys. Rev.* **D79** (2009) 081302, [arXiv:0903.0355].

[122] C. P. Burgess, H. M. Lee, and M. Trott, *Comment on Higgs Inflation and Naturalness*, *JHEP* **07** (2010) 007, [arXiv:1002.2730].

[123] M. P. Hertzberg, *On Inflation with Non-minimal Coupling*, *JHEP* **11** (2010) 023, [arXiv:1002.2995].

[124] R. N. Lerner and J. McDonald, *Higgs Inflation and Naturalness*, *JCAP* **1004** (2010) 015, [arXiv:0912.5463].

[125] F. Bezrukov, A. Magnin, M. Shaposhnikov, and S. Sibiryakov, *Higgs inflation: consistency and generalisations*, *JHEP* **01** (2011) 016, [arXiv:1008.5157].

[126] X. Calmet and R. Casadio, *Self-healing of unitarity in Higgs inflation*, *Phys. Lett.* **B734** (2014) 17–20, [arXiv:1310.7410].

[127] A. Escrivà and C. Germani, *Beyond dimensional analysis: Higgs and new Higgs inflations do not violate unitarity*, *Phys. Rev.* **D95** (2017), no. 12 123526, [arXiv:1612.06253].

[128] J. Fumagalli and M. Postma, *UV (in)sensitivity of Higgs inflation*, *JHEP* **05** (2016) 049, [arXiv:1602.07234].

[129] C. Germani and A. Kehagias, *New Model of Inflation with Non-minimal Derivative Coupling of Standard Model Higgs Boson to Gravity*, *Phys. Rev. Lett.* **105** (2010) 011302, [arXiv:1003.2635].

[130] C. Germani and A. Kehagias, *Cosmological Perturbations in the New Higgs Inflation*, *JCAP* **1005** (2010) 019, [arXiv:1003.4285]. [Erratum: JCAP1006,E01(2010)].

[131] M. Dhuria and G. Goswami, *Perturbativity, vacuum stability, and inflation in the light of 750 GeV diphoton excess*, *Phys. Rev.* **D94** (2016), no. 5 055009, [arXiv:1512.06782].

[132] A. Salvio and A. Mazumdar, *Higgs Stability and the 750 GeV Diphoton Excess*, *Phys. Lett.* **B755** (2016) 469–474, [arXiv:1512.08184].

[133] Y. Hamada, T. Noumi, S. Sun, and G. Shiu, *An O(750) GeV Resonance and Inflation*, *Phys. Rev.* **D93** (2016), no. 12 123514, [arXiv:1512.08984].

[134] S.-F. Ge, H.-J. He, J. Ren, and Z.-Z. Xianyu, *Realizing Dark Matter and Higgs Inflation in Light of LHC Diphoton Excess*, *Phys. Lett.* **B757** (2016) 480–492, [arXiv:1602.01801].

[135] J. McDonald, *The 750 GeV Resonance as Non-Minimally Coupled Inflaton: Unitarity Violation and Why the Resonance is a Real Singlet Scalar*, *Phys. Lett.* **B761** (2016) 408–411, [arXiv:1604.01711].

[136] D. H. Lyth and D. Wands, *Generating the curvature perturbation without an inflaton*, *Phys. Lett.* **B524** (2002) 5–14, [hep-ph/0110002].

[137] V. Vennin, K. Koyama, and D. Wands, *Encyclopædia curvatonis*, *JCAP* **1511** (2015) 008, [arXiv:1507.07575].

[138] D. Wands, *Multiple field inflation*, *Lect. Notes Phys.* **738** (2008) 275–304, [astro-ph/0702187].

[139] J. Frazer and A. R. Liddle, *Multi-field inflation with random potentials: field dimension, feature scale and non-Gaussianity*, *JCAP* **1202** (2012) 039, [arXiv:1111.6646].

[140] R. Klein, D. Roest, and D. Stefanyszyn, *Symmetry Breaking Patterns for Inflation*, arXiv:1712.05760.

[141] D. Marsh, L. McAllister, and T. Wrase, *The Wasteland of Random Supergravities*, *JHEP* **03** (2012) 102, [arXiv:1112.3034].

[142] M. C. D. Marsh, L. McAllister, E. Pajer, and T. Wrase, *Charting an Inflationary Landscape with Random Matrix Theory*, *JCAP* **1311** (2013) 040, [arXiv:1307.3559].

[143] M. Dias, J. Frazer, and M. c. D. Marsh, *Seven Lessons from Manyfield Inflation in Random Potentials*, arXiv:1706.03774.

[144] J. M. Maldacena, *Non-Gaussian features of primordial fluctuations in single field inflationary models*, *JHEP* **05** (2003) 013, [astro-ph/0210603].

[145] P. Creminelli and M. Zaldarriaga, *Single field consistency relation for the 3-point function*, *JCAP* **0410** (2004) 006, [astro-ph/0407059].

[146] D. Seery and J. E. Lidsey, *Primordial non-Gaussianities in single field inflation*, *JCAP* **0506** (2005) 003, [astro-ph/0503692].

[147] A. R. Liddle and S. M. Leach, *How long before the end of inflation were observable perturbations produced?*, *Phys. Rev.* **D68** (2003) 103503, [astro-ph/0305263].

[148] B. A. Bassett, S. Tsujikawa, and D. Wands, *Inflation dynamics and reheating*, *Rev. Mod. Phys.* **78** (2006) 537–589, [astro-ph/0507632].

[149] R. Allahverdi, R. Brandenberger, F.-Y. Cyr-Racine, and A. Mazumdar, *Reheating in Inflationary Cosmology: Theory and Applications*, *Ann. Rev. Nucl. Part. Sci.* **60** (2010) 27–51, [arXiv:1001.2600].

[150] J. Martin, C. Ringeval, and V. Vennin, *Observing Inflationary Reheating*, *Phys. Rev. Lett.* **114** (2015), no. 8 081303, [arXiv:1410.7958].

[151] M. S. Turner, *Coherent Scalar Field Oscillations in an Expanding Universe*, *Phys. Rev.* **D28** (1983) 1243.

[152] L. Kofman, A. D. Linde, and A. A. Starobinsky, *Reheating after inflation*, *Phys. Rev. Lett.* **73** (1994) 3195–3198, [hep-th/9405187].

[153] M. Kawasaki, K. Kohri, and T. Moroi, *Big-Bang nucleosynthesis and hadronic decay of long-lived massive particles*, *Phys. Rev.* **D71** (2005) 083502, [astro-ph/0408426].

[154] G. Barenboim and W.-I. Park, *Lepton number asymmetries and the lower bound on the reheating temperature*, *JCAP* **1712** (2017), no. 12 037, [arXiv:1708.04899].

[155] J. B. Munoz and M. Kamionkowski, *Equation-of-State Parameter for Reheating*, *Phys. Rev.* **D91** (2015), no. 4 043521, [arXiv:1412.0656].

[156] J. Martin, C. Ringeval, and V. Vennin, *Information Gain on Reheating: the One Bit Milestone*, *Phys. Rev.* **D93** (2016), no. 10 103532, [arXiv:1603.02606].

[157] G. N. Felder, L. Kofman, and A. D. Linde, *Instant preheating*, *Phys. Rev.* **D59** (1999) 123523, [hep-ph/9812289].

[158] M. A. Amin, M. P. Hertzberg, D. I. Kaiser, and J. Karouby, *Nonperturbative Dynamics Of Reheating After Inflation: A Review*, *Int. J. Mod. Phys.* **D24** (2014) 1530003, [arXiv:1410.3808].

[159] S. Saga, H. Tashiro, and S. Yokoyama, *Magnetic reheating*, *Mon. Not. Roy. Astron. Soc.* **474** (2018) L52, [arXiv:1708.08225].

[160] M. Endo, F. Takahashi, and T. T. Yanagida, *Inflaton Decay in Supergravity*, *Phys. Rev.* **D76** (2007) 083509, [arXiv:0706.0986].

[161] F. Takahashi, *Gravitino dark matter from inflaton decay*, *Phys. Lett.* **B660** (2008) 100–106, [arXiv:0705.0579].

[162] D. J. H. Chung, E. W. Kolb, and A. Riotto, *Production of massive particles during reheating*, *Phys. Rev.* **D60** (1999) 063504, [hep-ph/9809453].

[163] G. F. Giudice, E. W. Kolb, and A. Riotto, *Largest temperature of the radiation era and its cosmological implications*, *Phys. Rev.* **D64** (2001) 023508, [hep-ph/0005123].

[164] J. Ellis, M. A. G. Garcia, D. V. Nanopoulos, K. A. Olive, and M. Peloso, *Post-Inflationary Gravitino Production Revisited*, *JCAP* **1603** (2016), no. 03 008, [arXiv:1512.05701].

[165] M. Drees and F. Hajkarim, *Dark Matter Production in an Early Matter Dominated Era*, arXiv:1711.05007.

[166] J. L. Cook, E. Dimastrogiovanni, D. A. Easson, and L. M. Krauss, *Reheating predictions in single field inflation*, *JCAP* **1504** (2015) 047, [arXiv:1502.04673].

[167] L. Heurtier, *The Inflaton Portal to Dark Matter*, *JHEP* **12** (2017) 072, [arXiv:1707.08999].

[168] J. Martin, C. Ringeval, R. Trotta, and V. Vennin, *The Best Inflationary Models After Planck*, *JCAP* **1403** (2014) 039, [arXiv:1312.3529].

[169] J. Martin, C. Ringeval, and V. Vennin, *How Well Can Future CMB Missions Constrain Cosmic Inflation?*, *JCAP* **1410** (2014), no. 10 038, [arXiv:1407.4034].

[170] W. H. Kinney, *Inflation: Flow, fixed points and observables to arbitrary order in slow roll*, *Phys.Rev.* **D66** (2002) 083508, [astro-ph/0206032].

[171] A. R. Liddle, *Inflationary flow equations*, *Phys.Rev.* **D68** (2003) 103504, [astro-ph/0307286].

[172] E. Ramirez and A. R. Liddle, *Stochastic approaches to inflation model building*, *Phys.Rev.* **D71** (2005) 123510, [astro-ph/0502361].

[173] J.-O. Gong and E. D. Stewart, *The Density perturbation power spectrum to second order corrections in the slow roll expansion*, *Phys.Lett.* **B510** (2001) 1–9, [astro-ph/0101225].

[174] J. Martin, C. Ringeval, and V. Vennin, *K-inflationary Power Spectra at Second Order*, *J. Cosmol. Astropart. Phys.* **1306** (2013) 021, [arXiv:1303.2120].

[175] J. Choe, J.-O. Gong, and E. D. Stewart, *Second order general slow-roll power spectrum*, *JCAP* **0407** (2004) 012, [hep-ph/0405155].

[176] D. J. Schwarz, C. A. Terrero-Escalante, and A. A. Garcia, *Higher order corrections to primordial spectra from cosmological inflation*, *Phys.Lett.* **B517** (2001) 243–249, [astro-ph/0106020].

[177] D. J. Schwarz and C. A. Terrero-Escalante, *Primordial fluctuations and cosmological inflation after WMAP 1.0*, *J. Cosmol. Astropart. Phys.* **0408** (2004) 003, [hep-ph/0403129].

[178] A. Alho and C. Uggla, *Global dynamics and inflationary center manifold and slow-roll approximants*, *J. Math. Phys.* **56** (2015), no. 1 012502, [arXiv:1406.0438].

[179] A. R. Liddle, *The Inflationary energy scale*, *Phys. Rev.* **D49** (1994) 739–747, [astro-ph/9307020].

[180] P. Binetruy, E. Kiritsis, J. Mabillard, M. Pieroni, and C. Rosset, *Universality classes for models of inflation*, *JCAP* **1504** (2015), no. 04 033, [arXiv:1407.0820].

[181] S. Chongchitnan and G. Efstathiou, *Dynamics of the inflationary flow equations*, *Phys.Rev.* **D72** (2005) 083520, [astro-ph/0508355].

[182] G. Efstathiou and K. J. Mack, *The Lyth bound revisited*, *JCAP* **0505** (2005) 008, [astro-ph/0503360].

[183] B. A. Powell and W. H. Kinney, *Limits on primordial power spectrum resolution: An inflationary flow analysis*, *J. Cosmol. Astropart. Phys.* **0708** (2007) 006, [arXiv:0706.1982].

[184] W. H. Kinney, E. W. Kolb, A. Melchiorri, and A. Riotto, *WMAPping inflationary physics*, *Phys.Rev.* **D69** (2004) 103516, [hep-ph/0305130].

[185] L. Boubekeur, E. Giusarma, O. Mena, and H. Ramírez, *Phenomenological approaches of inflation and their equivalence*, *Phys.Rev.* **D91** (2015), no. 8 083006, [arXiv:1411.7237].

[186] A. D. Linde, *Axions in inflationary cosmology*, *Phys. Lett.* **B259** (1991) 38–47.

[187] **WMAP** Collaboration, H. V. Peiris et al., *First year Wilkinson Microwave Anisotropy Probe (WMAP) observations: Implications for inflation*, *Astrophys. J. Suppl.* **148** (2003) 213–231, [astro-ph/0302225].

[188] D. H. Lyth, *What would we learn by detecting a gravitational wave signal in the cosmic microwave background anisotropy?*, *Phys. Rev. Lett.* **78** (1997) 1861–1863, [hep-ph/9606387].

[189] L. Boubekeur and D. Lyth, *Hilltop inflation*, *JCAP* **0507** (2005) 010, [hep-ph/0502047].

[190] R. Easther and W. H. Kinney, *Monte Carlo reconstruction of the inflationary potential*, *Phys.Rev.* **D67** (2003) 043511, [astro-ph/0210345].

[191] K. Bamba, S. Nojiri, S. D. Odintsov, and D. Sáez-Gómez, *Inflationary universe from perfect fluid and $F(R)$ gravity and its comparison with observational data*, *Phys. Rev.* **D90** (2014) 124061, [arXiv:1410.3993].

[192] V. Mukhanov, *Quantum Cosmological Perturbations: Predictions and Observations*, *Eur.Phys.J.* **C73** (2013) 2486, [arXiv:1303.3925].

[193] D. Roest, *Universality classes of inflation*, *JCAP* **1401** (2014), no. 01 007, [arXiv:1309.1285].

[194] P. Creminelli, S. Dubovsky, D. López Nacir, M. Simonović, G. Trevisan, G. Villadoro, and M. Zaldarriaga, *Implications of the scalar tilt for the tensor-to-scalar ratio*, *Phys. Rev.* **D92** (2015), no. 12 123528, [arXiv:1412.0678].

[195] R. Gobbetti, E. Pajer, and D. Roest, *On the Three Primordial Numbers*, *JCAP* **1509** (2015), no. 09 058, [arXiv:1505.00968].

[196] J. Lin, Q. Gao, and Y. Gong, *The reconstruction of inflationary potentials*, *Mon. Not. Roy. Astron. Soc.* **459** (2016), no. 4 4029–4037, [arXiv:1508.07145].

[197] G. V. Chibisov and V. F. Mukhanov, *Galaxy formation and phonons*, *Mon. Not. Roy. Astron. Soc.* **200** (1982) 535–550.

[198] J. D. Barrow, *GRADUATED INFLATIONARY UNIVERSES*, *Phys. Lett.* **B235** (1990) 40–43.

[199] R. Myrzakulov and L. Sebastiani, *Inhomogeneous viscous fluids for inflation*, *Astrophys. Space Sci.* **356** (2015), no. 1 205–213, [arXiv:1410.3573].

[200] I. Brevik, E. Elizalde, S. D. Odintsov, and A. V. Timoshkin, *Inflationary universe in terms of a van der Waals viscous fluid*, *Int. J. Geom. Meth. Mod. Phys.* **14** (2017), no. 12 1750185, [arXiv:1708.06244].

[201] R. Myrzakulov, L. Sebastiani, and S. Zerbini, *Reconstruction of Inflation Models*, *Eur. Phys. J.* **C75** (2015), no. 5 215, [arXiv:1502.04432].

[202] D. Coone, D. Roest, and V. Vennin, *The Hubble Flow of Plateau Inflation*, *JCAP* **1511** (2015), no. 11 010, [arXiv:1507.00096].

[203] B. J. Broy, D. Coone, and D. Roest, *Plateau Inflation from Random Non-Minimal Coupling*, *JCAP* **1606** (2016), no. 06 036, [arXiv:1604.05326].

[204] R. Kallosh, A. Linde, and D. Roest, *Universal Attractor for Inflation at Strong Coupling*, *Phys. Rev. Lett.* **112** (2014), no. 1 011303, [arXiv:1310.3950].

[205] B. J. Broy, D. Roest, and A. Westphal, *Power Spectrum of Inflationary Attractors*, *Phys. Rev.* **D91** (2015), no. 2 023514, [arXiv:1408.5904].

[206] R. Kallosh and A. Linde, *Universality Class in Conformal Inflation*, *JCAP* **1307** (2013) 002, [arXiv:1306.5220].

[207] R. Kallosh, A. Linde, and D. Roest, *Superconformal Inflationary α-Attractors*, *JHEP* **11** (2013) 198, [arXiv:1311.0472].

[208] J. J. M. Carrasco, R. Kallosh, and A. Linde, *Cosmological Attractors and Initial Conditions for Inflation*, *Phys. Rev.* **D92** (2015), no. 6 063519, [arXiv:1506.00936].

[209] R. Kallosh, A. Linde, and D. Roest, *Large field inflation and double α-attractors*, *JHEP* **08** (2014) 052, [arXiv:1405.3646].

[210] J. J. M. Carrasco, R. Kallosh, and A. Linde, *α-Attractors: Planck, LHC and Dark Energy*, *JHEP* **10** (2015) 147, [arXiv:1506.01708].

[211] R. Kallosh and A. Linde, *Planck, LHC, and α-attractors*, *Phys. Rev.* **D91** (2015) 083528, [arXiv:1502.07733].

[212] A. Linde, *Single-field α-attractors*, *JCAP* **1505** (2015) 003, [arXiv:1504.00663].

[213] R. Kallosh and A. Linde, *Cosmological Attractors and Asymptotic Freedom of the Inflaton Field*, *JCAP* **1606** (2016), no. 06 047, [arXiv:1604.00444].

[214] Y. Ueno and K. Yamamoto, *Constraints on α-attractor inflation and reheating*, *Phys. Rev.* **D93** (2016), no. 8 083524, [arXiv:1602.07427].

[215] J. Martin, C. Ringeval, and V. Vennin, *Shortcomings of New Parametrizations of Inflation*, *Phys. Rev.* **D94** (2016), no. 12 123521, [arXiv:1609.04739].

[216] R. Kallosh and A. Linde, *Escher in the Sky*, *Comptes Rendus Physique* **16** (2015) 914–927, [arXiv:1503.06785].

[217] M. Galante, R. Kallosh, A. Linde, and D. Roest, *Unity of Cosmological Inflation Attractors*, *Phys. Rev. Lett.* **114** (2015), no. 14 141302, [arXiv:1412.3797].

[218] B. J. Broy, M. Galante, D. Roest, and A. Westphal, *Pole inflation – Shift symmetry and universal corrections*, *JHEP* **12** (2015) 149, [arXiv:1507.02277].

[219] C. L. Bennett, A. Banday, K. M. Gorski, G. Hinshaw, P. Jackson, P. Keegstra, A. Kogut, G. F. Smoot, D. T. Wilkinson, and E. L. Wright, *Four year COBE DMR cosmic microwave background observations: Maps and basic results*, *Astrophys. J.* **464** (1996) L1–L4, [astro-ph/9601067].

[220] J. Fumagalli, *Renormalization Group independence of Cosmological Attractors*, *Phys. Lett.* **B769** (2017) 451–459, [arXiv:1611.04997].

[221] S. P. Martin, *A Supersymmetry primer*, hep-ph/9709356. [Adv. Ser. Direct. High Energy Phys.18,1(1998)].

[222] A. Bilal, *Introduction to supersymmetry*, hep-th/0101055.

[223] R. Argurio, "Lecture notes: Introduction to supersymmetry." Retrieved from http://homepages.ulb.ac.be/~rargurio/susycourse.pdf.

[224] A. Brignole, *One loop Kahler potential in non renormalizable theories*, *Nucl. Phys.* **B579** (2000) 101–116, [hep-th/0001121].

[225] **CMS** Collaboration, A. M. Sirunyan et al., *Search for supersymmetry in multijet events with missing transverse momentum in proton-proton collisions at 13 TeV*, *Phys. Rev.* **D96** (2017), no. 3 032003, [arXiv:1704.07781].

[226] **ATLAS** Collaboration, M. Aaboud et al., *Search for squarks and gluinos in final states with jets and missing transverse momentum using 36 fb^{-1} of $\sqrt{s}$=13 TeV pp collision data with the ATLAS detector*, arXiv:1712.02332.

[227] G. F. Giudice and R. Rattazzi, *Gauge-mediated supersymmetry breaking*, *Adv. Ser. Direct. High Energy Phys.* **18** (1998) 355–377.

[228] S. Weinberg, *The quantum theory of fields. Vol. 2: Modern applications.* Cambridge University Press, 2013.

[229] D. V. Volkov and V. P. Akulov, *Is the Neutrino a Goldstone Particle?*, *Phys. Lett.* **46B** (1973) 109–110.

[230] R. Casalbuoni, S. De Curtis, D. Dominici, F. Feruglio, and R. Gatto, *Nonlinear Realization of Supersymmetry Algebra From Supersymmetric Constraint*, *Phys. Lett.* **B220** (1989) 569–575.

[231] Z. Komargodski and N. Seiberg, *From Linear SUSY to Constrained Superfields*, *JHEP* **09** (2009) 066, [arXiv:0907.2441].

[232] M. Rocek, *Linearizing the Volkov-Akulov Model*, *Phys. Rev. Lett.* **41** (1978) 451–453.

[233] E. A. Ivanov and A. A. Kapustnikov, *General Relationship Between Linear and Nonlinear Realizations of Supersymmetry*, *J. Phys.* **A11** (1978) 2375–2384.

[234] D. M. Ghilencea, *Comments on the nilpotent constraint of the goldstino superfield*, *Mod. Phys. Lett.* **A31** (2016), no. 12 1630011, [arXiv:1512.07484].

[235] D. Z. Freedman and A. Van Proeyen, *Supergravity*. Cambridge Univ. Press, Cambridge, UK, 2012.

[236] D. G. Cerdeno and C. Munoz, *An introduction to supergravity*, . [PoScorfu98,011(1998)].

[237] A. Sagnotti and S. Ferrara, *Supersymmetry and Inflation*, *PoS* **PLANCK2015** (2015) 113, [arXiv:1509.01500].

[238] M. Yamaguchi, *Supergravity based inflation models: a review*, *Class. Quant. Grav.* **28** (2011) 103001, [arXiv:1101.2488].

[239] E. Dudas, S. Ferrara, A. Kehagias, and A. Sagnotti, *Properties of Nilpotent Supergravity*, *JHEP* **09** (2015) 217, [arXiv:1507.07842].

[240] S. J. Gates, M. T. Grisaru, M. Rocek, and W. Siegel, *Superspace Or One Thousand and One Lessons in Supersymmetry*, *Front. Phys.* **58** (1983) 1–548, [hep-th/0108200].

[241] S. Ferrara, R. Kallosh, A. Van Proeyen, and T. Wrase, *Linear Versus Non-linear Supersymmetry, in General*, *JHEP* **04** (2016) 065, [arXiv:1603.02653].

[242] U. Lindstrom and M. Rocek, *Constrained Local Superfields*, *Phys. Rev.* **D19** (1979) 2300–2303.

[243] F. Farakos and A. Kehagias, *Decoupling Limits of sGoldstino Modes in Global and Local Supersymmetry*, *Phys. Lett.* **B724** (2013) 322–327, [arXiv:1302.0866].

[244] I. Antoniadis, E. Dudas, S. Ferrara, and A. Sagnotti, *The Volkov-Akulov-Starobinsky supergravity*, *Phys. Lett.* **B733** (2014) 32–35, [arXiv:1403.3269].

[245] N. Cribiori, G. Dall'Agata, F. Farakos, and M. Porrati, *Minimal Constrained Supergravity*, *Phys. Lett.* **B764** (2017) 228–232, [arXiv:1611.01490].

[246] N. J. Craig, *ISS-flation*, *JHEP* **02** (2008) 059, [arXiv:0801.2157].

[247] Y. Nakai and M. Sakai, *Inflation and Gauge Mediation in Supersymmetric Gauge Theory*, *Prog. Theor. Phys.* **125** (2011) 395–402, [arXiv:1004.2099].

[248] S. Choudhury, A. Mazumdar, and S. Pal, *Low & High scale MSSM inflation, gravitational waves and constraints from Planck*, *JCAP* **1307** (2013) 041, [arXiv:1305.6398].

[249] N. Arkani-Hamed, L. Motl, A. Nicolis, and C. Vafa, *The String landscape, black holes and gravity as the weakest force*, *JHEP* **06** (2007) 060, [hep-th/0601001].

[250] H. Ooguri and C. Vafa, *On the Geometry of the String Landscape and the Swampland*, *Nucl. Phys.* **B766** (2007) 21–33, [hep-th/0605264].

[251] N. Kaloper, M. Kleban, A. Lawrence, and M. S. Sloth, *Large Field Inflation and Gravitational Entropy*, *Phys. Rev.* **D93** (2016), no. 4 043510, [arXiv:1511.05119].

[252] D. Klaewer and E. Palti, *Super-Planckian Spatial Field Variations and Quantum Gravity*, *JHEP* **01** (2017) 088, [arXiv:1610.00010].

[253] R. Blumenhagen, I. Valenzuela, and F. Wolf, *The Swampland Conjecture and F-term Axion Monodromy Inflation*, *JHEP* **07** (2017) 145, [arXiv:1703.05776].

[254] M. Cicoli, D. Ciupke, C. Mayrhofer, and P. Shukla, *A Geometrical Upper Bound on the Inflaton Range*, arXiv:1801.05434.

[255] D. Escobar, A. Landete, F. Marchesano, and D. Regalado, *Large field inflation from D-branes*, *Phys. Rev.* **D93** (2016), no. 8 081301, [arXiv:1505.07871].

[256] R. Kallosh, F. Quevedo, and A. M. Uranga, *String Theory Realizations of the Nilpotent Goldstino*, *JHEP* **12** (2015) 039, [arXiv:1507.07556].

[257] I. Garcia-Etxebarria, F. Quevedo, and R. Valandro, *Global String Embeddings for the Nilpotent Goldstino*, *JHEP* **02** (2016) 148, [arXiv:1512.06926].

[258] S. Ferrara and R. Kallosh, *Seven-disk manifold, α-attractors, and B modes*, *Phys. Rev.* **D94** (2016), no. 12 126015, [arXiv:1610.04163].

[259] L. Aalsma, J. P. van der Schaar, and B. Vercnocke, *Constrained superfields on metastable anti-D3-branes*, *JHEP* **05** (2017) 089, [arXiv:1703.05771].

[260] J. Diaz Dorronsoro and M. Schillo, *Towards an explicit model of large field inflation*, arXiv:1712.04466.

[261] M. Kawasaki, M. Yamaguchi, and T. Yanagida, *Natural chaotic inflation in supergravity*, *Phys. Rev. Lett.* **85** (2000) 3572–3575, [hep-ph/0004243].

[262] A. Achucarro, S. Mooij, P. Ortiz, and M. Postma, *Sgoldstino inflation*, *JCAP* **1208** (2012) 013, [arXiv:1203.1907].

[263] A. Borghese, D. Roest, and I. Zavala, *A Geometric bound on F-term inflation*, *JHEP* **09** (2012) 021, [arXiv:1203.2909].

[264] S. V. Ketov and T. Terada, *Inflation in supergravity with a single chiral superfield*, *Phys. Lett.* **B736** (2014) 272–277, [arXiv:1406.0252].

[265] D. Roest and M. Scalisi, *Cosmological attractors from α-scale supergravity*, *Phys. Rev.* **D92** (2015) 043525, [arXiv:1503.07909].

[266] S. Ferrara and D. Roest, *General sGoldstino Inflation*, *JCAP* **1610** (2016), no. 10 038, [arXiv:1608.03709].

[267] S. Ferrara, R. Kallosh, and A. Linde, *Cosmology with Nilpotent Superfields*, *JHEP* **10** (2014) 143, [arXiv:1408.4096].

[268] G. Dall'Agata and F. Zwirner, *On sgoldstino-less supergravity models of inflation*, *JHEP* **12** (2014) 172, [arXiv:1411.2605].

[269] A. Linde, D. Roest, and M. Scalisi, *Inflation and Dark Energy with a Single Superfield*, *JCAP* **1503** (2015) 017, [arXiv:1412.2790].

[270] Y. Kahn, D. A. Roberts, and J. Thaler, *The goldstone and goldstino of supersymmetric inflation*, *JHEP* **10** (2015) 001, [arXiv:1504.05958].

[271] J. J. M. Carrasco, R. Kallosh, and A. Linde, *Minimal supergravity inflation*, *Phys. Rev.* **D93** (2016), no. 6 061301, [arXiv:1512.00546].

[272] S. Ferrara, R. Kallosh, and J. Thaler, *Cosmology with orthogonal nilpotent superfields*, *Phys. Rev.* **D93** (2016), no. 4 043516, [arXiv:1512.00545].

[273] A. Linde, *On inflation, cosmological constant, and SUSY breaking*, *JCAP* **1611** (2016), no. 11 002, [arXiv:1608.00119].

[274] E. McDonough and M. Scalisi, *Inflation from Nilpotent Kähler Corrections*, *JCAP* **1611** (2016), no. 11 028, [arXiv:1609.00364].

[275] W. Buchmuller, E. Dudas, L. Heurtier, and C. Wieck, *Large-Field Inflation and Supersymmetry Breaking*, *JHEP* **09** (2014) 053, [arXiv:1407.0253].

[276] W. Buchmuller, E. Dudas, L. Heurtier, A. Westphal, C. Wieck, and M. W. Winkler, *Challenges for Large-Field Inflation and Moduli Stabilization*, *JHEP* **04** (2015) 058, [arXiv:1501.05812].

[277] E. Dudas and C. Wieck, *Moduli backreaction and supersymmetry breaking in string-inspired inflation models*, *JHEP* **10** (2015) 062, [arXiv:1506.01253].

[278] E. Dudas, L. Heurtier, C. Wieck, and M. W. Winkler, *UV Corrections in Sgoldstino-less Inflation*, *Phys. Lett.* **B759** (2016) 121–125, [arXiv:1601.03397].

[279] R. Kallosh, L. Kofman, A. D. Linde, and A. Van Proeyen, *Gravitino production after inflation*, *Phys. Rev.* **D61** (2000) 103503, [hep-th/9907124].

[280] H. P. Nilles, K. A. Olive, and M. Peloso, *The Inflatino problem in supergravity inflationary models*, *Phys. Lett.* **B522** (2001) 304–314, [hep-ph/0107212].

[281] H. P. Nilles, M. Peloso, and L. Sorbo, *Nonthermal production of gravitinos and inflatinos*, *Phys. Rev. Lett.* **87** (2001) 051302, [hep-ph/0102264].

[282] J. J. M. Carrasco, R. Kallosh, A. Linde, and D. Roest, *Hyperbolic geometry of cosmological attractors*, *Phys. Rev.* **D92** (2015), no. 4 041301, [arXiv:1504.05557].

[283] R. Kallosh and A. Linde, *Superconformal generalization of the chaotic inflation model* $\frac{\lambda}{4}\phi^4 - \frac{\xi}{2}\phi^2 R$, *JCAP* **1306** (2013) 027, [arXiv:1306.3211].

[284] M. Kawasaki, K. Kohri, T. Moroi, and A. Yotsuyanagi, *Big-Bang Nucleosynthesis and Gravitino*, *Phys. Rev.* **D78** (2008) 065011, [arXiv:0804.3745].

[285] G. F. Giudice, A. Riotto, and I. Tkachev, *Thermal and nonthermal production of gravitinos in the early universe*, *JHEP* **11** (1999) 036, [hep-ph/9911302].

[286] T. Moroi, H. Murayama, and M. Yamaguchi, *Cosmological constraints on the light stable gravitino*, *Phys. Lett.* **B303** (1993) 289–294.

[287] M. Bolz, A. Brandenburg, and W. Buchmuller, *Thermal production of gravitinos*, *Nucl. Phys.* **B606** (2001) 518–544, [hep-ph/0012052]. [Erratum: Nucl. Phys.B790,336(2008)].

[288] V. S. Rychkov and A. Strumia, *Thermal production of gravitinos*, *Phys. Rev.* **D75** (2007) 075011, [hep-ph/0701104].

[289] M. Ibe and R. Kitano, *Gauge mediation in supergravity and gravitino dark matter*, *Phys. Rev.* **D75** (2007) 055003, [hep-ph/0611111].

[290] K. Hamaguchi, R. Kitano, and F. Takahashi, *Non-thermal Gravitino Dark Matter in Gauge Mediation*, *JHEP* **09** (2009) 127, [arXiv:0908.0115].

[291] K. Kamada, Y. Nakai, and M. Sakai, *Inflation in Gauge Mediation and Gravitino Dark Matter*, *Prog. Theor. Phys.* **126** (2011) 35–56, [arXiv:1103.5097].

[292] H. Fukushima, R. Kitano, and F. Takahashi, *Cosmologically viable gauge mediation*, *JHEP* **02** (2013) 140, [arXiv:1209.1531].

[293] H. Fukushima and R. Kitano, *Gravitino thermal production revisited and a new cosmological scenario of gauge mediation*, *JHEP* **01** (2014) 081, [arXiv:1311.6228].

[294] M. Ibe, Y. Nakayama, and T. T. Yanagida, *Conformal Gauge Mediation and Light Gravitino of Mass m(3/2) < O(10) eV*, *Phys. Lett.* **B671** (2009) 378–382, [arXiv:0804.0636].

[295] T. T. Yanagida, N. Yokozaki, and K. Yonekura, *Higgs Boson Mass in Low Scale Gauge Mediation Models*, *JHEP* **10** (2012) 017, [arXiv:1206.6589].

[296] E. Dudas, Y. Mambrini, and K. Olive, *The Case for an EeV Gravitino*, arXiv:1704.03008.

[297] F. Hasegawa, K. Nakayama, T. Terada, and Y. Yamada, *Gravitino problem in inflation driven by inflaton-polonyi Kähler coupling*, *Phys. Lett.* **B777** (2018) 270–274, [arXiv:1709.01246].

[298] F. Hasegawa, K. Mukaida, K. Nakayama, T. Terada, and Y. Yamada, *Gravitino Problem in Minimal Supergravity Inflation*, *Phys. Lett.* **B767** (2017) 392–397, [arXiv:1701.03106].

[299] M. Dine, L. Randall, and S. D. Thomas, *Supersymmetry breaking in the early universe*, *Phys. Rev. Lett.* **75** (1995) 398–401, [hep-ph/9503303].

[300] G. D. Coughlan, W. Fischler, E. W. Kolb, S. Raby, and G. G. Ross, *Cosmological Problems for the Polonyi Potential*, *Phys. Lett.* **131B** (1983) 59–64.

[301] J. R. Ellis, D. V. Nanopoulos, and M. Quiros, *On the Axion, Dilaton, Polonyi, Gravitino and Shadow Matter Problems in Supergravity and Superstring Models*, *Phys. Lett.* **B174** (1986) 176–182.

[302] T. Banks, D. B. Kaplan, and A. E. Nelson, *Cosmological implications of dynamical supersymmetry breaking*, *Phys. Rev.* **D49** (1994) 779–787, [hep-ph/9308292].

[303] T. Moroi, M. Yamaguchi, and T. Yanagida, *On the solution to the Polonyi problem with 0 (10-TeV) gravitino mass in supergravity*, *Phys. Lett.* **B342** (1995) 105–110, [hep-ph/9409367].

[304] S. Nakamura and M. Yamaguchi, *A Note on Polonyi Problem*, *Phys. Lett.* **B655** (2007) 167–171, [arXiv:0707.4538].

[305] R. Argurio, D. Coone, L. Heurtier, and A. Mariotti, *Sgoldstino-less inflation and low energy SUSY breaking*, *JCAP* **1707** (2017), no. 07 047, [arXiv:1705.06788].

[306] R. Kallosh, A. Linde, and M. Scalisi, *Inflation, de Sitter Landscape and Super-Higgs effect*, *JHEP* **03** (2015) 111, [arXiv:1411.5671].

[307] M. Scalisi, *Cosmological α-attractors and de Sitter landscape*, *JHEP* **12** (2015) 134, [arXiv:1506.01368].

[308] R. Kitano, H. Ooguri, and Y. Ookouchi, *Direct Mediation of Meta-Stable Supersymmetry Breaking*, *Phys. Rev.* **D75** (2007) 045022, [hep-ph/0612139].

[309] M. T. Grisaru, M. Rocek, and R. von Unge, *Effective Kahler potentials*, *Phys. Lett.* **B383** (1996) 415–421, [hep-th/9605149].

[310] K. A. Intriligator, N. Seiberg, and D. Shih, *Dynamical SUSY breaking in meta-stable vacua*, *JHEP* **04** (2006) 021, [hep-th/0602239].

[311] J. Ellis, M. A. G. Garcia, D. V. Nanopoulos, and K. A. Olive, *Calculations of Inflaton Decays and Reheating: with Applications to No-Scale Inflation Models*, *JCAP* **1507** (2015), no. 07 050, [arXiv:1505.06986].

[312] A. de Gouvea, T. Moroi, and H. Murayama, *Cosmology of supersymmetric models with low-energy gauge mediation*, *Phys. Rev.* **D56** (1997) 1281–1299, [hep-ph/9701244].

[313] K. Benakli, Y. Chen, E. Dudas, and Y. Mambrini, *A Minimal Model of Gravitino Dark Matter*, arXiv:1701.06574.

[314] R. T. Co, F. D'Eramo, and L. J. Hall, *Gravitino or Axino Dark Matter with Reheat Temperature as high as 10^{16} GeV*, *JHEP* **03** (2017) 005, [arXiv:1611.05028].

[315] R. T. Co, F. D'Eramo, L. J. Hall, and K. Harigaya, *Saxion Cosmology for Thermalized Gravitino Dark Matter*, arXiv:1703.09796.

[316] C. Cheung, G. Elor, and L. Hall, *Gravitino Freeze-In*, *Phys. Rev.* **D84** (2011) 115021, [arXiv:1103.4394].

[317] L. J. Hall, J. T. Ruderman, and T. Volansky, *A Cosmological Upper Bound on Superpartner Masses*, *JHEP* **02** (2015) 094, [arXiv:1302.2620].

[318] A. Monteux and C. S. Shin, *Thermal Goldstino Production with Low Reheating Temperatures*, *Phys. Rev.* **D92** (2015) 035002, [arXiv:1505.03149].

[319] R. T. Co, F. D'Eramo, L. J. Hall, and D. Pappadopulo, *Freeze-In Dark Matter with Displaced Signatures at Colliders*, *JCAP* **1512** (2015), no. 12 024, [arXiv:1506.07532].

[320] M. Drees and M. M. Nojiri, *The Neutralino relic density in minimal $N = 1$ supergravity*, *Phys. Rev.* **D47** (1993) 376–408, [hep-ph/9207234].

[321] J. D. Wells, *Supersymmetric dark matter with a cosmological constant*, *Phys. Lett.* **B443** (1998) 196–200, [hep-ph/9809504].

[322] J. D. Wells, *Mass density of neutralino dark matter*, hep-ph/9708285. [Adv. Ser. Direct. High Energy Phys.21,269(2010)].

[323] A. Boyarsky, J. Lesgourgues, O. Ruchayskiy, and M. Viel, *Lyman-alpha constraints on warm and on warm-plus-cold dark matter models*, *JCAP* **0905** (2009) 012, [arXiv:0812.0010].

[324] S. Dimopoulos, G. F. Giudice, and A. Pomarol, *Dark matter in theories of gauge mediated supersymmetry breaking*, *Phys. Lett.* **B389** (1996) 37–42, [hep-ph/9607225].

[325] A. D. Linde and V. F. Mukhanov, *Nongaussian isocurvature perturbations from inflation*, *Phys. Rev.* **D56** (1997) R535–R539, [astro-ph/9610219].

[326] N. Bartolo and A. R. Liddle, *The Simplest curvaton model*, *Phys. Rev.* **D65** (2002) 121301, [astro-ph/0203076].

[327] R. J. Hardwick, V. Vennin, K. Koyama, and D. Wands, *Constraining Curvatonic Reheating*, *JCAP* **1608** (2016), no. 08 042, [arXiv:1606.01223].

[328] R. Easther and J. T. Giblin, *The Hubble slow roll expansion for multi field inflation*, *Phys. Rev.* **D72** (2005) 103505, [astro-ph/0505033].

[329] R. Easther, J. Frazer, H. V. Peiris, and L. C. Price, *Simple predictions from multifield inflationary models*, *Phys. Rev. Lett.* **112** (2014) 161302, [arXiv:1312.4035].

[330] **CMB-S4** Collaboration, K. N. Abazajian et al., *CMB-S4 Science Book, First Edition*, arXiv:1610.02743.

[331] T. Matsumura et al., *Mission design of LiteBIRD*, arXiv:1311.2847. [J. Low. Temp. Phys.176,733(2014)].

[332] **CORE** Collaboration, F. Finelli et al., *Exploring Cosmic Origins with CORE: Inflation*, arXiv:1612.08270.

[333] A. Cooray, *21-cm Background Anisotropies Can Discern Primordial Non-Gaussianity*, *Phys. Rev. Lett.* **97** (2006) 261301, [astro-ph/0610257].

[334] M. Alvarez et al., *Testing Inflation with Large Scale Structure: Connecting Hopes with Reality*, arXiv:1412.4671.

[335] J. B. Muñoz, Y. Ali-Haïmoud, and M. Kamionkowski, *Primordial non-gaussianity from the bispectrum of 21-cm fluctuations in the dark ages*, *Phys. Rev.* **D92** (2015), no. 8 083508, [arXiv:1506.04152].